STRUCTURAL BEHAVIOUR OF SELF CONSOLIDATING STEEL FIBER REINFORCED CONCRETE BEAMS

by

Michael Cohen

Thesis submitted to the
Faculty of Graduate and Postdoctoral Studies
in partial fulfillment of the requirements for the degree of
Master of Applied Science
in Civil Engineering

uOttawa

Department of Civil Engineering
Faculty of Engineering
University of Ottawa

The M.A.Sc. in Civil Engineering is a joint program
with Carleton University administered by the
Ottawa-Carleton Institute for Civil Engineering

July 2012

Dedication

This thesis is dedicated to my parents, my sister and my brother.

Acknowledgement

I would like to express my sincere recognition to my supervisor Dr. Hassan Aoude for creating the opportunity and providing optimum conditions to carry out this Master's research project. His excellent supervision and invaluable guidance have contributed very much to the successful completion of this dissertation.

My deepest gratitude goes out to the professors of the Department of Civil Engineering at the University of Ottawa. The assistance of the administrative staff is also gratefully acknowledged.

I thankfully appreciate the generous financial support given by the Faculty of Engineering at the University of Ottawa. Words of thanks are also addressed to the Ontario Ministry of Training, Colleges and Universities for granting me the Ontario Graduate Scholarship (OGS). Without these great contributions this Master's programme would not come to realization.

The research presented in this thesis was carried out in the Structural Laboratory at the University of Ottawa. I would like to thank everyone who helped me during the construction and testing of the specimens.

The donation of materials by Bekaert Steel Wire Co. (steel fibers) and King Materials (SCC) was appreciated.

Finally, I would like to thank my parents, sister, and brother for their love, support, and patience.

Michael Cohen

Abstract

When subjected to a combination of moment and shear force, a reinforced concrete (RC) beam with either little or no transverse reinforcement can fail in shear before reaching its full flexural strength. This type of failure is sudden in nature and usually disastrous because it does not give sufficient warning prior to collapse. To prevent this type of shear failure, reinforced concrete beams are traditionally reinforced with stirrups. However, the use of stirrups is not always cost effective since it increases labor costs, and can make casting concrete difficult in situations where closely-spaced stirrups are required. The use of steel fiber reinforced concrete (SFRC) could be considered as a potential alternative to the use of traditional shear reinforcement. Concrete is very weak and brittle in tension, SFRC transforms this behaviour and improves the diagonal tension capacity of concrete and thus can result in significant enhancements in shear capacity. However, one of the drawbacks associated with SFRC is that the addition of fibers to a regular concrete mix can cause problems in workability. The use of self-consolidating concrete (SCC) is an innovative solution to this problem and can result in improved workability when fibers are added to the mix.

The thesis presents the experimental results from tests on twelve slender self-consolidating fiber reinforced concrete (SCFRC) beams tested under four-point loading. The results demonstrate the combined use of SCC and steel fibers can improve the shear resistance of reinforced concrete beams, enhance crack control and can promote flexural ductility.

Despite extensive research, there is a lack of accurate and reliable design guidelines for the use of SFRC in beams. This study presents a rational model which can accurately predict the shear resistance of steel fiber reinforced concrete beams. The thesis also proposes a safe and reliable equation which can be used for the shear design of SFRC beams.

Table of Contents

List of Figures

List of Tables

List of Symbols

A_f	Cross-sectional area of fiber
A_s	Cross-sectional area of steel reinforcement
A_v	Transverse reinforcement cross-sectional area
$A_{v,\min}$	Minimum area of shear reinforcement
a/d	Shear span-to-depth ratio
b_w	Beam web width
d	Effective depth
D_f	Diameter of fiber
d_v	Effective shear depth of the beam
e	Factor depending on the value of ratio
E_s	Modulus of elasticity of longitudinal steel reinforcement
F	Fiber factor
F_1	First-peak strength in the ASTM C1609 toughness test
F_{150}	Residual strength at net deflection of L/150 in the ASTM C1609 toughness test
F_{600}	Residual strength at net deflection of L/600 in the ASTM C1609 toughness test
$f_c^{'}$	Compressive strength of concrete
$f_{cf}^{'}$	Ultimate compressive strength of fiber reinforced concrete
f_{ct}	Tensile strength of concrete
$f_{cu}^{'}$	Ultimate compressive strength of plain concrete
$f_{ftd,res}$	Residual strength as defined in the Norwegian code
f_{fy}	Fiber tensile strength
$f_{\max}$	Peak tensile stress in concrete

F_p	Peak strength in the ASTM C1609 toughness test
$F_{pullout}$	Pullout strength of a single fiber
f_r	Modulus of rapture of concrete
F_{Ri}	Residual load at pre-determined crack-mouth opening displacement (CMOD)
f_{Ri}	Residual strength at pre-determined crack-mouth opening displacement (CMOD)
f_{sp}	Concrete cylinder splitting tensile strength
FT	Flexural toughness factor
f_u	Ultimate stress of longitudinal steel reinforcement
f_y	Yield stress of steel reinforcement
f_{yh}	Yield stress of transverse reinforcement
h	Beam height
h_o	Fiber dimension which is a function of hook geometry
jd	Flexural lever arm
K	Fiber participation factor
k	Factor referring to the type of test used to determine the tensile strength of concrete
k_o	Fiber dimension which is a function of hook geometry
k_{f1}, k_{f2}	Parameters used to define the descending branch of SFRC stress-strain curve
L	Span length in the ASTM C1609 toughness test
L_f	Length of fiber
$L_{f,straight}$	Length of straight portion of fiber neglecting the anchorage
L_f / D_f	Fiber aspect ratio
M_F	Factored moment applied to RC member
M_n	Nominal moment applied to RC member
n	Parameter that describes the shape of SFRC stress-strain diagram
N_{fibers}	Effective number of fibers per unit area

P_1	Load at onset of complete debonding during fiber pullout
P_2 , P_3	Load plateau at end of first hook contribution during fiber pullout
P_4	Load plateau at end of second hook contribution during fiber pullout
P_{150}	Residual load at net deflection of L/150 in the ASTM C1609 toughness test
P_{600}	Residual load at net deflection of L/600 in the ASTM C1609 toughness test
P_{crit}	Load that causes debonding to initiate during fiber pullout
P_p	Peak load in the ASTM C1609 toughness test
$\Delta P^{'}$	Mechanical pullout load contribution of hook due to the formation of two plastic hinges
$\Delta P^{''}$	Mechanical pullout load contribution of hook due to the formation of one plastic hinge
r_f	Fiber radius
RI	Steel fiber reinforcing index
s	Center-to-center spacing of transverse steel reinforcement in RC member
S_{ze}	Effective crack spacing parameter
T_{150}	Area under load versus net deflection curve in the ASTM C1609 toughness test
TR_c	Toughness ratio of plain concrete
TR_{cf}	Toughness ratio of fiber reinforced concrete
V	Shear force at a section of RC member
V_c	Concrete contribution to shear resistance
$V_{c,fib}$	Calculated shear capacity of SFRC beam for design
$V_{\exp}$	Experimental shear resistance
V_F	Factored shear load applied to RC member
V_f	Volume fraction of fibers in the concrete mixture
V_{fd}	Fiber contribution to shear resistance as defined in some design guidelines (RILEM, etc.)

V_{fib}	Fiber contribution to shear resistance in proposed model
V_{no}	Nominal shear resistance
V_{nf}	Shear resistance of the beam including the influence of the fibers
V_{pred}	Predicted shear resistance
V_r	Factored shear resistance of a RC member
V_s	Transverse steel contribution to shear resistance
υ_u	Ultimate shear strength of RC member
w	Crack width
W_F	Dissipated energy value in Stress – crack opening ($\sigma - w$) test
w_f	Weight fraction of fibers in the concrete mixture
α , α_θ	Fiber orientation factor
α_m	Fiber deformation contribution factor
α_v	Pullout reduction factor
β	Factor accounting for shear resistance of cracked concrete
β_1	Material parameter that controls shape of SFRC stress-strain diagram
Δ_1	Slip of the fiber at full-debonding
Δ_3	Slip of the fiber at load P_3 during debonding
Δ_4	Slip of the fiber at load P_4 during debonding
Δ_{exp}	Beam mid-span deflection at peak
Δ_{max}	Beam mid-span deflection at failure
δ_1	Net deflection at first-peak load in the ASTM C1609 toughness test
δ_p	Net deflection at peak load in the ASTM C1609 toughness test
ε_c	Elastic strain in concrete
$\varepsilon_{c,cr}$	Elastic strain in concrete at cracking
ε'_{cf}	Ultimate strain of fiber reinforced concrete
ε'_{cu}	Ultimate strain of plain concrete
ε_{sh}	Strain of longitudinal steel reinforcement at strain-hardening

ε_u	Ultimate strain of longitudinal steel reinforcement
ε_x	Average longitudinal strain at mid-depth of beam
ε_y	Yield strain of longitudinal steel reinforcement
η	Normalized compressive stress of fiber reinforced concrete
η_1	Length factor that accounts for variability in fiber embedment length
ϕ_c	Material resistance factor for concrete
ϕ_s	Material resistance factor for steel
γ_c	Unit weight of normal concrete
λ	Factor that accounts for concrete type
μ	Frictional coefficient of fiber-matrix interface
ω	Factor which accounts for fiber properties
Ψ	Size effect factor in several models proposed in the literature
ψ	Size effect factor used in proposed model
ρ	Longitudinal steel reinforcement ratio
σ_c	Elastic stress in concrete
$\overline{\sigma_p}(w)$	Residual post-cracking strength of SFRC
τ_{bond}	Bond shear strength
τ_{fd}	Fraction of the residual strength as defined in the Norwegian code
θ	Angle of inclination of diagonal compressive stresses to the longitudinal axis of the member

Chapter One: Introduction

1.1 Introduction

When subjected to a combination of moment and shear force, a reinforced concrete (RC) beam with either little or no transverse reinforcement can fail in shear before reaching its full flexural strength. This type of failure is sudden in nature and usually disastrous because it does not give sufficient warning prior to collapse. To prevent shear failure, beams are traditionally reinforced with stirrups. However, the use of stirrups is not always cost efficient, since it increases labor costs and can make casting concrete difficult in situations where closely-spaced stirrups are required.

The use of steel fiber reinforced concrete (SFRC) could be considered as a potential alternative to the use of traditional shear reinforcement. SFRC is the generic term used to define a composite material whose components include the traditional constituents of concrete and a dispersion of randomly oriented steel fibers. Concrete is very weak and brittle in tension, the use of steel fiber reinforced concrete (SFRC) can transform this behaviour. The addition of steel fibers improves the diagonal tension capacity of concrete and thus can result in significant enhancements in shear capacity. SFRC can potentially be used to completely or partially substitute conventional shear reinforcement in shear-critical beams.

However, one of the drawbacks associated with SFRC is that the addition of fibers to a regular concrete mix can cause problems in workability. The use of self-consolidating concrete (SCC) is an innovative solution to this problem and can result in improved workability when fibers are added to the mix.

Despite extensive research, the use of SFRC in load-carrying structural elements such as beams remains limited. One of the main reasons returns to the lack of accurate and reliable prediction models and design guidelines for SFRC.

1.2 Research Objectives

This thesis presents the results of a research program focusing on the shear and flexural behaviour of self-consolidating fiber reinforced concrete (SCFRC) beams and examines the potential of using SCFRC to substitute for the conventional shear reinforcement required by modern codes. In addition, the thesis also presents analytical studies aimed at developing prediction equations and design guidelines for the use of SFRC in shear-critical beams. The details of the experimental and analytical program are summarized below.

1.2.1. Experimental Program

The primary objective of the experimental research program is to study the main advantages that result from the combined use of steel fibers and self-consolidating concrete in shear-critical beams. A secondary objective is to examine the potential of using SCFRC to replace traditional shear reinforcement in beams. The objectives of the experimental research program will be achieved by:

- Examining the influence of steel fibers on the properties of traditional and customized SCC mixtures;
- Testing twelve beams constructed with SCC and steel fibers under four-point loading and studying the effect of various parameters on shear capacity, crack control and flexural ductility.

1.2.2 Analytical Program

The objective of the analytical program, which complements the experimental program, is to develop a model which can predict the shear resistance of SFRC and SCFRC beams. This objective will be achieved by:

- Performing a parametric study on a large database of SFRC beam test results in order to examine the effect of various parameters on the shear response of SFRC beams;
- Developing a rational model for predicting the shear strength of SFRC beams;
- Developing a safe and reliable equation which can be used in the shear design of SFRC beams;

1.3 Thesis Organization

The thesis consists of seven chapters. Chapter 2 starts with a comprehensive literature review of the subject addressed in this thesis. Thereafter, the thesis details the two main phases of the research program:

1. The first phase of the research program reviews the structural behaviour of twelve reinforced concrete beams constructed with steel fibers and self-consolidating concrete subjected to four-point loading:
   - Chapter 3 summarizes the details of the experimental program, including: material properties, beam properties and test setup.
   - Chapter 4 presents the experimental results for the twelve SCFRC beams tested in the experimental program.
   - Chapter 5 discusses and compares the experimental results to examine the influence of various parameters on the structural response of SCFRC beams.

2. The second phase of the research program presents analytical studies aimed at developing accurate models for predicting the shear resistance of SFRC beams:
   - Chapter 6 begins with a parametric study which examines the influence of various parameters on the shear response of SFRC beam. An analytical model that can be used to predict the shear strength of SFRC beams is then presented and design guidelines are proposed.

Finally, Chapter 7 features the concluding remarks regarding the experimental and analytical studies, and provides some recommendations for future research.

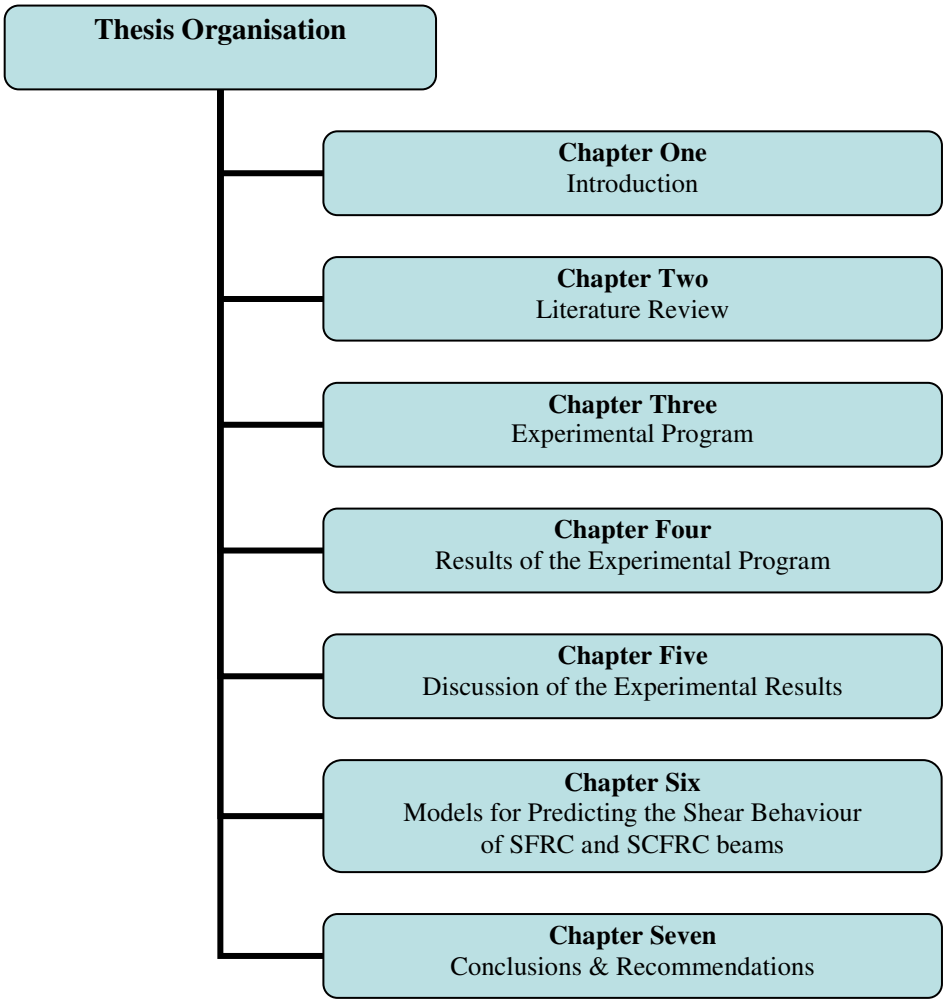

Figure 1.1: Thesis organization

Chapter Two: Literature Review

2.1 Overview

In this chapter a comprehensive review of Steel Fiber Reinforced Concrete (SFRC) as a structural material will be presented. Section 2.2 will introduce Steel Fiber Reinforced Concrete (SFRC), its uses and properties. In particular, a brief review of the pullout behaviour of fibers in concrete will be presented. In addition, the behaviour of SFRC in tension and compression will be discussed. Standard testing methods which can be used to evaluate the performance of SFRC will also be reviewed.

In addition, Section 2.3 will discuss the potential of using Self-consolidating fiber reinforced concrete (SCFRC) as an alternative to traditional SFRC. First methods for measuring the workability and fresh-state properties of self-consolidating concrete (SCC) will be discussed (slump flow test, V-funnel test, etc.) Thereafter, the concept of using fiber reinforced concrete in combination with self-consolidating concrete will be reviewed, with a summary of mix designs proposed by other researchers.

This thesis will focus on the use of SFRC and SCFRC to improve the shear behaviour of beams. Therefore the literature review will also review the benefits of using these materials in beams. Section 2.4 will review the shear behaviour of traditional reinforced concrete beams. North American code provisions related to shear will be also discussed. Section 2.5 will then review existing research on the shear behaviour of SFRC and SCFRC beams. Furthermore, this section will present existing empirical and rational models that have been proposed in the literature. Existing codes and guidelines related to the use of steel fibers in beams will also be summarized.

2.2 Fiber Reinforced Concrete (FRC)

The use of fibers to reinforce brittle materials is not a new concept. The use of straws to reinforce clay bricks can be found in ancient Egyptian construction. Similarly remains from ancient construction in Asia shows that similar "fiber" reinforcement was used in the construction of dwellings. One of the main purposes for using fibers is to “strengthen” the matrix to which it is added. Concrete is very weak and brittle in tension; the use of fiber reinforced concrete (FRC) can transform this behaviour. The most significant effect of fiber addition to concrete is the enhancement of post-cracking behaviour and toughness with the capability of FRC to carry tensile load after cracking (Li, 2000). Steel fiber reinforced concrete as we know it today was developed in the early 1960s. Other forms of fiber reinforcement such as polymeric fibers, glass fibers were developed shortly thereafter (Ando et al., 1990). Examples of various fibers are shown in **Figure 2.1**.

Figure 2.1: Different types of fibers with different lengths and shapes [Adapted from Kosmataka et al. (2002)]

2.2.1 Steel Fiber Reinforced Concrete (SFRC)

Steel fiber reinforced concrete (SFRC) is a composite material whose components include the traditional constituents of Portland cement concrete (hydraulic cement, fine and coarse aggregates, admixtures) and a dispersion of randomly oriented short discrete steel fibers. Just as with all FRC materials, compared to plain concrete the most noticeable differences are improved ductility and post-cracking performance.

In North America, the use of SFRC has grown over the years, albeit very slowly. In addition extensive experimental research has been conducted on SFRC. However, despite this fact the use of SFRC in structural applications remains very limited in the construction industry. One of the main reasons returns to the lack of reliable prediction models and the lack of detailed design guidelines for engineers. Other reasons include the cost of SFRC and the conservative nature of the construction industry (Li, 2000).

Current widespread use of fibers is mostly in nonstructural applications, where fibers are generally used as an alternative for the steel bars and wire mesh used to control cracking. Examples of non-structural applications include industrial floors and slabs, large concrete containers, and concrete pavements. In general, these structures and products have extensive exposed surface areas and movement constraints, resulting in high cracking potential. For such applications, fibers have a number of advantages over conventional steel reinforcement including uniform distribution of the fibers in the concrete matrix and savings in labor cost and construction time due to the ability of fibers to partially or completely replace traditional reinforcement.

In addition to the present use of fibers in non-structural applications there may be benefit in using this material in some structural applications. The use of fibers significantly enhances the diagonal-tension capacity of concrete, leading to improved shear resistance. Hence the use of fibers in beams and columns can potentially be used to replace traditional shear and transverse reinforcement. The addition of fibers also improves the energy-absorption capacity of concrete; hence the use of fibers may be beneficial in seismic and blast applications (beams, columns, walls). Examples of potential structural applications are shown in **Figure 2.2**.

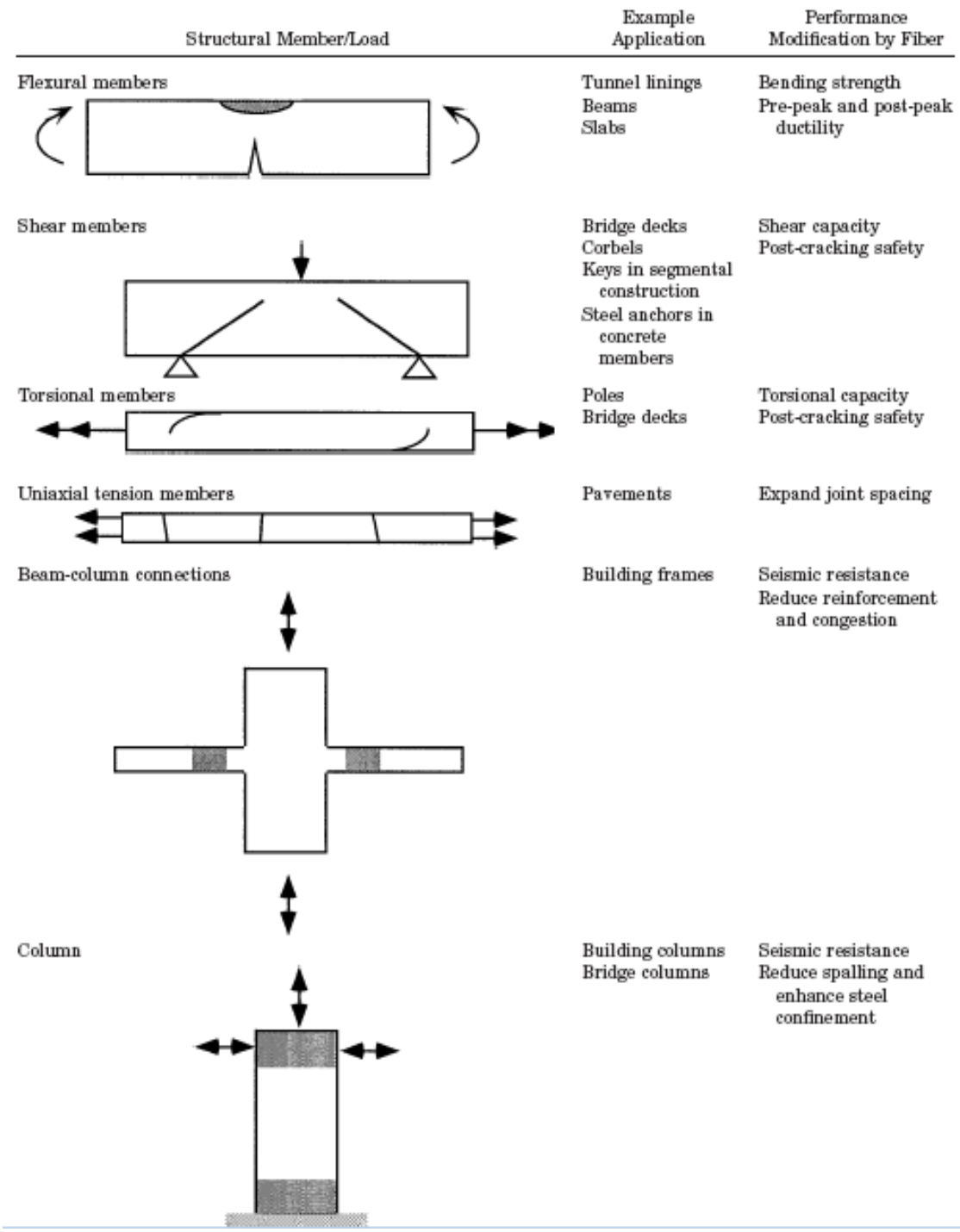

Figure 2.2: Potential structural applications for SFRC

[Adapted from Li (2000)]

2.2.2 Steel Fiber Typologies

Various steel fiber configurations can be used (see **Figure 2.3**). For example, some steel fibers have hooked ends while others have deformed or twisted shapes to improve pullout behaviour.

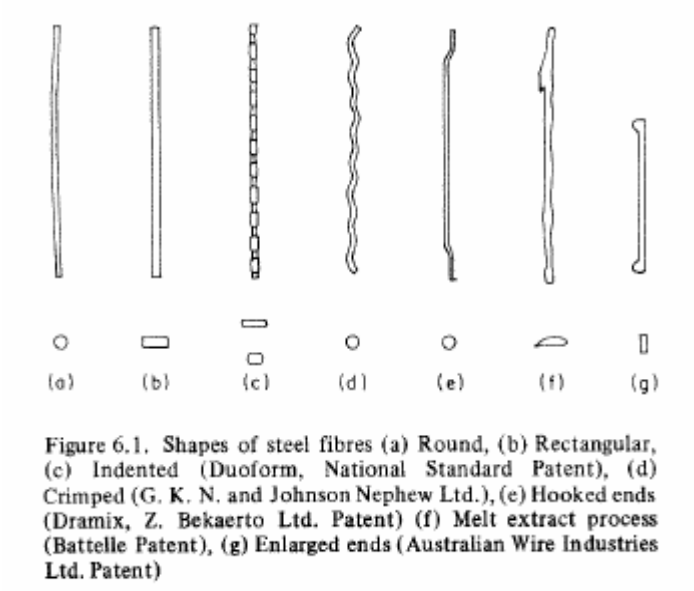

Figure 2.3: Examples of different steel fiber configurations
[Adapted from Johnston (2001)]

2.2.2.1 Hooked end steel fibers

Hooked-end steel fibers represent the most common fiber type used by researchers and in the construction industry. These fibers provide superior performance when compared to straight fibers because of the effect of the hooks on pullout resistance. After the initial debonding of the fiber from the concrete matrix, the hooked-ends must deform, resulting in an improvement in pullout strength.

Currently hooked-end fibers are manufactured by *Bekaert* under the *Dramix* brand. Extensive experimental data on the use of this type of fiber is available in the literature. The fibers are added to the concrete during mixing as glued bundles and disperse homogeneously during the mixing process (see **Figure 2.4**).

Examples of common brands of *Dramix* fibers include:

- *Dramix ZP305* fibers: tensile strength of 1100 N/mm^2, length of 30 mm and aspect ratio (L_f/D_f) of 55.
- *Dramix RC 80/60* fibers: tensile strength of 1035 N/mm^2, length of 60 mm and aspect ratio (L_f/D_f) of 80.
- *Dramix BP80/30* or *BP80/60* high strength fibers: tensile strength of 2000 N/mm^2, length of 30 or 60 mm and aspect ratio (L_f/D_f) of 80.

2.2.2.2 Crimped and twisted steel fiber

Another approach that can be used to enhance the pullout characteristics of steel fibers is to provide additional resistance to pullout through the use of a continuously deformed shape along the length of the fibers. Example of fibers in this category, are crimped and twisted steel fibers. In the case of crimped fibers, the deformed shape or "crimps" result in improved mechanical bonding (see **Figure 2.5**). This fiber configuration is the second most common fiber type used in research and field applications, and is supplied by several different manufacturers worldwide (e.g. *FiberMesh* and others). Some of the main advantages associated with the use of crimped steel fibers are related to cost efficiency, easy dispersion in concrete mixtures, and improvements in workability. On the other hand, when compared to hooked-end fibers, the use of crimped fibers generally results in reduced toughness properties (Banthia and Sappakittipakorn, 2007).

In addition to crimped fibers, recent research has led to the development of twisted steel fibers. These fibers provide improved frictional pullout due to the added energy required to untwist the "screw-shaped" fiber from the concrete matrix during pullout. In addition, rather than using a round wire shape, twisted fibers have a triangular cross-sectional shape. The triangular shape provides a greater surface area and thus leads to increased bond resistance. It is noted that with twisted fibers, the pullout behaviour is altered from a frictional pullout mechanism to a torsional untwisting pullout. **Figure 2.6** compares the properties of hooked-end and twisted fibers. Twisted fibers are currently manufactured under the *Helix* brand by *Polytorx*. Typical *Helix* fibers have a length of 25mm and a diameter of 0.5 mm, resulting in an aspect ratio of 50.

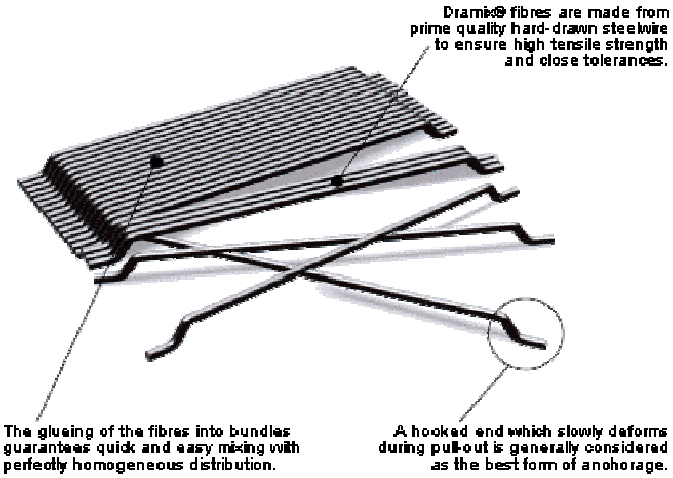

Figure 2.4: Dramix hooked end steel fibers

[Adapted from Bekaert website]

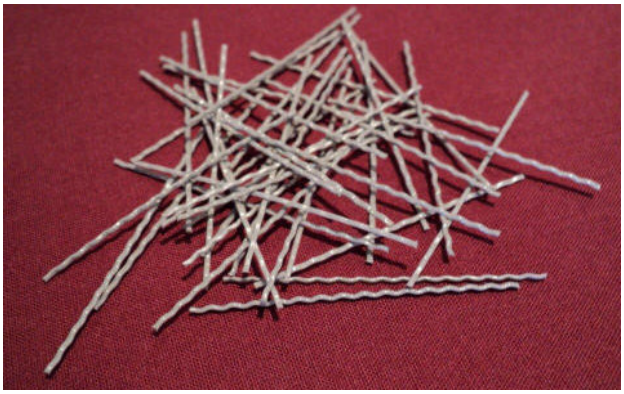

Figure 2.5: Example of crimped steel fibers

[Adapted from FiberMesh website]

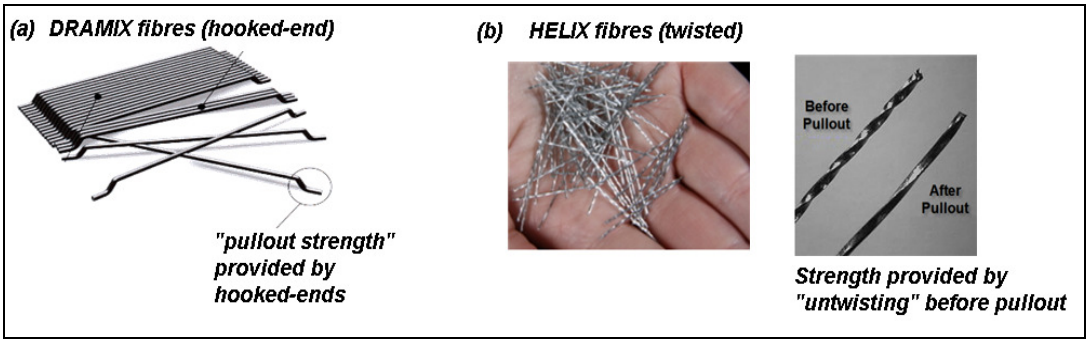

Figure 2.6: Difference in pullout behaviour: hooked-end vs. twisted fibers.

[Adapted from Aoude (2008)]

2.2.3 Introduction to SFRC and its properties

Since plain concrete shows poor response under tensile stresses and exhibits early primary cracking, it is considered a brittle material. The addition of steel fibers transforms concrete into a 'pseudo-ductile' material through the ability of fibers to bridge and control cracking. The mechanical properties of steel fiber reinforced concrete (SFRC) are influenced by a number of parameters related to the fibers and concrete matrix, including:

(a) Aspect ratio of the fiber;

(b) Fiber content and type;

(c) Bond between the fiber and the concrete matrix;

(d) Orientation factor.

2.2.3.1 Aspect ratio

Fiber lengths commonly vary between 10 to 60 mm. with round (or less commonly rectangular or triangular) cross sections with diameters in the range of 0.4 to 1 mm. Shorter fibers typically offer superior first crack strength while longer fibers are more efficient at enhancing post-cracking behaviour.

The ratio between the length of the fiber and the diameter of the fiber is termed as the "aspect ratio" (L_f/D_f). Research has shown that increasing the aspect ratio improves the mechanical properties of the SFRC matrix in tension and compression. However it should be noted that with greater aspect ratio steel fibers are difficult to disperse uniformly during mixing, and hence using a high aspect ratio has a negative effect on the fresh-state properties and workability of SFRC. As such there exists a tradeoff between enhanced mechanical properties and reduced workability. For this reason, most mixes discussed in the literature use fibers with aspect ratios of 80 or less (Minelli, 2005).

2.2.3.2 Fiber content and type

Addition of 78 kg/m^3 results in 1% of steel fibers per volume of concrete. Typical fiber contents in SFRC range between 20 to 120 Kg/m^3 (or 0.25% to 1.5%). Typical non-structural applications such as slabs on grade limit the fiber content to less than 40 kg/m^3 (or 0.5%). For structural applications quantities greater than 1.0% are typically required (Aoude, 2008).

In addition, as noted in the previous section fiber typology (straight, hooked-end, corrugated and twisted) has an important impact on the pullout strength of fibers and hence performance of SFRC.

2.2.3.3 Bond between the fiber and the concrete matrix

Bond strength is a parameter that has a direct effect on the pullout strength of steel fibers. There exists a direct relationship between the matrix strength and the resulting average bond shear strength between the fiber and the matrix (τ_{bond}). Kutzing (2000) proposed typical values of τ_{bond} as a function of concrete compressive strength based on a review of pullout data (from tests on straight steel fibers) available in the literature (see **Table 2.1**).

Table 2.1: Range of bond shear strength values for various concrete matrices [Adapted from Grunewald (2004) based on work by Kutzing (2000)]

Matrix Compressive strength class	Compressive strength range f'_{co} (MPa)	Bond shear strength τ_{bond} (MPa)
Normal strength	≤ 50	2.0-3.0
Medium strength	≥ 50 & ≤ 70	3.4-4.5
High strength	> 70	5.0-6.0

2.2.3.4 Orientation factor and number of fibers crossing the cracking plane

Another important variable that has an impact on the mechanical properties of SFRC is the "orientation factor", α. This factor represents the random orientation of the fibers along the crack interface (see **Figure 2.7**). According to some researchers, for fibers in "bulk" the orientation factor value can be taken to be 0.5 (Dupont, 2003). Foster (2003) has suggested taking this factor to be 3/8. To arrive at this value Foster assumed that only fibers which are oriented from $\theta = 30^{o}$ to 90^{o} to the cracking plane can be considered to be effective, based on data published by Maage (1977) which suggested that the fibers oriented from $\theta = 0^{o}$ and 30^{o} have a reduced pullout efficiency (see **Figure 2.8**).

If the orientation factor is known, Equation 2-1 can be used to calculate the effective number of fibers per unit area, N_{fibers}. For fibers oriented randomly in three dimensions the following expression can be used to calculate N_{fibers} (Lee, 1990):

$$N_{fibers} = \frac{V_f}{A_f} \times \alpha \times \eta_l \tag{2-1}$$

Where V_f is the fiber content (by volume of concrete), A_f is the cross sectional area of the fiber and α is the orientation factor used to describe the random orientation of the fibers along the crack face. The length factor, η_1, accounts for the differences in embedded fiber length across the crack interface and is typically taken as being 0.5.

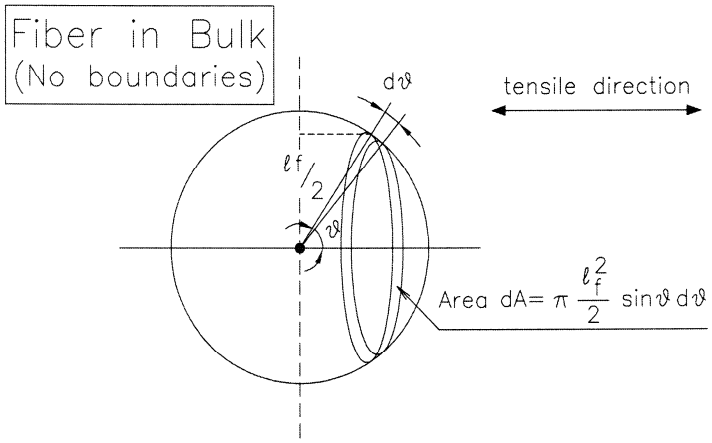

Figure 2.7: Dupont's Graphical representation to calculate α
[Adapted from Dupont (2003)]

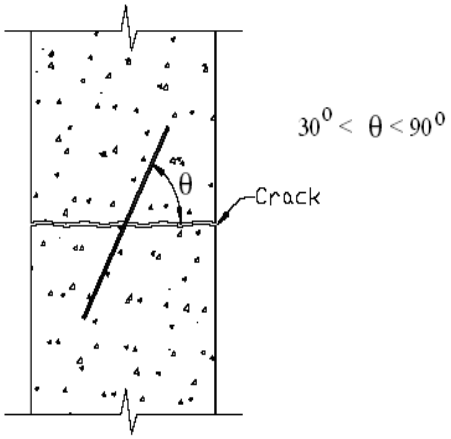

Figure 2.8: Foster's Graphical representation to calculate α
[Adapted from Foster (2001)]

2.2.4 Pullout behaviour of fibers

2.2.4.1 Steel Fiber Pullout Behaviour - overview

The tensile behaviour of SFRC is directly influenced by the pullout behaviour of the fibers. Bond between the concrete matrix and the fiber, and the deformed shape of the fiber have important influences on pullout response, and hence post-cracking behaviour of SFRC.

At initial stages, tensile stresses are resisted by the bond at the concrete-fiber interface. After the fiber has debonded, fiber pullout through frictional slip will govern the pullout response. The geometry of the deformed shape plays an important role in improving the pullout contribution during pullout (Chanvillard, 1996).

Over the years, several researchers have proposed models to predict the pullout response of straight and deformed fibers. For brevity the pullout of straight fibers is reviewed and a model for the pullout of hooked-end fibers is presented.

2.2.4.2 Pullout behaviour of straight fibers

To predict the pullout response for straight round fibers, Hannant (1978) suggested the formula shown in Equation 2-2:

$$F = \tau_{bond} \times \pi \times D_f \times \frac{L_f}{2} \qquad (2\text{-}2)$$

Where D_f is the fiber diameter and τ_{bond} is the bond shear strength that is a function of the matrix properties. The equation assumes constant bond shear strength τ_{bond} along the length, L_f, of the fiber.

For straight fibers the pullout stages involve partial debonding, full debonding and frictional pullout (see **Figure 2.9**). A typical pullout curve (pullout load versus slip) for a straight undeformed fiber is shown in **Figure 2.10**.

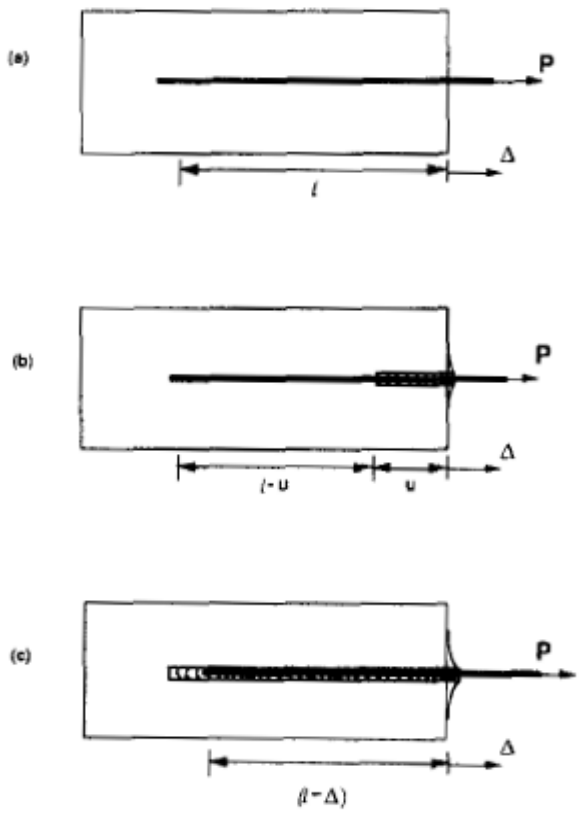

Figure 2.9: Different mechanical pullout stages: (a) pre-critical loading (b) partial debonding (c) full debonding

[Adapted from Naaman et al. (1991)]

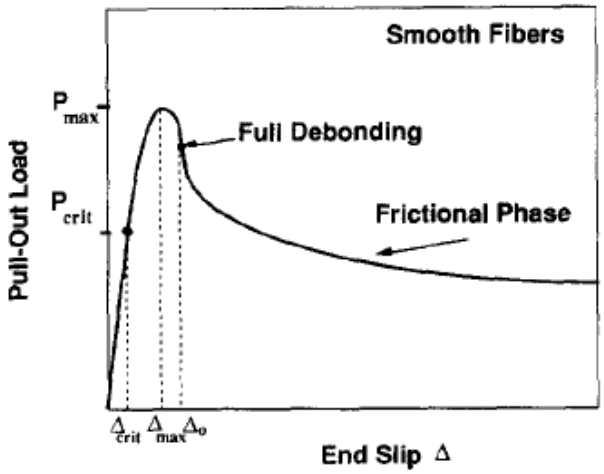

Figure 2.10: Pullout load vs. slip curve for a straight fiber

[Adapted from Naaman et al. (1991)]

2.2.4.3 Pullout behaviour for deformed fibers

It is now well understood that deformed fibers (hooked end, crimped, twisted, etc.) have an improved pullout performance due to the mechanical contribution of the deformations during pullout. This mechanical contribution arises from the additional energy required to pull the deformed fiber out of the matrix.

In the case of hooked-end fibers, the deformed ends significantly enhance the pullout performance. Several authors have proposed models to predict the pullout behaviour of hooked end fibers, among them Alwan et al. (1991). In this model, the pullout response of straight fibers is modified to account for the contribution of the hooked ends during pullout. This contribution represents the additional load required to straighten the deformed shape of the fiber as it is pulled out from the matrix. Taking into account this contribution, the pullout response can be described by several stages (**Figure 2.11 & 2.12**).

The first stage the pullout behaviour is characterized by an elastic response with P_{crit} representing the load that initiates debonding. In the second stage shear and frictional stresses will govern the response until full fiber debonding at a load P_1.

The third stage represents the contribution of the hooks through mechanical clamping. At this stage the deformed shape of fiber will increase the pullout load (P_2 through P_4) due to the additional energy required to straighten and pull the fiber out of the matrix. At this stage, the pullout resistance is a function of the hook geometry and would be independent of the matrix strength. After the mechanical clamping stage, the fiber will finally be pulled out of the matrix due to loss of frictional stresses at the matrix-fiber interface (fourth stage).

It is noted that this model is an adaption of the Naaman et al. model for straight fiber (particularly in stages 1,2 and 4) with the exception being that a third stage that accounts for the hook contribution to pullout has been added.

The following equations can be used to estimate the loads P_3 and P_4:

$$P_3 = P_1 + \Delta P^{'} \tag{2-3}$$

$$P_4 = P_1 + \Delta P^{''} \tag{2-4}$$

$$\Delta P^{'} = \frac{\left[\frac{f_{fy}\pi r_f^2}{3\cos\theta}\right][1+\frac{\mu\cos\beta}{(1-\mu\cos\beta)}]}{[1-\mu\cos\beta]} \tag{2-5}$$

$$\Delta P'' = \frac{\left[\frac{f_{fy}\pi r_f^2}{6\cos\theta}\right]}{[1-\mu\cos\beta]} \tag{2-6}$$

P_1 is the load at the debonding stage and P_3 and P_4 are the first and the second pullout plateaus respectively (see **Figure 2.11**) The mechanical pullout load contribution is represented by the parameters $\Delta P'$ and $\Delta P''$ which account for the formation of plastic hinges. f_{fy} refers to the fiber yield strength, r_f refers to fiber radius and μ is the frictional coefficient at the fiber-matrix interface. The parameters θ and β are related to angle of inclination of the hook with respect to the straight portion of the fiber.

It is noted that for a typical Dramix hooked end fiber the following values can be used: θ=45°, β=67.5°, and μ=0.5. Therefore, the expression for $\Delta P'$ simplifies to **Equation 2-7**:

$$\Delta P' = \frac{3.05}{\cos\left(45^o \times \pi/180^o\right)}\left(f_{fy} * \frac{\pi\left(D_f/2\right)^2}{6}\right) \tag{2-7}$$

The value f_{fy} is the fiber yield strength (in psi) and d_f is the fiber diameter (in inches). As an example for a typical Dramix ZP305 fiber, $\Delta P'$ is found to be 34 lbs (152 N).

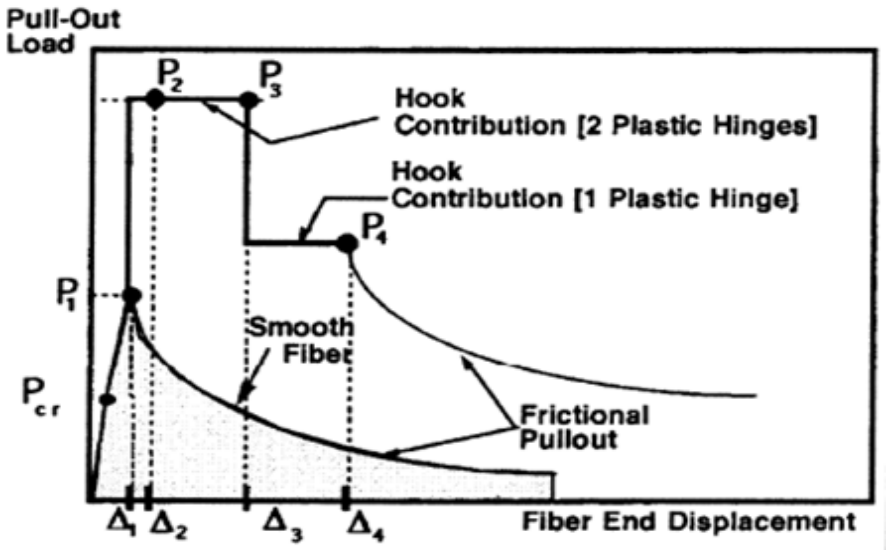

Figure 2.11: Hooked end fiber pullout behaviour

[Adapted from Alwan et al. (1991)]

The fiber end-displacement values Δ_3 and Δ_4 shown in **Figure 2.11** can be computed using the following formulas:

$$\Delta_3 = \Delta_1 + k_o \tag{2-8}$$

$$\Delta_4 = \Delta_3 + h_o \tag{2-9}$$

Where Δ_1 refers to the fiber slip at full debonding stage, and k_o and h_o are a function of the fiber geometry (see **Figure 2.12**).

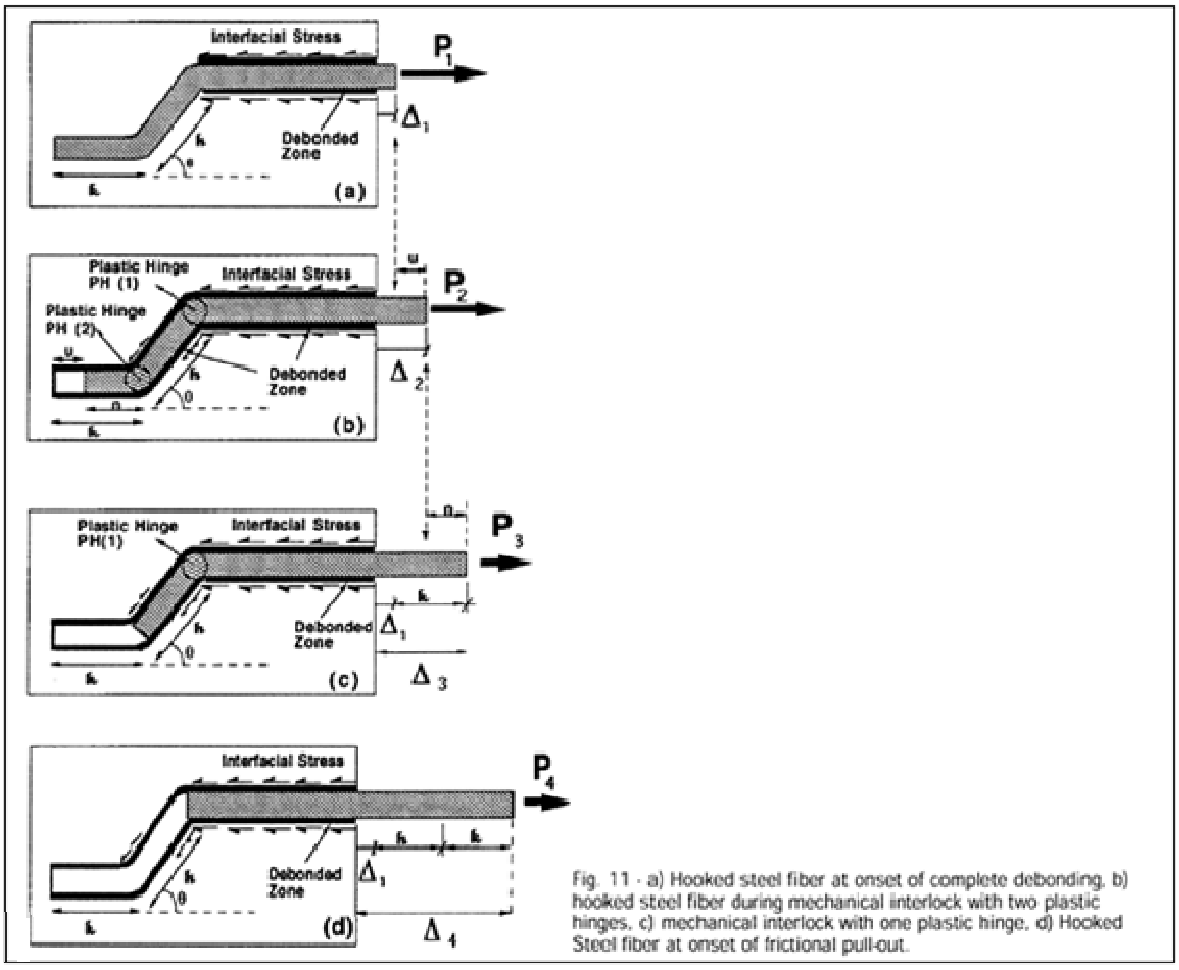

Figure 2.12: Four stages of Alwan's pullout model.
[Adapted from Alwan et al. (1999)]

2.2.5 Behaviour of SFRC in pure tension

Figure 2.13 compares the tensile behaviour of concrete and SFRC. As shown in **Figure 2.13 (a)**, the tensile stress-strain ($\sigma_c - \varepsilon_c$) relationship for plain concrete shows a rapid loss in tensile resistance after the formation of the first crack.

If steel fibers are added, the composite material will show higher fracture toughness in uniaxial tension due to the ability of the fibers to bridge stresses at crack surfaces. The overall improvement in tensile post-cracking resistance has a strong dependence on the fiber volume fraction in the matrix, V_f (Fantilli et al, 2009).

As shown in **Figure 2.13 (b)**, there is a modest improvement in response at low fiber contents. At higher fiber contents the post cracking behaviour is greatly enhanced (see **Figure 2.13 (c)**), resulting in a peak stress ($f_{\max}$) which is higher than the first cracking stress (f_{ct}). The post-cracking behaviour is therefore characterized as being strain-hardening (as opposed to strain-softening). In addition, the behaviour will be characterized by multiple cracking in the range $\varepsilon_c > \varepsilon_{c,cr}$ and $f_{ct} < \sigma_c < f_{\max}$ (Fantilli et al, 2009).

It is noted that traditional concrete begins to have workability issues at fiber contents greater than 1.5%. However, recent research has now led to the development of high performance fiber reinforced concretes (HPFRC). Through careful mix design HPFRC mixes can exhibit strain-hardening behaviour at fiber contents of 1.5-2% while also exhibiting excellent fresh-state properties (see Section 3).

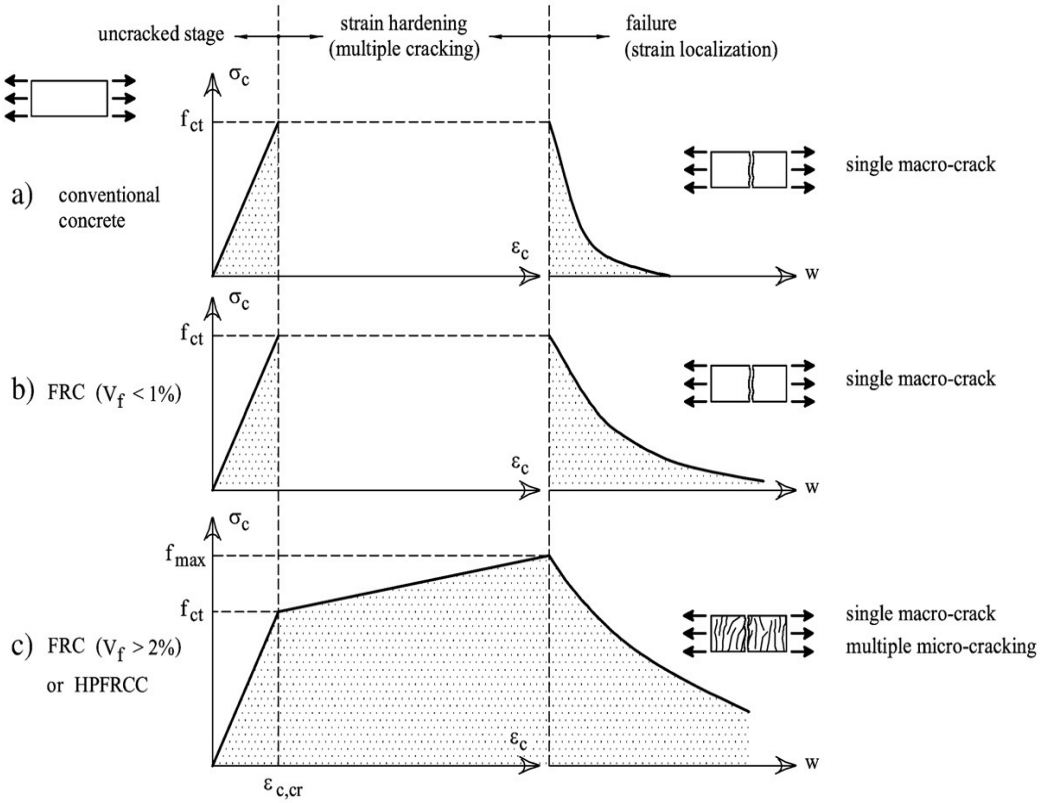

Figure 2.13: Mechanical response of cement-based composites under uniaxial tension

a) $\sigma_c - \varepsilon_c$ and $\sigma_c - w$ diagrams of ordinary concretes.

b) $\sigma_c - \varepsilon_c$ and $\sigma_c - w$ diagrams of FRC with low fiber volume fraction (V_f <1%).

c) $\sigma_c - \varepsilon_c$ and $\sigma_c - w$ diagrams of HPFRC with high fiber volume fractions (V_f >2%).

[Adapted from Fantilli et al. (2009)]

2.2.6 Direct tensile testing methods

2.2.6.1 Dog-Bone test

This test is considered a direct tensile test because it measures the tensile stresses directly in "dog-bone" shaped specimens tested under pure tension. An example of a dog-bone specimen used by some researchers with typical dimensions is shown in **Figure 2.14**. In the test setup the end regions of the specimen are held using fixtures connected to the test

machine by steel rods (see **Figure 2.14**). The strains and stresses are measured to obtain a tensile stress versus strain relationship (Liao et al., 2006).

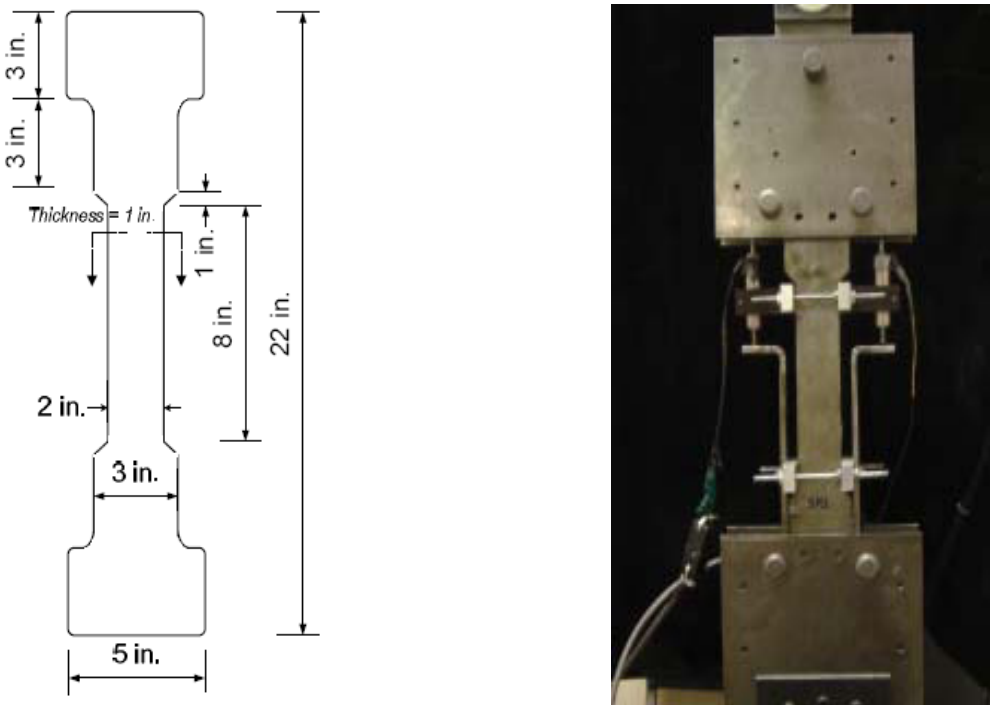

Figure 2.14: Dog-Bone Specimen and the testing machine
[Adapted from Liao et al. (2006)]

Although the test allows for the direct measurement of tensile properties, some disadvantages with this test include the difficulty in running the test (requires a special test setup), and the lack of a standardized testing methodology. The lack of standardized dimensions is also an issue as some researchers have found that there may be a size effect when different specimen sizes are used (see **Figure 2.15**). **Figure 2.16** shows a comparison of SFRC dog-bone specimens of two different sizes, it is clear that the strain at peak stress is significantly higher for the large specimen when compared to the small one. Therefore it is important to specify the size of the member prior to testing to consider size effects (Naaman & Reinhardt, 2006).

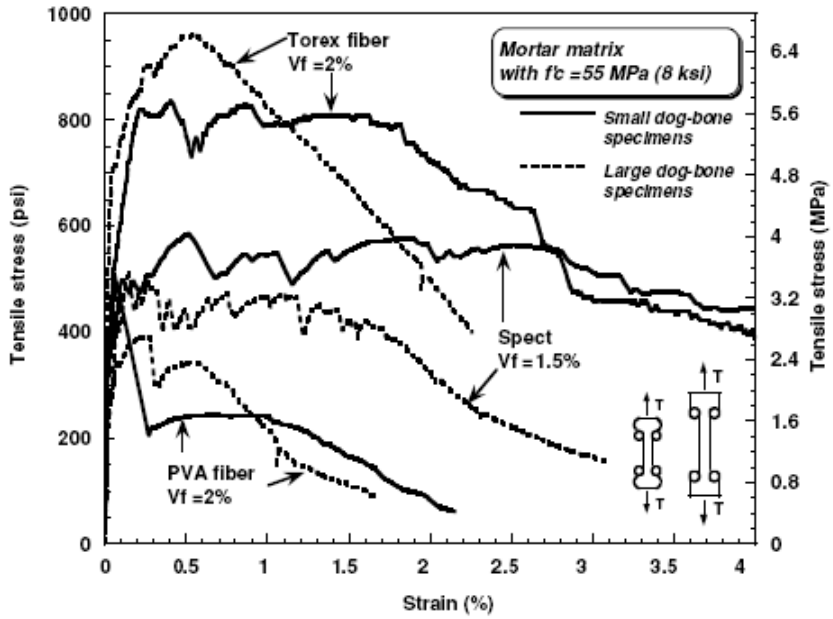

Figure 2.15: Size effect observed in direct tensile testing of SFRC [Adapted from Naaman & Reinhardt (2006)]

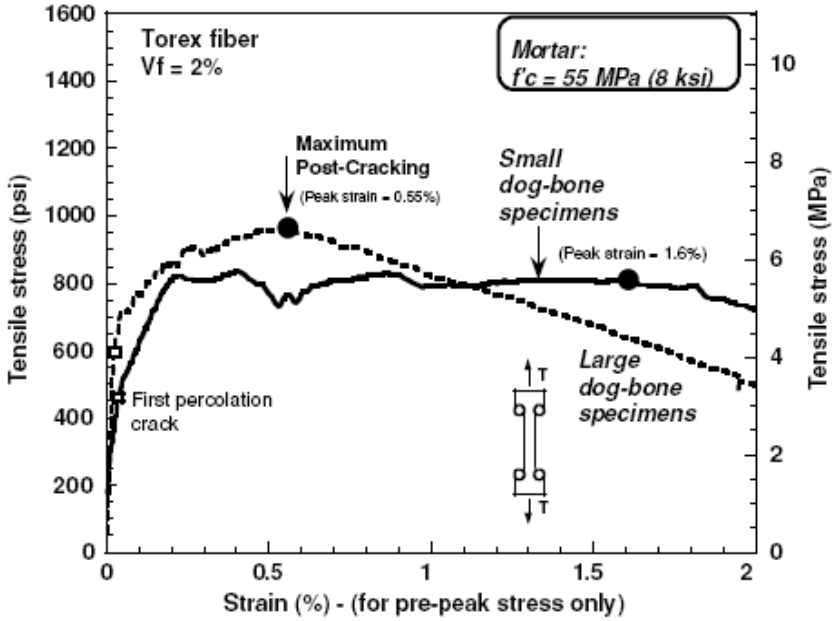

Figure 2.16: The difference in peak strains for different size dog-bone specimens. [Adapted from Naaman & Reinhardt (2006)]

2.2.6.3 Stress – crack opening $\sigma - w$ test

This test has been developed by RILEM committee TC 162-TDF, and is conducted to determine the tensile stresses versus crack opening behaviour of SFRC (RILEM, 2001). As shown in **Figure 2.17**, the test method uses a cylindrical specimen (150 mm diameter and 150 mm length) which is notched using a diamond saw along its circumference (notching is to a depth of 15 mm and a width of 2-5 mm). After preparation, the specimen is glued to the metal blocks with the crack opening measured using displacement transducers at the notch location. A typical setup is shown in **Figure 2.18**. Using the load and displacement measurements the stress-crack opening relationship is obtained ($\sigma - w$). In addition the dissipated energy can be calculated using the equation below:

$$W_F = \int_{w_i}^{w_m} \sigma_w(w)dw \qquad (2\text{-}10)$$

An advantage of the method is that it is a standardized test method (RILEM TC-162-TDF). However the method has not been widely adopted in North America due to the relative difficulty in conducting the test when compared to more simple indirect test methods (e.g. Flexural beam/ Toughness test methods).

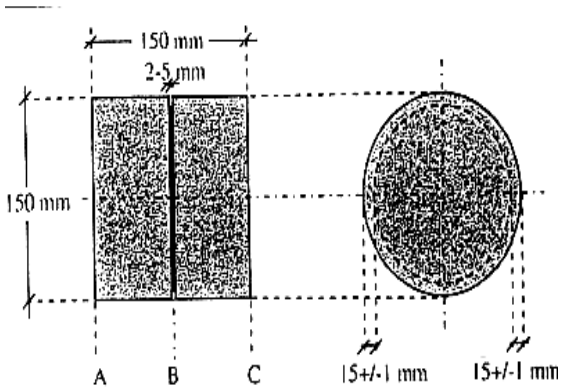

Figure 2.17: RILEM tensile test specimen geometry.

[Adapted from RILEM (2001)]

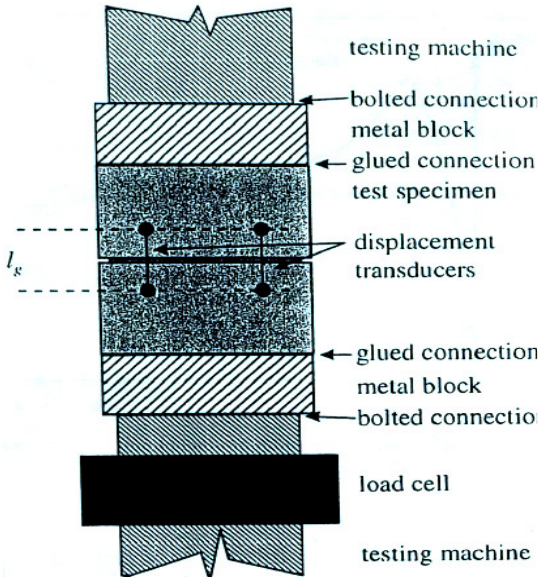

Figure 2.18: RIILEM tensile test setup

[Adapted from RILEM (2001)]

2.2.7 Indirect tensile testing methods

2.2.7.1 Toughness tests for SFRC

Toughness can be defined as the capacity of a composite subjected to fracturing load to resist fracture or failure. Various methods have been proposed to quantify SFRC toughness (tension, compression, or flexure). The flexural toughness test method is simple to perform and has been adopted as one of the main standardized test methods for SFRC in North America (Chen, 1995).

2.2.7.1.1 ASTM third-point bending test

In this test, third-point bending is applied on a 100 x 100 x 350 mm beam. The load displacement curve is then used to compute various indices and residual strength factors over several cracking intervals to assess toughness (ASTM, 1998, 2010b).

Although the method is widely accepted and used in industry, the method has several disadvantages. For instance, it is somewhat difficult to precisely locate the "first crack" deflection; this is especially problematic in the ASTM C1018 method since all quantities were defined as a function of this deflection, resulting in vagueness in the interpretation of the test results (see **Figure 2.19**). Furthermore, the results can be affected by extraneous effects due seating and twisting of the specimens, though this can be corrected using a "Yoke" setup for measuring deflections (see **Figure 2.20**). Finally, the test often results in high variability of results.

It is noted that the ASTM C1018 method has been replaced by ASTM C1609 which uses the same testing methodology but a more reliable method for quantifying toughness and residual strength values (see **Figure 2.21**).

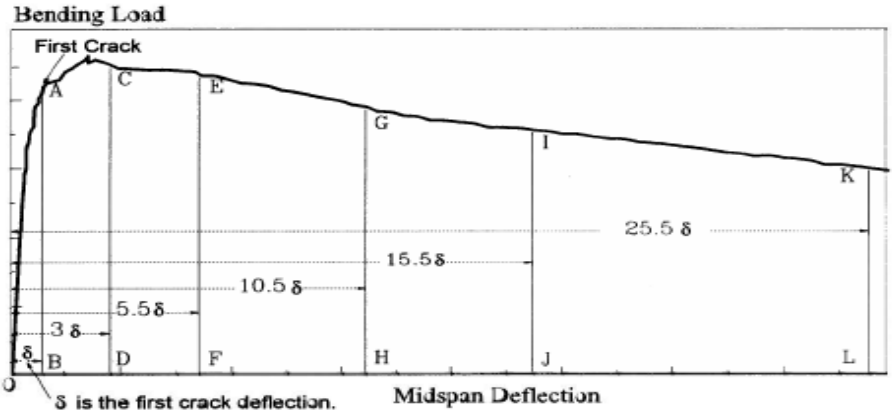

Figure 2.19: Different toughness Indices in the ASTM C1018 method [Adapted from Chen (1995)]

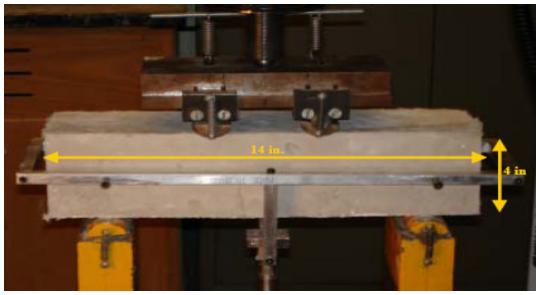

Figure 2.20: "Yoke" setup for measuring deflection [Adapted from Liao et al. (2006)]

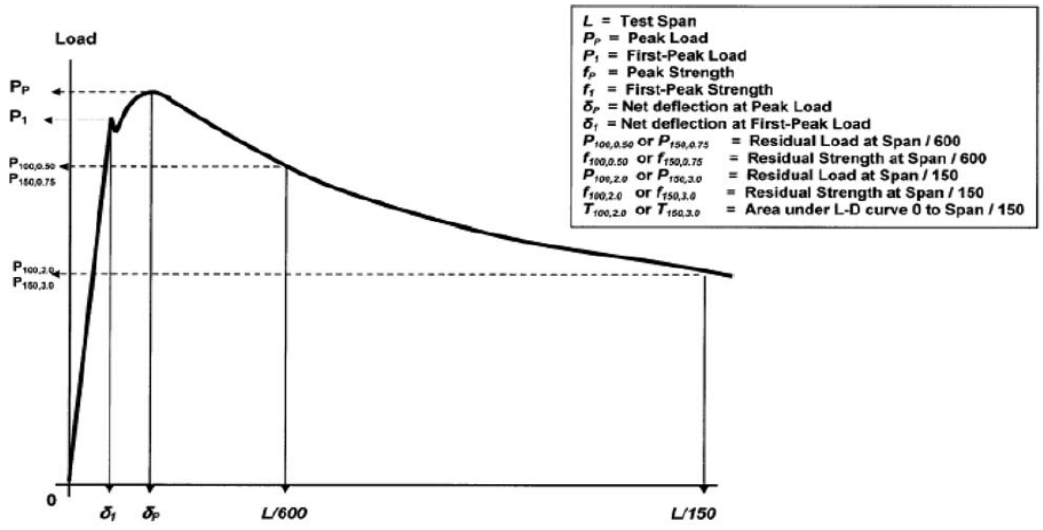

Figure 2.21: Definition of toughness Indices in the ASTM C1609 method [Adapted from Skazlic & Bjecovic (2009)]

2.2.7.1.2 JSCE SF-4 method

This test method uses the same setup used in the ASTM C1018 method but uses a different methodology to quantify toughness. When comparing to the methodology in the ASTM method, the JSCE method does not require the measurement of the first crack deflection to obtain toughness, therefore resulting in more simple data interpretation. Using the load versus deflection response (up to a deflection of span/150), a single flexural toughness factor is obtained (see **Figure 2.22**). It is noted that the ASTM C1609 method which replaces the ASTM C1018 method uses a similar procedure to quantify toughness.

However this test has some disadvantages including the fact that the toughness is size dependent as compared to the relative toughness values. Furthermore, the test doesn't distinguish between the pre-crack and post crack behaviour so different mixtures with different behaviour may theoretically have the same toughness values (Banthia & Trottier, 1995).

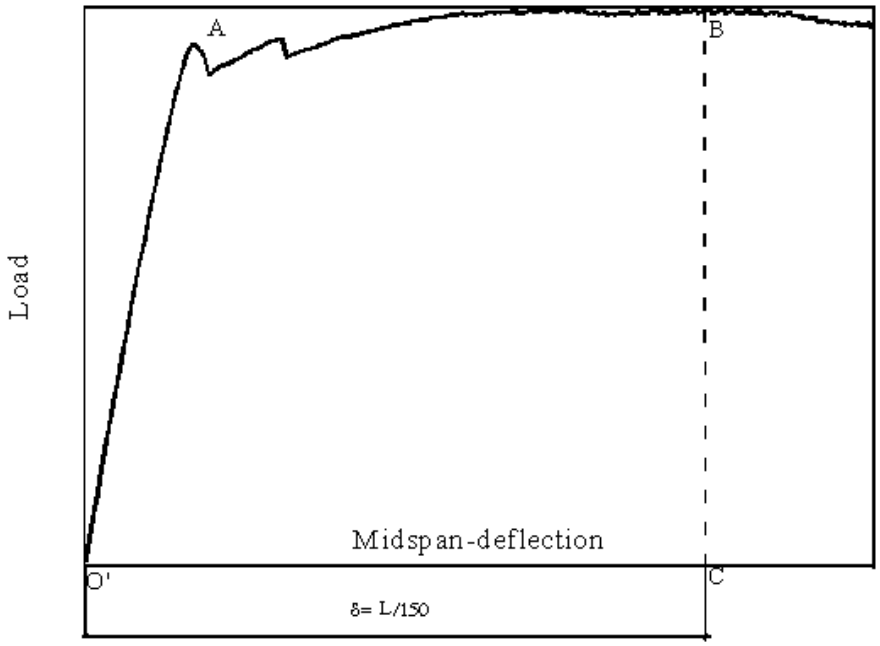

Figure 2.22: Flexural toughness values according to JSCE SF-4 method [Adapted from Banthia & Trottier (1995)]

2.2.7.1.3 ASTM C1399 method

Some researchers have found that the ASTM C1018 can result in difficulty in accurately measuring the post-peak behaviour of SFRC composites due to instability after first-crack, particularly with higher strength SFRC. To overcome this problem, the ASTM C1399 method has been proposed. In the method the beam is seated on a steel plate in order to prevent the complete failure of the beam after first-crack. After cracking, the plate is removed and the beam is reloaded again; the curve obtained from this experiment represents the reload stress and deflection response. The data is then used to quantify the residual strength of the beam for different deflection values. **Figure 2.23** shows a schematic comparison between the previously mentioned test methods as well as the analysis model used in each method (Banthia & Mindess, 2004).

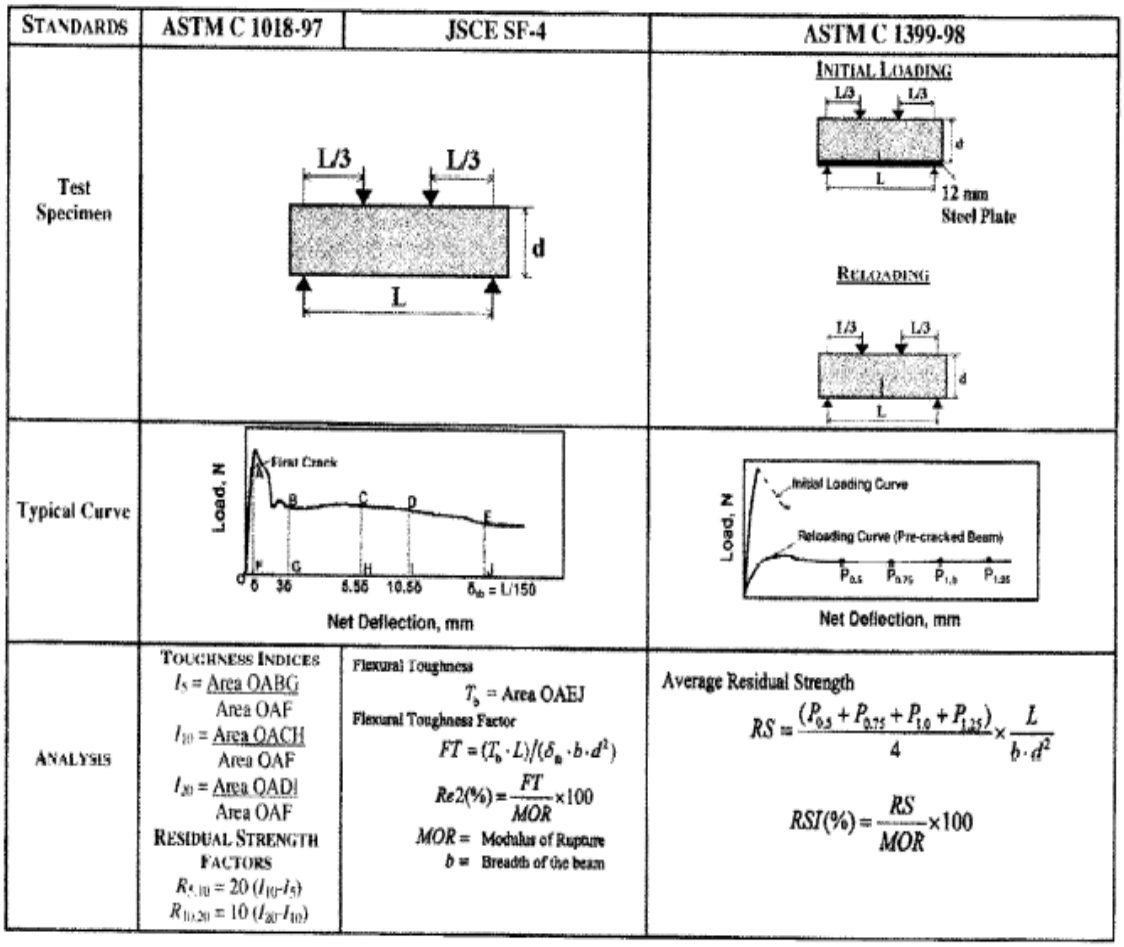

Figure 2.23: A schematic comparison between different toughness test methods [Adapted from Banthia and Mindess (2004)]

2.2.7.2 Round Panel test

One of the recent methods to quantify the post cracking behaviour of SFRC is the round panel test which was standardized by ASTM Committee C09 in 2002 in the ASTM C1550 standard (ASTM, 2010a). This test permits a reliable and economical estimation of the post cracking response of SFRC. In the test, a plate having a diameter of 800 mm and a thickness of 75 mm is placed on three pivots and loaded with a concentrated compressive load until failure (see **Figure 2.24**). The data can then be used to obtain a load deflection curve which can be used to quantify the tensile behaviour of the composite. An average crack rotation angle ϕ can be estimated for a given central deflection (Bernard, 2003).

The advantage of using this test is the relative simplicity of the test method, the relatively low variability between test results and the ability to use standard forms (see **Figure 2.24**). Disadvantages include the large specimen sizes (800 mm diameter) and the need to use specialized testing equipment.

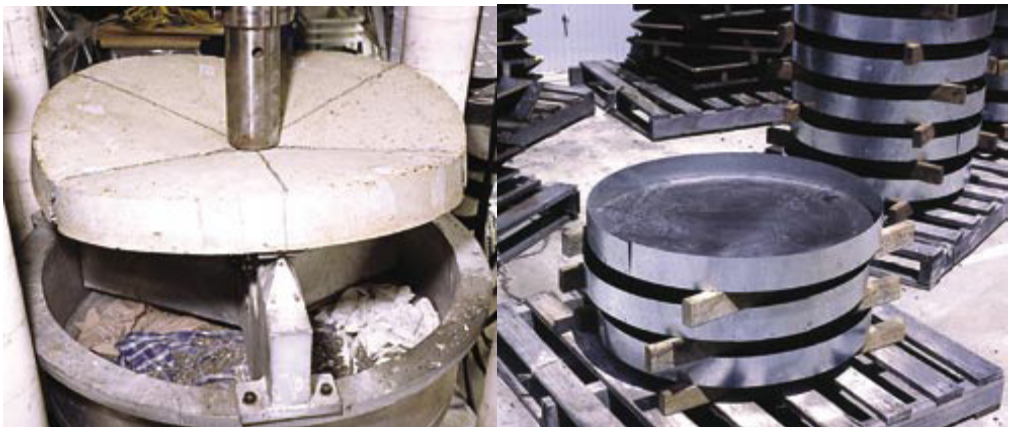

Figure 2.24: The round panel under test and the panel forms
[Adapted from Bernard (2003)]

2.2.7.3 Double Punch test

It is noted that most of the current standardized methods to quantify the tensile strength of SFRC, are based on flexural loading. In addition as discussed in the previous section there is some concern over the variability/scatter of results that often result when using these methods. On the other hand the flexural tests are very simple to perform when compared to direct tensile test methods.

Another relatively new indirect tensile method with the simplicity of the flexural tests is the Double Punch Test (DPT), also known as Barcelona test (Molins et al., 2009). This test is an adaptation of the Brazilian test which is used to measure the tensile strength of plain concrete which has been adapted to quantify the tensile response in FRC samples.

As shown in **Figure 2.25**, the test sample consists of a vertical cylindrical specimen, with identical height and diameter (150 mm) and two centered circular punches placed at the top and the bottom surface of the specimen (punches have a diameter equal to 0.25 of the overall cylinder diameter). The mechanism of the test consists of compressing the cylinder by a concentrated load applied directly on the punches resulting in radial cracking in three dimensions. Using the test data a relationship between the crack width and the load is obtained, from which the tensile strength can be estimated.

Table 2.2 summarizes the various test methods that can be used to study the tensile properties of SFRC.

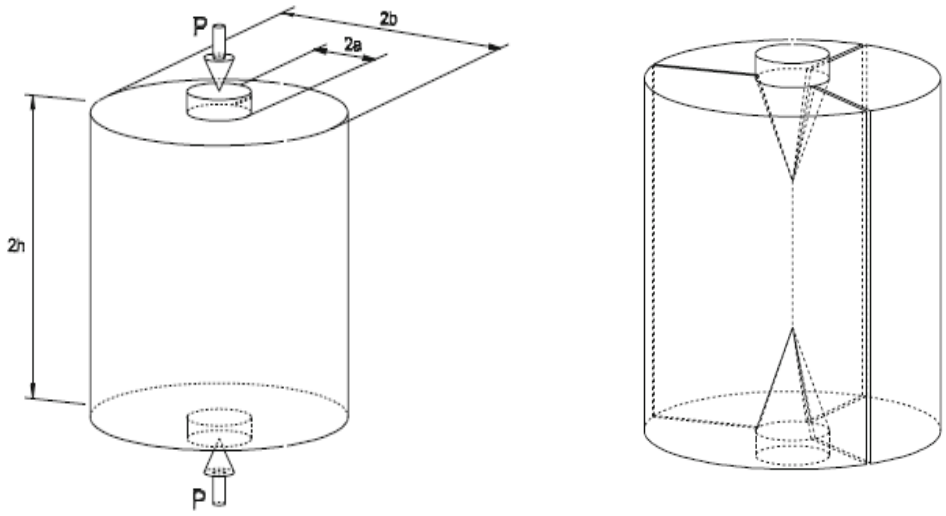

Figure 2.25: Barcelona Double Punch sample dimensions and the failure crack mechanism [Adapted from Molins et al. (2009)]

Table 2.2: Different indirect tensile tests for SFRC

[Adapted from Molins et al. (2009)]

Test	Layout	Dimensions (cm)	Weight[a] (N)	Failure surface (cm^2)	Specific failure surface	CV[b] (%)
ASTM C-1018	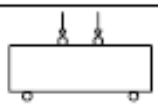	35 × 10 × 10	84.0	100.0	0.0286	15[c]
NBN B 15-238	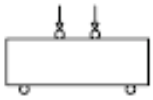	(60−75) × 15 × 15	405.0	225.0	0.0133	12–20[d]
EFNARC beam		55 × 7.5 × 12.5	123.7	93.8	0.0182	20[e]
3-point bending test		55 × 7.5 × 12.5	123.7	93.8	0.0182	17[f]
RILEM 3-point bending test	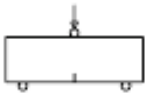	(55–60) × 15 × 15	297.0	187.5	0.0152	10–25[g]
EFNARC panel		60 × 60 × 10	864.0	2,597.7	0.0722	9[f]
Round determinate panel		7.5 × ϕ80	906.5	900.0	0.0238	6–13[f]
Double Punch Test		15 × ϕ15	63.6	337.5	0.1274	13[h]

2.2.8 Behaviour of SFRC in compression

Many researchers have shown that the influence of steel fibers to the peak compressive strength of concrete is not substantial (Minelli, 2005). However the addition of fibers will improve the descending branch of the compressive stress-strain curve. Under compressive loading, as lateral expansion takes place due to Poisson's effect, the fibers restrain and control cracking and lateral expansion and thus significant improvement in toughness results. Several investigators have proposed models to predict the compressive stress strain behaviour of SFRC. Although not used in the subsequent chapters of the thesis, for completeness some of these models are described in the sections that follow.

2.2.8.1 Nataraja et al. model

Natarja et al. (1999) proposed an empirical model to predict the complete compressive stress-strain curve based on experimental test results on specimens having fiber volume fractions of 0.5-1%. The distinguished parameter in his model is the steel fiber reinforcing index (RI) which can be obtained from equation (2-11):

$$RI = w_f \frac{L_f}{D_f} \tag{2-11}$$

The following equations are then used to estimate the maximum compressive stress and strain of SFRC using the RI value:

$$f_{cf}^{'} = f_{cu}^{'} + 2.1604(RI) \tag{2-12}$$

$$\varepsilon_{cf}^{'} = \varepsilon_{cu}^{'} + 0.0006(RI) \tag{2-13}$$

Where $f_{cf}^{'}$ is the ultimate compressive strength of fiber reinforced concrete, and $f_{cu}^{'}$ is the ultimate compressive strength of plain concrete. $\varepsilon_{cf}^{'}$ and $\varepsilon_{cu}^{'}$ represent the ultimate strain for fiber reinforced and plain concrete respectively.

The equation shown below is then used to obtain the complete compressive stress-strain curve for SFRC:

$$\frac{f_{cf}}{f_{cf}^{'}} = \frac{\beta 1\left(\frac{\varepsilon_{cu}^{'}}{\varepsilon_{cf}^{'}}\right)}{\beta 1 - 1 + \left(\frac{\varepsilon_{cu}^{'}}{\varepsilon_{cf}^{'}}\right)^{\beta 1}} \tag{2-14}$$

Where β_1 represents the material parameter that controls the stress-strain diagram shape, and it's value can be calculated from equation (2-15):

$$\beta_1 = 0.5811 + 1.93RI^{-0.7406} \tag{2-15}$$

Natarja et al. also proposed an equation to quantify the steel fiber toughness ratio TR_{cf}, where TR_c is the plain concrete toughness ratio:

$$TR_{cf} = TR_C + 0.0978RI \tag{2-16}$$

2.2.8.2 Hsu and Hsu model

To arrive at their model, Hsu and Hsu (1994) tested a series of high strength SFRC cylindrical specimens with hooked end steel fibers at a volume fraction of 0.25% -1.0%. Using the experimental results they proposed empirical expressions to evaluate the ratio of compressive stress in SFRC to that of plain concrete (no fibers), $\frac{f_{cf}}{f_{cu}^{'}}$ expressed as η:

$$\eta = \frac{f_{cf}}{f_{cu}^{'}} = \frac{n\beta_1 x}{n\beta_1 - 1 + x^{n\beta 1}} \qquad \text{For } 0 \le x \le x_d \tag{2-17}$$

$$\eta = \frac{f_{cf}}{f_{cu}^{'}} = \eta_d \exp\left\{-k_d\left(\frac{\varepsilon_{cf}}{\varepsilon_{cu}^{'}} - x_d\right)^a\right\} \qquad \text{For } x_d \le x \tag{2-18}$$

Where β_1 and n are material parameters which represent the stress-strain curve shape.

The resulting expressions can then be used to obtain the entire compressive stress-strain curve of SFRC.

2.2.8.3 Mansur et al. model

Mansur et al. (1999) proposed a model to predict the stress-strain relationship based on an experimental program on high strength concrete (70 to 120 MPa) reinforced with hooked end steel fiber with volume fractions of 1.0%-1.5%.

The following equations describe the ascending branch of the stress-strain curve:

$$f_{cf} = f_{cu}^{'}\left[\frac{\beta_1\left(\frac{\varepsilon_{cf}}{\varepsilon_{cu}^{'}}\right)}{\beta 1 - 1 + \left(\frac{\varepsilon_{cf}}{\varepsilon_{cu}^{'}}\right)^{\beta 1}}\right] \tag{2-19}$$

$$\beta_1 = \frac{1}{1 - \frac{f_{cu}^{'}}{\varepsilon_{cu}^{'} E_a}} \tag{2-20}$$

Where $f_{cf}^{'}$ and $f_{cu}^{'}$ are the ultimate compressive strength of fiber reinforced and plain concrete respectively, $\varepsilon_{cf}^{'}$ and $\varepsilon_{cu}^{'}$ are the ultimate strain for fiber reinforced and plain concrete respectively. β_1 is a parameter which controls the shape of the stress-strain curve.

For the descending branch of the curve the following equations are used, where k_{f1} and k_{f2} are parameters to reflect the use of fiber in the stress-strain curve. These parameters are function of fiber volume fraction and fiber aspect ratio.

$$f = f_{cu}^{'}\left[\frac{k_{f1}\beta_1\left(\frac{\varepsilon_{cf}}{\varepsilon_{cu}^{'}}\right)}{k_{f1}\beta_1 - 1 + \left(\frac{\varepsilon_{cf}}{\varepsilon_{cu}^{'}}\right)^{kf2\beta 1}}\right] \tag{2-21}$$

$$k_{f1} = \left(\frac{50}{f_{cu}^{'}}\right)^{3.0}\left[1 + 2.5\left(\frac{v_f L_f}{D_f}\right)^{2.5}\right] \tag{2-22}$$

$$k_{f2} = \left(\frac{50}{f_{cu}^{'}}\right)^{1.3}\left[1 - 0.11\left(\frac{v_f L_f}{D_f}\right)^{-1.1}\right] \tag{2-23}$$

2.3 Combined Use of SCC and Fibers

2.3.1 Introduction to Self-Consolidating Concrete (SCC)

Self Consolidating Concrete (SCC) is a highly flowable concrete with the ability to compact under its self weight and was first proposed by researchers at the University of Tokyo in 1986. ACI Committee 237 defines SCC as a cementitious material with high flowability and non-segregation characteristics which allow the concrete to spread into place, fill formwork, and flow around reinforcement without exhibiting any blocking (Liao et al., 2006). Furthermore using SCC in pre-cast and cast-in-place applications can result in reduced construction times and labor costs (Liao et al., 2006).

SCC has several properties that make it attractive as an alternative to traditional concrete, these include:

(a) Filling ability: SCC can flow and fill formwork without vibration or compaction. Common tests to measure the filling ability for SCC in fresh state are: slump flow, V-funnel, U-Box, and L-Box tests.

(b) Segregation resistance: despite being highly flowable, SCC has the ability to maintain a cohesive matrix during mixing and casting. Some tests that can be used to measure segregation resistance are: V-funnel test and visual observation during the slump flow test.

(c) Passing ability: SCC can flow through narrow sections without blocking, or loss in homogeneity. The tests that can be used to determine the passing ability of SCC are: the V-funnel test, J-ring in combination with slump flow test, L-Box and U-Box tests.

2.3.1.1 Slump flow test

The slump flow test is one of the simplest and most widely used tests for determining the fresh state properties of SCC. The test has similarities to the ASTM standard slump test of fresh concrete, but instead of measuring the height difference of the spread concrete, the diameter of the spread in two directions is measured. In the test the SCC is placed in a standard slump cone on a horizontal table. The cone is then lifted and the diameter of the spread sample is measured (see **Figure 2.26**). In addition, the time at which the concrete spreads to 500 mm diameter is recorded. The test gives an indication of the flowability and

filling ability of the SCC (Curjar, 2004). Visual inspection can also give an indication of the segregation resistance of the SCC.

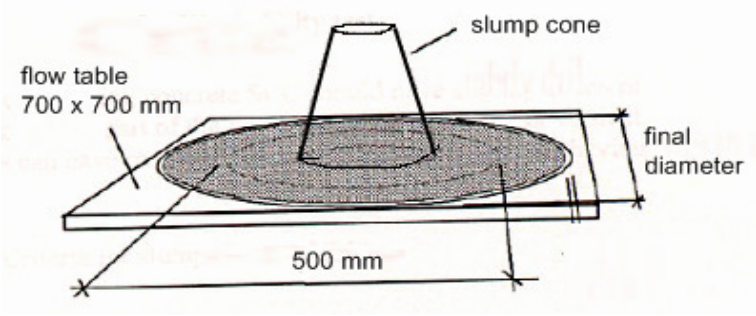

Figure 2.26: Slump flow test set up
[Adapted from Curjar (2004)]

2.3.1.2 V-funnel test

The V-funnel test can be used to evaluate the SCC's segregation resistance. During the test a V- shaped funnel is filled and the time the SCC takes to exit the funnel is recorded (see **Figure 2.27**). After the first trial, a second V-funnel time is recorded after first letting the concrete remain in the funnel for a period of 5 minutes before opening the lid (Curjar, 2004).

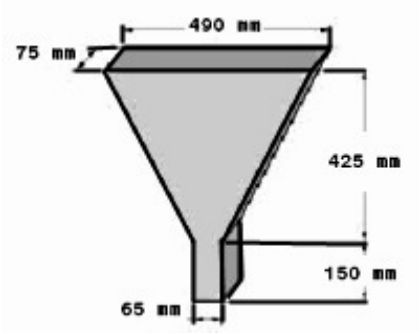

Figure 2.27: V-funnel shape and dimensions
[Adapted from Curjar (2004)]

2.3.1.3 L-Box test

The L-Box test can be used to measure the passing ability of SCC (see **Figure 2.28**). The test consists of using an L- shaped box with a sliding gate and some vertical steel rebars to simulate the reinforcement obstruction to the concrete. At the start of the test the concrete is poured in the vertical part and the gate is closed. The gate is then opened and the concrete is allowed to flow and time the SCC takes to reach marked distances is recorded (200 mm and

400 mm point on the horizontal box). After the concrete settles, the ratio between the heights at both ends of the box is also measured (Curjar, 2004).

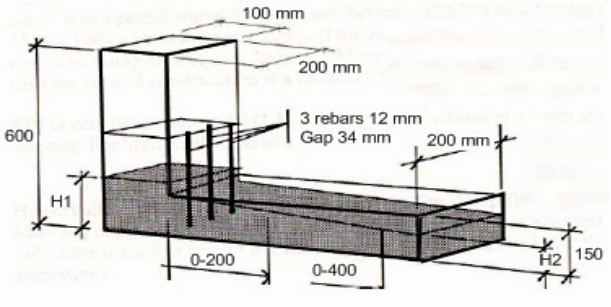

Figure 2.28: L-Box apparatus shape and measurements
[Adapted from Curjar (2004)]

2.3.2 Self Consolidating Fiber Reinforced Concrete (SCFRC)

Although fibers can improve many of the properties of traditional concrete, the addition fibers in volumes greater than 1.0% can result in placement problems in the fresh-state. One solution to this problem is the combined use of SCC and fibers. Due to SCC's high flowability, higher fiber contents can be used without compromising workability.

2.3.2.1 Factors influencing properties of SCFRC

Even in the case of SCC, the addition of fibers improves performance only within a limited range of fiber properties (L_f / D_f) and volume fractions (V_f), with researchers demonstrating that higher aspect ratios and volume fractions can result in reduced flowability and the eventual loss of SCC properties (Liao et al., 2006). Although flowability and filling ability of SCC typically decrease gradually as fibers are added to the SCC matrix, researchers have found that some flowability can be maintained at moderate fibers contents. Higher fiber contents (typically $V_f > 2\%$) result in loss of SCC properties (Grunewald, 2004).

Other factors that can affect flowability of SCC are the maximum aggregate size and the percentage of the coarse and fine aggregate in the concrete. The use of larger aggregate size

can result in fiber "balling" and eventually lead to loss of SCC properties (Swamy & Mangat, 1974; Johnston, 1996; Grunewald, 2004). **Figure 2.29** shows the effect of maximum aggregate size on fiber "balling". In addition, increasing the coarse aggregate content also results in reduced workability. **Figure 2.30** shows an example of a recommendation on maximum fiber contents as a function of coarse aggregate content.

Therefore, to maintain acceptable performance of SCFRC in the fresh-state it is of importance to limit the fiber content, the maximum aggregate size and the coarse aggregate content (by increasing the fines-to-aggregate ratio).

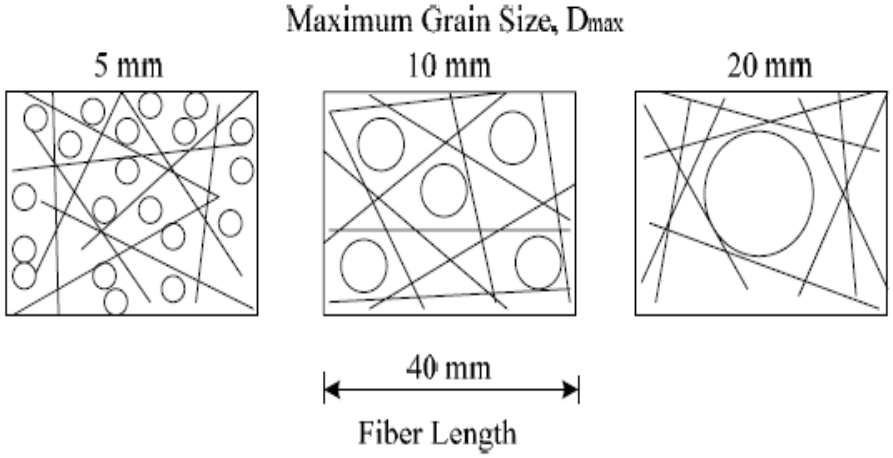

Figure 2.29: The relationship between fiber orientation and aggregate size [Adapted from Johnston (1996)]

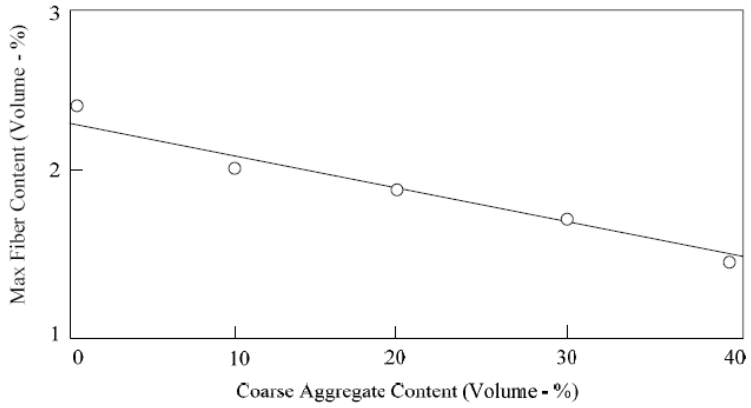

Figure 2.30: The relationship between coarse aggregate content and maximum fiber content [Adapted from Swamy & Mangat (1974)]

2.3.2.2 Tests for measuring fresh-state properties of SCFRC

Just as with traditional SCC, it is also important to measure the fresh state properties of self-consolidating fiber-reinforced concrete (SCFRC). However, to date there are no standard fresh-state tests that have been specially adapted for SCFRC. Most researchers have therefore used traditional SCC tests such as the Slump flow, J-ring and V-funnel tests to measure the fresh-state properties of SCFRC. Some researchers have also proposed changing some of the detailing in standard SCC tests for SCFRC, for example increasing the bar spacing to two times the fiber length in the J-ring test and changing the spacing of the rebars in the L-box test as a function of fiber aspect ratio as shown in **Table 2.3** (Groth, 2000).

Table 2.3: Recommended bar spacing for different fiber aspect ratios [Adapted from Groth (2000)]

c/L_f [-]	L_f/d_f [-]	Max. m_f [kg/m^3]
≥ 3	80	30
	65	60
≥ 2	65	30
	45	60
≥ 1.5	45	30

2.3.3 High Performance Fiber Reinforced Concrete (HPFRC)

Research initiated by Naaman & Reinhardt has led to the development of a new generation of fiber reinforced concretes which have enhanced mechanical properties when compared to traditional SFRC. The main distinguishing feature between traditional SFRC and High Performance Fiber Reinforced Concrete (HPFRC) is in the improved post cracking response under tensile stresses (Naaman & Reinhardt, 2006).

In traditional SFRC, the behaviour under tension is characterized by a "strain-softening" response after first-cracking. As shown in **Figure 2.31**, the response is linear until first cracking and then a descending branch will follow up to failure. In the case of HPFRC, the post cracking performance is enhanced due to multiple cracking and results in a "strain-

hardening" response after first-cracking which imparts additional toughness and ductility in tension and flexure.

The behaviour of HPFRC in tension can be described by three stages as shown in **Figure 2.32**. The first stage OA is similar to that of normal SFRC prior to cracking, however after first-cracking significant strain-hardening behaviour occurs (this is shown as stage AB in **Figure 2.32**). The last stage after B results in crack localization and a descending branch as pullout of the fibers occurs. It is noted that the strain-hardening behaviour is accompanied by multiple cracking with cracks having smaller widths and spacing when compared to conventional SFRC (Naaman & Reinhardt, 2006).

In addition to enhanced behaviour in the hardened state, it is now possible to produce HPFRCs which have flowable properties in the fresh-state (Liao et al., 2006). This is achieved through careful mix design, limitations on coarse aggregate size (typically less than 13 mm), the use of moderate fiber contents (1.5-2.0%) and the use of superplasticizers, viscosity modifying agents and mineral admixtures (Fly Ash).

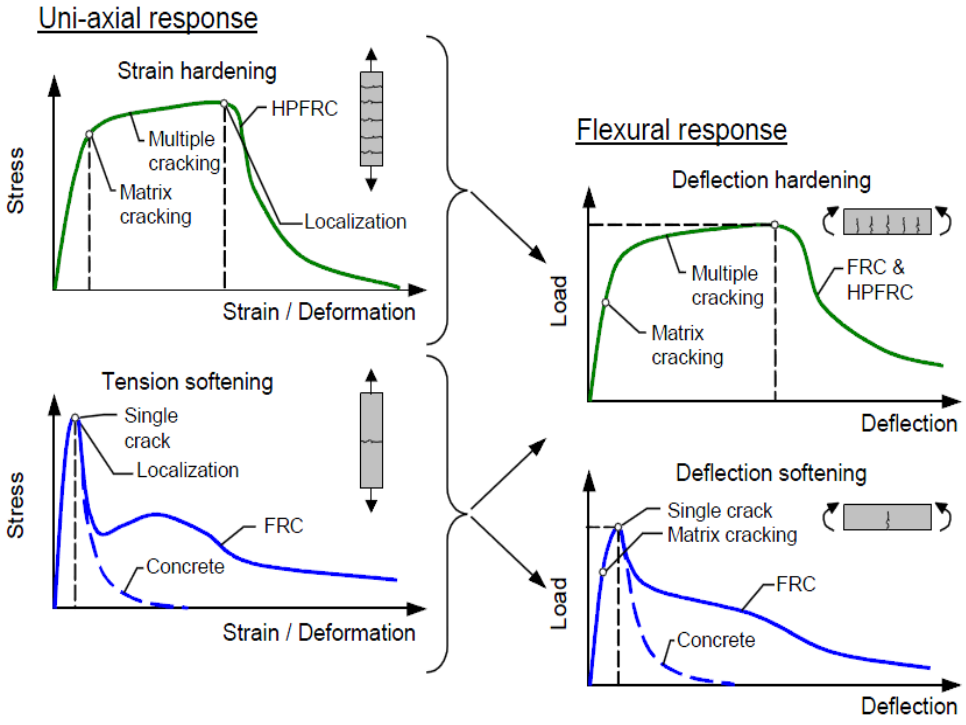

Figure 2.31: Comparison between the behaviour of conventional FRC and HPFRC showing strain-softening behaviour in FRC and strain-hardening behaviour in HPFRC [Adapted from Löfgren (2005)]

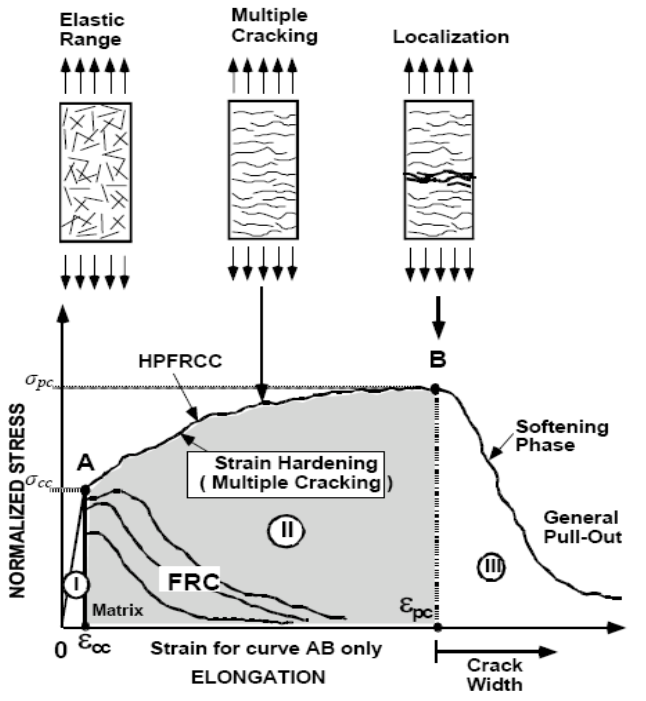

Figure 2.32: Stages in the tensile response of HPFRC [Adapted from Liao et al. (2006)]

2.3.4 Examples of SCFRC and HPFRC mix designs

2.3.4.1 SCFRC mix designs proposed by different researchers

Several research studies have been performed on the combined use of steel fibers and SCC. This includes studies performed by Sahmaran and Yurtseven (2005); Grunewald and Walraven (2001); Dehn (2005); Bui et al. (2003, 2005). A summary of the mixture proportions proposed in some of these studies was tabulated by Liao et al. (2006) and is reproduced herein in **Tables 2.4 &2.5**. To indicate the effect of fiber volume fraction on the mixture properties, the studies are divided into two groups: the first group for fiber content less than 1.5%, and the second group for fiber volume fraction greater than 1.5%.

It should be noted that SCC is more sensitive to mixing time and procedure than conventional concrete. The sequence of mixing is also important and therefore special care is required. Typically the aggregates, cement and mineral admixtures are dry-mixed first, then

water and superplasticizers is slowly added followed by the fibers. SCFRC mixing procedures are described in more detail in Grunewald's work (Grunewald, 2004).

Table 2.4: SCC mix designs in previous research studies ($V_f < 1.5\%$)

[Adapted from Liao et al. (2006)]

Author(researcher)		Sahmaran et al. 2005			Sahmaran et al. 2007			Grunewald 2001			Dehn 2005	
kg/m^3												
Cement	C1	500	500	500	250	250	250				382	490
	C3							362	386	386	1044	982
Fine aggregate	0.15-4mm	977	977	977	977	977	977	641	676	676	489	745
Coarse aggregate	4-16mm	578	578	578	578	578	578	942	855	855	183	157
Water		200	200	200	226	205	205	164	171	171		
steel fiber	Dramix ZP 305	60	30		60	30						
	OL 6/16		30	60		30	60					
	Dramix-RL 45/30							100		100		
	Arbed/Euro steel 50/50								100			
	Dramix 65/60 BN										60	
	F 60/30											78
V_f (%)		0.76	0.8	0.84	0.76	0.8	0.84	1.27	1.27	1.27	0.76	1.00
Comp. strength (MPa)		49.5	56.3	58.9	19.6	22.8	22.5	55.9	56.9	56.9	N/A	N/A
Slump flow (cm)		62	61.5	67.5	66	63	70	64	58	60	N/A	N/A

Table 2.5: SCC mix designs in previous research studies ($V_f \geq 1.5\%$)

[Adapted from Liao et al. (2006)]

Author(researcher)		Grunewald 2001	V.K. Bui (2003)		V.K. Bui (2005)	
kg/m^3						
Cement	C1		592	574	480	480
	C3	386				
Fine aggregate	0-2mm		1184	1149		
	0-4mm	676				
	sand				819	819
Coarse aggregate	4-16mm	855				
	coarse aggregate				546	546
Water		171	355	373	214	214
steel fiber	Dramix-RL 45/30	120				
	F1 37.5/6		140	140		
	length 60mm				156	
	length 35mm					156
V_f (%)		1.53	2	2	2	2
Comp. strength (MPa)		56.9	N/A	N/A	75	64
Slump flow (cm)		59	N/A	N/A	N/A	N/A

2.3.4.2 HPFRC mixtures proposed by University of Michigan researchers

Liao et al. (2006) proposed several HPFRC mixtures which exhibit the high flowability and segregation resistance of SCC and the improved post cracking response of HPFRC. In this study six mixtures with compressive strength varying from 35 to 64 MPa were proposed and validated using SCC fresh-state tests as well as hardened-state tests to assess behaviour in tension and compression. The proposed mixtures used moderate steel fiber contents (1.5 and 2%) and five of the mixtures used high-strength hooked-end fibers (details are shown in **Table 2.6**). The mix proportions by weight of cement and weight of HPFRC mix are shown in **Table 2.7** and **Table 2.8**. All mixtures used Type III Portland Cement and mineral admixtures (fly ash) to achieve high early strength. In addition to using a low coarse-fine aggregate ratio, to ensure flowable properties and prevent segregation, superplasticizers and viscosity modifying admixtures (VMA) were used.

Based on the test results, it was found that "Mix 3" and "Mix 6" were most optimal in terms of combined fresh-state and hardened-state performance.

Table 2.6: Steel fiber types used in the uMichigan study
[Adapted from Liao et al. (2006)]

Fiber ID	Product	Material	Shape	Specific gravity	Diameter (mm)	Length (mm)	Aspect Ratio	Tensile Strength (MPa)
SF 1	Dramix® RC-80/30-BP	Steel	Hooked	7.85	0.38	30	79	2300
SF 2	Dramix® ZP305	Steel	Hooked	7.85	0.55	30	50	1100

Table 2.7: Mixture Proportions by weight of cement in the uMichigan study

[Adapted from Liao et al. (2006)]

Mix Proportion by weight of cement							
Series ID		Mix 1	Mix 2	Mix 3	Mix 4	Mix 5	Mix 6
Cement	C3*	1	1	1	1	1	1
Mineral Admixture	FA**	0.48	0.5	0.5	0.875	0.67	0.875
Fine Aggregates	Silica Sand (Flint)***	1.7	1.7	1.7	2.5	2.1	2.2
Coarse Aggregates	Crushed Limestone +	1.1	1	1	1.25		1.2
	Pea gravel ++					1.1	
Water	Water	0.45	0.6	0.6	0.84	0.67	0.8
Chemical Admixture	ADVA® Cast 530 ×	0.027	0.015	0.01		0.013	
	Glenium® 3200HES ××				0.0055		0.005
	RHEOMAC® VMA 362×××		0.012	0.0095	0.065	0.013	0.038
Steel Fiber	SF 1		0.325	0.244	0.31	0.289	0.315
	SF 2	0.325					
Total Weight		5.082	5.152	5.0635	6.8455	5.871	6.433
V_f (%)		1.96	1.92	1.47	1.38	1.50	1.50

Note: * ASTM Type III Portland cement.
** fly ash class C.
*** ASTM 50-70.
+ max size about 12mm.
++ max size about 8mm.
× these three chemical admixtures are typically added with the initial mix water and their concentration could be seen as 1.0; that is, it is not necessary to consider the amount of water in these chemical admixtures while calculating the total amount of water needed.

Table 2.8: Mixture proportions by mix weight in the uMichigan study [Adapted from Liao et al. (2006)]

Mix Proportion by weight							
Series ID		Mix 1	Mix 2	Mix 3	Mix 4	Mix 5	Mix 6
Cement	C3*	0.197	0.194	0.197	0.146	0.170	0.155
Mineral Admixture	FA**	0.094	0.097	0.099	0.128	0.114	0.136
Fine Aggregates	Silica Sand (Flint)***	0.335	0.330	0.336	0.365	0.360	0.342
Coarse Aggregates	Crushed Limestone +	0.216	0.194	0.197	0.183		0.187
	Pea gravel ++					0.189	
Water	Water	0.089	0.116	0.119	0.123	0.114	00.124
Chemical Admixture×	ADVA® Cast 530	0.005	0.0029	0.0020		0.0022	
	Glenium® 3200HES				0.0008		0.00078
	RHEOMAC® VMA 362		0.0023	0.0019	0.0095	0.002	0.0059
Steel Fiber	SF 1		0.063	0.048	0.0453	0.049	0.049
	SF 2	0.064					
Total Weight		1.00					
V_f (%)		1.96	1.92	1.47	1.38	1.50	1.50

Note: * ASTM Type III Portland cement.
** fly ash class C.
*** ASTM 50-70.
+ max size about 12mm.
++ max size about 8mm.
× these three chemical admixtures are typically added with the initial mix water and their concentration could be seen as 1.0; that is, it is not necessary to consider the amount of water in these chemical admixtures while calculating the total amount of water needed.

2.3.4.3 University of Michigan mixing procedure

As mentioned before the sequence of adding the materials is an important factor to obtain the desired properties of SCFRC. The importance of mixing sequence and procedure applies (even more so) to HPFRC. Based on their research study, Liao et al. (2006) proposed the mixing procedure described below:

(1) The cement, fly ash, and sand are mixed in a dry condition for 30 seconds;

(2) The water and chemical admixtures are premixed. Initially ½ of the total amount of liquid is poured to the mixture and mixed for 1 minute;

(3) Thereafter, another ¼ of liquid is added, followed by 1/8 of the liquid and 1/16 of liquid with one minute of mixing accompanying each addition;

(5) The remaining liquid is then poured and mixed for 1 minute after which all the coarse aggregates are added with mixing for 2 minutes;

(6) The steel fibers are added slowly to the mixture and mixing continues for about 3 minutes.

2.4 Shear Behaviour and Modeling of Reinforced Concrete Beams

2.4.1 Introduction

Catastrophic failures such as the collapse of large RC beams in the 1950s at US Air-force warehouses as well as more recent failures such as the collapse of the "de La Concorde Bridge" in 2006 (see **Figure 2.33**) have emphasized the importance of properly accounting for shear in the design of reinforced concrete structures. These failures have shown that beams without shear reinforcement can fail suddenly and without warning prior to reaching their flexural capacity.

Beams without web reinforcement typically fail in shear shortly after the formation of inclined cracks (diagonal shear cracks). For this reason, it is important to accurately quantify the shear resistance of concrete. This concrete contribution to resistance is a function of several parameters (including cross-sectional geometry, beam dimensions, loading, and material properties) and is not fully understood. When the concrete contribution to shear resistance is deemed inadequate, modern codes require the provision of additional shear resistance in the form of transverse steel reinforcement (or stirrups).

(a) Beams failed in shear at the US Air-force warehouses

(b) The collapse of de La Concorde Bridge due to shear failure

Figure 2.33: Examples of brittle shear failures in RC beams without web reinforcement [Adapted from Sherwood (2008)]

2.4.2 Shear behaviour of RC beams

2.4.2.1 Classification of RC beam behaviour in flexure

As shown in **Figure 2.34** the failure of a rectangular reinforced concrete beam without web reinforcement is strongly influenced by the beam's span-to-depth ratio (*a/d*). The constant line in **Figure 2.34 (b)** represents the nominal moment M_n, and the shaded area indicates the strength loss due to shear (Wight & Macgregor, 2009). As seen in **Figure 2.34 (b)** the behaviour can be grouped into three categories as a function of the *a/d* ratio:

- Deep Beams: Beams with short spans ($1< a/d <2.5$). In these load is carried by a combination of redistribution of internal forces and arch and strut action;
- Slender Beams: Beams having a span-to-depth ratio in between 2.5 to 6 are termed slender. In slender beams without web reinforcement, the development of inclined cracks affects the equilibrium between internal resistance and applied load, and the beam will fails soon after the formation of the flexure-shear cracks;
- Very Slender Beam: Beams having a span-to-depth ratio which exceeds 6. In these beams failure may occur in flexure before the formation of inclined shear cracks.

It is common for researchers to describe failure mechanisms based on the primary failure crack patterns shown in **Figure 2.35** and listed below:

- Flexural failure;
- Shear-Tension failure;
- Diagonal-Tension failure and;
- Shear-Compression failure.

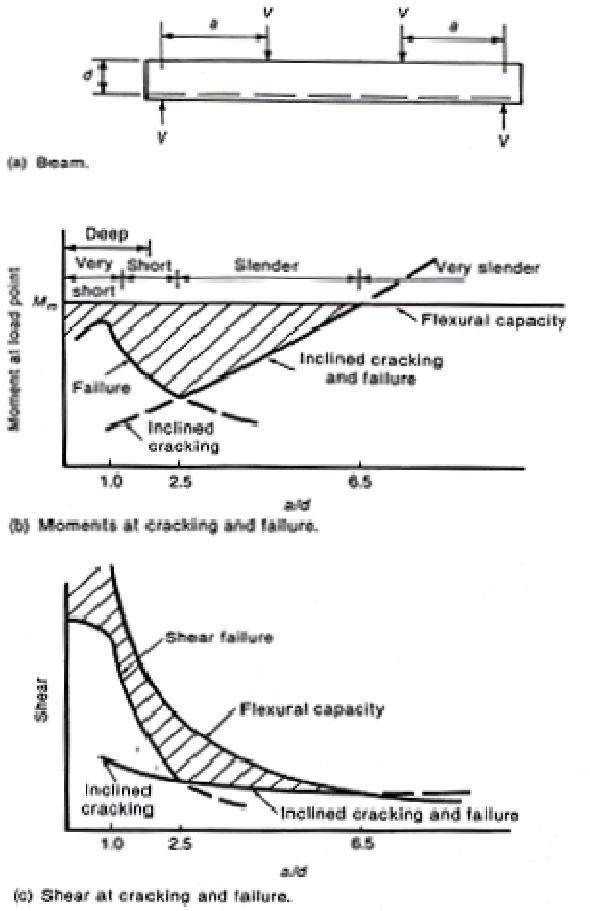

Figure 2.34: Beam's Span-to-depth ratio (*a/d*)

[Adapted from Wight and Macgregor (2009)]

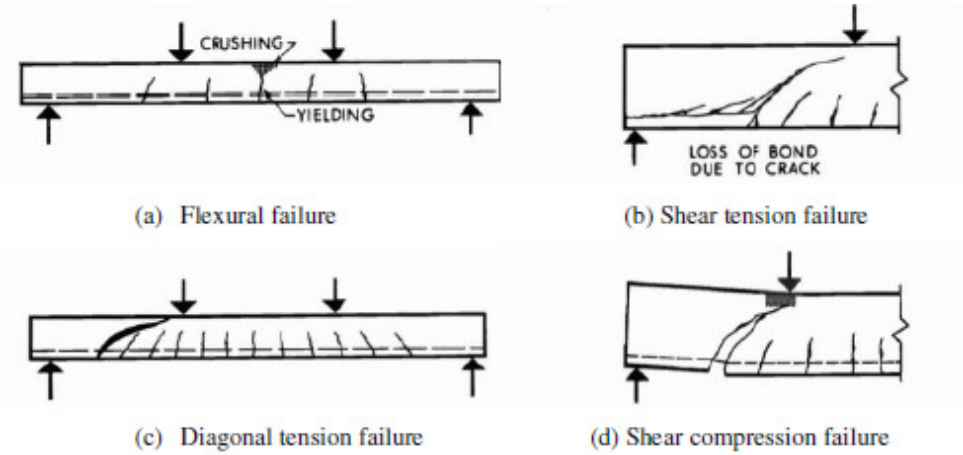

Figure 2.35: Beam failure modes

[Adapted from Dinh (2009)]

2.4.2.2 Shear resistance mechanisms in beams without web reinforcement

Over the past few decades, extensive research has led to important advancements in our understanding of the shear behaviour of reinforced concrete beams. That being said, the shear behaviour of RC beams is yet to be completely understood, partly because of the various mechanisms involved. As shown in **Figure 2.36**, the contribution to shear resistance in a RC beam without web reinforcement is function of several mechanisms: shear stresses in the uncracked concrete, aggregate interlock (or interface shear), dowel action of the longitudinal reinforcement, arching action and residual tensile stresses that are transmitted across the cracks (Minelli, 2005).

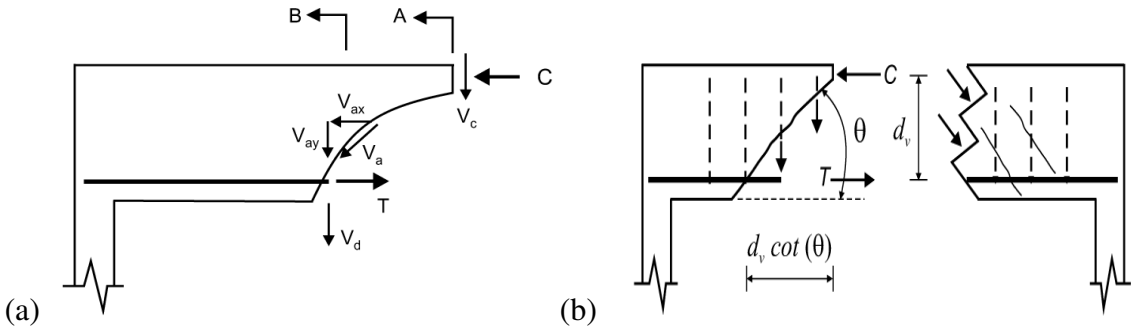

Figure 2.36: (a) Shear resistance mechanisms (b) Contribution of transverse reinforcement [Adapted from Brzev and Pao (2006)]

2.4.2.3 Factors affecting shear resistance mechanisms in beams without web reinforcement

In slender beams without web reinforcement failure takes place soon after the initiation of inclined shear cracks. The shear capacity of such beams is thus governed by the inclined shear cracking load. This capacity is influenced by several factors including compressive resistance of the concrete, amount of longitudinal reinforcement, shear span-to depth ratio, beam size, axial load, etc.

2.4.2.3.1 Concrete Compressive Strength

One of the factors affecting the shear strength of RC beams is compressive strength. The concrete contribution to shear resistance is directly influenced by the diagonal tensile capacity of the concrete. When shear forces are present diagonal tension and compression stresses result, and when diagonal tension exceeds the tensile capacity of the concrete diagonal cracks form. It is noted that in the case of normal-strength concrete, since the concrete strength is lower than the aggregate crushing strength, cracking will typically go around the aggregates; thus the shear resistance is improved due to the rough and uneven surface at the crack. In the case of high-strength concrete, the cracks may go through the aggregates rather than going around them; this results in a smoother crack surface reducing the contribution due to aggregate interlock and may result in a lower shear capacity (Sherwood, 2008).

2.4.2.3.2 Longitudinal Reinforcement

The longitudinal reinforcement ratio (ρ) is another factor which has an influence on the shear capacity of beams without web reinforcement. Research has shown that an increase in longitudinal reinforcement ratio (ρ) leads to an improvement in shear capacity of RC beams (see **Figure 2.37**). When compared to an equivalent beam with higher longitudinal reinforcement ratio, a reduced amount of ρ results in larger tensile strains, wider crack widths and a drop in shear capacity. This reduced shear capacity is likely due to reduction in aggregate interlock as ρ reduces (Sherwood, 2008). In addition as the reinforcement ratio increases an increase in dowel action and a deeper compression zone may result, leading to a higher shear capacity (Dinh, 2009).

2.4.2.3.3 Shear span-to-depth ratio

As discussed previously the shear span-to-depth ratio (*a/d*) has a strong influence on the mechanisms governing the failure of reinforced concrete beams. In deep beams ($a/d < 2.5$), redistribution of stresses occurs and results in the development of arch action and the transmission of larger shear stresses to the supports by the compression struts (Wight and Macgregor, 2009). Due to the complex nature of this type of failure mechanism, such beams

are best modeled using strut and tie models or other analysis techniques. **Figure 2.37** shows the influence of *a/d* ratio on shear capacity. As shown in the figure, beams with small *a/d* ratio can carry significantly higher shear stresses when compared to slender beams (*a/d* > 2.5). The figure also shows that the *a/d* ratio has less influence on shear capacity in beams with a shear span-to-depth ratio greater than 2.5.

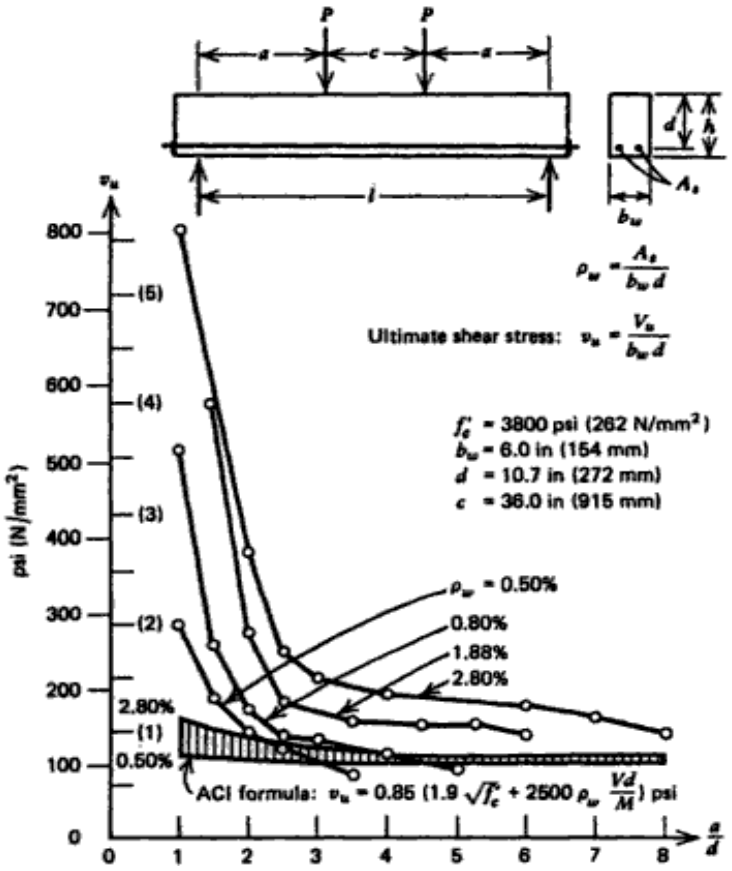

Figure 2.37: The relationship between the ultimate shear stress and *a/d* ratio [Adapted from Park and Paulay (1975)]

2.4.2.3.4 Beam Size

As shown in **Figure 2.38,** for a beam without web reinforcement, increasing the depth has the effect of decreasing the shear stress at failure if all other properties are left constant. Increasing beam depth results in an increase in crack widths which in turn reduces the maximum concrete shear stress which is transferred across the crack by aggregate interlock, thus reducing shear capacity (Wight and Macgregor, 2009). Studies have demonstrated that

the size effect has less of an impact on the shear strength in beams with web reinforcement or containing well distributed longitudinal reinforcement along the depth. In such case the size effect will be more related to the spacing between the layers of longitudinal reinforcement rather than the beam depth.

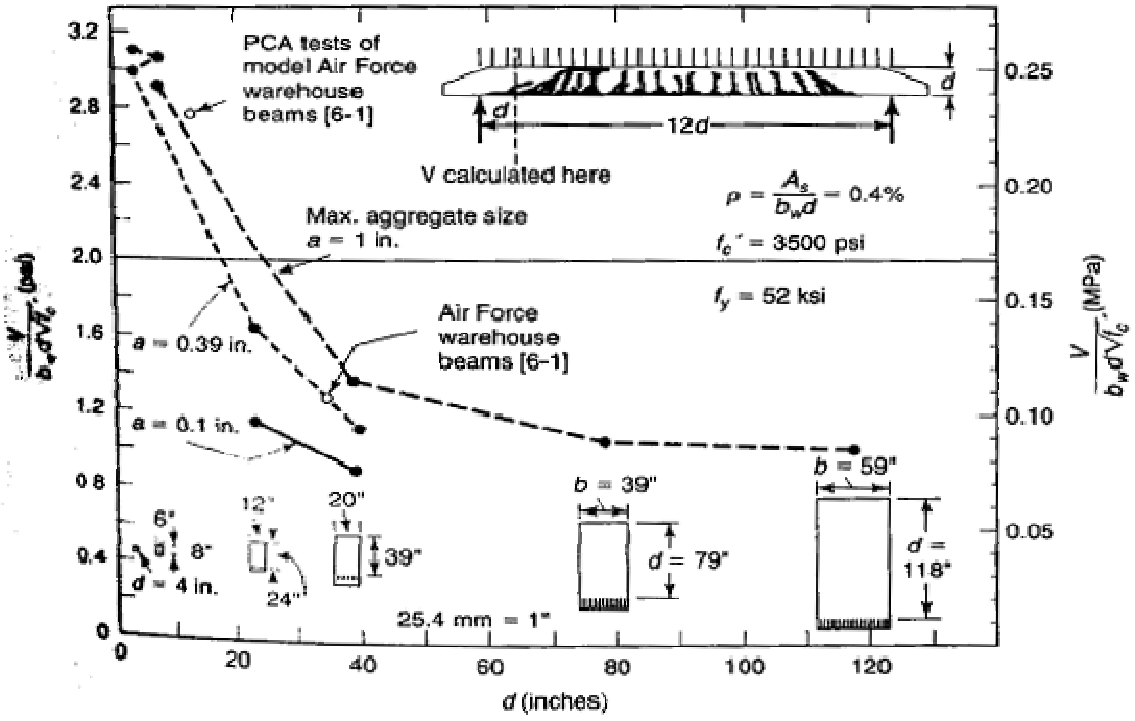

Figure 2.38: the effect of the beam size on shear failure
[Adapted from Wight and Macgregor (2009)]

2.4.2.3.5 Axial Force

In case of the absence of transverse reinforcement, studies have shown that the shear strength is influenced by the application of axial load. The application of external compressive axial load or prestressing reduces longitudinal strains and hence prompting less crack widths, which in turn can lead to an increase in shear capacity. On the other hand the application of additional axial tension forces directly increase the stress and longitudinal strain resulting in increased crack widths and a reduction in shear capacity (see **Figure 2.39**).

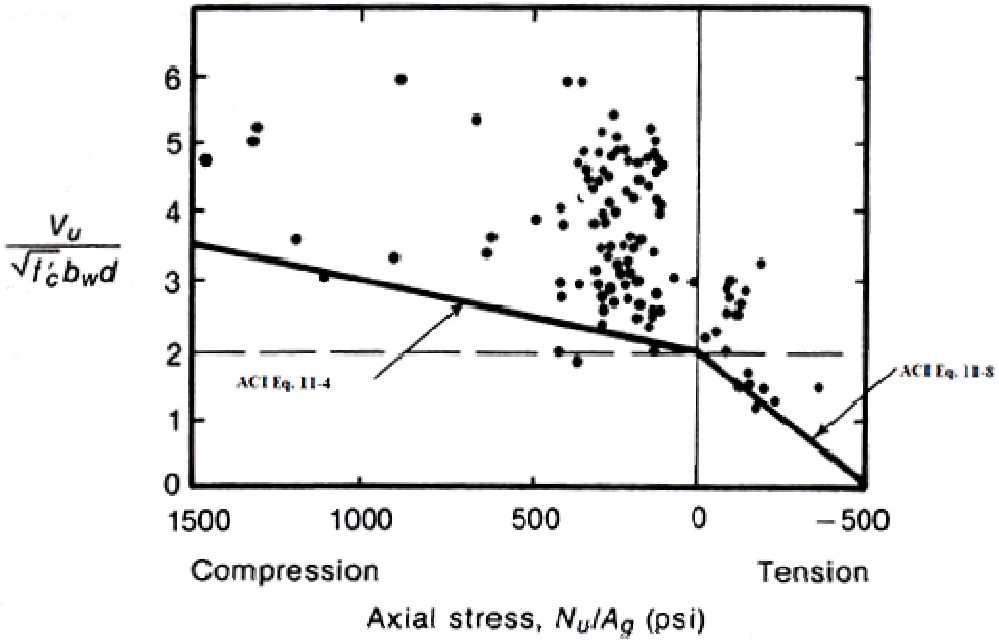

Figure 2.39: The effect of the axial load on the shear capacity

[Adapted from Wight and Macgregor (2009)]

2.4.2.3.6 Other Parameters

Other parameters which may have an influence on the shear strength of RC beams, include:

- Load Condition (e.g. concentrated load, uniformly or non-uniformly distributed load);
- Cross Section Shape;
- Longitudinal Reinforcement Distribution along the beam's depth;
- Use of reduced aggregate size;
- Use of lightweight aggregate concrete.

2.4.2.4 Shear resistance of beams with web reinforcement

To ensure a ductile flexure failure mode (and prevent brittle shear failure), steel reinforcement in the form of transverse stirrups is often added to provide an additional shear resistance mechanism (see **Figure 2.36 (b)**). After cracking, the stirrups (which intercept the inclined cracks) provide additional shear resistance as shear is transferred by tension in the stirrups. If sufficient web reinforcement is provided the shear failure due to inclined cracking

can be prevented and the full flexural capacity of the beam can be developed. In the presence of stirrups as shown in **Equation 2-24** , the shear capacity of a beam can be taken as the sum of the contributions of the concrete (V_c) and the steel web reinforcement (V_s):

$$V_r = V_c + V_s \tag{2-24}$$

2.4.3 Models for the shear behaviour of RC beams

2.4.3.1 Early truss models

Truss analogy was first introduced by Mörsch (1905) to model the shear behaviour of reinforced concrete beams. In this model the reinforced concrete beam is idealized as a truss where the "vertical tension members" are represented by the transverse reinforcement, the "diagonal members" by the inclined compressive concrete stresses, and the "bottom and top cords" are represented by longitudinal reinforcement and the concrete compression zone respectively. In this model the post cracking tensile stresses in concrete is conservatively ignored, and due to the complexity of determining the inclined concrete compressive stresses angle, the angle of diagonal cracking is conservatively taken as 45^o (Aoude, 2008).

A more accurate approach can be made by modifying the Mörsch model through a more accurate estimation of the angle of inclination of the diagonal concrete compressive stresses. As seen in (**Figure 2.40**) the free body diagram has four variables (the principal compressive stress, the tensile forces in the longitudinal reinforcement, the stress in the stirrups, and the inclination of the principal compressive stresses) while there are only three equilibrium equations, therefore the diagonal compressive struts angle must be estimated before starting the analysis (Collins and Mitchell 1997).

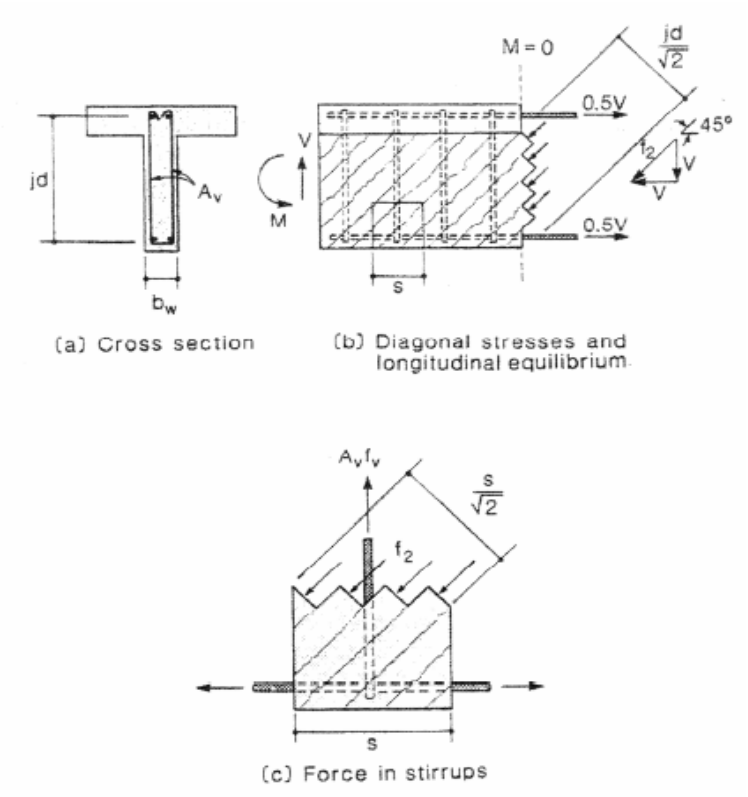

Figure 2.40: The modified Mörsch truss model and the equilibrium conditions [Adapted from Collins and Mitchell (1997)]

2.4.3.2 Compression Field Theory

Mitchell and Collins (1974) proposed the Compression Filed Theory (CFT) to solve the equilibrium equations in the Mörsch truss model. In this model, Mitchell and Collins ignored the tensile stress in concrete after cracking and assumed that the shear stresses are resisted by the diagonal compressive stresses. Using Mohr's circle the stress-strain relationship of the different materials, and the strain compatibly between the concrete and the reinforcement can be obtained. The inclined compressive stress angle is taken as a function of those strains (see **Figure 2.41**). Although the CFT neglected the post cracking tensile stresses in concrete, it allows for a reasonable prediction of the shear response of reinforced concrete members.

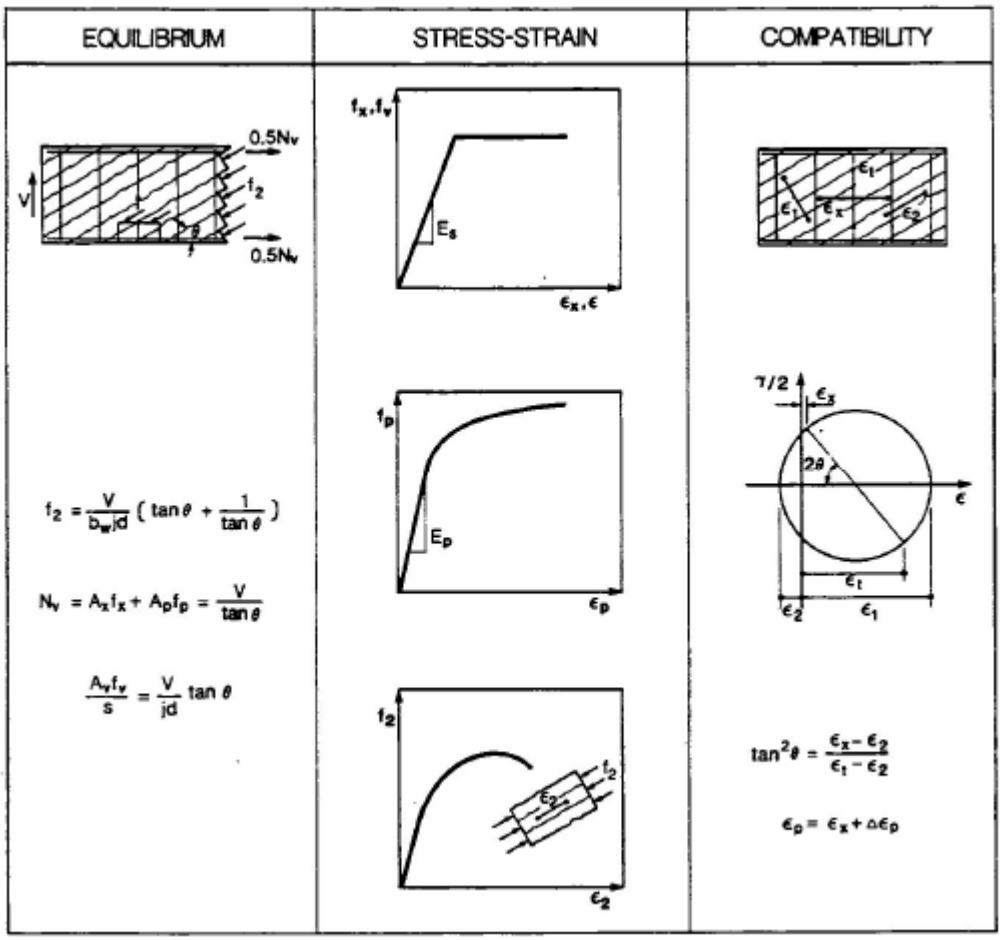

Figure 2.41: Different criteria in the CFT method

[Adapted from Collins and Mitchell (1997)]

2.4.3.3 Modified Compression Field Theory

Vecchio and Collins (1986) developed the Modified compression field theory (MCFT) which further refines the CFT model, by accounting for the contribution of the tensile stresses of concrete after cracking. To arrive at the relationships used in the MCFT, numerous tests were performed on reinforced concrete panels under pure shear loading. Based on the equilibrium equations, stress-strain relationship, and the strain compatibility relationships, a practical analysis of the complete shear load-deformation response can be obtained (see **Figure 2.42**). The development of user-friendly computer programs such as RESONSE 2000 have facilitated the practical implementation of the MCFT to predict the shear capacity and complete load-deformation response of RC beams (Bentz, 2000).

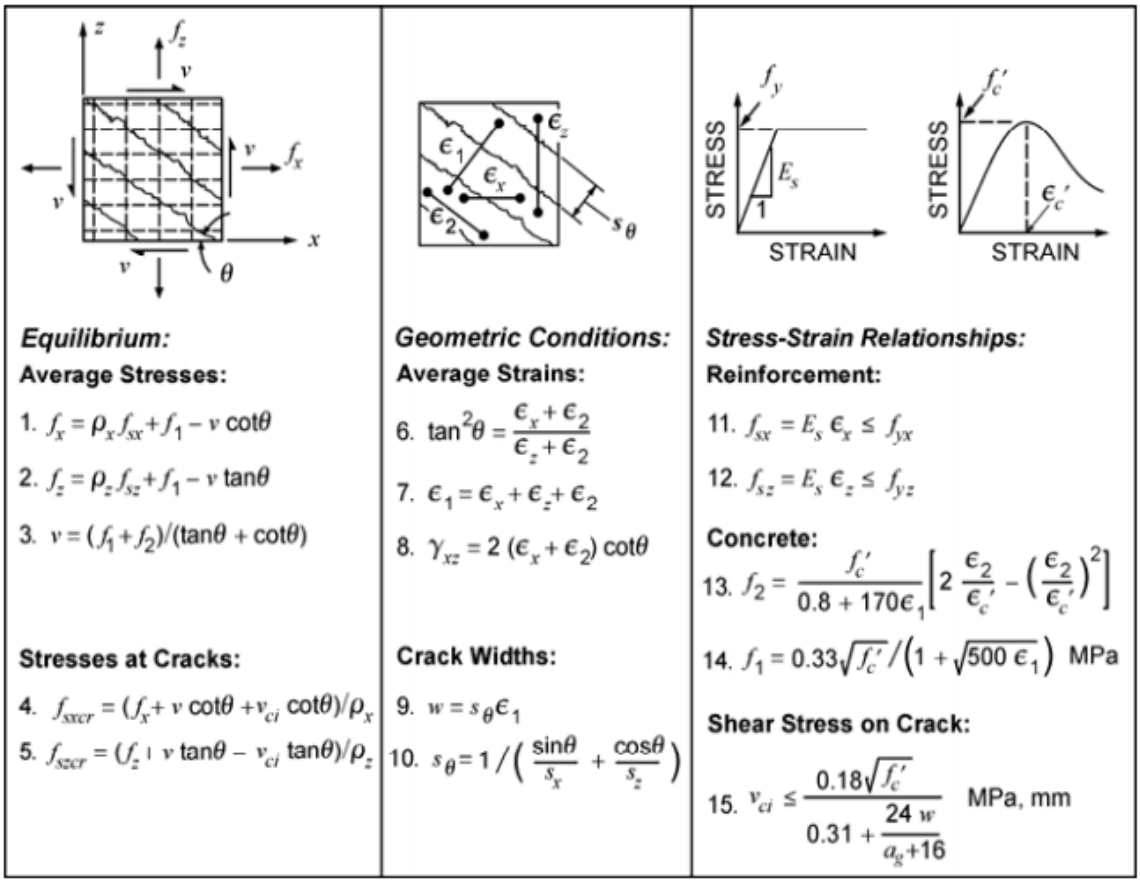

Figure 2.42: Relations of the Modified Compression Filed Theory (MCFT) [Adapted from Sherwood (2008)]

2.4.4 ACI 318 shear design provisions

The simplified 45^o truss model proposed by Mörsch formed the basis of early shear design guidelines in North America. The model, which assumes shear cracks form at an angle of 45^o permitted engineers to quickly estimate the shear strength of a reinforced concrete member with web reinforcement. This simplified model still forms the basis of the expressions for shear resistance provided by stirrups in several design codes, including the current ACI expressions (Sherwood, 2008). However, as noted previously, this model assumed shear resistance to be provided solely by transverse reinforcement and ignores the contribution of the concrete to shear resistance. Research was therefore initiated to quantify this concrete

contribution. Based on these research efforts, an empirically derived working shear stress of 0.03*f'c* (psi) was proposed to "safely" account for the shear contribution provided by the concrete, V_c. (Sherwood, 2008). Combined with the simplified truss model of Mörsch, this empirically derived concrete contribution formed the basis of the ACI shear design provisions in the 1950s. However, the 1955 collapse of the Air Force Warehouse roof beams (see **Figure 2.33 (a)**) indicated the unsafe nature of these early shear design provisions. The large beams had been designed without web reinforcement based on the assumption they could resist the "safe" working shear stress of 0.03*f'c* (Sherwood, 2008). As a result of this incident, significant research was initiated to develop a safe and reliable model to account for the shear resistance provided by concrete. Based on a large database of experimental data, a simplified expression for predicting concrete shear capacity was proposed for use in the 1963 ACI code (**Equation 2-25, 2-26**). The equation, along with the 194 experimental data points used in the curve-fit of the expression is plotted in **Figure 2.43** (Sherwood, 2008).

$$\frac{V_c}{b_w d} = 1.9\sqrt{f_c'} + 2500\frac{\rho_w V d}{M} \le 3.5\sqrt{f_c'} \quad \text{(psi)} \tag{2-25}$$

$$\frac{V_c}{b_w d} = 0.142\sqrt{f_c'} + 17\frac{\rho_w V d}{M} \le 0.29\sqrt{f_c'} \quad \text{(MPa)} \tag{2-26}$$

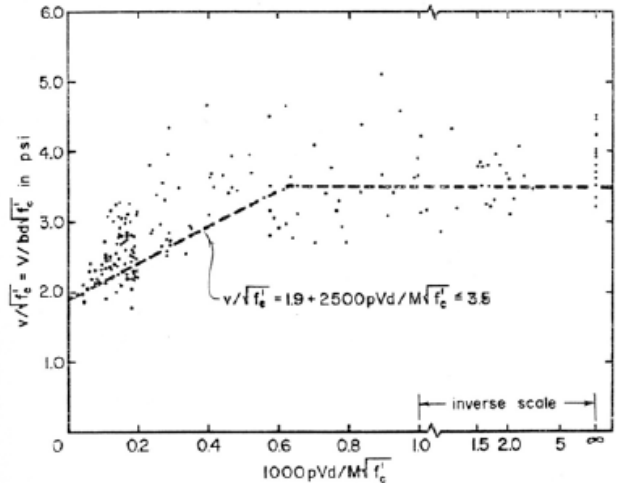

Figure 2.43: Plot showing derivation of ACI 318 shear equation
[Reproduced from ACI Committee 326 (1962)]

For most practical beam configurations values of $1000\rho_w Vd/M\sqrt{f_c'}$ are located to the left of **Figure 2.43**, and therefore, **Equations 2-25, 2-26** can be simplified to the following expression, which is the simplified formulation used in the current shear provisions of the ACI 318 code (ACI Committee 318, 2008).

$$V_c = 2\sqrt{f_c'}\,b_w d \qquad \text{(psi)} \tag{2-27}$$

$$V_c = 0.167\sqrt{f_c'}\,b_w d \quad \text{(MPa)} \tag{2-28}$$

It is also noted that the ACI 318 Code requires the provision of minimum shear reinforcement in the form of stirrups in RC flexural members when the factored shear force, V_u, exceeds one-half the shear strength provided by concrete, V_c (ACI Committee 318, 2008). This minimum area of shear reinforcement can be calculated using the flowing expression:

$$A_{v,\min} = 0.75\sqrt{f_c'}\,\frac{b_w s}{f_y} \quad \text{(psi)} \tag{2-29}$$

$$A_{v,\min} = 0.06\sqrt{f_c'}\,\frac{b_w s}{f_y} \quad \text{(MPa)} \tag{2-30}$$

2.4.5 CSA shear design provisions

2.4.5.1 Overview

In the last few decades the Canadian shear design provisions have evolved several times in order to better predict the shear strength of reinforced concrete flexural members. In the early 1980s the Canadian provisions relied generally on empirical relationships. A more rational approach was introduced in 1984 based on the Compression Filed Theory (CFT). Later on in 1986, Vecchio and Collins have developed the Modified Compression Field Theory (MCFT). This method was the backbone of the general design method adopted in the 1994 CSA shear design provisions. However using the general shear design method presented in the 1994 edition of the CSA A23.3 standard was relatively complex due to the way in which factors such as the inclination angle, θ, and β factor had to be calculated. The 2004 edition of the CSA A23.3 standard introduced a set of simplified analytical relationships that can be

used to accurately predict the shear resistance of RC members based on the Modified Compression Field Theory (MCFT), making the Canadian shear design method independent from the ACI provisions (Bentz and Collins, 2005). In order to satisfy the CSA A23.3 2004 shear design requirements the factored shear resistance for an RC member, V_r, has to exceed the factored external applied shear load ($V_r \geq V_{fa}$). V_r can be found using **Equation 2-24** ($V_r = V_c + V_s$), while V_c and V_s can be calculated respectively using the equations below:

$$V_c = \phi_c \lambda \beta \sqrt{f_c'} b_w d_v \tag{2-31}$$

$$V_s = \frac{\phi_s A_V f_{yh} d_v \cot\theta}{s} \tag{2-32}$$

Where b_w and d_v represent the web width and the shear depth of the beam; λ is a factor which accounts for concrete type, ϕ_c and ϕ_s are material reduction factors for the concrete and the steel respectively; A_v is the cross sectional area of the transverse steel reinforcement; f_{yh} is the yield strength of that steel and; s is the spacing of the transverse reinforcement.

2.4.5.2 Simplified and general shear design methods

In the general shear design method the angle of the principal diagonal stresses, θ, and the β factor need to be computed in order to predict the factored shear resistance.

The β factor represents the ability of the concrete to carry stresses in between cracks and is a function of the aggregate interlock mechanism. This factor is computed using a simplified equation developed based on the MCFT. As shown in **Equation 2-33**, both the strain effect and size-effect are incorporated in the β equation (Bentz and Collins, 2005):

$$\beta = \frac{0.40}{(1+1500\varepsilon_x)} \times \frac{1300}{(1000+S_{ze})} \tag{2-33}$$

S_{ze} is the effective cracking spacing in the member and is a function of the member's depth and the aggregate size. ε_x represents the longitudinal strain at mid depth of the member and can be calculated using the following equation:

$$\varepsilon_x = \frac{\left(\frac{M_F}{d_v}\right) + V_F}{2 \times E_s \times A_s} \tag{2-34}$$

Where M_F and V_F are the factored applied moment and shear respectively; E_s and A_s are the modulus of elasticity and the cross sectional area of the longitudinal steel reinforcement respectively.

Equation 2-35 can be used to calculate the angle of inclination of the diagonal compressive stresses, θ:

$$\theta = 29^o + 7000\varepsilon_x \quad (2\text{-}35)$$

The simplified shear design method is considered as a modification of the general shear design method where some assumptions are made to avoid the iteration procedure. In the simplified method the longitudinal strain at mid depth of the member ε_x is taken to be equal to 0.85 x 10^{-3}. After substituting ε_x in **Equation 2-33** and **Equation 2-35** the β value will be 0.18 and θ will be 35^o. Moreover to use this method the yield strength of the steel reinforcement should not be greater than 400 MPa and the concrete compressive strength must be less than 60 MPa.

2.5 Shear Behaviour and Modeling of SFRC and SCFRC Beams

2.5.1 Previous research on shear behaviour of SFRC beams

One of the possible applications of SFRC is in beams that are shear critical. Research over the past three decades has shown that the use of steel fibers in reinforced concrete beams can be used to enhance shear resistance. Adding steel fibers to a concrete beam without transverse reinforcement improves shear behaviour due to the ability of SFRC to resist and redistribute diagonal tensile stresses after cracking. In addition, the fiber crack-bridging capabilities delay and control the development of cracks. Thus, very much like traditional transverse reinforcement, the use of fibers results in an increase in the overall shear resistance of the beam and can promote flexural failure and ductility. If added in sufficient quantities, the use of steel fibers can replace traditional transverse reinforcement and promote flexural failure and ductility. Parra-Montesinos (2006) presented a large database of SFRC beam test results which included results from 16 studies. The results showed that all SFRC beams in the database having $V_f \geq 0.5\%$ exhibited shear stress at failure greater than

$0.17\sqrt{f_c'}$, equivalent to V_c as defined in the ACI-318 code (ACI, 2008) with beams having $V_f \geq 0.75\%$ failing at shear stresses not less than $0.3\sqrt{f_c'}$. Based on the experimental evidence reported in the literature, the use of steel fibers in flexural members is now permitted in several international design codes (see Section 2.6).

2.5.2 Models for predicting the shear resistance of SFRC beams

Over the past two decades several researchers have proposed equations to predict the shear resistance of SFRC beams (see **Table 2.9**). These include models proposed by Sharma (1986), Ashour et al. (1992), Narayanan and Darwish (1987), Mansur et al. (1986) and others. It is noted that the majority of the models account for the contribution of SFRC to shear resistance using the so-called fiber factor (F) which as shown in **Equation 2-36** is a function of fiber content (V_f) and fiber aspect-ratio (L_f/D_f). Other models use material tests to quantify the improvement in tensile resistance and the enhancement in shear capacity.

$$F = V_f \frac{L_f}{D_f} \tag{2-36}$$

Most of these models are from empirical formulae derived from regression analysis of limited experimental data. Therefore the results obtained from these models can't be relied on in many cases to evaluate the shear capacity in SFRC beams (Minelli, 2005). In particular, it is noted that the model proposed by Sharma (1986) and initially recommended by ACI Committee 544 shows very poor accuracy. The model proposed by Minelli and Plizzari (2006) modifies the shear capacity formula given in Eurocode 2. In this formulation, a toughness parameter is used to adjust the longitudinal reinforcement ratio; the rationale being that fibers improve shear capacity and ductility in the same way longitudinal reinforcement uniformly distributed along the depth of a member improves shear capacity.

In addition to the empirical models discussed above, several researchers have proposed more rational models to predict the shear response of SFRC beams. Models in this category include the Variable Engagement Model (VEM) proposed by Foster and Voo (2003) and the strain-based shear strength model developed by Choi et al. (2007). These two models have

been shown to result in more accurate predictions of shear resistance when compared to the empirically-based equations, though more computational effort is typically required.

Table 2.9: SFRC beam models for calculating the shear resistance

Researcher	Predictive model for ultimate shear strength [MPa]
Kwak et al. (2002)	$\upsilon_u = 3.7 e f_{spfc}^{2/3}\left(\rho\frac{d}{a}\right)^{1/3} + 0.8\left(0.41\tau\frac{L_f V_f d_f}{D_f}\right)$
Sharma (1986)	$\upsilon_u = k f_t^{'}\left(\frac{d}{a}\right)^{0.25}$
Li et al. (1992)	$\upsilon_{frc} = 1.25 + 4.7\left[\left(f_f f_{sp}\right)^{\frac{3}{4}}\left(\rho\frac{d}{a}\right)^{\frac{1}{3}} d^{-\frac{1}{3}}\right]$
Khuntia et al. (1999)	$\upsilon_u = \left(0.167\alpha + 0.25\frac{L_f V_f d_f}{D_f}\right)\sqrt{f_c^{'}}$
Imam et al. (1995)	$\upsilon_u = 0.6\Psi\sqrt[3]{\omega}\left[\left(f_c^{'}\right)^{0.44} + 275\sqrt{\frac{\omega}{\left(a/d\right)^5}}\right]$
Cucchiara et al. (2004)	$\upsilon_c = 0.83\xi\sqrt[3]{\rho}\bullet\chi + \frac{1.67\sqrt{f_c^{'}}}{\chi}\rho_w f_{yw}$
Mansur at al. (1986)	$\upsilon_u = \left(0.16\sqrt{f_c^{'}} + 17.2\frac{\rho V d}{M}\right) + 0.41\left(\tau V_f\frac{L_f}{D_f}\right)$
Narayanan & Darwish (1987)	$\upsilon_u = e\left(0.24 f_{spfc}^{'} + 80\rho\frac{d}{a}\right) + 0.41\left(\tau\frac{L_f V_f d_f}{D_f}\right)$
Ashour et al. (1992)	$\upsilon_u = \left(0.7\sqrt{f_c^{'}} + 7\frac{L_f V_f d_f}{D_f}\right)\frac{d}{a} + 17.2\rho\frac{d}{a}$
Cassanova (1996)	$V = 0.9bd\cdot\overline{\sigma_p}(w) + V_s$
Minelli & Plizzari (2006)	$\upsilon_u = \left[\frac{0.18}{\gamma_c}k\left(100\rho_1\left(1 + 2.5\frac{f_{eq(0.6-3)}}{f_{ct}}\right)f_{ck}\right)^{1/3} + 0.15\sigma_{CP}\right]$

Note: e is a function of the (a/d) ratio; f_{spfc} is the split cylinder strength, ρ is the longitudinal steel reinforcement ratio; d is the beam effective depth; a is the shear span; τ is the fiber bond shear strength; L_f, V_f, D_f are the fiber length, fiber volume fraction, and fiber diameter, respectively; d_f is a factor which accounts for the fiber geometry; k is a factor that refers to the type of the test used to determine the concrete tensile resistance; f_{sp} is the split cylinder strength (a different expression is used for $a/d < 2.5$); $f_c^{'}$ is the concrete compressive strength; Ψ is the size factor defined by Imam et al.; ω is a function of the fiber properties; a/d is the shear span-to-effective depth ratio; χ is a function of the concrete strength and the (a/d) ratio; V/M is shear-moment ratio; $\overline{\sigma_p}(w)$ is the residual post-cracking strength of SFRC at crack width w; γ_c is the unit weight of normal concrete.

2.5.3 Design Guidelines for use of SFRC in Beams

The utilization of steel fiber as complete replacement for shear reinforcement remains a matter of debate, and this returns to the complexity and lack of full understanding of the shear contribution of the steel fiber in beams with and without stirrups. Another reason returns to the absence of reliable and accurate code-based equations for predicting the shear resistance of SFRC beams. Nonetheless, several codes in Europe and North America now permit and give guidelines for the use of SFRC in beams (see **Table 2.10**).

Table 2.10: Summary of some design guidelines for the shear resistance of SFRC beams.

Design Guideline	Design Equation	Fiber contribution is ...
RILEM TC-162 TDF σ-*w* method	$V_u = V_c + \bar{\sigma}_{pd}(w_m) \cdot bz$	-separate term that is additional to the concrete contribution -function of mean residual post-cracking stress obtained from stress-crack opening (σ-*w*) relationship -obtained using uni-axial tension test
RILEM TC-162-TDF σ-ϵ method	$V_u = V_{cd} + 0.7 k_f k_1 \tau_{fd} b_w d$ where $\tau_{fd} = 0.12 f_{Rk,4}$	-separate term that is additional to the concrete contribution -function of a fraction of the residual post-cracking strength (f_{Rk}) -obtained from bending test
DaftStb German Guidelines	$V_u = V_{cd} + 0.7 k_f k_1 \tau_{fd} b_w d$ where $\tau_{fd} = 0.37 f_{Rk}^{f}$	
Swedish Betongrapport nr 4	$V_u = V_{cd} + V_{fd}$	
Norwegian Recommendations	$V_u = V_{cd} + 0.8 f_{ftd,res} b_w d$	-similar to above, except residual post-cracking strength is used directly in equation -obtained from bending test
Italian Recommendation	$V_u = \left[\frac{0.18}{\gamma_c} k \left(100 \rho_1 \left(1 + 7.5 \frac{f_{Ftuk}}{f_{ctk}} \right) f_{ck} \right)^{1/3} + 0.15 \sigma_{CP} \right] b_w d$	-not a separate term; taken as an addition to the effect of the longitudinal reinforcement ratio (ρ_1) -function of residual post-cracking strength (f_{Ftuk}) -obtained from uni-axial tension or bending test
ACI 318 (2008)	No equation	

2.5.3.1 ACI 318 code

The 2008 edition of the ACI-318 code was the first North American code to permit the use of SFRC as shear reinforcement in beams. In particular the code allows the limited use of steel fiber as a replacement for the minimum shear reinforcement under certain conditions (ACI Committee 318, 2008).

In terms of the fibers, clause 3.5.8 specifies that the steel fibers should have a length-to-diameter ratio of not less than 50 and not greater than 100.

At the material level, ACI 318 clause 5.6.6.2 proposes that SFRC shall be considered acceptable for shear resistance if the following conditions are satisfied:

(a) The weight of steel fibers per cubic yard should be greater than or equal to 100 lb/yd^3 (60 kg/m^3, which is equivalent to a volume fraction of 0.75%);

(b) In accordance with the ASTM C1609 four point bending test, the residual strength obtained at a midspan deflection of 1/300 of the span length should be greater than or equal to 90% of the first peak strength measured from the flexural test, or 90% of f_r value which is calculated using **Equation 2-37**, whichever is greater; and

(c) For the same flexural test and at mid span deflection of 1/150 of the span length, the measured residual strength should be greater than or equal to 75% of the first peak strength obtained from the same test, or 75% of f_r calculated using **Equation 2-37**, whichever is greater.

$$f_r = 7.5\lambda\sqrt{f_c'} \tag{2-37}$$

In terms of using SFRC as a replacement for the minimum shear stirrups, clause 11.4.6.1(f) allows using hooked or crimped steel fibers on condition that:

(a) The concrete strength, f_c' does not exceed 60 psi (41 MPa);

(b) The beam depth, h, does not exceed 24 in (610 mm); and

(c) The ultimate shear stress V_u does not exceed $\phi 2\sqrt{f_c'} b_w d$

2.5.3.2 RILEM TC-162-TDF Method

Also known as the $\sigma - \varepsilon$ method, the RILEM TC-162-DF method uses the residual post-cracking strength of FRC to determine the shear strength of a FRC member. Crack-mouth-opening displacements (CMOD) or deflection-controlled bending tests are used to obtain residual load values (F_{Ri}) at pre-determined CMOD or deflection values (see **Figure 2.44**). These load values are then used to determine the residual post-cracking strength of the FRC material at the various CMOD/deflections (f_{Ri}).

The design shear strength of the FRC beam is taken as the shear resistance of a traditional concrete member without shear reinforcement, V_c, plus an additional contribution provided by the fibers. The contribution of the fibers, V_{fd}, is taken as a fraction of the residual post-cracking strength of the FRC (see **Equations 2-38** & **2-39**).

$$V_u = V_c + 0.7 k_f k_1 \tau_{fd} b_w d \tag{2-38}$$

$$\tau_{fd} = 0.12 f_{Rk,4} \tag{2-39}$$

It is noted that the RILEM guidelines also propose a second method for estimating shear design strength based on the RILEM uni-axial σ-*w* test method (see **Table 2.10**).

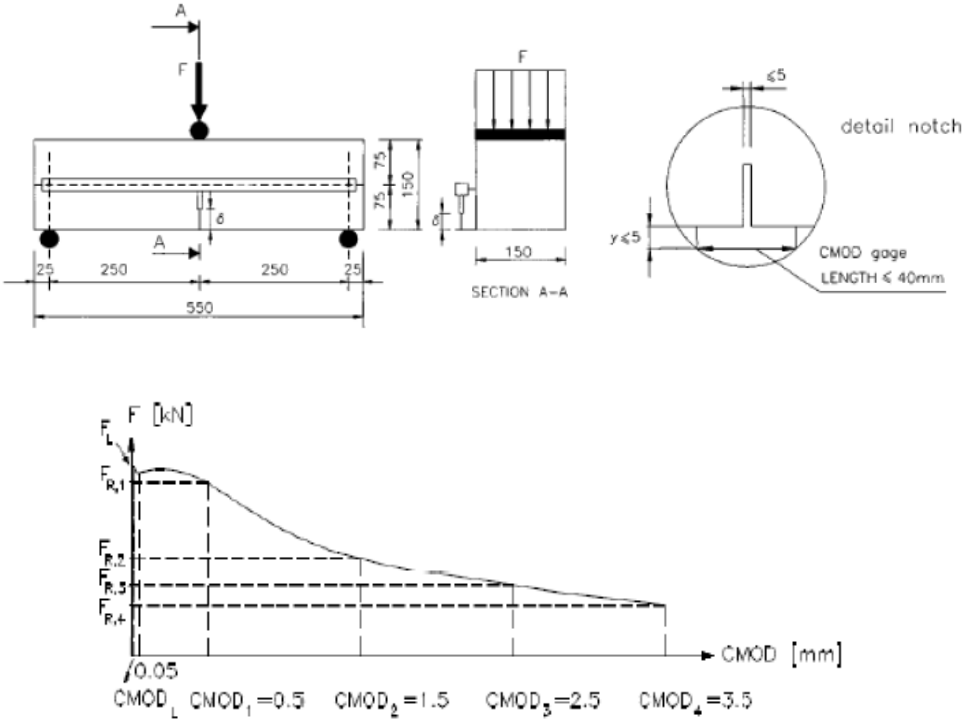

Figure 2.44: RILEM TC-162-TDF post-cracking residual strength

[Adapted from Jansson (2007)]

2.5.3.3 German, Swedish and Norwegian guidelines

Other design guidelines for SFRC include the Swedish (Betongrapport nr4), German (DAfStb) and Norwegian (Veiledning stålfiberarmert betong) recommendations. Just as in the RILEM method, in these recommendations the shear resistance provided by the fibers is accounted for by an additional term V_{fd} which is taken as a fraction of the residual post-cracking strength of FRC as obtained from bending tests (see **Table 2.10**)

2.5.3.4 Italian guidelines

The Italian guidelines differ from the previously mentioned guidelines in that the shear resistance provided by the fibers is not accounted for using a separate term. The method, which is based on the previously mentioned formulation proposed by Minelli and Plizzari (2006) modifies the shear strength formula found in EN 1992-1-1 and modifies it with regard to the residual capacity of the FRC material (see **Equation 2-40**). The residual strength of FRC is obtained from standard uni-axial tension or bending tests.

$$V_{Rd,F} = \left\{ \frac{0.18}{\gamma_c} k \left[100\rho_1 \left(1 + 7.5 \frac{f_{Ftuk}}{f_{ctk}} \right) f_{ck} \right]^{1/3} + 0.15\sigma_{cp} \right\} b_w d \qquad (2\text{-}40)$$

2.5.4 Shear behaviour of SCFRC beams

As discussed previously, the addition of steel fibers in traditional concrete mixes can cause problems in workability and placement, particularly when high fiber contents are used. The use of self-consolidating concrete (SCC) has been proposed to reduce these problems and facilitate placement. SCC can flow into place under its own weight without vibration and without exhibiting segregation or bleeding. Studies have shown that by utilizing a highly flowable SCC mix, self-consolidating properties can be maintained at low or moderate fiber contents, while adequate workability can be maintained at higher fiber contents (with some loss of self-consolidating properties) (Aoude, 2008).

2.5.5 Previous Research on Shear Behaviour of SCFRC beams

While there has been several studies focusing on the development of SCFRC mix designs, there is limited data in the literature related to the structural use of SCFRC in beams. Greenough and Nehdi (2008) performed a study on 13 slender SCFRC beams having *a/d* ratios equal to or greater than 3 and having fiber contents ranging from 0.5-1.0%. Three different fiber types were used including: hooked-end, flat-end and wavy type fibers. The authors noted that SCC is particularly well suited for fiber addition due to its improved rheological properties. The authors found that the addition of steel fibers improves the shear behaviour of SCC slender beams, with results showing that addition of 1.0% fiber content results in a 128% increase in shear capacity. The authors also proposed an empirical equation which modifies the traditional ACI shear equation (see **Equation 2-41**). The authors of this study also proposed a second equation that modifies a previously developed equation for shear capacity of RC slender beams developed by the same authors (see **Equation 2-42**).

$$V = \left(0.167\sqrt{f_c^{'}} + \alpha F \rho \frac{d}{a} + 0.9\eta_0 \tau F \right) b_w d \tag{2-41}$$

$$V = \left(0.35\left(1 + \sqrt{\frac{400}{d}} \right) f_c^{'0.18} + \left((1+F)\rho \frac{d}{a} \right)^{0.4} + 0.9\eta_o \tau F \right) b_w d \tag{2-42}$$

Where α is taken as 1 N/mm^2, F is the fiber factor, η_o is the fiber orientation factor, ρ is the reinforcement ratio, b_w and d are the beam width and depth, respectively. It is noted, as in previous models, the fiber contribution to shear resistance is taken into account empirically using the previously mentioned fiber factor (F).

Finally, there is limited published data on the behavior of plain SCC beams in shear. Lachemi et al. (2004) tested a series of 18 normal concrete (NC) and SCC beams and found that a decrease in aggregate size from 19 mm to 12 mm resulted in a reduction in ultimate shear capacity. Similarly a comparison between the behavior of the NC and SCC series showed the SCC beams had reduced shear capacity when compared to the NC beams. In both cases the behaviour was linked to the reduced contribution of aggregate interlock when smaller aggregates or lesser aggregate content are used.

Chapter Three: Experimental Program

3.1 Introduction

Although there has been extensive research focusing on the shear behaviour of traditional steel fiber reinforced concrete (SFRC) beams, there is limited research in the literature on the behaviour of beams constructed with self-consolidating concrete (SCC) and steel fibers. The main objective of the experimental phase of this research program was to study the structural shear strength, flexural ductility and crack control of self-consolidating fiber reinforced concrete (SCFRC) beams. A secondary objective was to examine if the use SCFRC could substitute for traditional shear reinforcement in reinforced concrete beams. The experimental program involved the construction and testing of twelve simply-supported beam specimens constructed with SCC and steel fibers. This chapter summarizes the details regarding specimen and material properties.

3.2 Description of Test Specimens

The experimental program involved the testing of twelve reinforced concrete beams constructed with SCC and steel fibers. **Figure 3.1** shows the geometry for a typical specimen. All of the beams were 125 mm wide, 250 mm deep, and had a length of 2.8 m. The beams where simply-supported over a span of 2.4 m and had a shear span of 800 mm resulting in a shear span-to-depth ratio, *a/d*, of 3.8. Each beam was reinforced with two longitudinal reinforcing bars and a 30 mm clear concrete cover was provided in each specimen. In addition none of the beams contained any transverse reinforcement. The details regarding the cross-sectional properties are given in **Table 3.1**.

As shown in **Table 3.1** the experimental program included four series of specimens grouped based on longitudinal reinforcement ratio and concrete type. The M15-KING series consisted of 6 beams reinforced with two 15M longitudinal steel bars, and constructed using a traditional self-consolidating concrete (SCC) mix manufactured by KING materials (see details in section 3.3.3). The series included a control beam without fibers (specimen M15-0.0%) and five other beams with varying fiber contents and types. Specimens M15-0.5%, M15-1.0% and M15-1.5% contained normal strength hooked-end steel fibers with a fiber content, V_f, of 0.5%, 1.0% and 1.5%, respectively. Specimens M15-0.5%H and M15-0.75%H were reinforced with 0.5% and 0.75% of high strength hooked-end steel fibers, respectively. The M20-KING series consisted of 2 beams reinforced with two 20M longitudinal steel bars and constructed with same SCC mix used in the M15-KING series. Specimens M20-0.75% and M20-1.0% contained normal strength hooked-end steel fibers with V_f of 0.75% and 1.0%, respectively.

The final two series of beams (M20-CustomA,B) were constructed with two different customized SCC mixes (designated as Custom SCC-Mix A and Custom SCC-Mix B; see section 3.3.3 for details) and reinforced with normal strength hooked-end steel fibers. Specimens M20-1.0%A, M20-1.0%B had a fiber content, V_f of 1.0% whereas Specimens M20-1.5%A, M20-1.5%B had a V_f of 1.5%.

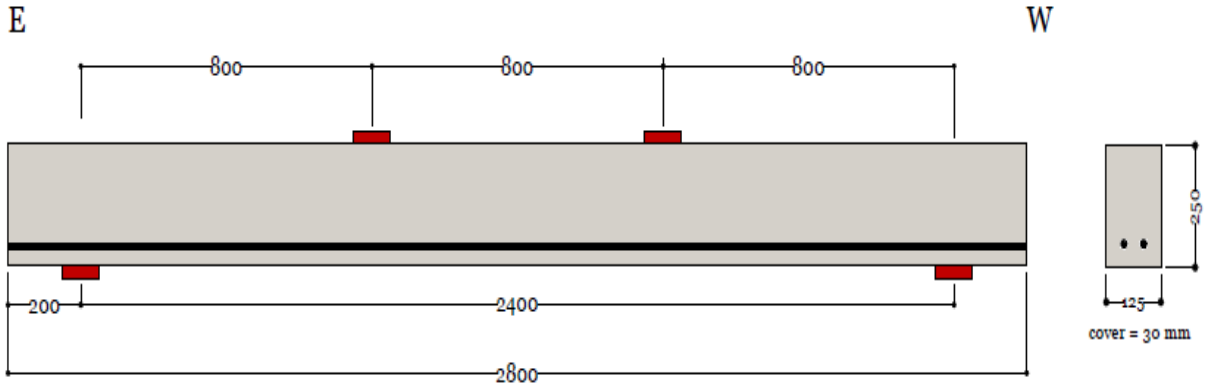

Figure 3.1: Typical Beam Specimen

Table 3.1: Design properties for beam specimens

Series	*Beams*	*Concrete Type*	*Cross-section*	*Reinforcement*	**Transverse reinforcement**	*Shear span to depth ratio (a/d)*	*Fiber type*	*Fiber content (% by volume)*
M15-KING	M15-0.0%	KING SCC	125 mm x 250 mm	2 - 15M (ρ=1.55%)	N/A	3.8	ZP-305	0.0
	M15-0.5%						ZP-305	0.5
	M15-1.0%						ZP-305	1.0
	M15-1.5%						ZP-305	1.5
	M15-0.5%H						BP80/30	0.5
	M15-0.75%H						BP80/30	0.75
M20-KING	M 20-0.75%	KING SCC		2 - 20M (ρ =2.33%)	N/A		ZP-305	0.75
	M 20-1.0%						ZP-305	1.0
M20-CustomA	M 20-1.0%A	Custom SCC (Mix A)					ZP-305	1.0
	M 20-1.5%A						ZP-305	1.5
M20-CustomB	M 20-1.0%B	Custom SCC (Mix B)					ZP-305	1.0
	M 20-1.5%B						ZP-305	1.5

3.3 Material Properties

3.3.1 Reinforcing Steel

Two sizes of deformed reinforcing bars were used in this experimental program. The longitudinal steel reinforcement consisted of 15M in the first series of beams, while 20M bars were utilized to reinforce the specimens in the remaining beams. Standard tensile coupon tests were performed on two samples of each bar size using a 600 kN MTS testing machine located at the University of Ottawa Structures Laboratory (see **Figure 3.2**). **Figure 3.3** shows typical stress – strain relationships for each bar size and **Table 3.2** summarizes the properties of the reinforcing steel bars, including: yield strength (f_y), ultimate strength (f_u), as well as yield, strain hardening and ultimate strains (ε_y, ε_{sh}, ε_u, respectively).

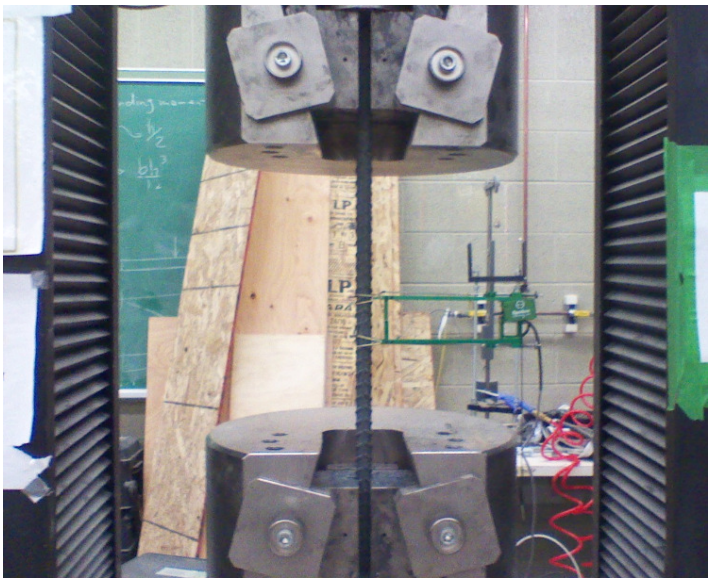

Figure 3.2: MTS testing machine for testing steel coupons

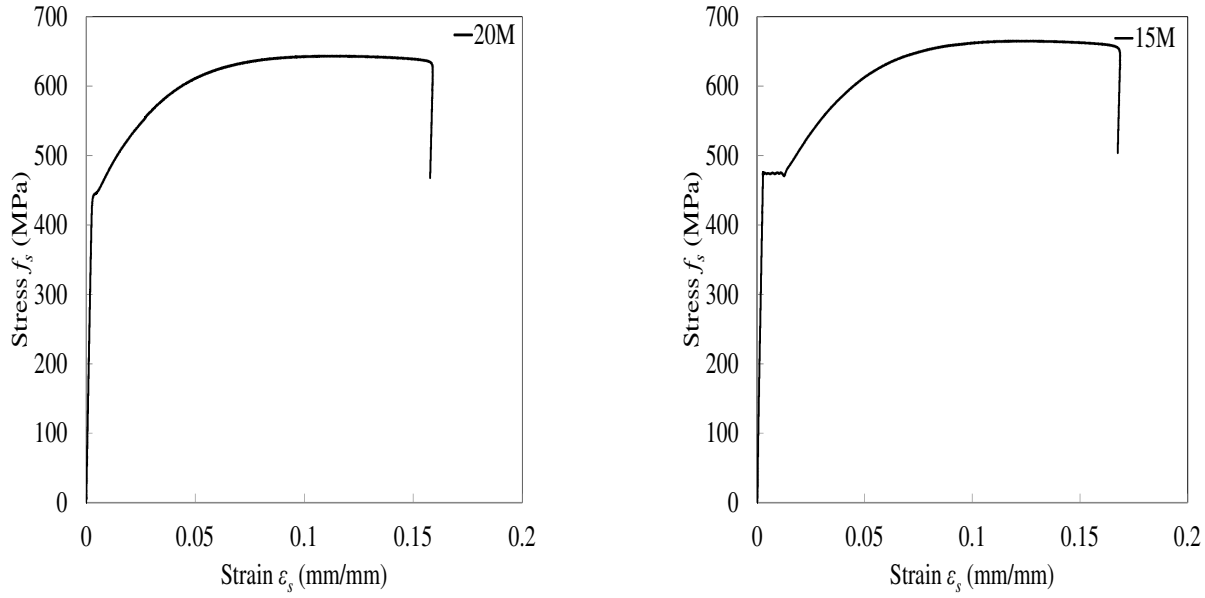

(a) Stress-strain relationship for 20M steel bar

(b) Stress-strain relationship for 15M steel bar

Figure 3.3: Stress – strain responses for 20M and15M reinforcing bars

Table 3.2: Properties of reinforcing bars

Bar description	Area (mm^2)	f_y (MPa) [std. dev.]	ε_y (mm/mm) [std. dev.]	ε_{sh} (mm/mm) [std. dev.]	f_u (MPa) [std. dev.]	ε_u (mm/mm) [std. dev.]
20M	300	441 [0.6]	0.0022 [0.000003]	0.0034 [0.00024]	643 [0.0]	0.1475 [0.0162]
15M	200	474 [0.1]	0.0023 [0.0000005]	0.0063 [0.00516]	663 [2.9]	0.1947 [0.0368]

3.3.2 Steel Fibers

Two types of steel fibers were used in this experimental program. Nine of the twelve specimens contained Dramix ZP305 fibers, whereas two of the specimens (M15-0.5%H and M15-0.75%H) contained Dramix BP80/30 fibers. These two types of fibers were manufactured by Bekaert Cooperation. Both types of fibers were 30 mm long with hooked ends and collated into bundles by dissolvable glue as shown in **Figure 3.4**.

The Dramix ZP305 fibers are made of normal strength steel wire with a tensile strength of 1100 MPa, have an aspect-ratio (L_f/D_f) of 55 and are likely the most common type of fiber studied in previous research and used in practice.

The Dramix BP 80/30 fibers have a higher tensile strength of approximately 2300 MPa and have a higher aspect-ratio (L_f/D_f) of 80. It is noted that this fiber type has been used to a lesser extent in previous research and is more often employed in high strength concrete or extreme load applications (earthquake and blast).

Different amounts of fibers were used in reinforcing the specimens in order to examine the effect of varying fiber content on shear response of SCFRC beams. The fiber contents varied from 0.5 % (38.4 kg/m^3) to 1.5% (115.2 kg/m^3) by volume of concrete. The properties of both steel fibers are summarized in **Table 3.3**.

Table 3.3: Properties of hooked-end steel fibers used in the experimental program

Fiber type	Length L_f (mm)	Diameter D_f (mm)	Aspect ratio L_f/D_f (mm/mm)	Tensile strength f_{fy} (MPa)
Dramix ZP-305	30	0.55	55	1100
Dramix BP80/30	30	0.38	80	2300

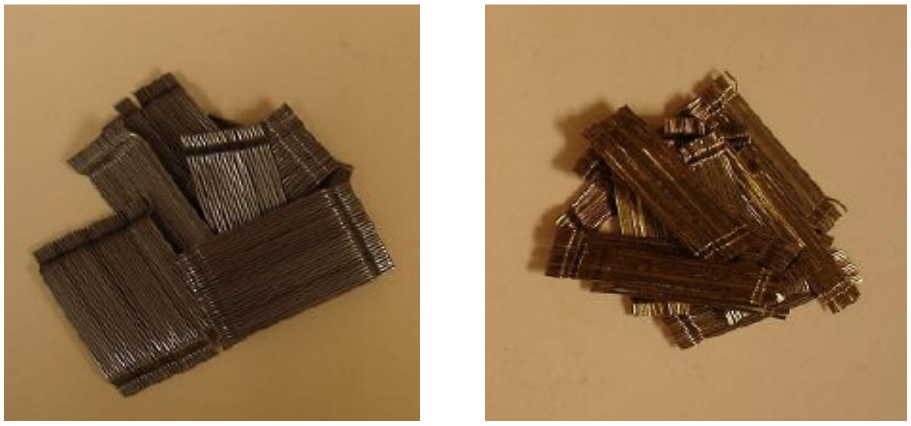

(a) Dramix ZP305 (normal strength) (b) Dramix BP80/30 (high strength)

Figure 3.4: Dramix hooked-end steel fibers used in this study

3.3.3Concrete

The concrete for all beam specimens was produced at the University of Ottawa's Pomerleau Concrete Laboratory. As discussed earlier, three types of self-consolidating concrete (SCC) mixtures were used in this experimental program. KING self-consolidating concrete was used in eight of the tested specimens, while the last four beams were constructed using two different customized SCC mixtures.

3.3.3.1 KING-SCC Mix

The KING-SCC mix consisted of a pre-packaged, self-consolidating concrete mix with a specified strength of 50 MPa (MS Self-Consolidating Concrete, KING Packaged Materials

Company). The mix contained a maximum aggregate size of 10 mm with a sand-to-aggregate ratio of approximately 0.55 and a water-cement ratio of approximately 0.42. An air-entraining admixture, a superplasticizer and a viscosity modifying admixture (VMA) are incorporated into the mix in the form of dry powder. **Table 3.4** lists the composition of this concrete as specified by the manufacturer. As mentioned in Chapter Two, SCC can be used to reduce the potential of low workability when high percentage of fibers are added (typically at fiber contents greater than 1.0%) and facilitate the placement of concrete. This mix was utilized in eight of the specimens used in the experimental program. The first "control" batch contained no fibers, while the fiber contents of the remaining batches ranged from 0.0% to 1.5% and included two fiber types (Dramix ZP305 and BP80/30).

Table 3.4: Self-Consolidating Concrete composition

Component	Content
HSF Cement	500 (kg/m^3)
Water-cement ratio	0.42
Coarse Aggregate	765 (kg/m^3)
Fine aggregate	915 (kg/m^3)
Ratio Fine/Total Aggregate	0.55
Mass Density	2300 (kg/m^3)
Air Content	7 (%)

3.3.3.2 Customized SCC Mixtures

The last four beams in this experimental program where constructed using two different customized SCC mixtures. The objective was to produce a regular-strength SCFRC mixture with good workability at high fiber contents (1.0% and above). This was accomplished by limiting coarse aggregate size, using cement with mineral admixtures (Fly Ash) and the use of chemical admixtures (superplasticizer & viscosity-modifying agent).

Both mixtures contained Type 10 cement and class C fly ash. The coarse aggregate size was limited to 12 mm while silica sand was used as fine aggregate. In addition, a superplastizer

(ADVA CAST 575) and viscosity modifying admixture (V-MAR 3) were used in order to improve workability and prevent segregation. The mix proportions were selected using a series of trial batches and were based on an extensive review of mixtures proposed by other researchers. Both mixtures incorporate normal-strength hooked-end steel fibers (Dramix ZP305) at fiber contents that varied from 1.0% to 1.5%. **Table 3.5** summarizes the composition of both customized mixtures.

Table 3.5: Properties of customized SCC mixtures

Component	**Content (Mix A)**	**Content (Mix B)**
Cement	473 (kg/m^3)	350 (kg/m^3)
Fly Ash	238 (kg/m^3)	307 (kg/m^3)
Water-cement ratio	0.33	0.36
Coarse Aggregate	439 (kg/m^3)	439 (kg/m^3)
Fine Aggregates (silica)	806 (kg/m^3)	876 (kg/m^3)
Mass Density	2400 (kg/m^3)	2400 (kg/m^3)
Superplastizer* *ADVA CAST 575* *GRACE Concrete Products*	292 ml/100 kg	380 ml/100 kg
Viscosity modifying admixture * *V-MAR 3* *GRACE Concrete Products*	52.8 ml/100 kg	76 ml/100 kg
Steel Fiber	(1.0-1.5)%	(1.0-1.5)%

*Superplastizer and VMA quantities are measured per 100 kg of cementitious materials

3.4 Mixing and Casting of concrete

3.4.1 Effect of mixer type

Different mixers were used in the study to assess the effect of mixer type on the fresh-state properties of the mixes (see **Figure 3.5**). The first type of mixer was a portable gas-powered rotating drum mixer. The mixing action in this type of mixer was provided by small ledges on the interior of the drum that would lift the material to a certain point, and then allow it to be dropped to the base of the drum. However, the efficiency of this mixer was limited due to

its slower mixing rate (≈30rpm) and its smaller mix capacity. Although this mixer type was found adequate for the KING SCC mix even at higher fiber contents, it was much less effective in mixing the customized SCC mixtures in this study. The second mixer was a 420 volt electric multiflow pan mixer that uses 3 fixed paddle blades that are arranged in such a way as to create a forced mixing action as the pan revolves at high velocity. A side scraper blade is also used to ensure that material does not build up on the side of the pan. When working properly, this mixer was the ideal mixer for both the KING and customized SCC mixtures due to its ability to force material at high velocity into defined flow path and resulted in an excellent distribution of steel fibers, and excellent mix uniformity.

(a) Drum Mixer (b) Pan Mixer

Figure 3.5: Concrete Mixers used in the experimental program

3.4.2 Mixing procedure

The KING-SCC mix was prepared by adding the designed amount of prepackaged materials to the mixer and pouring the water in several stages (dry-mixing for 30 seconds, adding half of the mix water and mixing for 1 minute, adding the remaining water in 4 steps at 60 second intervals). After the initial SCC mixing steps, steel fibers were added gradually and mixed until uniform distribution was attained.

The customized SCC mixtures were essentially prepared by adapting the mixing procedure proposed by Liao et al. (2006). Initially, the dry mix (cement, fly ash, silica sand) was

thrown into the mixer and the materials were mixed for 30 seconds. Thereafter half of the liquid (water pre-mixed with the chemical admixtures) was poured into the mixer and mixing continued for 1 minute. Subsequently half of the remaining amount of liquid was added in 4 steps at 60 second intervals. This was followed by the addition of the coarse aggregates and two minutes of mixing. The steel fibers were then added gradually to the mixture and after all fibers were added, mixing continued for 2 minutes to ensure uniform fiber distribution. It is noted that following the proposed sequence in mixing was crucial in order to achieve the desired workability in both mix types.

3.4.3 Casting and Curing

At the time of casting the specimens in this experimental program the Pan mixer was initially not available. As such all the beams which contained the KING-SCC mix were cast using a pair of gas-powered rotating drum mixers (see **Figure 3.5 (a)**). The last four specimens which contained the customized SCC mixtures were cast using a Pan mixer (see **Figure 3.5 (b)**).

The mix procedures detailed in the previous section were used to mix the concrete used in all the specimens. After mixing, concrete was poured directly into wooden forms (see **Figure 3.6**) layer by layer. Vibration was required in the case of using high strength and/or high percentage of fibers (1% and above) to ensure proper concrete consolidation. At the end of casting, the concrete surface was leveled in order to obtain a fairly smooth surface.

After completion of casting, all beam specimens were cured and covered with plastic sheets and a layer of moist burlap. Curing of the beams continued for seven days and then they were demolded and air-cured in the laboratory until the day of testing.

Figure 3.6: The form work used to cast all the beam specimens

3.4.4 Fresh-State Concrete Properties

As mentioned in Chapter Two, SCC in the fresh state should maintain fair workability and segregation resistance. Workability was examined using the slump flow test, whereas visual inspection was used to observe if segregation occurred. The slump flow test was carried out for each mixed batch. The diameter of the spread concrete was measured in two perpendicular directions and recorded as slump flow. **Figure 3.7** lists measured slump flow diameters for each batch associated with the type of concrete and the steel fibers properties used in each mixture. It is noted many factors govern the flowability of SCFRC such as the concrete type, aggregate size, and steel fiber properties. In this study the type and the content of steel fibers were the driving parameters affecting workability as observed in the slump flow test results. As expected, increasing the fiber content reduced the workability of the KING-SCC mix. Results from a previous test series using the same concrete mix indicated that the 1.5% fiber content is an upper limit for a semi-workable self-consolidating mix (Aoude et al., 2009). In this test series, although self-consolidation was no longer possible at a fiber content of 1% ZP305 fibers, the mix was sufficiently workable. During casting of the specimens no vibration was required at a fiber content of 0.5% or 0.75%, while slight vibration with a small 25 mm (1 in.) vibrator was requiring at a fiber content of 1%. The flowability was also significantly influenced by fiber type, with recorded slump flow values declining in the case of using steel fiber with larger aspect ratio (L_f /D_f) such in case of Dramix BP 80/30. For example while good workability was attained when normal strength fibers were used at moderate fiber contents, the use of 0.75% of high-strength fibers significantly reduced workability owing to the higher aspect ratio of this fiber, and required vibration during casting (some segregation was observed for this mix). Observations made during this test program indicate that a fiber content of 0.5-0.75% BP80/30 may be an upper limit for the mix used in this study. Similar workability results were observed for the customized SCC mixtures, and although slump flows were reduced, placement of these mixtures was quite improved based on visual inspection during casting.

Slump Flow Photos			
Mix[Fiber Type]	SCC-0.0%	SCC-0.5% [ZP305]	SCC-1.0% [ZP305]
slump flow(mm)	600	530	485
Slump Flow Photos			
Mix[Fiber Type]	SCC-1.5% [ZP305]	SCC-0.5H% [BP80/30]	SCC-0.75H%[BP80/30]
slump flow(mm)	460	440	410
Slump Flow Photos			
Mix[Fiber Type]	SCC-0.75% [ZP305] *	SCC-1.0% [ZP305] *	Custom.1.0%A [ZP305]
slump flow(mm)	525	495	440
Slump Flow Photos			
Mix[Fiber Type]	Custom.1.0%B [ZP305]	Custom.1.5%A [ZP305]	Custom.1.5%B [ZP305]
slump flow(mm)	450	360	400

*Two beams in the second series in which two 20M steel reinforcing bars were used

Figure 3.7: Slump Flow Properties

3.4.4 Hardened- State Concrete Properties

A series of lab cured cylinders and flexural beams were prepared during the mixing of the concrete. Three cylinders, taken from each batch were tested to determine the concrete properties used in the beams. The concrete compressive strengths were obtained by testing standard cylinders having a diameter of 100 mm and a height of 200 mm at the day of testing (see **Table 3.6**). The cylinders were tested using a hydraulic pressure machine located at the University of Ottawa Structures Laboratory (see **Figure 3.8 (a)**). Another series of compressive strength tests were carried out on a similar set of cylinders to plot the full stress-strain relationship of SCFRC material under compression. The second series was tested by a hydraulic pressure machine (MTS) located at the Jamieson Structures Laboratory at McGill University (see **Figure 3.8 (b)**). The stress-strain plots are shown in the left side of **Figures 3.9** and **3.10**. As expected increasing the fiber content improves the post-peak behaviour and ductility observed in the stress-strain responses.

As elaborated in Chapter Two, steel fibers are mainly used to enhance concrete toughness properties, and several methods to estimate this toughness were described in the Literature review. In this experimental program the third-point bending test method described in ASTM C1609 was used. The flexural toughness tests were conducted on specimens which were 100 mm by 100 mm by 400 mm in size and were subjected to third point loading over a span of 300 mm (see **Figure 3.8 (c)**). The rate of loading was 0.2 mm/min and the test was conducted with a hydraulic pressure machine (MTS) located at the University of Ottawa Structures Laboratory. Full load-deflection relationships for each specimen are presented in the right side of **Figures 3.9** and **3.10**. As expected, one can see that the addition of fibers has significantly improved toughness properties, which could be clearly noted by the significant improvement in the post-peak stage of the SCFRC specimen responses. It is also noted that the deflection-hardening behaviour is observed at a fiber content of 1.5% for both the KING SCC and customized SCC mixtures.

A full analysis of the results was performed using toughness parameters defined in ASTM C1609 and JSCE SF-4 standards (see **Table 3.7**).

Table 3.6: Concrete Properties

Concrete Type	Fiber type	Fiber Content, (V_f) %	Compressive strength at day of testing, f'_{co}(MPa)	Modulus of Rupture, f_r(MPa)
SCC	-	0	51.94	5.93
SCC	ZP305	0.50	59.43	7.02
SCC	ZP305	1.00	51.52	6.72
SCC	ZP305	1.50	55.78	7.70
SCC	BP 80/30	0.50	49.56	6.46
SCC	BP 80/30	0.75	45.94	5.74
SCC*	ZP305	0.75	44.70	6.96
SCC*	ZP305	1.00	45.00	6.72
Customized (A)	ZP305	1.00	54.49	8.45
Customized (B)	ZP305	1.00	52.58	8.22
Customized (A)	ZP305	1.50	50.51	7.25
Customized (B)	ZP305	1.50	51.54	7.28

*SCC beams in the second series in which two 20M steel reinforcing bars were used

(a) Cylinder testing machine located at uOttawa Laboratory

(b) Cylinder testing machine located at McGill University

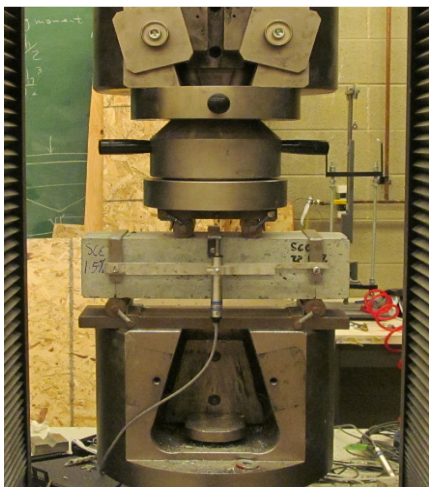

(c) Flexural beam testing machine located at uOttawa Laboratory

Figure 3.8: Hydraulic pressure machines used to test concrete cylinders and flexural beams

Table 3.7: Flexural toughness parameter according to the ASTM C1609 and JSCE SF-4 standards

Mixture Name	ASTM C1609											JSCE SF-4
	P_1	δ_1	P_p	δ_p	f_1	f_p	P_{600}	f_{600}	P_{150}	f_{150}	T_{150}	FT
KING-SCC 0.0%	-	-	19.39	-	-	5.93	-	-	-	-	-	-
KING-SCC 0.5%	-	-	23.88	0.068	-	7.02	17.21	5.06	5.70	1.68	23.40	0.003
KING-SCC 1.0%	-	-	23.08	0.07	-	6.72	18.06	5.26	8.88	2.59	27.23	0.004
KING-SCC 1.5%	20.38	0.05	25.68	0.208	6.11	7.70	0.49	0.15	15.58	4.67	40.44	0.006
KING-SCC 0.5%H	21.97	0.05	20.02	1.28	6.46	5.89	17.8	5.24	18.93	5.57	37.68	0.005
KING-SCC 0.75%H	19.14	0.07	19.07	0.48	5.74	5.72	19.07	5.72	13.99	4.20	32.18	0.005
Custom-SCC 1.0%A	16.35	0.06	28.18	0.577	4.91	8.45	27.35	8.21	20.47	6.14	48.43	0.007
Custom-SCC 1.0%B	24.77	0.23	27.94	0.42	7.29	8.22	24.54	7.22	12.70	3.74	40.13	0.006
Custom-SCC 1.5%A	20	0.18	25.14	0.836	5.77	7.25	23.09	6.66	20.51	5.92	44.47	0.006
Custom-SCC 1.5%B	16.94	0.05	24.52	0.385	5.03	7.28	21.61	6.42	16.31	4.84	39.64	0.006

L = Span Length (300 mm), (L/600 = 0.5, L/150 =2)
P_1= First-Peak Load (kN)
δ_1= Net Deflection at First-Peak Load (mm)
P_p= Peak Load (kN)
δ_p= Net Deflection at Peak Load (mm)
f_1= First-Peak Strength (MPa)
f_p= Peak Strength (MPa)
P_{600}= Residual Load at net deflection of L/600 (kN)
f_{600}= Residual Strength at net deflection of L/600 (MPa)
P_{150}= Residual Load at net deflection of L/150 (kN)
F_{150}= Residual Strength at net deflection of L/150 (MPa)
T_{150}= Area under load vs. net deflection curve (0 to L/150)
FT = Flexural Toughness Factor = $(T_{150}*L)/(L/150 *b*d^2)$

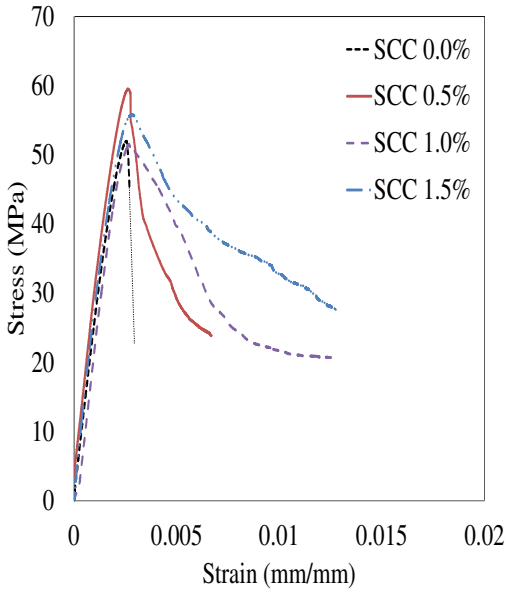

(a) Comparison of stress-strain realtionships which reflects the effect of fiber content

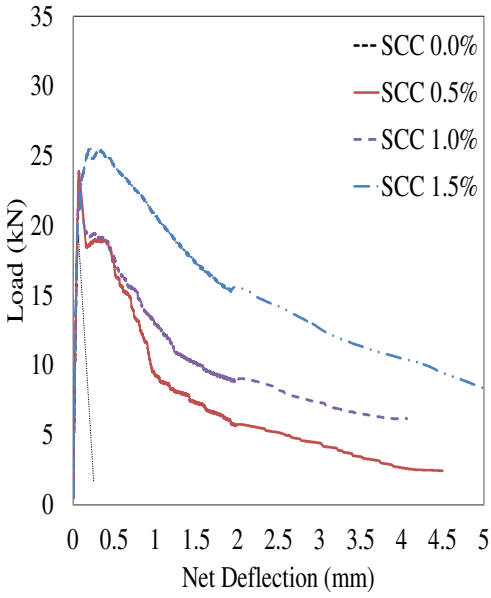

(b) Flexural beam load-deflection curves

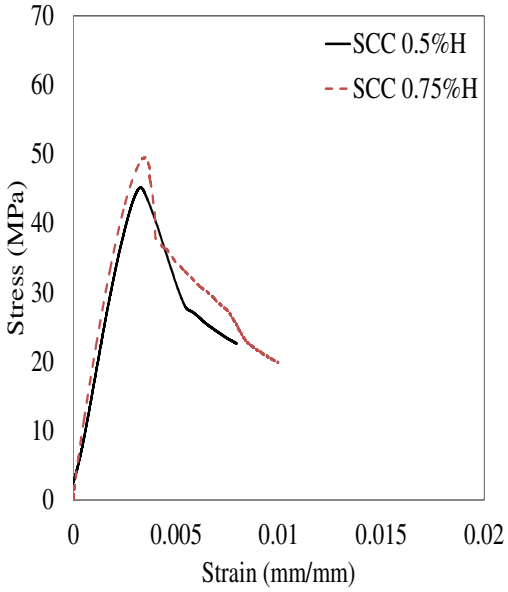

(c) Comparison of stress-strain realtionships which reflects the effect of fiber type

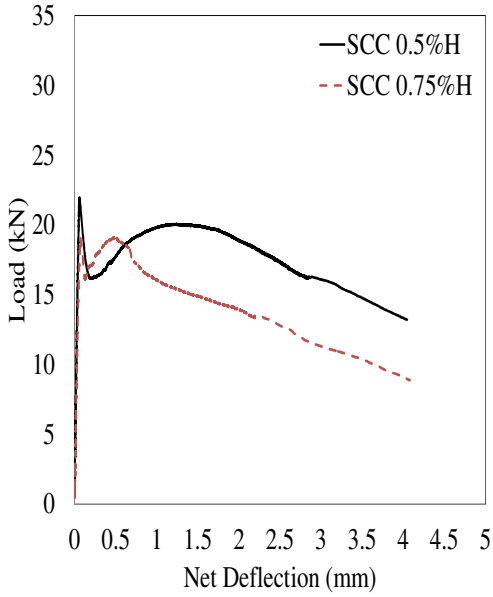

(d) Flexural beam load-deflection curves

Figure 3.9: Results from compression tests & toughness tests for the KING-SCC mix

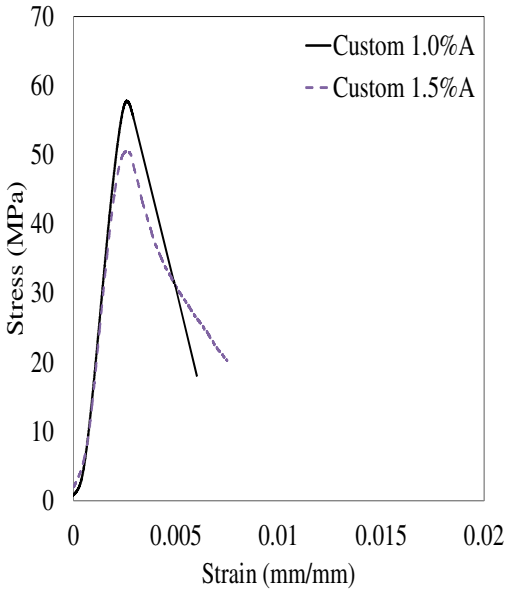

(a) Comparison of stress-strain realtionships of the customized concrete type A

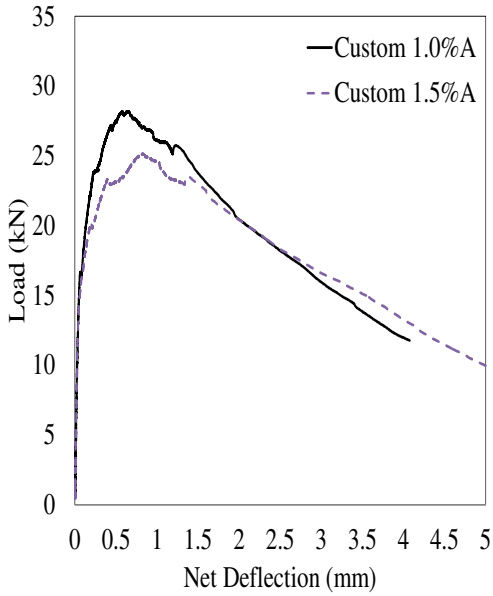

(b) Flexural beam load-deflection curves

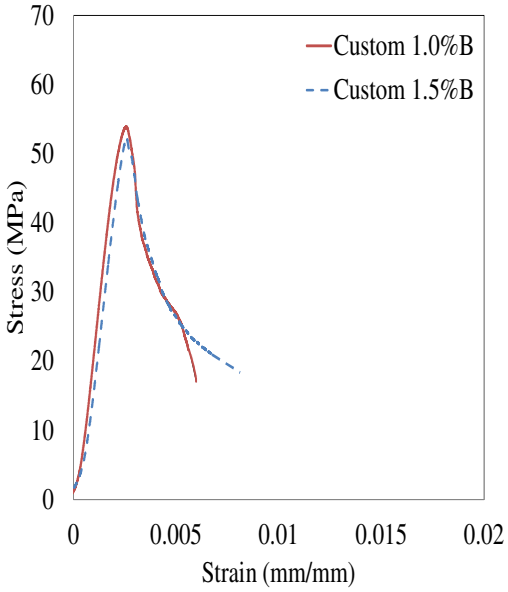

(c) Comparison of stress-strain realtionships of the customized concrete type B

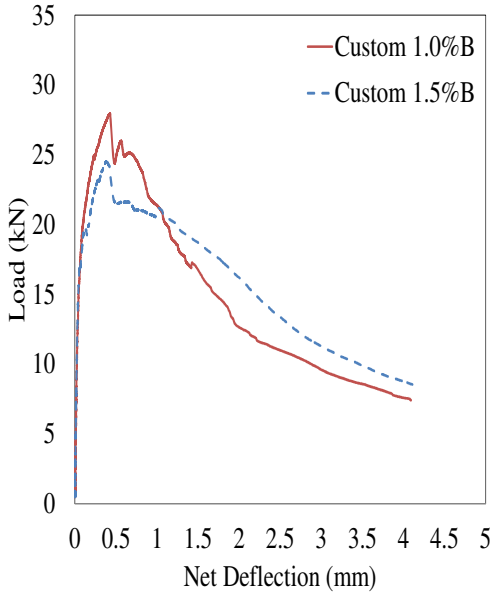

(d) Flexural beam load-deflection curves

Figure 3.10: Results from compression tests & toughness tests for customized mixes

3.4.5 Load setup and Instrumentation

The setup shown in **Figure 3.11** was used to test all of the beam specimens monotonically under four-point bending load. All the beams were simply supported over a length of 2400 mm and subjected to two central loads, spaced 800 mm apart, to ensure a constant moment region in the middle of the beam. The shear span was 800 mm (resulting in shear span-to-effective depth ratio *a/d*, of approximately 3.8). The loading was applied by a hydraulic jack, mounted on a circular load cell, and both rested on a small rigid steel assembly in order to obtain a uniform load transfer to the beam. The load and support details are shown in **Figure 3.12**.

The tensile strains in steel reinforcement were monitored using electrical resistance strain gages, glued to one reinforcing bar in each specimen. These gages were located in the midspan and at the point-load locations. Beam deflections were recorded at midspan and the two point-load positions using three displacement cable transducers (DCT). **Figure 3.13** shows the locations of the tensile strain gages attached to the steel bar, and the position of the DCT's. The load cell, the three strain gage wires and the three DCT's were hooked to a data acquisition system programmed to record loading and deformation readings.

3.4.6 Testing Sequence

All the specimens were subjected to the same loading sequence. Initially the specimens were tested under load-control and an interval of 2.5 kN was left between load stages. The load interval was increased to 5 kN once the load reached 15 kN (corresponding to a shear, V, of 7.5 kN) and testing continued until failure in shear or the onset of yielding. After yielding, loading was switched to deflection-control (with 5 mm left in between load stages) and continued until the load dropped below 85% of the peak value or when the maximum deflection reached 70 mm, which represented the travel capacity of the loading apparatus.

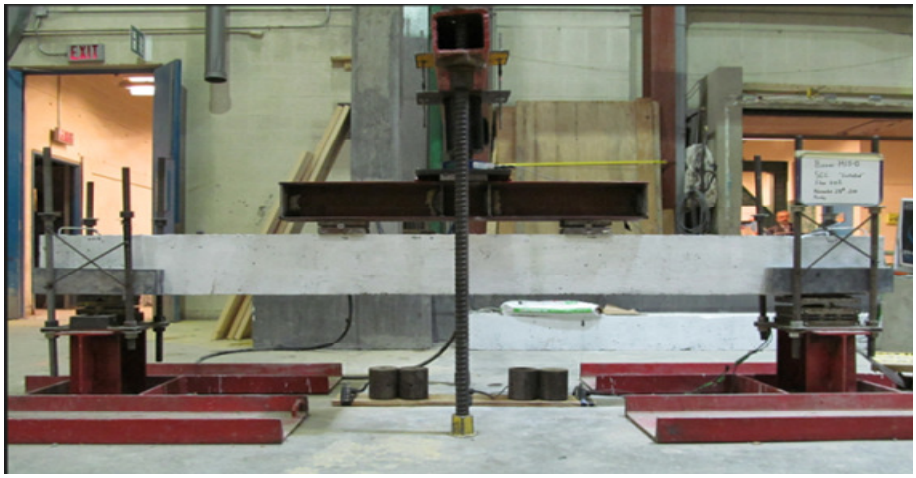

Figure 3.11: Beam specimen just prior to testing

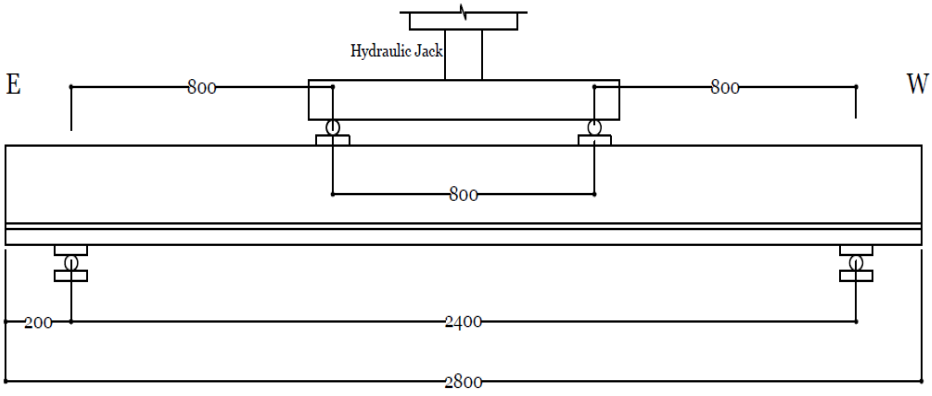

Figure 3.12: Loading device and support details

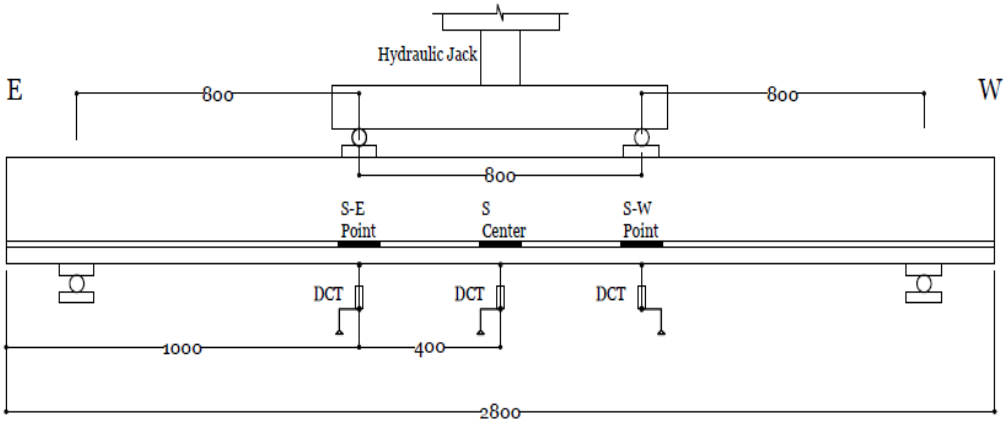

Figure 3.13: Locations of the strain gages and the DCTs

Chapter Four: Results of the Experimental Program

4.1 Introduction

In this chapter the behaviour of the twelve beams tested in the experimental program is discussed. The results of each specimen in terms of shear load-deflection response, reinforcement strains, cracking behaviour, major events during testing and failure modes are presented. All the specimens were subjected to the same loading sequence. Initially loading was applied under "load control", with intervals of 2.5 & 5 kN between stages. This mode of testing continued until shear failure or the onset of flexural yielding at which point loading was switched to "deflection control", with 5 mm between stages. Testing continued until the load dropped below 85% of the peak value or when the maximum deflection reached 70 mm. While this chapter presents the detailed response of each beam, the results are compared and discussed in Chapter 5.

4.1.1 Beam M15-0.0%

This specimen was the first beam to be tested in the KING-M15 series. The beam was the "controlled" specimen in this series and was constructed with a traditional self-consolidating concrete (SCC), and contained neither steel fibers nor transverse shear reinforcement.

The first hairline cracks in the form of flexural cracks occurred at an applied load of approximately 12.53 kN (V = 6.27 kN) and occurred at the center of the beam in the constant moment region. As the load increased, flexural cracks started to propagate outside the constant moment region. The first flexural-shear crack took place on the east shear span of the beam at load of 35.24 kN (V = 17.62 kN). Thereafter, further flexural-cracks were

observed on the west shear span of the beam at load of 55.25 kN (V = 27.63 kN). At a load of approximately 59.7 kN (V = 29.35 kN) a sudden shear crack formed on the west side of the beam and was immediately followed by a brittle shear failure with a sudden loss in load carrying capacity. **Figure 4.1 (a)** shows a plot of the shear load that was applied to the specimen versus the corresponding mid-span deflection. The maximum deflection recorded in the mid span of the beam just before failure was 10.77 mm. **Figure 4.1 (b)** shows a plot of the measured strains in the steel reinforcement. It is noted that the steel didn't exhibit any yielding. As expected, the brittle failure occurred well before the flexural capacity could be reached due to the lack of transverse shear reinforcement in this specimen. **Figures 4.1 (c) & (d)** show the growth of shear and flexural crack widths as a function of load. The maximum flexural crack width prior to failure was 0.3 mm. It is noted that the crack that caused failure occurred suddenly and without warning. The major events are summarized in **Figure 4.2**.

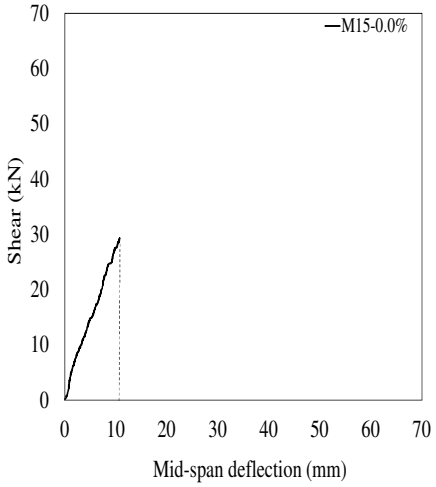

(a) Shear load versus mid span deflection

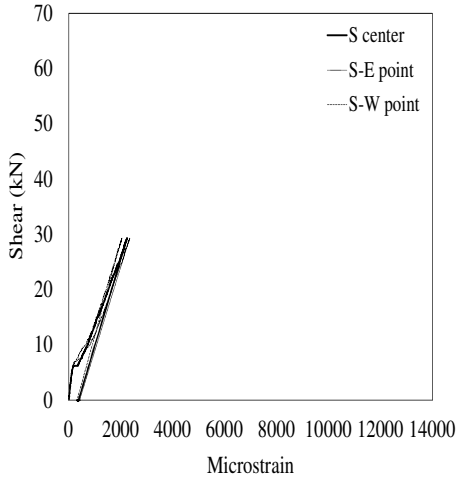

(b) Tensile strains in longitudinal steel bars

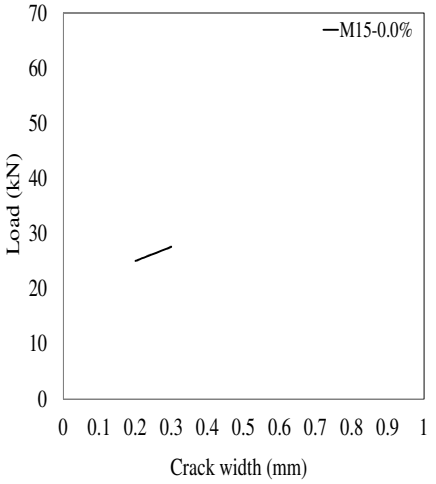

(c) Maximum crack width (shear)

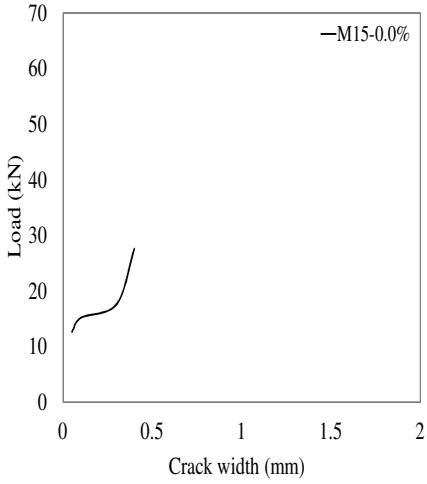

(d) Maximum crack width (flexure)

Figure 4.1: Experimental results for Beam M15-0.0%

Load stage	V (kN)	Mid-span Δ (mm)	
L5	6.27	1.63	- First hairline cracks appear in the constant moment region
			
Load stage	V (kN)	Mid-span Δ (mm)	
L7	10	3.26	- First cracks appear outside the constant moment region
			
Load stage	V (kN)	Mid-span Δ (mm)	
L9	15.2	5.39	- Cracks at the center propagate and reach 0.2 mm in width
			
Load stage	V (kN)	Mid-span Δ (mm)	
L10	17.6	6.40	- Flexural-shear crack beginning to form on the E-side of the beam
			
Load stage	V (kN)	Mid-span Δ (mm)	
L14	27.63	9.96	- Flexural-shear crack beginning to form on the W-side of the beam - Cracks at the center reach 0.3 mm in width
			
Load stage	V (kN)	Mid-span Δ (mm)	
Failure	29.35	10.77	- Specimen fails: brittle shear failure on the W-side of the beam
			

Figure 4.2: Major events for specimen M15-0.0%

4.1.2 Beam M15-0.5%

This beam had identical properties to the previous specimen with the exception of addition of steel fibers at a fiber content of 0.5% by volume of concrete. The fibers used in this beam were Dramix ZP305, normal strength hooked-end steel fibers. The objective of adding this quantity of fibers was to study the effect on ultimate shear capacity and to examine the potential enhancement in crack control.

The same loading sequence used in the testing of Specimen M15-0.0% was used in the testing of this specimen. The first hairline crack was observed in the middle of the beam at a load of 12.55 kN (V = 6.27 kN). Multiple flexural cracks formed outside the constant moment region at load of 30.16 kN (V = 15.08 kN). At load of 40 kN (V = 20 kN) a flexural-shear crack started to develop on the east shear span of the beam. As loading continued another flexural-shear crack appeared on the west shear span of the beam when the load reached 75.26 kN (V = 37.63 kN). The east side flexural-shear crack eventually developed into a shear crack which led to a brittle shear failure at a load of 86.66 kN (V = 43.33 kN) and corresponding mid-span deflection of 17.85 mm.

Figure 4.3 (a) shows a plot of the shear load that was applied to the specimen versus mid-span deflection. **Figure 4.3 (b)** shows the measured strains in the longitudinal steel reinforcement, with failure occurring prior to the yielding due to the brittle shear response. Due to the presence of fibers, the ultimate shear capacity of this specimen was increased by 47% when compared to the control specimen. However, the quantity of fibers used in this beam wasn't sufficient to transform the shear failure into a ductile flexural response.

The maximum flexural crack width was 0.4 mm before failure, and the largest diagonal crack width was also 0.4 mm (see **Figures 4.3 (c) & (d)**). The major events during testing are summarized in **Figure 4.4**.

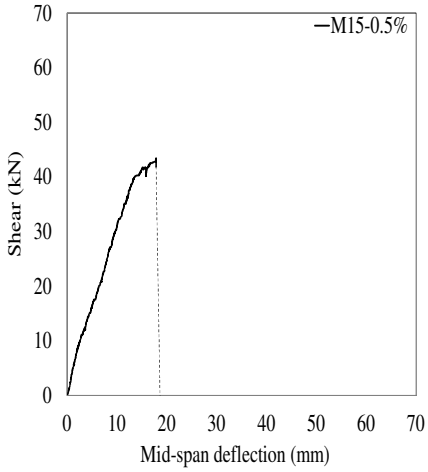

(a) Shear load versus mid span deflection

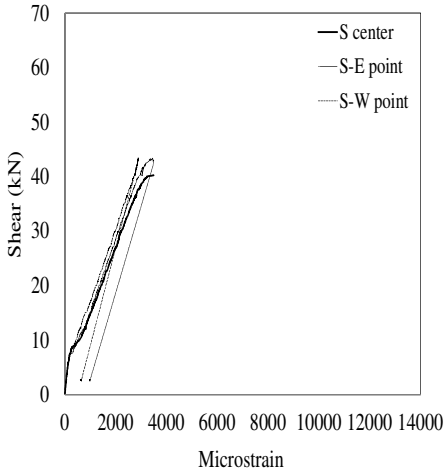

(b) Tensile strains in longitudinal steel bars

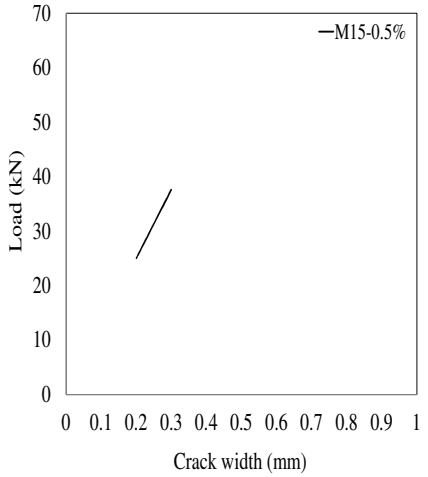

(c) Maximum crack width (shear)

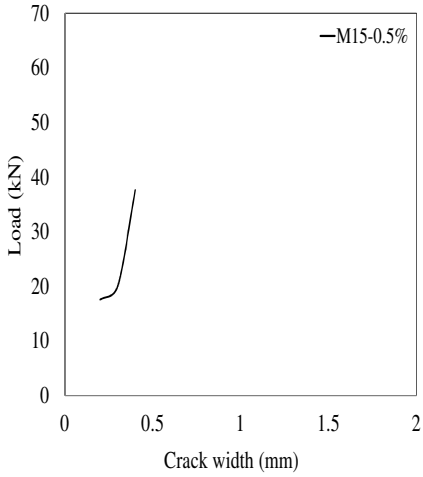

(d) Maximum crack width (flexure)

Figure 4.3: Experimental results for Beam M15-0.5%

Load stage	V (kN)	Mid-span Δ (mm)	
L5	6.27	1.51	- First hairline cracks appear in the constant moment region
			
Load stage	V (kN)	Mid-span Δ (mm)	
L9	15.08	4.47	- First cracks appears outside the constant moment region
			
Load stage	V (kN)	Mid-span Δ (mm)	
L11	20	6.41	- Flexural-shear crack beginning to form on the E-side of the beam - Crack at the center become 0.3 mm wide
			
Load stage	V (kN)	Mid-span Δ (mm)	
L18	37.63	12.42	- Flexural-shear crack beginning to form on the W-side of the beam
			
Load stage	V (kN)	Mid-span Δ (mm)	
L20	42.52	16.8	- Shear crack suddenly forms on the W-side of the beam
			
Load stage	V (kN)	Mid-span Δ (mm)	
Failure	43.33	17.85	- Specimen fails: brittle shear failure on the E-side of the beam
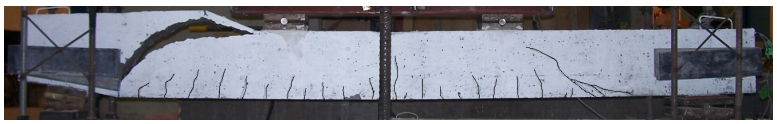			

Figure 4.4: Major events for specimen M15-0.5%

4.1.3 Beam M15-1.0%

This specimen was built in the same manner as beam M15-0.0% but included steel fibers at a fiber content of 1.0% by volume of concrete. In addition to improving the shear capacity of the beam and crack control, it was expected that this fiber content would be sufficient to transform the failure mechanism of the specimen from a brittle shear failure to a ductile flexural failure.

The same loading sequence used in the previous beams was followed in testing this specimen. The first hairline crack formed at load of 15.10 kN (V = 7.55 kN) in the constant moment region. It is noted that the load required to cause first cracking was slightly higher than that observed in the control specimen. When the load reached 50.06 kN (V = 25.03 kN), in addition to the formation of new flexural cracks outside the middle region, a flexural-shear crack began to form on the west shear span of the beam. For the east shear span, the first flexural-shear cracks started to appear at load of 70.48 kN (V = 35.24 kN). With further loading, "forking" cracks (secondary cracks growing out of primary cracks) began to develop in the tensile face of the member. This was followed by the sudden appearance of a diagonal shear crack on the east shear span of the beam at a load of 90.16 kN (V = 45.08 kN). Despite the occurrence of the shear crack, the crack was controlled and there was no observed drop in load carrying capacity. This can be attributed to the improvement in diagonal tension capacity provided by this quantity of steel fibers. The increased shear capacity allowed the beam to reach its full flexural strength, with associated yielding of the longitudinal reinforcement. After yielding occurred, testing continued under deflection control. As the mid-span deflection increased the concrete in the compression zone started to show signs of crushing when the load approached 91.78 kN (V = 45.89 kN). Subsequently, crushing of concrete continued and when the deflection at mid-span reached 41 mm the load started to drop steadily (maximum sustained load was 96 kN, V = 48 kN). Testing was stopped when the capacity of the beam dropped to 85% of peak resistance at a mid-span deflection of 55.12 mm. **Figure 4.5 (a)** shows a plot of the shear load that was applied to the specimen versus the mid-span deflection. **Figure 4.5 (b)** shows the measured strains in the longitudinal steel reinforcement. The largest shear crack width was 0.4 mm, while the flexural cracks in the

center of the beam exceeded 4.0 mm (see **Figure 4.5 (c) & (d)**). **Figure 4.6** summarizes all the major events that occurred during the test.

The major observation in this test is that addition of 1.0% steel fibers resulted in an increase in shear capacity, and transformed the brittle shear failure observed in the control specimen (and Beam M15-0.5%) into a ductile flexural response. The flexural failure allowed the specimen to carry large deflections prior to failure with the recorded maximum deflection corresponding to approximately four times that carried by Beam M15-0.5%.

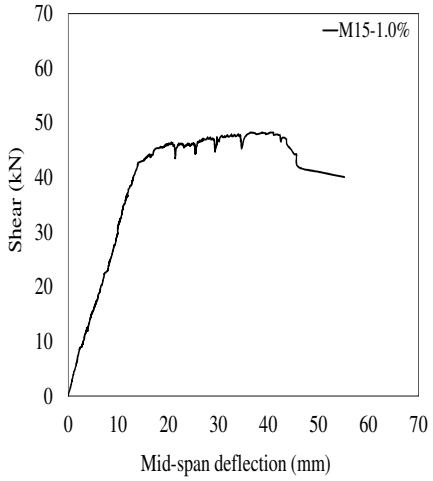

(a) Shear load versus mid span deflection

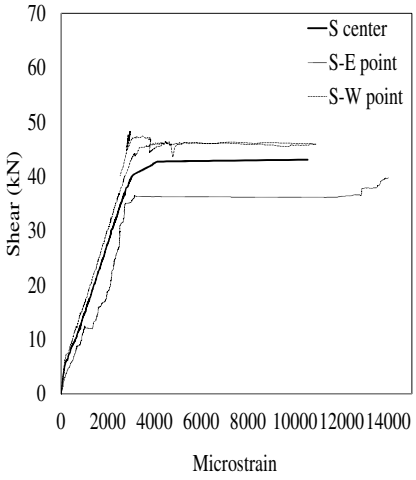

(b) Tensile strains in longitudinal steel bars

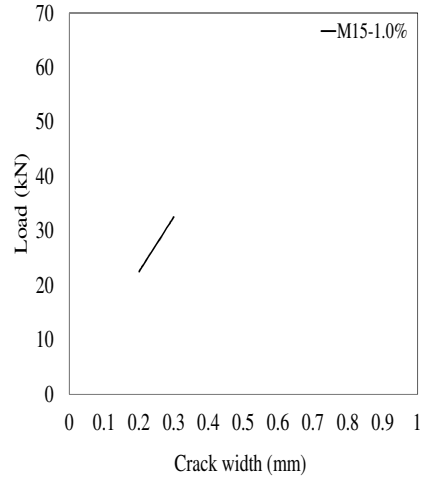

(c) Maximum crack width (shear)

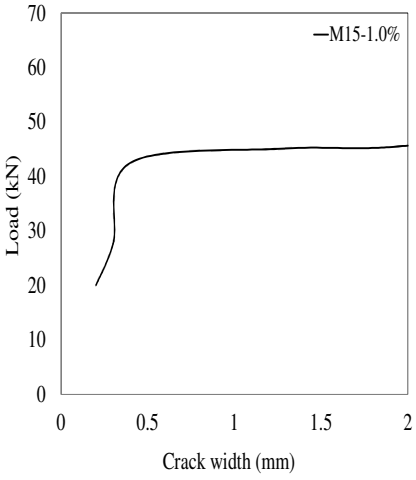

(d) Maximum crack width (flexure)

Figure 4.5: Experimental results for Beam M15-1.0%

Load stage	V (kN)	Mid-span Δ (mm)	
L7	10.11	2.99	- First hairline cracks appear in the constant moment region
			
Load stage	V (kN)	Mid-span Δ (mm)	
L13	25.03	8.33	- Crack at the center become 0.2 mm wide - Flexural-shear crack beginning to form on the W-side of the beam
			
Load stage	V (kN)	Mid-span Δ (mm)	
L17	35.24	11.20	- Flexural-shear crack beginning to form on the E-side of the beam
			
Load stage	V (kN)	Mid-span Δ (mm)	
L21	45.08	17.17	- Forking cracks beginning to form - Web shear crack suddenly forms on the E-side of the beam
			
Load stage	V (kN)	Mid-span Δ (mm)	
L24	45.89	29.18	- Cracks at the center reach 2.0 mm in width - Signs of crushing on the compression side of the beam at mid-span
			
Load stage	V (kN)	Mid-span Δ (mm)	
Failure	40.8	55.12	- Flexural cracks (>4.0 mm) - Failure of specimen (capacity drops to 85% of peak value)
			

Figure 4.6: Major events for specimen M15-1.0%

4.1.4 Beam M15-1.5%

This beam was the fourth specimen in the M15-KING test series and contained 1.5% of normal-strength hooked-end fibers by volume of concrete. The main objective of testing this specimen was to study the enhancement in flexural capacity and crack control which could be gained from adding such an amount of steel fibers.

The first flexural crack appeared on the constant moment region of the beam at load of 15.18 kN (V = 7.59 kN). Soon thereafter, more flexural cracks developed outside the middle of the beam at load of 20.06 kN (V = 10.03 kN). Flexural-shear cracks started to occur in both the east and the west shear spans of the beam simultaneously when the load approached 35.45 kN (V = 17.73 kN). Prior to reaching the beam flexural capacity flexural cracks were propagating, whereas their widths remained relatively small (0.3 mm) due to the ability of this relatively high amount of steel fibers to control cracking. Once yielding occurred and the flexural capacity was reached, the loading was switched to deflection-control. With further loading, concrete started to exhibit crushing in the middle top portion of the beam when the deflection reached 25 mm at mid-span with a corresponding load of 92.18 kN (V = 46.09 kN) and. As testing continued the load started to drop and continued until the deflection at mid-span reached 70 mm as shown in **Figure 4.7 (a)** (it is noted that the beam capacity dropped near 85% of peak capacity at this load stage). The peak recorded load was 93.4 kN, corresponding to a shear load of 46.7 kN. **Figure 4.7 (b)** shows yielding of the longitudinal reinforcement strains as recorded by the gages.

As shown in **Figure 4.7 (c)**, the largest shear crack was 0.4 mm. The flexural cracks in at the center of the beam exceeded 5.0 mm in width at the end of testing (see **Figure 4.7 (d)**). This specimen showed a slight improvement in controlling cracks when compared to the previous specimen that failed in flexure (Beam M15-1.0%), thus the additional amount of fibers efficiently bridged the crack openings beyond the onset of flexural yielding. It is also noted that concrete crushing was better controlled in this specimen when compared to the specimen with 1.0% fibers. **Figure 4.8** shows a summary of the major events which took place during testing.

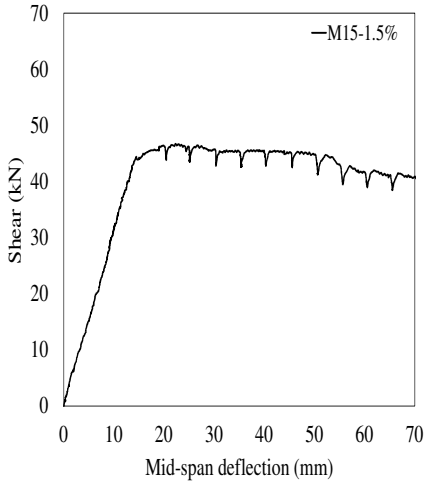

(a) Shear load versus mid span deflection

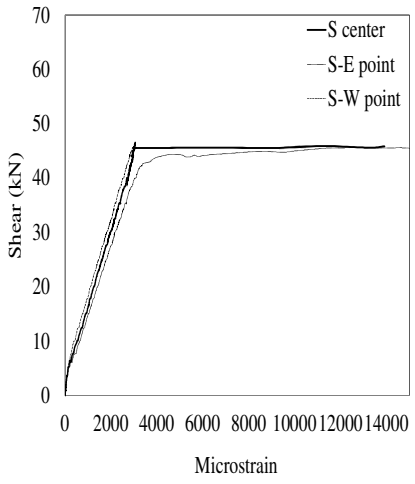

(b) Tensile strains in longitudinal steel bars

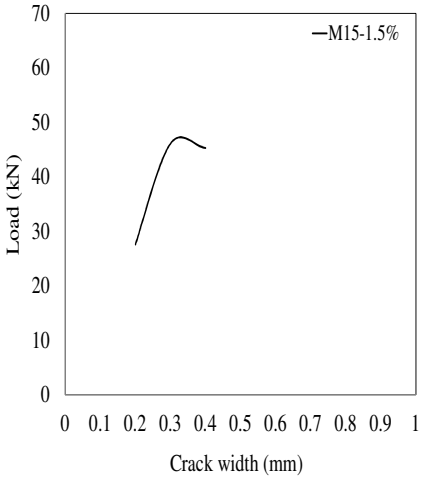

(c) Maximum crack width (shear)

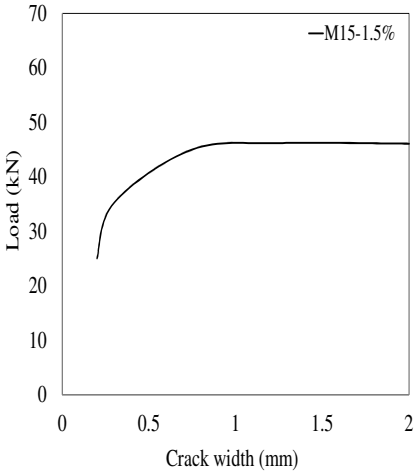

(d) Maximum crack width (flexure)

Figure 4.7: Experimental results for Beam M15-1.5%

Load stage	V (kN)	Mid-span Δ (mm)	
L6	7.59	2.29	- First hairline cracks appear in the constant moment region
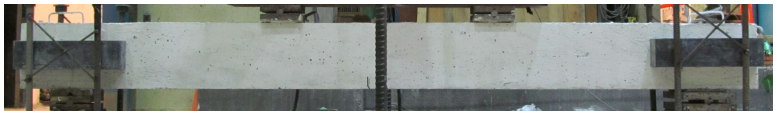			
Load stage	V (kN)	Mid-span Δ (mm)	
L7	10.03	3.14	- Flexural cracks start to form outside the middle region
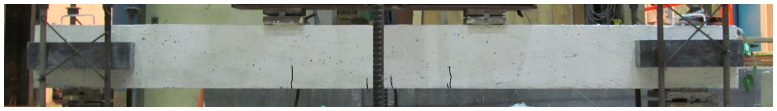			
Load stage	V (kN)	Mid-span Δ (mm)	
L10	17.73	5.7	- Flexural-shear crack beginning to form on the E-side & W-side of the beam
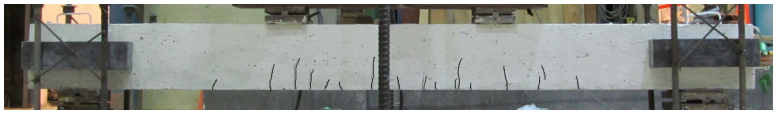			
Load stage	V (kN)	Mid-span Δ (mm)	
L17	35.31	11.09	- Extension of Flexural-shear crack - Cracks at the center reach 0.3 mm in width
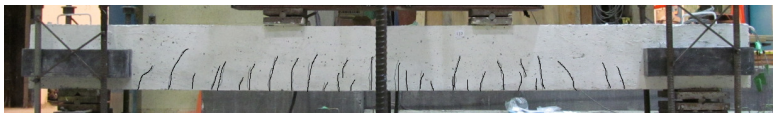			
Load stage	V (kN)	Mid-span Δ (mm)	
L22b	46.09	25	- Initiation of concrete crushing in compression zone - Forking cracks - Cracks at the middle reach 2.0 mm in width
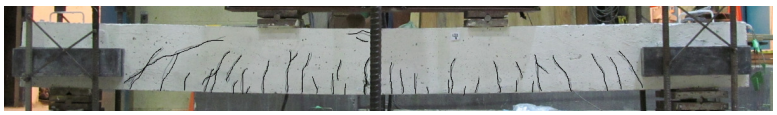			
Load stage	V (kN)	Mid-span Δ (mm)	
L27	44.80	50.20	- Further concrete crushing - Multiple cracking and slightly reduced spacings - Flexural cracks exceed 5.0 mm in width
			
Load stage	V (kN)	Mid-span Δ (mm)	
Failure	39.7	70.5	- Failure of specimen (capacity drops to 85% of peak value)
			

Figure 4.8: Major events for specimen M15-1.5%

4.1.5 Beam M15-0.5%H

The main new feature in this specimen in comparison to the previous specimens in the M15-KING series is the use of Dramix BP 80/30 fibers at a fiber content of 0.5%. To recall these fibers have higher tensile strength and a greater aspect ratio when compared to the Dramix ZP305 fibers used in the previous specimens. It is noted that while the use of this fiber caused a reduction in SCC workability in the fresh-state, the two aforementioned fiber properties were expected to lead to some improvement in member response in terms of shear capacity and crack control. To investigate the improvements in behaviour a comparison can be made between the response of this specimen and beam M15-0.5% which was reinforced with normal-strength Dramix ZP305 fibers.

Similar to the two previous SCFRC specimens in this test series, the first hairline crack formed at a load of 14.67 kN (V = 7.33 kN). When the load reached 20.04 kN (V = 10.02 kN) additional flexural cracks started to form outside the middle region of the beam. The first flexural-shear crack was seen on the east shear span of the beam at a load of 30.16 kN (V = 15.08 kN), and at the same stage some of flexural cracks had a width of 0.2 mm. As the applied load was increased, the flexural cracks started to widen until they reached 0.3 mm in width, along with the appearance of first flexural-shear crack on the west side of the beam at a load of 55.26 kN (V = 27.63 kN). A very visible web-shear crack formed on the west shear span of the beam at a load of 75.20 kN (V = 37.60 kN). Subsequently the specimen started to show some flexural response with significant deflections at mid-span. Nevertheless, the previously formed web-shear crack continued to increase in size with the beam failing in shear at a load of 90.35 kN (corresponding to shear load of 45.17 kN). The maximum deflection in the mid-span of the beam was 39.88 mm corresponding to more than 2.2 times the maximum deflection in Beam M15-0.5% (see **Figure 4.9 (a)**). It is noted that the gages attached to the longitudinal steel reinforcement did show some yielding before failure (see **Figure 4.9 (b)**). During testing, after the main shear crack formed it could be clearly seen that the fibers at the crack interface were bridging the crack. However as the loading continued the fibers eventually were pulled out and failure occurred resulting in a sudden loss in load carrying capacity. While the maximum flexural crack width was 0.3 mm at

failure, remarkably the largest shear crack before failure was over 1.0 mm in width which allowed for some warning prior to the brittle collapse of the beam (see **Figure 4.9 (c) & (d)**). The major events for this beam are summarized in **Figure 4.10**.

It can be concluded that the use of Dramix BP 80/30 fibers in this mixture has allowed the specimen to exhibit a more ductile response when compared to Beam M15-0.5% due to the enhanced fiber characteristics.

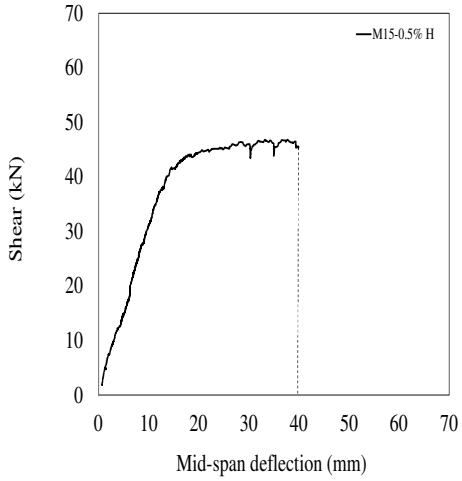

(a) Shear load versus mid span deflection

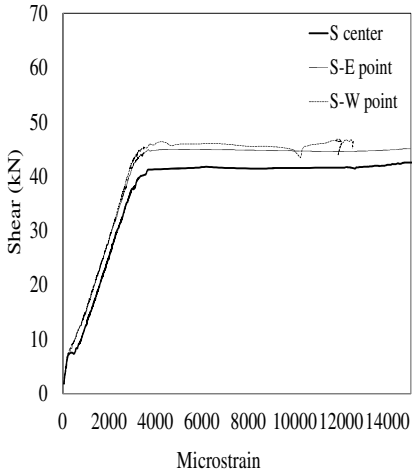

(b) Tensile strains in longitudinal steel bars

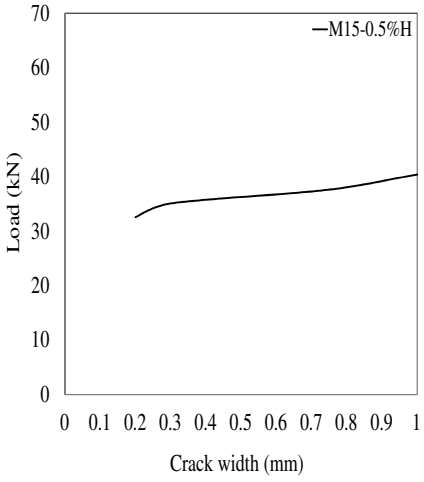

(c) Maximum crack width (shear)

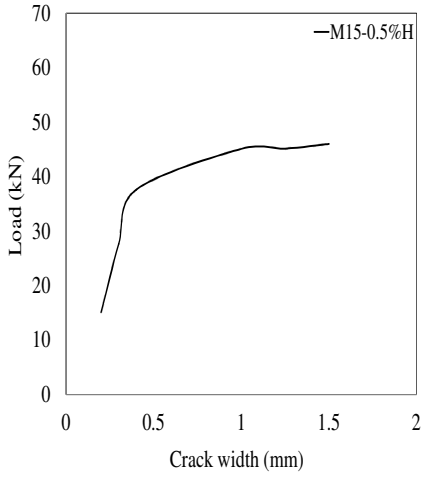

(d) Maximum crack width (flexure)

Figure 4.9: Experimental results for Beam M15-0.5%H

Load stage	V (kN)	Mid-span Δ (mm)	
L5	7.33	2.05	- First hairline cracks appear in the constant moment region
			
Load stage	V (kN)	Mid-span Δ (mm)	
L7	10.02	2.98	First cracks appears outside the constant moment region
			
Load stage	V (kN)	Mid-span Δ (mm)	- Flexural-shear crack beginning to form on the E-side of the beam - Flexural crack in the middle reaches 0.2 mm
L9	15.08	11.20	
			
Load stage	V (kN)	Mid-span Δ (mm)	- Flexural-shear crack starting to appear on the E-side of the beam - Flexural Cracks at the center are 0.3 mm wide
L14	27.63	8.68	
			
Load stage	V (kN)	Mid-span Δ (mm)	- Formation of web shear crack at the W-side of the beam - Some shear cracks become 1.0 mm wide
L18	37.60	12.36	
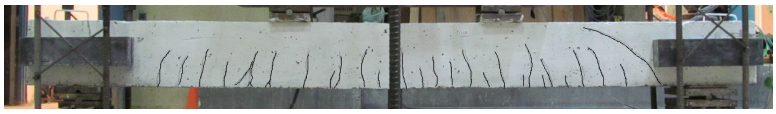			
Load stage	V (kN)	Mid-span Δ (mm)	- Brittle shear failure on the W-side of the beam
Failure	45.17	39.88	
			

Figure 4.10: Major events for specimen M15-0.5%H

4.1.6 Beam M15-0.75%H

As indicated in the previous test, the addition of 0.5% Dramix BP80/30 wasn't quite sufficient to develop a fully ductile flexural response in Beam M15-0.5%H. The objective of testing this specimen is to verify the optimum additional content of Dramix BP80/30 fibers required to avert a brittle shear failure. This specimen was designed with the same details as the previous specimen but was reinforced with 0.75% of BP80/30 fibers. It was expected that the additional 0.25% of fibers would allow the beam to exhibit a more ductile flexural response. However, this was the last beam in the M15-KING test series.

The tensile face of the concrete showed the first hairline cracks at a load of 20.23 kN (V = 10.12kN), corresponding to a higher cracking load than observed in the previous beams. Soon thereafter multiple flexural cracks formed outside the constant moment region at a load of 25.24 kN (V = 12.62 kN). Some of the flexural cracks reached 0.3 mm in width, along with the appearance of flexural-shear crack on the east shear span of the beam at a load of 55.40 kN (V = 27.70 kN). When the load started to exceed 70 kN (V = 35 kN) cracking in the shear span was well controlled and behaviour switched to a flexural response along with the yielding of the longitudinal steel reinforcement. As loading continued in deflection control, the flexural cracks continued to extend and enlarge. The concrete started to show the first signs of crushing at a load of 93.27 kN (V = 46.64 kN) and a deflection near 40 mm. When the specimen reached a mid-span deflection of 50.78 mm the load dropped to 85% of the peak load which is similar to the failure deflection recorded in beam M15-1.0%. The peak load for this beam was 95.66 kN (V = 47.83 kN). It is noted that testing continued until deflection reached 70 mm to allow for a comparison with the response of Beam M15-1.5%.

Figure 4.11 (a) shows the shear-deflection response while **Figure 4.11 (b)** shows the measured strains in the longitudinal steel reinforcement for this specimen. The growth in shear and flexural crack widths as a function of load are shown in **Figures 4.11 (c) & (d)**. The maximum shear crack was 0.2 mm, while the flexural cracks in the middle region of the beam were over 2 mm in width at failure. **Figure 4.12** summarizes the most important test stages for this specimen.

From the results of this test it is concluded that the additional 0.25% of Dramix BP80/30 fibers was the optimum amount to let the beam in this test series fail in flexure.

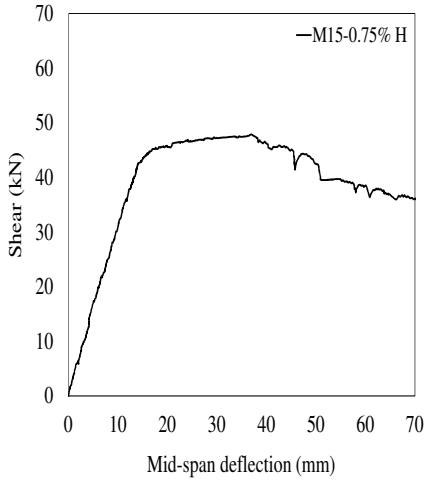

(a) Shear load versus mid span deflection

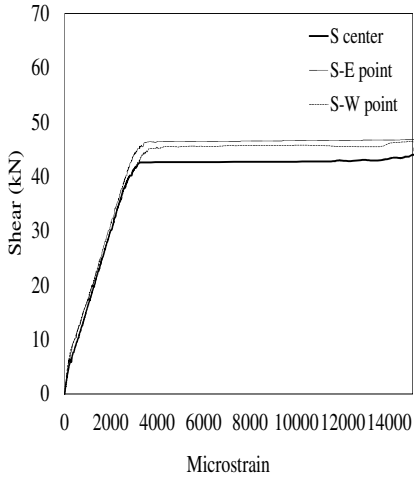

(b) Tensile strains in longitudinal steel bars

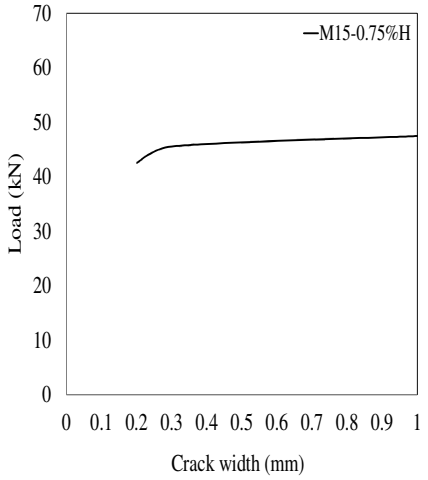

(c) Maximum crack width (shear)

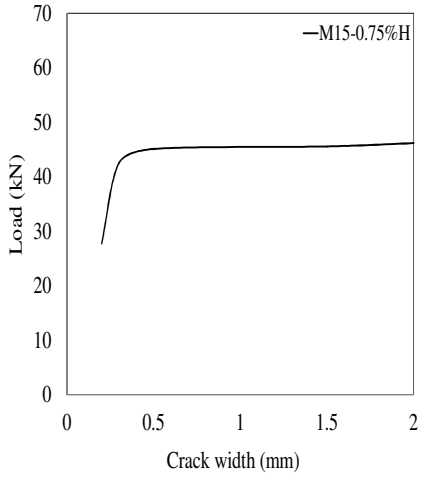

(d) Maximum crack width (flexure)

Figure 4.11: Experimental results for Beam M15-0.75%H

Load stage	V (kN)	Mid-span Δ (mm)	
L7	10.12	3.18	- First hairline cracks appear in the constant moment region
			
Load stage	V (kN)	Mid-span Δ (mm)	
L8	12.62	4.03	- Flexural cracks start to form outside the middle region
			
Load stage	V (kN)	Mid-span Δ (mm)	
L14	27.70	8.67	- Flexural-shear crack beginning to form on the E-side of the beam - Cracks at the center becomes 0.3 mm wide
			
Load stage	V (kN)	Mid-span Δ (mm)	
L17	35	11.20	- Flexural-shear crack beginning to form on the W-side of the beam
			
Load stage	V (kN)	Mid-span Δ (mm)	
L21	45.10	16.90	- Cracks at the center reach 0.5 mm in width - Hairline shear cracks continue to grow
			
Load stage	V (kN)	Mid-span Δ (mm)	
L22b	46.64	25	- Flexural cracks exceed 2 mm in width - Onset of concrete crushing in the compression zone
			
Load stage	V (kN)	Mid-span Δ (mm)	
Failure	40.6	50.78	- Failure of specimen (capacity drops to 85% of peak value)
			

Figure 4.12: Major events for specimen M15-0.75%H

4.1.7 Beam M20-0.75%

This beam represented the first specimen in the second series of this experimental program (M20-KING series). As mentioned earlier the key parameter to be investigated in this series is the effect of increasing the ratio of longitudinal reinforcement and the corresponding shear strength required to cause flexural failure. To study this effect the two 15M bars used in the previous series were replaced with two 20M reinforcing steel bars. All other parameters remained unchanged, including the use of the KING SCC mixture. In this specimen the SCC was mixed with Dramix ZP305, normal-strength hooked-end steel fibers at a fiber content of 0.75% by the volume of concrete.

In terms of response, the first hairline crack was observed when the load reached 15.06 kN (V = 7.53 kN). With further loading multiple hairline cracks appeared outside the constant moment region at a load of 25.23 kN (V = 12.62 kN). The first flexural-shear crack formed on the east side of the beam at a load of 35.30 kN (V = 17.65 kN), followed by the formation of another flexural-shear crack on the west shear span of the beam when the load reached 45.08 kN (V = 22.54 kN). This was followed by sudden appearance of an inclined shear crack on the west side of the beam when the load approached 60.13 kN (V = 30.07 kN). Consequently this diagonal crack started to develop until it reached 1.75 mm in width at a load of 85.08 kN (V = 42.54 kN). Soon thereafter the diagonal tension capacity of the fiber reinforced concrete was exceeded leading to the sudden failure of the beam in shear at a load of 88.06 kN (corresponding to shear load of 44.03 kN). The maximum mid-span deflection recorded just before failure was 14.61 mm. **Figure 4.13 (a)** shows the shear-deflection response for this beam; while **Figures 4.13 (b)** shows that no yielding was observed in the 20M reinforcing steel bars. Although the ultimate shear capacity was higher than that observed in Beam M15-0.5% due to the 0.25% increase in fiber content, this increase in strength was modest and a higher ultimate capacity would have been expected.

Figures 4.13 (c) & (d) show the cracking response. The largest flexural crack was 0.2 mm in width while the critical diagonal shear crack exceeded 1.0 mm in width at failure. **Figure 4.14** shows all the major events observed during the testing of this beam.

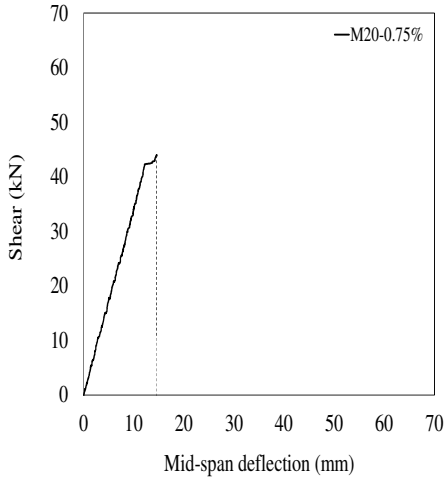

(a) Shear load versus mid span deflection

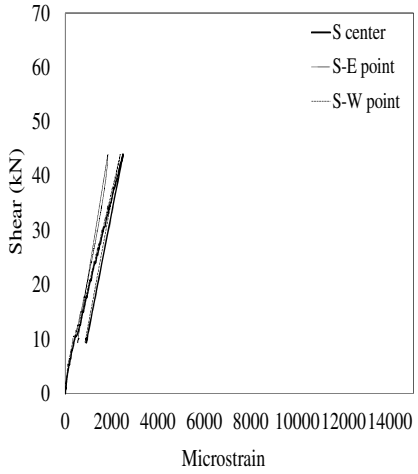

(b) Tensile strains in longitudinal steel bars

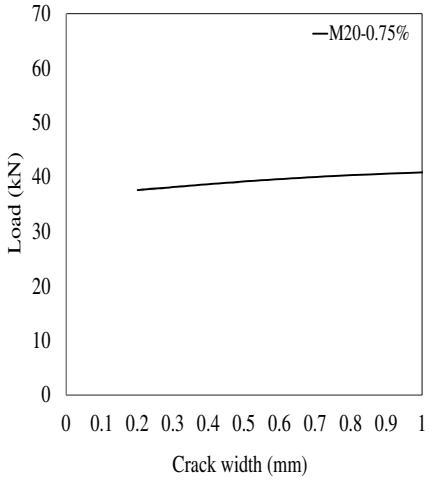

(c) Maximum crack width (shear)

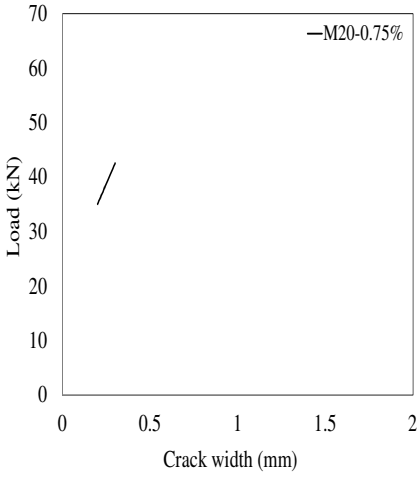

(d) Maximum crack width (flexure)

Figure 4.13: Experimental results for Beam M20-0.75%

<table>
<tr><td>Load stage</td><td>V (kN)</td><td>Mid-span Δ (mm)</td><td rowspan="3">- First hairline cracks appear in the constant moment region</td></tr>
<tr><td>L5</td><td>6.27</td><td>1.51</td></tr>
<tr><td colspan="3">  </td></tr>
<tr><td>Load stage</td><td>V (kN)</td><td>Mid-span Δ (mm)</td><td rowspan="3">- First cracks appears outside the constant moment region</td></tr>
<tr><td>L9</td><td>15.08</td><td>4.47</td></tr>
<tr><td colspan="3">  </td></tr>
<tr><td>Load stage</td><td>V (kN)</td><td>Mid-span Δ (mm)</td><td rowspan="3">- Flexural-shear crack beginning to form on the E-side of the beam
- Crack at the center become 0.3 mm wide</td></tr>
<tr><td>L11</td><td>20</td><td>6.41</td></tr>
<tr><td colspan="3">  </td></tr>
<tr><td>Load stage</td><td>V (kN)</td><td>Mid-span Δ (mm)</td><td rowspan="3">- Flexural-shear crack beginning to form on the W-side of the beam</td></tr>
<tr><td>L18</td><td>37.63</td><td>12.42</td></tr>
<tr><td colspan="3">  </td></tr>
<tr><td>Load stage</td><td>V (kN)</td><td>Mid-span Δ (mm)</td><td rowspan="3">- Some forking cracks beginning to form
- Shear crack suddenly forms on the W-side of the beam</td></tr>
<tr><td>L20</td><td>42.52</td><td>16.8</td></tr>
<tr><td colspan="3">  </td></tr>
<tr><td>Load stage</td><td>V (kN)</td><td>Mid-span Δ (mm)</td><td rowspan="3">- Specimen fails: brittle shear failure on the E-side of the beam</td></tr>
<tr><td>Failure</td><td>44.03</td><td>14.61</td></tr>
<tr><td colspan="3"> 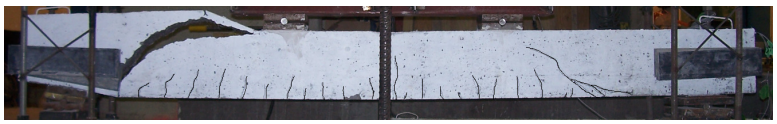 </td></tr>
</table>

Figure 4.14: Major events for specimen M20-0.75%

4.1.8 Beam M20-1.0%

This is the second specimen in the M20-KING series and the last beam where KING self-consolidating concrete was used in a combination with steel fibers. The beam had the same details as the previous specimen but had an increased fiber content of 1.0%. It was expected that this specimen would show higher capacity than Beam M20-0.75%, and the objective of the experiment was to estimate the optimum amount of fibers required to allow the M20 beams to fail in flexure.

As in previous specimens, the first flexural cracks in the tension zone of the beam started to appear when the load approached 15 kN (V = 7.56 kN). The first hairline cracks outside the constant moment region began to form at a load of 30.04 kN (V = 15.02 kN). Thereafter the first flexural-shear crack occurred on the west span when the load reached 35.14 kN (V = 17.57 kN). A sudden formation of multiple flexural-shear cracks took place on the east shear span of the beam at a load of 55.08 kN (V = 27.54 kN). Two large diagonal shear cracks formed on the east and the west side of the beam simultaneously at a load of 75.18 kN (V = 37.59 kN), and at the same stage the flexural crack in the middle of the beam were 0.2 mm in width. Both diagonal cracks developed rapidly as the load increased, and when the load reached to 110.12 kN (V = 55.06 kN) their width exceeded 0.75 mm. After a slight increase in the load the shear crack on the west side of the beam suddenly propagated to cause failure of the beam and a sudden drop in load-carrying capacity. As shown in **Figure 4.15 (a),** at failure the maximum deflection measured at mid-span was 19.54 mm with an associated ultimate capacity of 115 kN (corresponding to a shear load of 57.5 kN). As expected, **Figure 4.15 (b)** shows that strains in the longitudinal steel reinforcement remained below yield values due to the onset of the brittle shear failure. **Figures 4.15 (c) & (d)** show the growth of shear and flexural crack widths in this test specimen. The widest flexural crack was 0.2 mm, while the diagonal crack on the east side of the beam has exceeded 1.75 mm. The main events for this specimen are listed in **Figure 4.16**.

Comparing to beam M20-0.75%, the shear capacity of M20-1.0% has increased by nearly 30%, along with a relatively higher mid-span deflection at failure. It is also noted that although beam M15-1.0% was constructed with SCC and the same amount and type of steel

fibers, this beam failed in flexure. This can be explained by the higher shear demand required to reach flexure in Beam M20-1.0% due to the corresponding increase in longitudinal reinforcement ratio. For this reason the beams in the customized series were designed with fiber contents of 1% and 1.5%.

The result puts into evidence the importance of developing rational and accurate equations for predicting the shear capacity of SFRC beams.

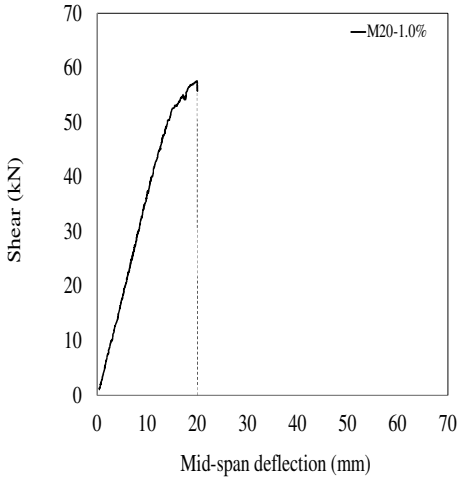

(a) Shear load versus mid span deflection

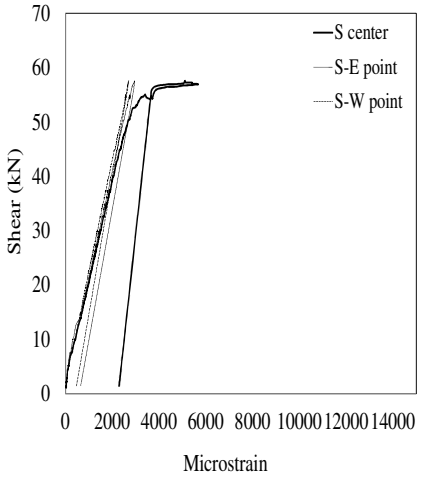

(b) Tensile strains in longitudinal steel bars

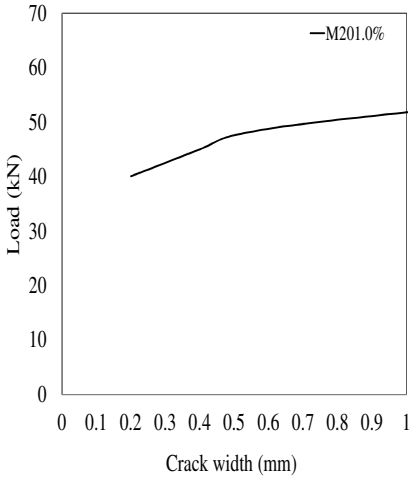

(c) Maximum crack width (shear)

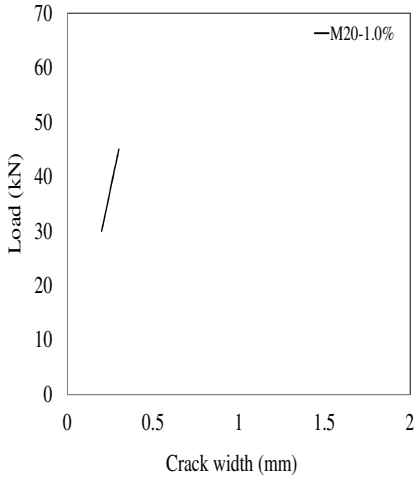

(d) Maximum crack width (flexure)

Figure 4.15: Experimental results for Beam M20-1.0%

Load stage	V (kN)	Mid-span Δ (mm)	
L6	7.56	2.13	- First hairline cracks appear in the constant moment region
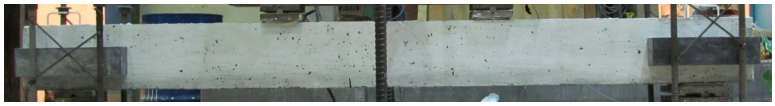			
Load stage	V (kN)	Mid-span Δ (mm)	
L9	15.02	4.26	- Formation of flexural cracks outside the constant moment region
			
Load stage	V (kN)	Mid-span Δ (mm)	
L10	17.57	4.88	- Flexural-shear crack beginning to form on the W-side of the beam
			
Load stage	V (kN)	Mid-span Δ (mm)	
L14	27.54	7.64	- Sudden formation of multiple flexural-shear cracks on the E-side of the beam
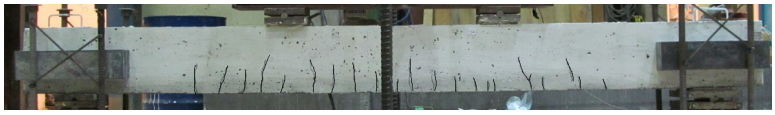			
Load stage	V (kN)	Mid-span Δ (mm)	
L18	37.59	10.31	- Development of web shear crack on both sides of the beam - Cracks in the middle reach 0.2 mm in width
			
Load stage	V (kN)	Mid-span Δ (mm)	
L25	55.06	17.17	- Diagonal shear crack at the E &W-sides of the beam reach 1.5 mm and 0.75 mm in width respectively
			
Load stage	V (kN)	Mid-span Δ (mm)	
Failure	57.5	19.54	- Sudden shear failure on the E-side of the beam
			

Figure 4.16: Major events for specimen M20-1.0%

4.1.9 Beam M20-1.0%A

The final two series of beams were constructed with two different customized SCFRC mixtures (Custom SCC Mix A & Mix B) and reinforced with normal strength hooked-end steel fibers. The main objective from testing these four beams was to study the effect of using a customized SCFRC mix on member response.

Beam M20-1.0%A had identical properties to the specimens in the M20-KING series but was constructed with the first of two customized concrete mixtures (Mix A) and reinforced with Dramix ZP305 steel fibers at a fiber content of 1.0% by volume of concrete. It was expected that this specimen would have a similar response to that observed in Beam M20-1.0%, although it was expected that the improved tensile properties of the customized mixture would lead to improvements in crack control.

As in the previous tests the first hair line crack appeared at a load of 15.25 kN (V = 7.62 kN), and after the load reached 20.20 kN (V = 10.10 kN) several hairline cracks started to form within and outside the constant moment region. A flexural-shear crack formed on the west shear span of the beam at a load of 35.38 kN (V = 17.69 kN). With further loading a new flexural-shear crack then formed on the east side of the beam at load of 45.26 kN (V = 22.63 kN) followed by the formation of multiple inclined cracks on the west side of the beam at a load of 75.20 kN (V = 37.6 kN). As the load increased to 115.18 kN (V = 57.59 kN), one of the inclined cracks on the west-side of the beam began to propagate and increase in width at a rapid rate, reaching a width of 1.25 mm. This was accompanied by yielding of the flexural reinforcement (see **Figure 4.17 (b)**) with the specimen sustaining significant deflection after reaching its peak capacity. Nonetheless with further increase in mid-span deflection the specimen failed suddenly in shear. At failure the ultimate capacity reached 118.04 kN (V = 59.02 kN) and was associated with a maximum mid-span deflection of 30.66 mm (see **Figure 4.17 (a)**). Comparing to Beam M20-1.0%, this specimen developed a slightly higher shear capacity but showed a noticeable enhancement in ductility, with a 50% increase in mid-span deflection before failure.

Figures 4.17 (c) & (d) show the growth of shear and flexural crack widths in this specimen while **Figure 4.18** summarizes the major events that occurred during the test. It is noted that

when compared to Beam M15-1.0%, this specimen showed a slightly more diffused cracking pattern.

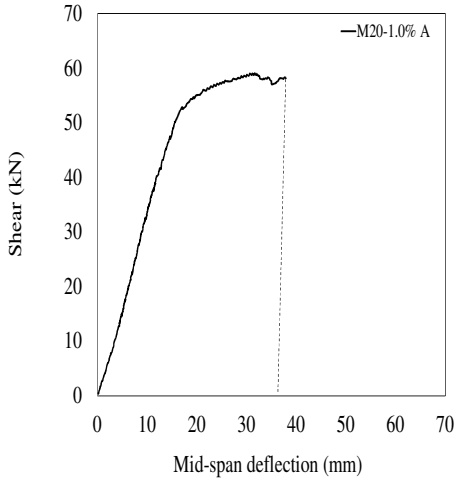

(a) Shear load versus mid span deflection

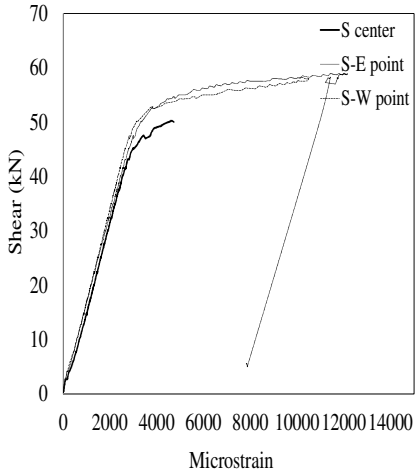

(b) Tensile strains in longitudinal steel bars

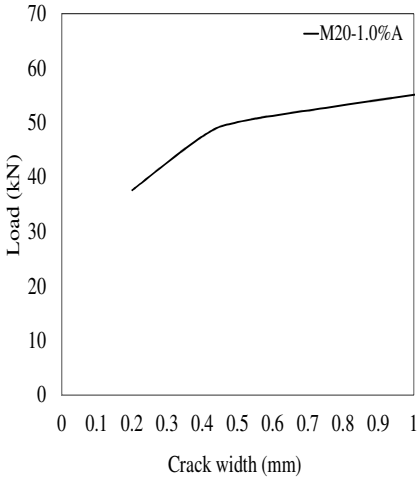

(c) Maximum crack width (shear)

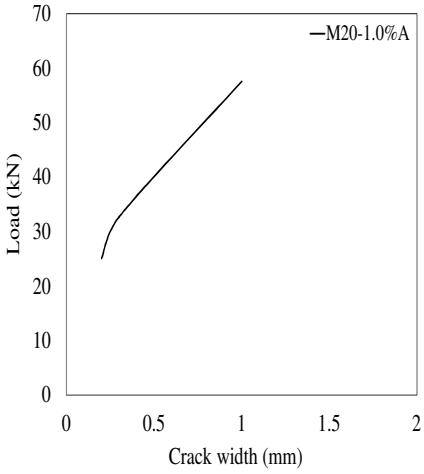

(d) Maximum crack width (flexure)

Figure 4.17: Experimental results for Beam M20-1.0%A

Load stage	V (kN)	Mid-span Δ (mm)	
L6	7.62	2.71	- Hairline cracks appear in the constant moment region
			
Load stage	V (kN)	Mid-span Δ (mm)	
L7	10.10	3.45	- Extension of the flexural cracks and formation of new cracks outside the constant moment region
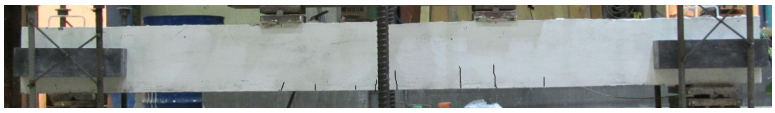			
Load stage	V (kN)	Mid-span Δ (mm)	
L10	17.69	5.58	- Flexural-shear crack beginning to form on the W-side of the beam
			
Load stage	V (kN)	Mid-span Δ (mm)	
L12	22.63	6.9	- Flexural-shear cracks forming on the E-side of the beam - Flexural cracks reach 0.2 mm in width
			
Load stage	V (kN)	Mid-span Δ (mm)	
L18	37.60	11.13	- Formation of multiple web shear cracks on the W-side of the beam - Middle cracks reach 0.3 mm in width
			
Load stage	V (kN)	Mid-span Δ (mm)	
L26	57.59	26.70	- Web shear crack on the W-side of the beam exceeds 1.25 mm in width
			
Load stage	V (kN)	Mid-span Δ (mm)	
Failure	59.02	30.66	- Brittle shear failure on the E-side of the beam
			

Figure 4.18: Major events for specimen M20-1.0%A

4.1.10 Beam M20-1.0%B

This specimen had identical cross-section properties to the previous specimen and contained the same quantity of fibers (1.0% by volume of concrete) with the only exception being that this specimen was constructed with the second customized mix (Mix B). It was expected that this specimen would show similar response to that observed in Beam M15-1.0%A.

The load at which the first flexural cracks occurred was 15.20 kN (V = 7.60 kN). With increasing load the flexural cracks started to extend and more began to form outside the middle region at a load of 20.70 kN (V = 10.35 kN). The first flexural-shear crack was observed on the west shear span of the beam at a load of 33.62 kN (V = 16.18 kN). A new flexural-shear crack formed on the east side of the beam at a load of 65.04 kN (V = 32.52 kN), and at the same stage the largest flexural crack at the center of the beam reached 0.3 mm in width. Thereafter, a large web-shear crack formed on the east side of the beam at a load of 85.08 kN (V = 42.54 kN). Just as in the previous specimen, this web-shear crack began to propagate and increase in size rapidly and reached 0.75 mm in width when the load approached 95.54 kN (V = 47.77 kN) and was followed by a brittle shear failure shortly thereafter. Just before failure the load reached a maximum value of 102.92 kN (V = 51.46 kN) with a corresponding mid-span deflection of 16.51 mm (see **Figure 4.19 (a)**). It is noted that the shear capacity has dropped by 13% when compared to the ultimate capacity recorded in Beam M20-1.0%A, and this beam did not show any significant ductility before failure (**Figure 4.19 (b)** shows that no yielding was recorded in the steel reinforcement).

Figures 4.19 (c) & (d) summarize the cracking behaviour recorded during testing. **Figure 4.20** illustrates all the main events that occurred during the testing of this specimen. It is noted that the cracking pattern at the end of testing was less diffused in this specimen when compared to the companion beam constructed with Mix A.

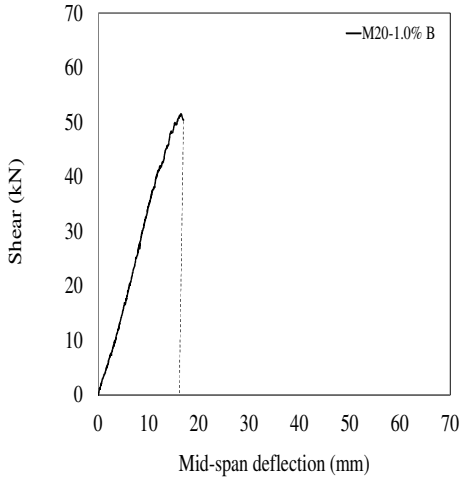

(a) Shear load versus mid span deflection

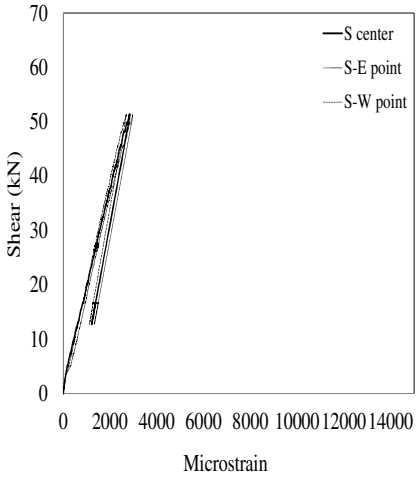

(b) Tensile strains in longitudinal steel bars

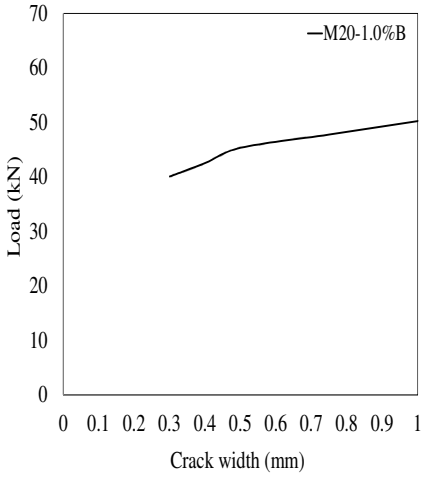

(c) Maximum crack width (shear)

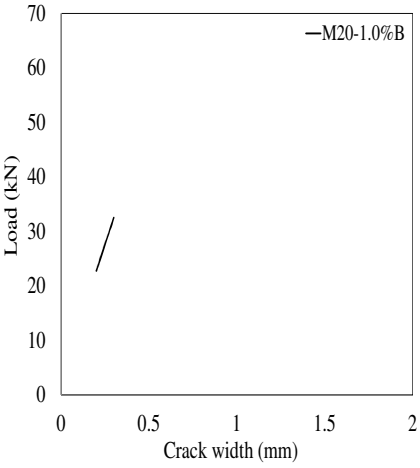

(d) Maximum crack width (flexure)

Figure 4.19: Experimental results for Beam M20-1.0%B

Load stage	V (kN)	Mid-span Δ (mm)	
L6	7.6	2.44	- Multiple hairline cracks appear in the constant moment region
			
Load stage	V (kN)	Mid-span Δ (mm)	
L7	10.35	3.53	- Extension of flexural cracks outside the constant moment region
			
Load stage	V (kN)	Mid-span Δ (mm)	
L9	16.81	5.27	- Flexural-shear crack beginning to form on the W-side of the beam
			
Load stage	V (kN)	Mid-span Δ (mm)	
L16	32.52	9.46	- Flexural-shear cracks appear on the E-side of the beam - Crack widths at the center approach 0.3 mm
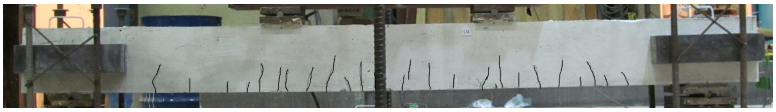			
Load stage	V (kN)	Mid-span Δ (mm)	
L20	42.54	12.71	- Formation of 0.4 mm web shear crack on the E-side of the beam
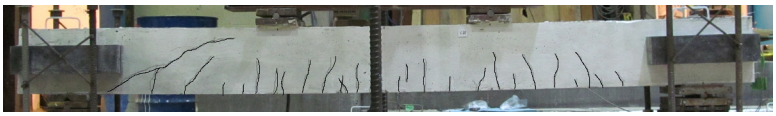			
Load stage	V (kN)	Mid-span Δ (mm)	
L22	47.77	14.23	- Web shear crack reaches 0.75 mm in width
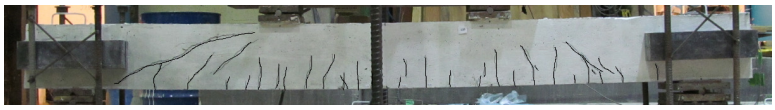			
Load stage	V (kN)	Mid-span Δ (mm)	
Failure	51.46	16.51	- Beam fails in shear on the E-side of the beam
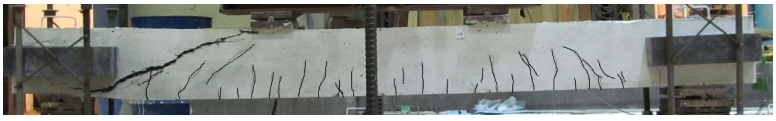			

Figure 4.20: Major events for specimen M20-1.0%B

4.1.11 Beam M20-1.5%A

As observed in the previous four beams in the M20 series the addition of 1.0% ZP305 fibers was not sufficient to result in a ductile flexural response. The last two beams in this test program were therefore reinforced with 1.5% fibers by volume of concrete. Beam M20-1.5%A had identical details and the same concrete mixture used in Beam M20-1.0%A but contained an additional percentage of 0.5% of steel fibers. It was expected that this quantity of fibers would be sufficient for the beam to develop its full flexural capacity.

The first hairline crack in this beam as in the previous tests occurred in the middle region of the beam at a load of 15.04 kN (V = 7.52 kN). Thereafter, at a load of 20.30 kN (V = 10.15 kN) multiple flexural cracks occurred outside the constant moment region. Flexural-shear crack started to initiate on the west shear span of the beam when the load reached 55.04 kN (V = 27.52 kN). The cracks in the constant moment region continued to propagate and reached 0.2 mm in width at a load of 65.02 kN (V = 32.51 kN), along with the sudden formation of a visible inclined shear crack on the west side of the beam. Diagonal shear cracks started to develop on the east side of the beam and reached 0.5 mm in width when the load approached 119 kN (V = 59.50 kN). At this stage yielding was recorded in the longitudinal steel reinforcement (it is noted that the strain gages failed right after reaching yielding (see **Figure 4.21 (b)**) with the specimen reaching its flexural capacity. The mid-span deflection measured at this stage was 25.45 mm. As shown in **Figure 4.21 (a)** loading was then continued under deflection control. Multiple cracking and "forking" type cracks started to occur as further loading was applied. When the load reached 120.04 kN (V = 60.02 kN) concrete in the compression zone started to show signs of crushing and the load began to drop steadily. The peak load was 123.70 kN (V = 61.85 kN) and associated with a maximum mid-span deflection of 38.84 mm. Loading continued until the load dropped below 85% of the peak value at a deflection of 56.6 mm. At failure the largest flexural crack was approximately 2.5 mm in width while the maximum diagonal crack width was 0.5 mm. **Figures 4.21 (c) & (d)** summarize the growth in crack widths as a function of load in this specimen, while **Figure 4.22** summarizes the major events during testing. When compared to Beam M20-1.0%A, this specimen showed a 5% improvement in flexural capacity but

resulted in a ductile flexural failure with the mid-span deflection at failure recorded as being significantly high when comparing to the failure deflection in beam M20-1.0%A. Therefore it can be concluded that the inclusion of 1.5% of steel fibers was sufficient to carry the extra load required to reach flexural failure in the M20 series. An interesting observation is that the beam showed a significantly more diffused cracking pattern when compared to the other beams tested in this experimental program.

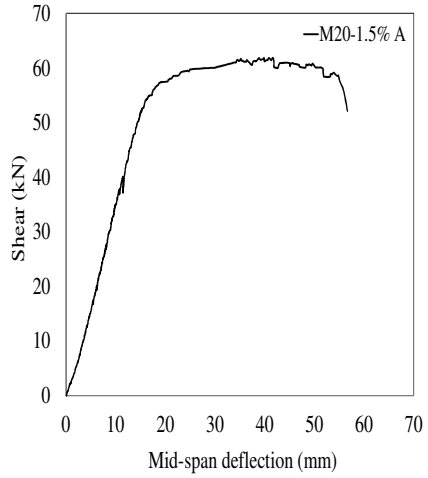

(a) Shear load versus mid span deflection

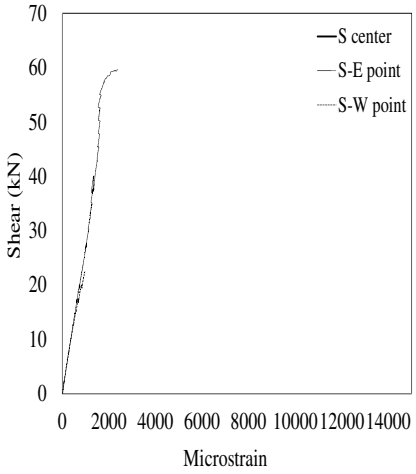

(b) Tensile strains in longitudinal steel bars

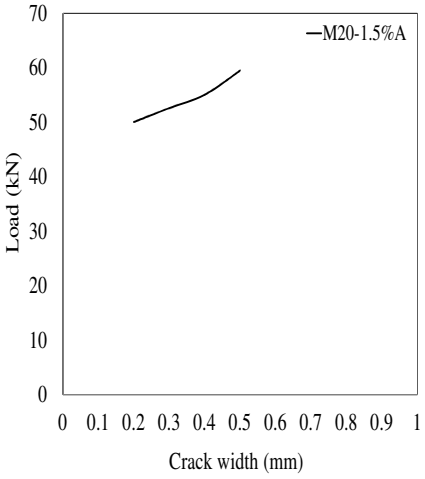

(c) Maximum crack width (shear)

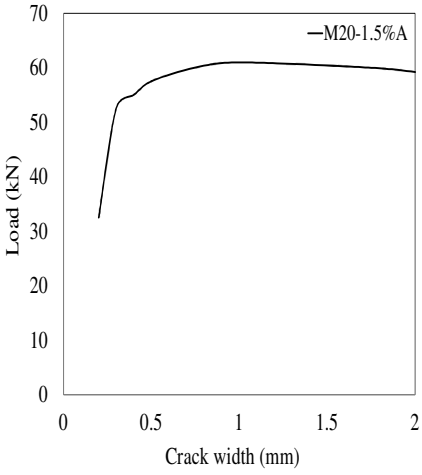

(d) Maximum crack width (flexure)

Figure 4.21: Experimental results for Beam M20-1.5%A

Load stage	V (kN)	Mid-span Δ (mm)	
L6	7.52	2.71	- First hairline crack forms in the constant moment region
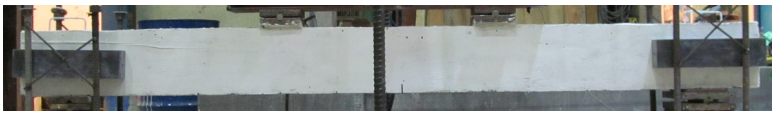			
Load stage	V (kN)	Mid-span Δ (mm)	
L7	10.15	3.49	- New flexural cracks form outside the constant moment region
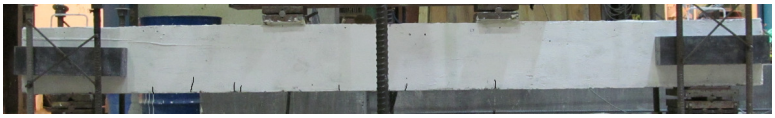			
Load stage	V (kN)	Mid-span Δ (mm)	
L14	27.52	8.10	- Flexural-shear crack beginning to form on the W-side of the beam
			
Load stage	V (kN)	Mid-span Δ (mm)	
L16	32.51	9.30	- Sudden formation of web shear crack on the W-side of the beam - Flexural cracks width become 0.2 mm
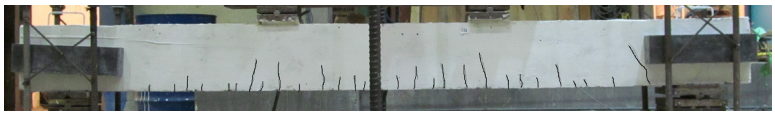			
Load stage	V (kN)	Mid-span Δ (mm)	
L27	59.50	24.54	- Diagonal crack width on the E-side of the beam becomes 0.5 mm - Onset of concrete crushing
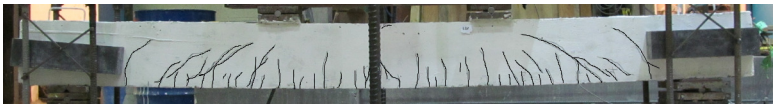			
Load stage	V (kN)	Mid-span Δ (mm)	
L30	60.02	42.6	- Formation of Forking cracks and multiple cracking - Flexural crack at the center reaches 1.75 mm in width
			
Load stage	V (kN)	Mid-span Δ (mm)	
Failure	52.6	56.6	- Flexural Failure (capacity drops to 85% of peak value)
			

Figure 4.22: Major events for specimen M20-1.5%A

4.1.12 Beam M20-1.5%B

This beam was the last specimen tested in this experimental program and had identical properties as the previous beam (Beam M20-1.5%A), but was constructed with the second of the two customized SCC mixtures used in the experimental program. When compared to Beam M20.1.0%B this beam had an increased fiber content of 1.5%, and it was expected that the increased quantity of fibers would permit this beam to fail in flexure. It was also expected that the response of this specimen would be similar to the response of Beam M20-1.5%A.

The first hairline cracks in this beam occurred at a load of 18.58 kN (V = 9.29 kN) close to the center of the beam. More flexural cracks started to extend outside the constant moment region when the load approached 30.40 kN (V = 15.20 kN). Flexural and inclined shear cracks began to form on the west side of the beam at a load of 60.12 kN (V = 30.06 kN). Soon thereafter a new flexural-shear crack formed on the east shear span of the beam at a load of 65.06 kN (V = 32.53 kN). Loading continued until the beam reached its flexural capacity with corresponding yielding observed in the longitudinal steel reinforcement. As loading continued under deflection-control the concrete in the compression zone began to show signs of crushing when the load reached 117.98 kN (V = 58.99 kN). After reaching a maximum capacity of 119.36 kN (V = 59.68 kN) and a mid-span deflection of 22.37 mm, the load began to drop with increasing deflections and testing continuing until the load dropped below 85% of the peak value corresponding to a mid-span deflection of 45.08 mm. **Figures 4.23 (a) & (b)** shows the load-deflection response and recorded strains in the longitudinal steel reinforcement. This test result demonstrated that the additional amount of steel fiber used in this specimen when compared to M20-1.0%B Beam was adequate to transform the brittle failure into a ductile flexural response with the mid-span deflection before failure increasing by 173% comparing to specimen M20-1.0%B.

Figures 4.23 (c) & (d) shows the load-crack widths responses while the main events recorded during testing are summarized in **Figure 4.24**. At failure the maximum crack width recorded in the flexural zone was over 2 mm while the largest diagonal crack was 0.4 mm in width. Just as with the previous specimen it is noted that this beam showed multiple cracking and reduced crack spacing.

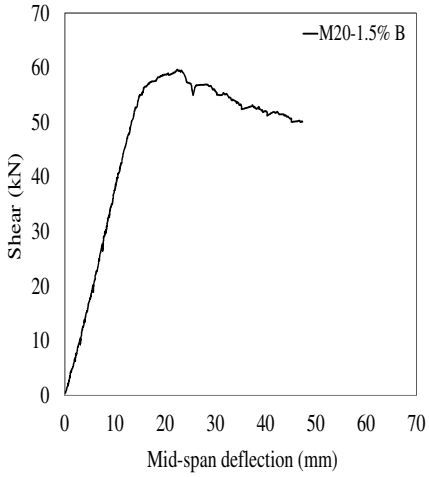

(a) Shear load versus mid-span deflection

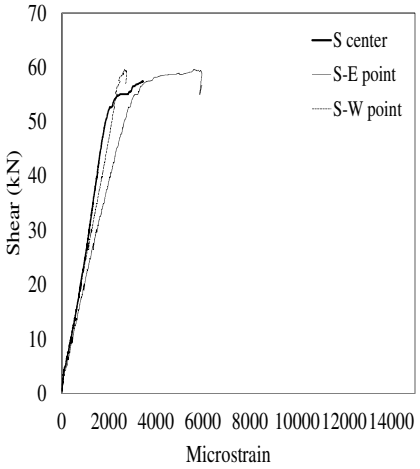

(b) Tensile strains in longitudinal steel bars

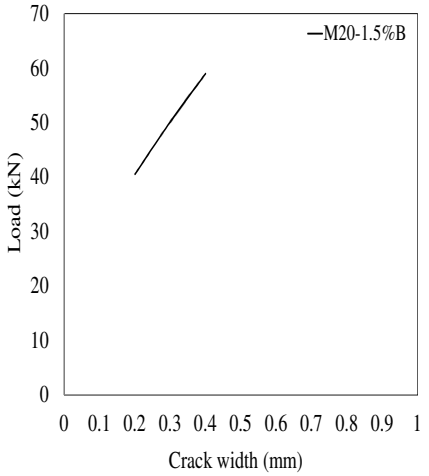

(c) Maximum crack width (shear)

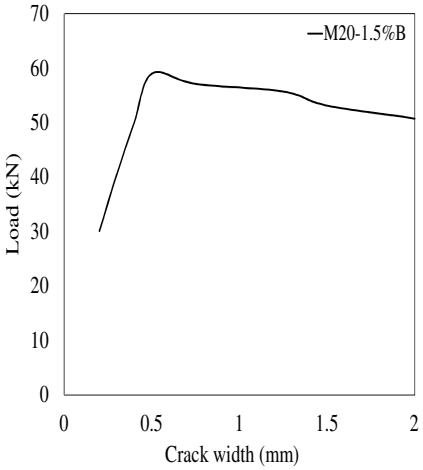

(d) Maximum crack width (flexure)

Figure 4.23: Experimental results for Beam M20-1.5%B

Load stage	V (kN)	Mid-span Δ (mm)	
L7	9.29	3.06	- First hairline cracks appear in the constant moment region
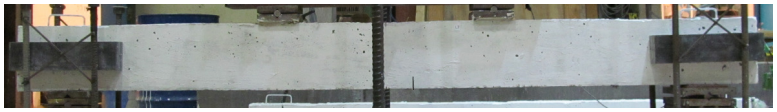			
Load stage	V (kN)	Mid-span Δ (mm)	
L9	15.20	4.30	- Flexural cracks form outside the middle region
			
Load stage	V (kN)	Mid-span Δ (mm)	
L15	30.06	8.02	- Flexural-shear crack beginning to form on the W-side of the beam - Web crack forms on the W-side of the beam
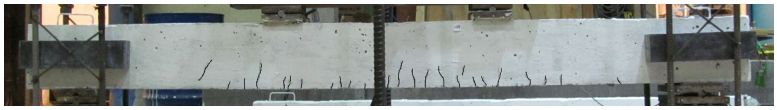			
Load stage	V (kN)	Mid-span Δ (mm)	
L16	32.53	8.64	- Appearance of flexural shear crack on the E-side of the beam - Cracks in the middle reach 0.2 mm in width
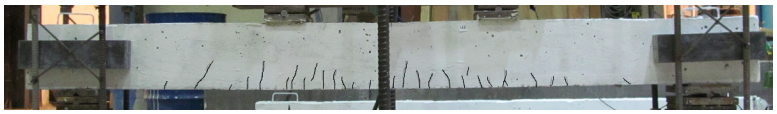			
Load stage	V (kN)	Mid-span Δ (mm)	
L27	58.99	20.58	- Concrete crushing starts in compression zone - Forking cracks and multiple cracking - Cracks at the middle reach 0.5 mm in width
			
Load stage	V (kN)	Mid-span Δ (mm)	
L30	53.13	35.12	- Further concrete crushing - Further development of secondary cracks - Diagonal crack width approaches 0.4 mm
			
Load stage	V (kN)	Mid-span Δ (mm)	
Failure	50.74	45.08	- Flexural Failure (capacity drops to 85% of peak value)
			

Figure 4.24: Major events for specimen M20-1.5%B

Chapter Five: Discussion of the Experimental Results

5.1 Introduction

This chapter compares the results from the twelve SCFRC beams tested in the experimental program. The response of the beams in terms of shear capacity, load-deflection behaviour, ductility and crack control is discussed. Furthermore, a discussion is provided on the concept of "critical fiber content", and the ability of steel fibers to replace the minimum shear reinforcement required by the ACI-318 code is investigated.

5.2 Shear Capacity, Load-Deflection Response & Failure Mode

This section compares the ultimate shear capacity, load-deflection response and failure mode of the various specimens tested in this experimental program. Comments are made regarding the effect of various parameters including: fiber content, fiber type, longitudinal reinforcement ratio and concrete type.

5.2.1 M15 series – Effect of Fiber Content

To recall, the six beams in the M15-KING series had identical cross-sectional properties and were cast using a traditional SCC. The series included one control beam (Beam M15-0.0%) and five beams having varying fiber contents (ranging from 0.5% to 1.5%) and fiber types (Dramix ZP305 normal strength fibers and Dramix BP80/30 high-strength fibers). **Table 5.1**

and **Figures 5.1&5.2** compare the shear capacities, deflections (at maximum and at failure) and the load-deflection responses of the various beams tested in this series.

In terms of shear resistance, as has been reported for traditional SFRC beams, one can see that the addition of steel fibers in SCFRC beams leads to improvements in shear capacity. In addition, as the fiber content is increased so does the relative increase in shear strength. For example, as shown in **Table 5.1**, the addition of 0.5% fibers in Beam M15-0.5% increased the shear capacity of the beam by 47% when comparing to the strength of the control beam. A further increase in fiber content to 1.0% has led to 63% improvement in shear strength when compared to the control beam. The use of 1.5% fibers did not lead to a further increase in capacity when compared to the companion beam with 1.0% fibers. It is noted that both beams failed in flexure and the result demonstrates that addition of steel fibers does not have a significant influence in increasing moment capacity in beams failing in flexure.

In terms of member response and failure modes, as expected, the control beam, which contained no shear reinforcement or fibers, failed in shear at relatively low load and deflection (see **Figure 5.1**). The use of 0.5% fibers did not result in a transformation of failure mode, and this beam also failed in shear. The use of 1.0% fibers in Beam M15-1.0% was sufficient to transform the brittle shear failure into a ductile flexural failure and allowed the beam to carry large deflections prior to failure (approximately 5.5 times more than the control specimen). A further addition of 0.5% fibers in Beam M15-1.5% led to further improvements in ductility allowing the beam to sustain 28% larger deflections prior to failure when compared to the companion beam with 1.0% fibers.

5.2.2 M15 series – Effect of Fiber Type

In addition to the effect of fiber quantity, two of the beams in this series were constructed with high-strength BP80/30 steel fibers. A comparison of the results from **Table 5.1** and **Figure 5.2** shows the beneficial impact of using high-strength fibers. Besides the improvement in shear capacity, the use of high-strength fibers has contributed to an enhanced post-peak response and ductility. Just as in the case of the normal strength fibers,

the use of high-strength fibers was shown to improve ultimate shear capacity and member response. When compared to the control beam, increases in strength of 54% and 63% for Beams M15-0.5%H and M15-0.75%H were observed. The response of Beam M15-0.5%H shows that the use of high-strength fibers allowed the beam to sustain significant deflections before failure when compared to the control specimen. Similarly, although both Beams M15-0.5% and M15-0.5%H failed in shear at similar failure loads, a comparison between the deflections at failure (see **Table 5.1**) and the member responses (see **Figure 5.2**) demonstrates an improved level of ductility for the beam reinforced with high-strength fibers (with Beam M15-0.5%H experiencing 200% increase in deflections before failure). The results also show that an increase in high-strength fiber content to 0.75% resulted in a further increase in strength and was sufficient to produce a ductile flexural failure in Beam M15-0.75%H (compare the response of Beams M15-0.75%H and M15-0.5%H). It is noted that the structural response of Beam M15-0.75%H is rather similar to the response of Beam M15-1.0% in terms of flexural ductility.

Table 5.1: Summary of results for beams in the M15-KING series

Beam specimen	Maximum Load P_{exp} (kN)	Shear at Max. Load V_{exp} (kN)	Increase in Shear $\frac{(V_{exp} - V_{exp_0})}{V_{exp}}\%$	Deflection at Peak Δ_{exp} (mm)	Deflection at Failure Δ_{max} (mm)
M15-0.0%	59.70	29.85	---	10.77	10.77
M15-0.5%	86.66	43.33	47%	17.85	17.85
M15-1.0%	96.00	48.00*	63%	41	55.12
M15-1.5%	93.40	46.70*	60%	24.3	70.5
M15-0.5%H	90.35	45.17	54%	39.88	39.88
M15-0.75%H	95.66	47.83*	63%	37	50.78

*Beam failed in flexure

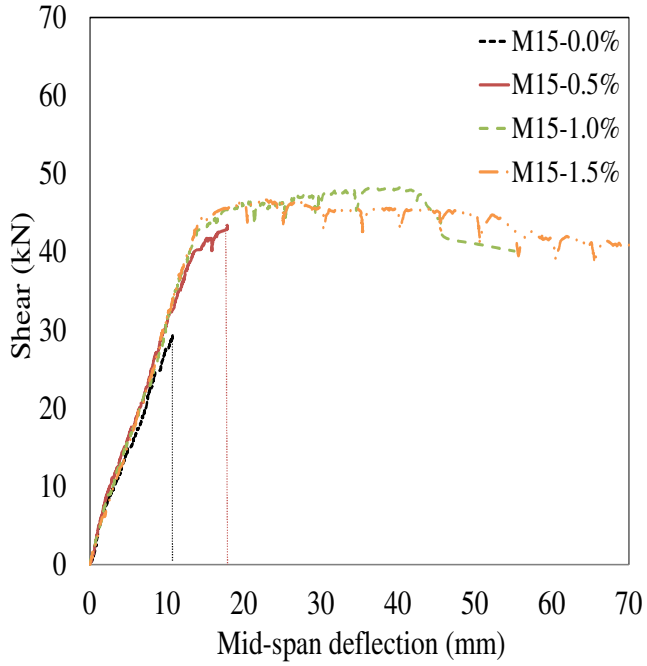

Figure 5.1: The effect of fiber content on the shear-deflection response in the M15 series

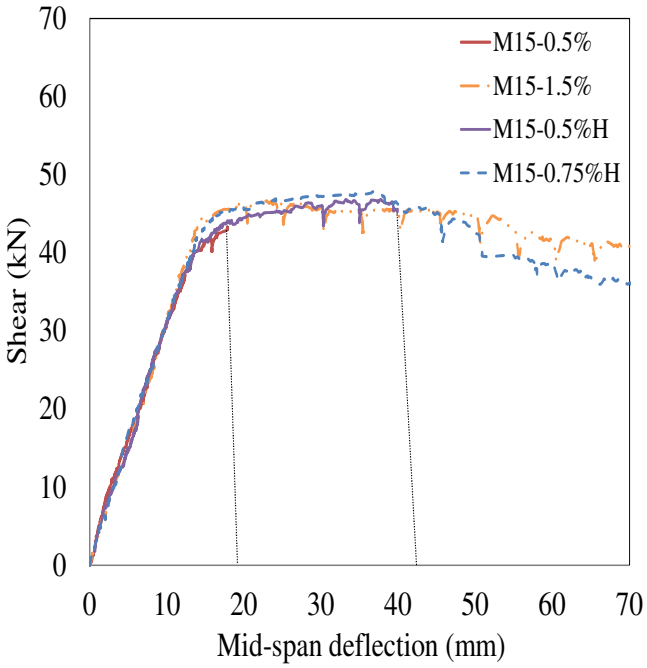

Figure 5.2: The effect of fiber type on the shear-deflection response in the M15 series

5.2.3 M20 series – Effect of Fiber Content

Beams M20-0.75% and M20-1.0% were constructed with a traditional SCC mix, normal strength hooked-end steel fibers and fiber contents of 0.75% and 1.0% by volume of concrete, respectively. It is noted that no control beam was tested in this test series. To allow for a comparison of shear capacities, the expected shear strength of a reinforced concrete beam having identical properties but without fibers was predicted using the program RESPONSE-2000 (the program, which was developed at the University of Toronto can accurately predict the shear response of traditional reinforced concrete beams). The calculated shear capacity of this beam was found to be 34 kN. **Table 5.2** compares the maximum shear capacities of the two beams in this series with the expected capacity of the hypothetical beam without fibers. The addition of fibers results in an increase in capacity when comparing to the case of a beam with no fibers. In addition, the results show that increasing the fiber content from 0.75% to 1.0% is accompanied by a relative increase in peak capacity. As shown in **Figure 5.3**, despite the enhancement in shear capacity, the failure pattern for both beams in this series was brittle and the beams failed in shear with a sudden loss in load-carrying capacity at failure.

5.2.4 M20 series – Effect of Longitudinal Reinforcement Ratio

The beams discussed in the previous section were reinforced with two 20M bars, whereas all other properties including concrete type remained unchanged from the M15 test series. A comparison of the responses of Beams M15-1.0% and M20-1.0% in **Figure 5.4** shows that while 1.0% of steel fibers was sufficient to transform the brittle shear response in the M15 series beam, the use of 1.0% fibers in the beam with 20M reinforcement was not sufficient to avoid a brittle shear failure. The reason returns to the higher flexural capacity in the beams with larger reinforcement ratio. That is to say that the additional shear capacity provided by 1.0% steel fibers was not sufficient to “make up” the shear required to reach the beam’s flexural capacity and cause flexural failure in the beam with larger reinforcement ratio. The

result clearly puts into evidence the importance of developing accurate and reliable equations for predicting the shear resistance of steel fiber reinforced concrete beams.

5.2.5 M20 series – Effect of Concrete Type

In addition to the two beams constructed with traditional SCC, the M20 series also included four beams constructed with two different customized concrete mixtures (SCC-Custom Mix A and Mix B). In comparing the results in **Table 5.2** Beams M20-1.0%A and M20-1.0%B have shown a 74% and 51% higher shear capacity respectively when compared to the expected capacity of the hypothetical companion beam without fibers.

A comparison of the responses of Beam M20-1.0% from the M20-KING series and Beams M20-1.0%A and M20-1.0%B allows for an investigation into the effect of concrete type on response. All beams were reinforced with 1.0% normal-strength hooked-end fibers and had identical properties with the exception of concrete mix type. In comparing the results in **Figure 5.5** one can see that while the capacities of all three beams was similar and failure in all cases was in shear, the beam constructed with the first customized SCC mix (Beam M20-1.0%A) showed an improved level of ductility when compared to the two companion beams. This may be linked to the improved concrete tensile properties of this SCFRC mixture and the fact that yielding was initiated in the longitudinal reinforcement before the brittle failure in this specimen.

Based on the observations made in section 5.2.4, the fiber content used in the remaining two beams of this test program was selected to be 1.5% fibers by volume of concrete. As shown in **Figure 5.6**, while 1.0% fibers was not sufficient to prevent a brittle shear failure in the previous two beams in this series (Beams M20-1.0%A,B), the use of 1.5% fibers in Beams M20-1.5%A,B was adequate to transform the failure into a ductile flexural response.

One can also note that the beam with the first customized mix (Mix A) showed a more ductile response when compared to the beam constructed with the second customized mixture (Mix B) due to the differences in mix design.

Table 5.2: Summary of results for beams in the M20-KING and M20-Custom series

Beam specimen	Maximum Load P_{exp} (kN)	Shear at Max. Load V_{exp} (kN)	Increase in Shear $\frac{(V_{exp} - V_{exp_0})}{V_{exp_0}}\%$	Deflection at Peak Δ_{exp} (mm)	Deflection at Failure Δ_{max} (mm)
Control-0.0%†	68.00	34.00	---	---	---
M 20-0.75%	88.06	44.03	30%	14.61	14.61
M 20-1.0%	115.00	57.50	69%	19.54	19.54
M 20-1.0%A	118.04	59.02	74%	30.66	30.66
M 20-1.0%B	102.92	51.46	51%	16.51	16.51
M 20-1.5%A	123.70	61.85*	82%	38.84	56.6
M 20-1.5%B	119.36	59.68*	76%	22.37	45.08

†No control beam was tested in the M20 series, the capacity indicated is the shear strength predicted using the program RESPONSE for an RC beam having identical cross-sectional properties and $f_c^{'}$ of 50 MPa.
*Beam failed in flexure

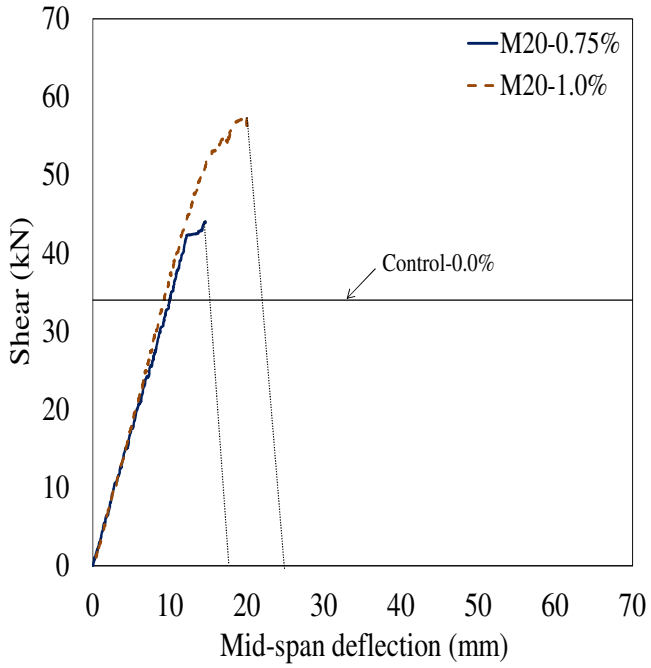

Figure 5.3: The effect of fiber content on the shear-deflection response in the M20-KING series

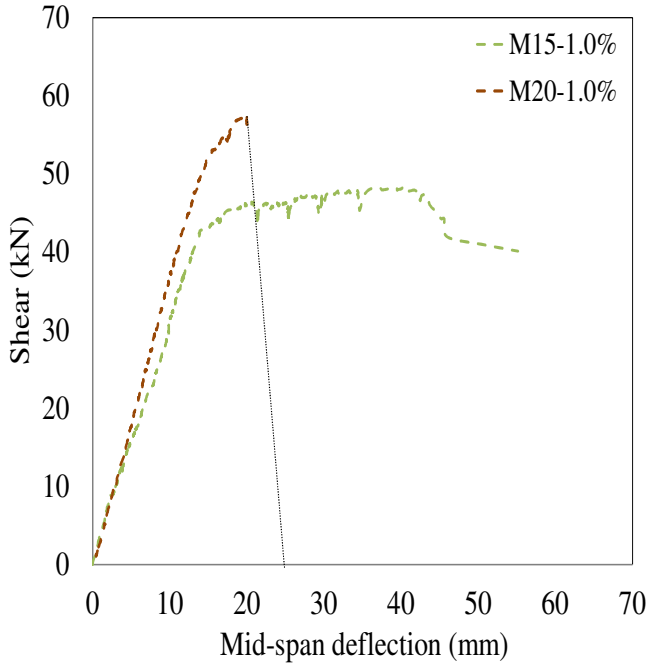

Figure 5.4: The effect of longitudinal reinforcement on shear-deflection response

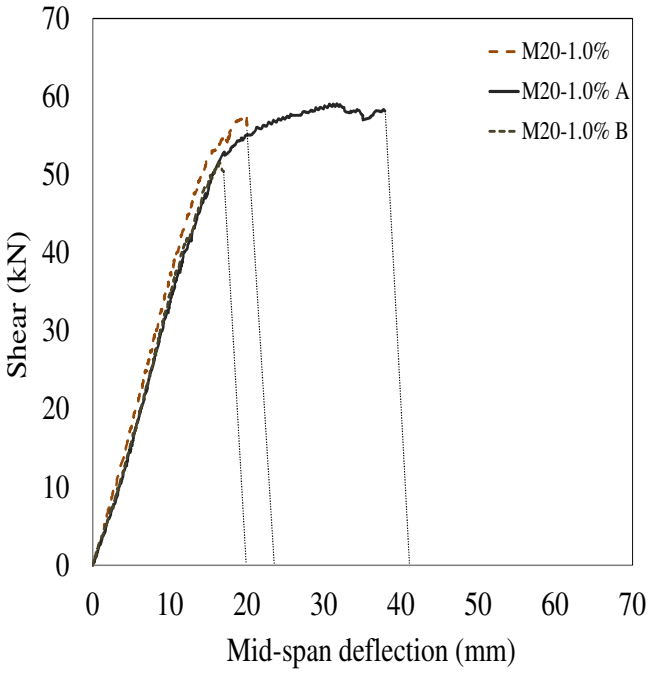

Figure 5.5: The effect of concrete type on shear-deflection response in the M20 series

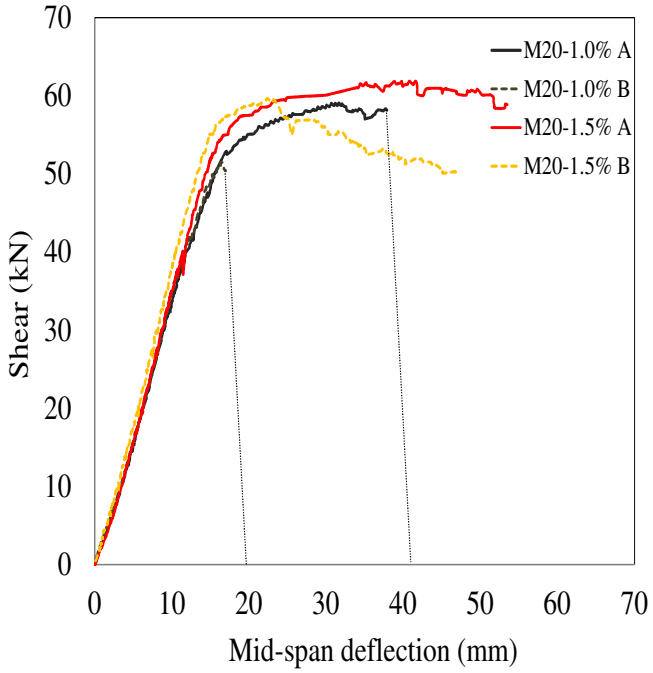

Figure 5.6: The effect of fiber content on shear-deflection response in the Custom series

5.3 Shear and Flexural Crack Widths

As expected the utilization of steel fibers in the SCFRC beams had an important influence on shear and flexural crack widths.

Figure 5.7(a) and **Figure 5.8(a)** compare the growth in shear crack widths as a function of load for the beams in the M15 and M20 series, respectively. For the M15-series, the control specimen (Beam M15-0.0%) as well as the beams with 0.5% normal strength and high-strength fibers (Beams M15-0.5% and M15-0.5%H, respectively) failed suddenly in shear. For the control beam the failure was accompanied with very little warning of the imminent shear failure with the crack width just before the sudden failure remaining at around 0.3 mm. Beam M15-0.5% which also failed under shear, was able to resist a slightly larger crack width of approximately 0.4 mm before failure, and consequently gave a slight warning before collapse. The use of high-strength BP 80/30 fibers in Beam M15-0.5%H permitted this specimen to show a remarkably larger critical shear crack width (exceeding 1.0 mm)

prior to failure (see **Figure 5.9**). This enhancement is linked to the higher tensile strength and increased aspect-ratio of this fiber type, which results in enhanced pullout behaviour allowing the BP 80/30 fibers to more effectively bridge the critical diagonal shear crack.

A comparison of the growth in shear crack widths in the M20-series beams with 1.0% fibers (Beams M20-1.0%, M20-1.0%A and M20-1.0%B), shows that although all three beams failed in shear, the inclusion of fibers allowed for the bridging of large shear crack widths (over 1.0 mm) prior to failure.

Beams M15-1.0% and M15-1.5% of the M15-series and Beams M20-1.5%A and M20-1.5%B of the M20 series failed in flexure and thus showed a good control of shear crack widths at equivalent load stages when compared to the control and shear-critical specimens. The results also show that increasing the fiber content results in further improvements in crack control.

A comparison of the flexure crack widths in the beams that failed in flexure in the M15 series (see **Figure 5.7(b)**) demonstrates that increasing the fiber content from 1.0% to 1.5% results in a better control of flexural crack widths at equivalent load stages (compare the plots for Beams M15-1.0% and M15-1.5%). The results also show that using 0.75% high-strength BP80/30 fibers results in a better control of crack widths when compared to the companion specimens with 1.0% and 1.5% normal strength fibers (compare the plots for Beam M15-0.75% H with that of Beams M15-1.0% and M15-1.5%). Finally a comparison of the growth in flexural crack widths in the M20 series, shows that the use of 1.5% fibers in the first customized mix results in improved control of crack widths when compared to the second customized mix (compare the results of Beams M20-1.5%A and M20-1.5%B).

In addition to the above observations, examination of the diagonal shear cracks in the SCFRC beams reveals that the fibers pullout rather than fracture across the cracking plane when shear failure occurs. An interesting observation is that the hooked-end fibers deform and straighten during pullout (see **Figure 5.10**).

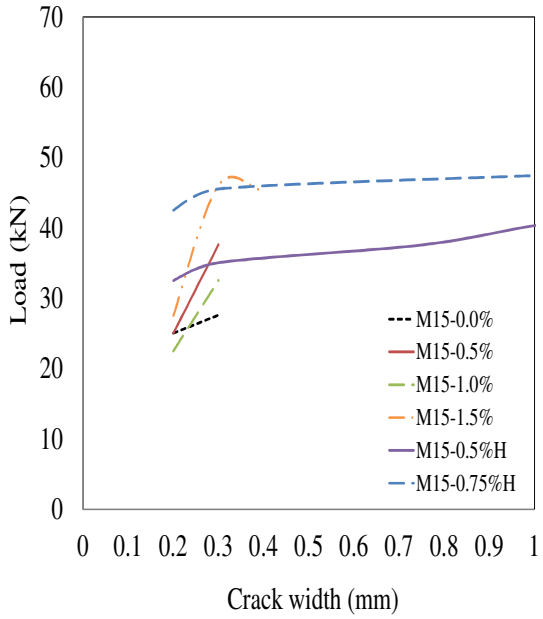

(a) Maximum crack width (shear)

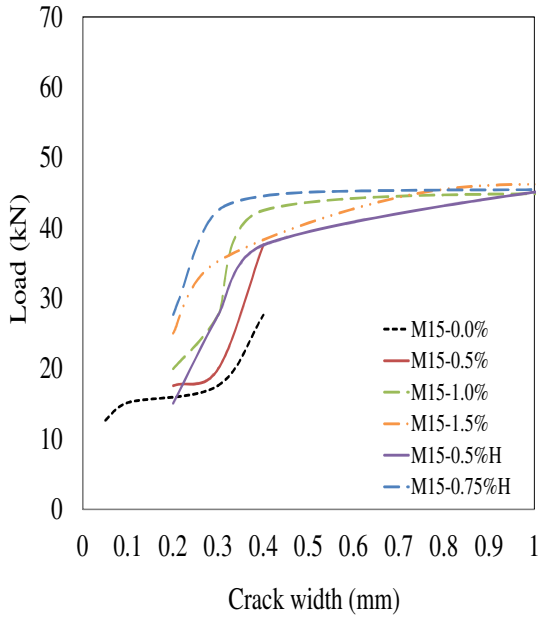

(b) Maximum crack width (flexure)

Figure 5.7: Load vs. crack width relationship for various beams in the M15 series

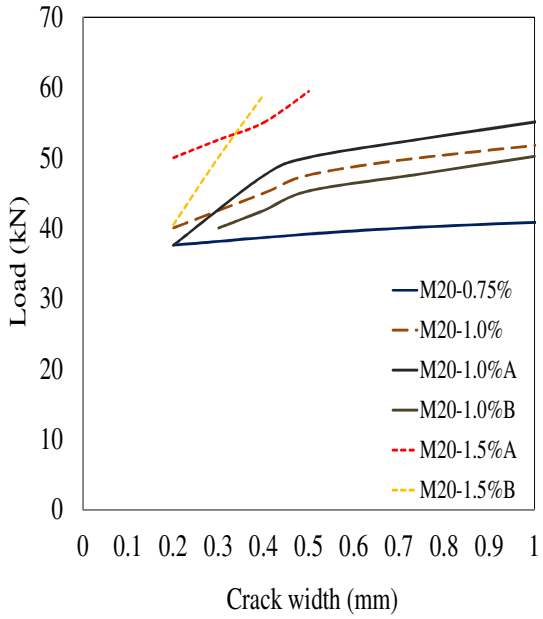

(a) Maximum crack width (shear)

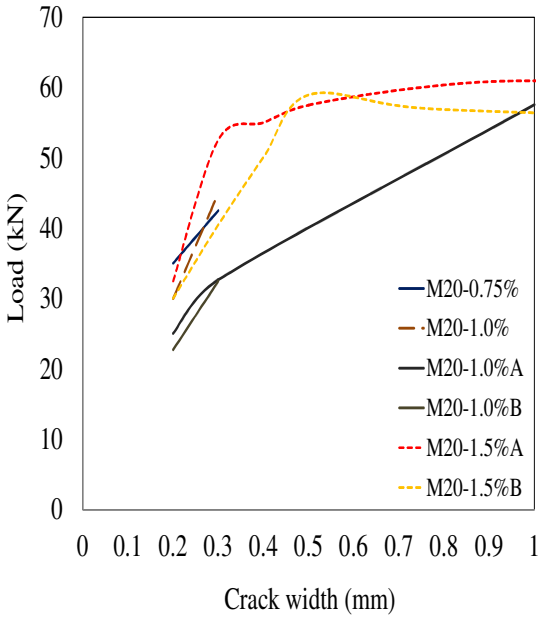

(b) Maximum crack width (flexure)

Figure 5.8: Load vs. crack width relationship for various beams in the M20 series

Figure 5.9: The influence of high-strength fibers on crack width

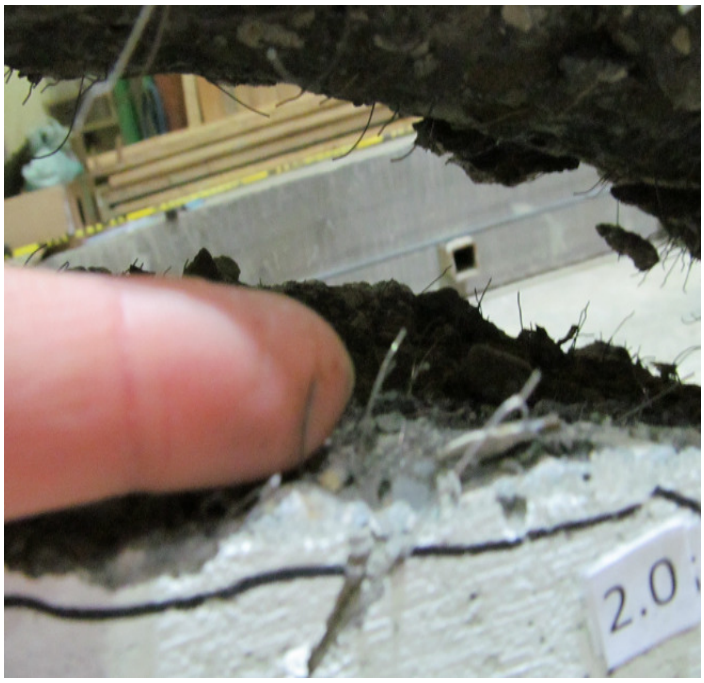

Figure 5.10: Pullout and straightening of hooked-end fibers after shear failure

5.4 Cracking Patterns

In addition to the improvements in controlling crack widths, the use of steel fibers had a noticeable influence on crack patterns in the beams tested in the experimental program.

Figures 5.11 and **5.12** show the crack patterns for the various specimens at the end of testing in the M15 and M20 series, respectively.

For the M15 series the crack patterns for the control beam and the SCFRC beams were noticeably different. Comparing the inclined cracks for the beams that failed in shear, the control specimen (Beam M15-0.0%) exhibited a single inclined crack followed by a brittle shear failure. On the other hand the SCFRC beams which failed in shear showed at least two diagonal shear cracks before failure (Beams M15-0.5% and M15-0.5%H). Comparing the same three beams it can be seen that use of 0.5% fibers has reduced the spacing between cracks when compared to the control specimen. The specimen with 0.5% high-strength fibers shows further reductions in crack spacing when comparing to the control beam and the companion specimen constructed with normal-strength fibers.

When comparing the control beam with the specimens that failed in flexure (Beams M15-1.0%, M15-1.5%, M15-0.75%H) one can see that the use of higher fiber content (greater or equal to1.0%) led to both reductions in crack widths and spacing. In addition, the higher fiber contents resulted in a more diffused cracking pattern with the formation of “forking” cracks with secondary cracks growing out of primary cracks. This is particularly evident in the failure photo of Beam M15-0.75%H which contained high-strength fibers.

Similar observations can be made in comparing the results of the M20 series beams. When examining the failure photos of the four beams that failed in shear it is noticed that the beams have reduced spacing of cracks when compared to the M15-0.0% beam of the previous test series. It is noted that the beam constructed with 1.0% fibers and the first customized mix (Beam M20-1.0%A) showed significant reductions in crack spacing with multiple flexural and inclined shear cracks despite having failed in shear. The results of the two beams constructed with 1.5% fibers and the customized mixtures (in particular, Beam M20-1.5%A) showed greatly reduced crack spacings, multiple cracking and very diffused cracking

patterns when compared to the other beams in the M20 series and Beam M15-1.5% of the previous test series.

M15-0.0% Single shear crack Large crack spacings	
M15-0.5% Two shear cracks Reduced crack spacings	
M15-0.5%H Shear crack ≥ 1.0 mm Reduced crack spacings	
M15-1.0% Forking cracks Diffused cracking pattern	
M15-1.5% Forking cracks Diffused cracking pattern Reduced crack widths	
M15-0.75%H Multiple cracking Forking cracks Diffused cracking pattern	

Figure 5.11: Crack patterns for the beams in the M15 series

M20-0.75% Two diagonal cracks Large crack spacings	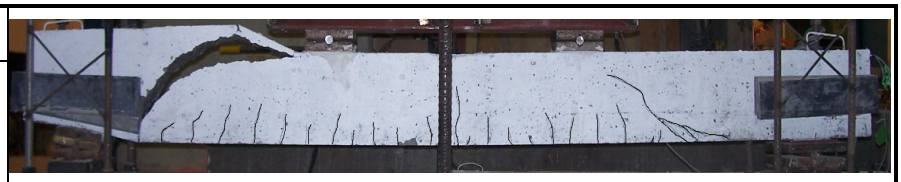
M20-1.0% Sveral diagonal cracks Reduced crack spacings	
M20-1.0%A Shear crack ≥ 1.0 mm Reduced crack spacings	
M20-1.0%B Similar to M20-1.0%	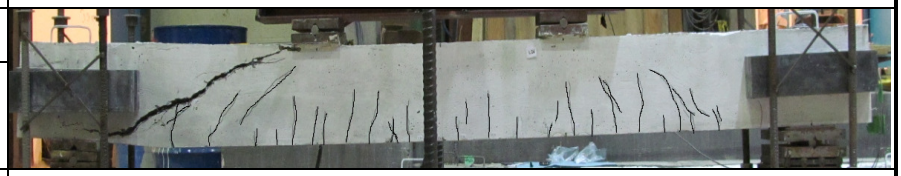
M20-1.5%A Very diffused pattern Multiple cracking Forking cracks	
M20-1.5%B Multiple cracking Forking cracks	

Figure 5.12: Crack patterns for the beams in the M20 series

5.5 Discussion on Critical Fiber Content

One of the most fundamental observations from the experimental program is the importance of selecting the most efficient fiber quantity for a given beam, which we may refer to as the "critical fiber content". As has been demonstrated in this experimental program using fibers in a quantity lower than the critical content would lead to a beam that fails in shear and does not show a ductile failure response (e.g. in this test series 1% fibers was sufficient to transform failure mode into flexure in the M15-series, but was not sufficient in the M20 series). On the other hand, adding fibers beyond the critical content will not result in significant enhancements in capacity since fibers play a minimal role in increasing flexural strength (e.g. compare beams M15-1.0% and M15-1.5%), although the addition of fibers beyond this limit could lead to improvements in flexural ductility and crack control. That is to say adding fibers up to the critical limit has an important effect on the ultimate capacity in beams failing in shear, however once the flexural capacity is reached, the effect on nominal moment capacity is minimal. Hence, for design practice it is important to be able to select the most appropriate fiber content in order to provide safe design while simultaneously optimizing material costs. Moreover, in certain situations the shear demand is too large to be accommodated by using steel fibers, due to the limitations on the amount of fibers which can be added without affecting workability. It is important to note that this "critical fiber content" is governed by many parameters such as material properties (of both the concrete and the fibers) as well as beam properties. These parameters should be considered in prediction and design equations used to select fiber requirements for a given application.

5.6 Discussion on Minimum Shear Reinforcement in the ACI-318 Code

5.6.1 Ability of fibers to replace minimum shear reinforcement - SFRC

As previously discussed in the literature review, the ACI-318 Code permits the use of steel fibers to replace the minimum shear reinforcement required in beams subjected to shear

forces ranging from $0.5V_c$ to V_c, ($V_c = 0.17\sqrt{f_c'}b_w d$, MPa). In order to qualify as an alternative to traditional shear reinforcement, the SFRC must have a minimum fiber dosage of 60 kg/m^3 (0.75% by volume of concrete). This recommendation was based on a parametric study conducted by Parra-Montesinos (2006) on a large database of SFRC beam test results reported in the literature. The study showed that all SFRC beams in the database having a fiber content greater or equal to 0.5% exhibited shear stress at failure larger than $0.17\sqrt{f_c'}$ (MPa) which corresponds the shear stress attributed to concrete, V_c, in the ACI-318 code. The study also showed that beams having $V_f \geq 0.75\%$ had shear stresses at failure not less than $0.3\sqrt{f_c'}$ (MPa), which can be considered as a lower bound value for beams having this quantity of fibers (see **Figure 5.13**). Based on this result Parra-Montesinos recommended that a minimum steel fiber content of 0.75% in order to substitute for minimum shear reinforcement. This minimum fiber requirement was implemented in the 2008 edition of the ACI-318 code, which permits the use of SFRC to replace minimum shear reinforcement in flexural members meeting certain material, dimensional and loading limits.

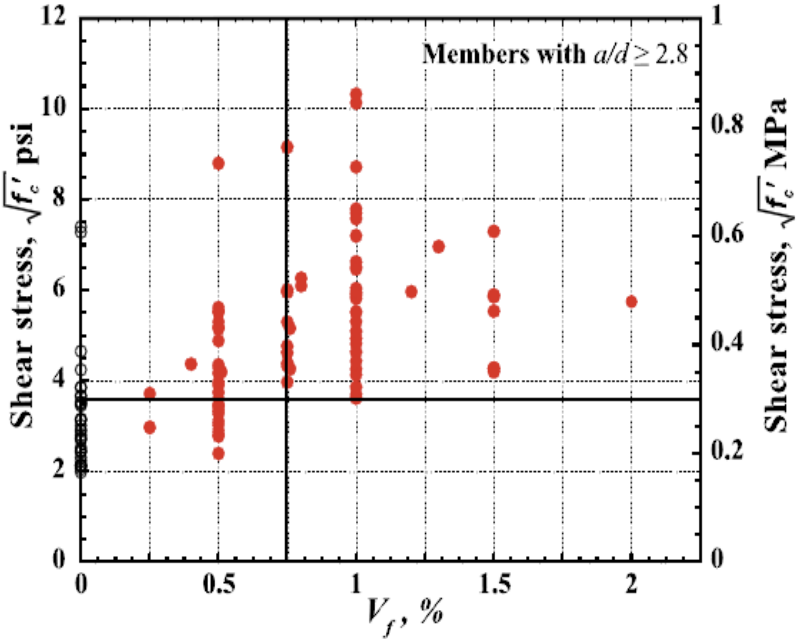

Figure 5.13: The influence of fiber content on the normalized shear stress [Adapted from Parra- Montesinos (2006)]

5.6.2 Ability of fibers to replace minimum shear reinforcement - SCFRC

Although there is much data to support the use of SFRC as a replacement for minimum shear reinforcement in traditional reinforced concrete beams, it is important to examine if this statement is also valid for beams constructed with self-consolidating concrete and steel fibers. The data plotted in **Figure 5.14** shows the shear stress at failure for all the beams tested in this experimental program (it is noted that all beams had $V_f \geq 0.5\%$). Although there is limited data in the literature on SCFRC beams, **Figure 5.15** shows the shear stress at failure for all the beams that failed in shear in this experimental program along with the failure stresses of SCFRC beams from two other studies in the literature (Greenough and Nehdi (2008), Zighuo et al. (2010)). The properties of the SCFRC specimens in these two studies are summarized in **Table 5.3**. The analysis shows that all the SCFRC beams tested in this study and reported in the literature failed at shear stresses greater than $0.17\sqrt{f_c'}$. Considering this limited set of SCFRC beam test results, the estimated lower bound value is found to be $0.25\sqrt{f_c'}$ for beams having $V_f \geq 0.75\%$ (see **Figure 5.15**). This value is found to be somewhat lower than the value of $0.3\sqrt{f_c'}$ reported for SFRC beams. Nonetheless, the above analysis, though limited to a few beams, could be considered preliminary evidence to support the use of steel fibers as a replacement for minimum shear reinforcement in SCFRC beams having $V_f \geq 0.75\%$. However further research is required to validate this statement.

It is also interesting to note that the shear stress at failure for the control SCC beam in this study was lower than the nominal shear stress corresponding to V_c in the ACI code.

Table 5.3: The parameters of the specimens tested by the other researchers

Beam Designation	b (mm)	d (mm)	ρ	a/d	f_c' (MPa)	D_f (mm)	L_f/D_f	V_f (%)	V_{exp} (kN)
S-HE-50-0.5*	200	265	0.017	3.02	40	1.00	50	0.50	90.80
S-HE-50-0.75*	200	265	0.017	3.02	40	1.00	50	0.75	105.60
S-HE-50-1.0*	200	265	0.017	3.02	40	1.00	50	1.00	148.90
SFSCCB50-∞**	200	260	0.028	3.00	56	0.55	64	0.50	137.50

* tested by Greenough and Nehdi (2008)
** tested by Zighuo et al. (2010)

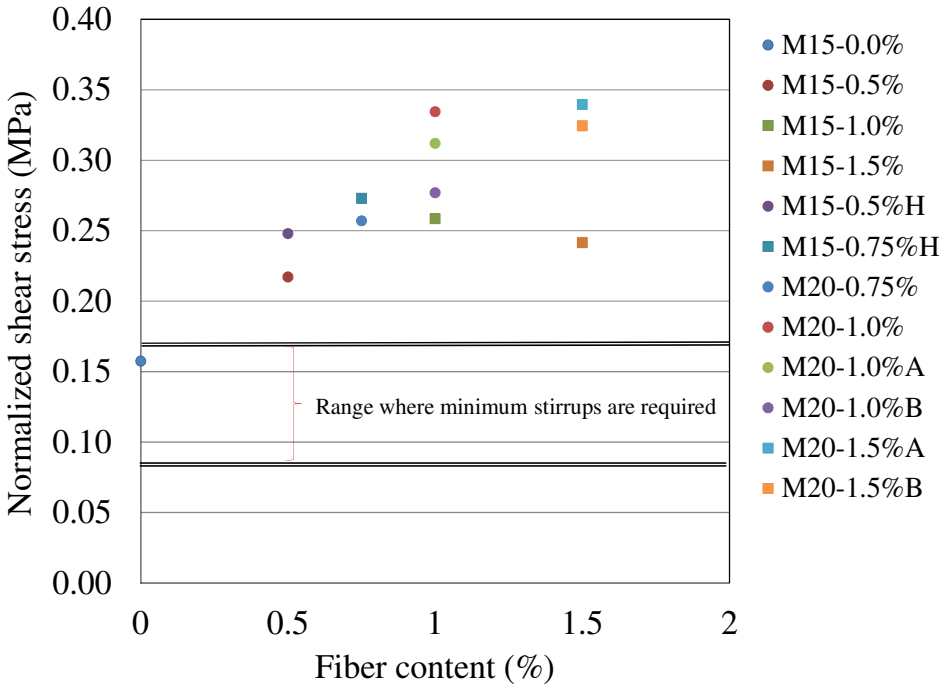

Figure 5.14: Shear stress at failure versus fiber content for beams tested in this study

● beams failed in shear failure ■ beams failed in flexure

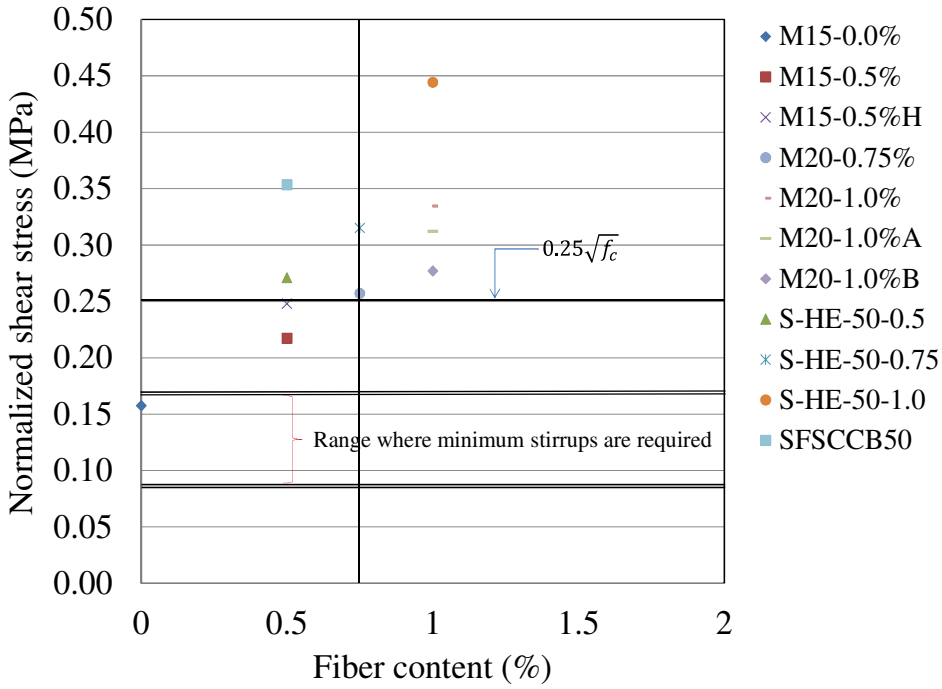

Figure 5.15: Data showing the lower bound value for shear stress at failure for SCFRC beams

Chapter Six: Models for Predicting Shear Behaviour of SFRC and SCFRC Beams

6.1 Introduction

Research over the past three decades has shown that the use of steel fibers in reinforced concrete beams can be used to enhance shear resistance and promote flexural failure and ductility. Adding steel fibers to a concrete beam without transverse reinforcement improves the shear strength due to the ability of SFRC to resist and redistribute diagonal tensile stresses after cracking.

This chapter begins with a parametric study investigating the effect of various factors on the shear strength of SFRC beams. In addition, existing models proposed by other researchers for predicting shear strength of SFRC beams are reviewed. A simple analytical model for predicting the shear capacity of SFRC beams is also proposed. The proposed model and empirical models presented in the literature are validated against a database of SFRC and SCFRC beam test results. Finally, the chapter concludes by an equation and guidelines for predicting the design shear strength of SFRC beams.

6.2 Parametric Study: Parameters Affecting Shear Strength of SFRC Beams

Despite the large amount of research data, the behaviour of SFRC beams remains a problem whose complexity is not completely understood. The complexity returns to the fact that the behaviour of SFRC beams is a function of several factors both at the material and structural

level. These factors are related to the geometry and the cross-section of the member, the material properties, and the fiber characteristics.

This section presents a parametric study that examines the effect of various factors on the shear response of SFRC beams, including effective depth, shear span-to-depth ratio, longitudinal reinforcement ratio, concrete matrix strength and fiber properties. Included in the study is a database of 173 SFRC beams having rectangular cross-section reported in 19 research studies. It is noted that several of the studies come from a previously published database compiled by Parra-Montesinos (2006). The database includes test results from SFRC beams having effective depths (d) ranging from 180-570 mm, shear-span to depth ratio (*a/d*) ranging from 1.0-6.0, compressive strength (f_c') between 18-104 MPa, longitudinal reinforcement ratios (ρ) ranging from 0.4%-5%, fiber volume fractions (V_f) ranging from 0.25%-2% and having straight, hooked or crimped fibers.

Table 6.1 summarizes the different parameters investigated in the 19 research studies reported in the database. The properties of the various beams are summarized in the appendix section of the thesis (see **Table A1**).

6.2.1 SFRC compressive strength

At the material level, the post-cracking resistance of SFRC is directly dependent on the fiber type, volume, and the bond strength developed between the fibers and the concrete matrix. This last parameter has a direct influence on fiber pullout strength and is a function of the concrete matrix strength. **Figure 6.1** presents research data from seven series of beams in three different studies. The beams in each series have identical properties but have different concrete matrix strengths. The figure shows that increasing the compressive strength of the matrix produces larger SFRC beam shear resistance when all other properties are kept constant. Kwak et al. (2002) has previously suggested that doubling the concrete strength of a beam increases shear strength by 20%.

6.2.2 Fiber volume fraction

Figure 6.2 presents data from 5 studies and 7 series of beams having the same properties but having varying fiber contents. As expected increasing the fiber content improves the shear resistance of an SFRC beam. However it should be noted that many other factors related to the fibers themselves can also have a significant effect on shear response; this includes factors such as the type of fiber, and the fiber strength.

As discussed previously, Parra-Montesinos (2006) has proposed that using a minimum fiber content of $V_f \geq 0.75\%$ produces an average shear stress not less than the conservative lower bound of $0.3\sqrt{f_c'}$ MPa. Para-Montesinos found that in case of V_f less than or equal 0.5% the shear stress value approaches the ACI-318 code value of $0.17\sqrt{f_c'}$ MPa which represents the concrete contribution to shear resistance.

It is worth mentioning that although fiber content has an important effect on the ultimate capacity in beams failing in shear, once the flexural capacity is reached the effect of increasing fiber content on nominal moment capacity is minimal. Thus, using fibers as a supplement to traditional longitudinal reinforcement may not be effective (Minelli, 2005).

6.2.3 Fiber aspect ratio L_f/D_f

As noted in the literature one of the key parameters affecting the performance of fibers in SFRC in general is the aspect ratio (L_f/D_f). **Figure 6.3** plots the effect of aspect-ratio on shear resistance in six series of beams from studies performed by Adebar et al. (1997) and Dinh (2009). The figure shows that the use of fiber with higher aspect-ratio can result in a improvement in shear capacity. It should be noted that using a higher aspect-ratio can impact workability and placement of concrete when higher fiber contents are used.

6.2.4 Longitudinal reinforcement ratio

Another parameter related to cross-sectional properties that can affect shear response is ratio of longitudinal steel reinforcement. As shown in **Figure 6.4**, when all other properties are kept similar, increasing the reinforcement ratio results in an increase in shear resistance. As noted in the literature review, this same effect has also been reported in the case of traditional reinforced concrete beams without fibers. This goes back to the fact that increasing this ratio results in an increase in dowel action and a deeper compression zone which results in increased shear capacity (Dinh, 2009).

6.2.5 Shear span-to-depth ratio

Several researchers have studied the effect of shear span-to-depth ratio (*a/d*) on the behaviour of SFRC beams. Based on the research data it can be concluded that decreasing the *a/d* ratio leads to an increase in SFRC shear resistance. This effect is shown in **Figure 6.5** where test data (from 5 studies, 13 series) shows that using beams with a shear span-to-depth ratio less than 2 can result in a significant increase in ultimate shear strength (Dinh, 2009). The figure also shows that as the *a/d* ratio increases beyond 3.0 the effect of increasing the *a/d* ratio is present but less pronounced.

It is noted that mechanisms governing shear response in beams with small *a/d* ratio is different than in slender beams (due to strut-and-tie action). It should also be mentioned that many of the studies reported in the literature involve beams with an *a/d* ratio less than 2 (see **Figure 6.6**). This should be kept in mind, since the shear strength of such SFRC beams is strongly influenced by arch and strut action.

6.2.6 Effective depth

Research has shown that the shear stress at failure in RC beams without web reinforcement reduces as the size increases (Collins and Mitchell, 1997). Some researchers have postulated that this "size effect" is eliminated in SFRC beams. However, Gustafsson and Noghabai (1999) tested a series of SFRC beams with varying depths and observed that as the beam depth increased the ductility decreased. The authors used fracture mechanics to show that as the ratio of stored elastic energy to dissipated fracture energy increases, the brittleness increases. Hence, the larger the beam, the greater the energy release, and thus the more brittle the behaviour.

There is limited data in the literature comparing the behaviour of smaller and larger SFRC beams, however **Figure 6.7** shows a plot of normalized shear stress ($v_u / \sqrt{f_c'}$) as a function of beam effective depth from four studies reported in the literature. It can be seen that the specimens show a drop in ultimate shear stress as the beam depth is increased.

It should be noted that the large majority of the test data available in the literature (more than 85%) has dealt with SFRC beams with small effective depths (d < 280 mm) (see **Figure 6.8**). Thus, the statement above has not been fully verified and there is a need for further experimental research on the effect of size in larger SFRC beams.

Table 6.1: Summary of the database results of SFRC beams in this parametric study

Author	Range of main parameters											
	Beams #	Cross sec.	b_w (mm)	h (mm)	d (mm)	f_c' (MPa)	a/d	ρ (%)	Fiber type	L_f (mm)	d_f (mm)	V_f (%)
Montesinos et al. (2006)	10	R	152	457	381	31-49	3.4-3.5	0.20-0.27	H	30-60	0.50	1.0-1.5
Adebar et al. (1997)	6	R	150	610	556	41-56	1.6	0.023	H	30-50	0.5	0.4-1.5
Ashour et al.(1992)	18	R	127	254	216	92-101	1.0-6.0	0.004-0.046	H	60	0.80	0.5-1.5
Casanova et al. (1999)	3	R	127	254	226	90	2.9	0.022-0.036	H	30	0.50	1.3
Cucchiara et al. (2004)	4	R	150	250	218	41-43	2.0-2.8	0.019	H	30	0.50	1.0-2.0
Kwak et al. (2002)	9	R	127	254	213	31-69	2.0-4.0	0.015	H	50	0.80	0.5-0.75
Li et al. (1992)	2	R	127	229	203	23-26	3.0	0.022	H	30-50	0.50	1.0
Lim et al. (1987)	12	R	152	254	221	34	1.5-3.5	0.012-0.024	H	30	0.50	0.5-1.0
Mansur et al. (1986)	20	R	152	229	198-201	21-33	2.0-4.4	0.008-0.020	H	30	0.50	0.50-1.0
Noghabai (2000)	5	R	201-300	500-701	236-569	68-102	2.9-3.3	0.029-0.043	S-H, H	30-60	0.60-0.70	0.5-0.75
Rosenbusch et al. (2002)	17	R	201	300-599.4	259-541	39-41	2.5-4.0	0.018-0.031	H	60	0.90	0.25-0.76
Sharma (1986)	1	R	152	305	277	49	1.8	0.045	H	50	0.60	0.9
Swamy & Bahia (1985)	6	R	175	249	211	35 -42	4.5	0.020-0.040	C	50	0.50	0.4-1.2
Swamy et al. (1993)	9	R	56	305	264	32 -41	2.0-4.9	0.016-0.043	C	50	0.50	1.0
Tan et al. (1993)	5	R	61	376	340	32-36	1.5-2.0	0.034	H	30	0.50	0.5-1.0
Barragan (2002)	6	R	200	300-600	260-540	38-39	3.5	0.026-0.029	H	60	0.92	0.5
Aoude (2008)	2	R	150	250	202	20-21	3.0	0.013	H	30	0.55	0.5-1.0
Narayanan (1987)	33	R	85	150	126-130	36-64	2.0-3.5	0.02-0.057	C	30-40	0.30	1.25-3.0
Furlan (1997)	5	R	100	100	86	49-55	3.5	0.06-0.1	C	25-38	0.20	1.0-2.0

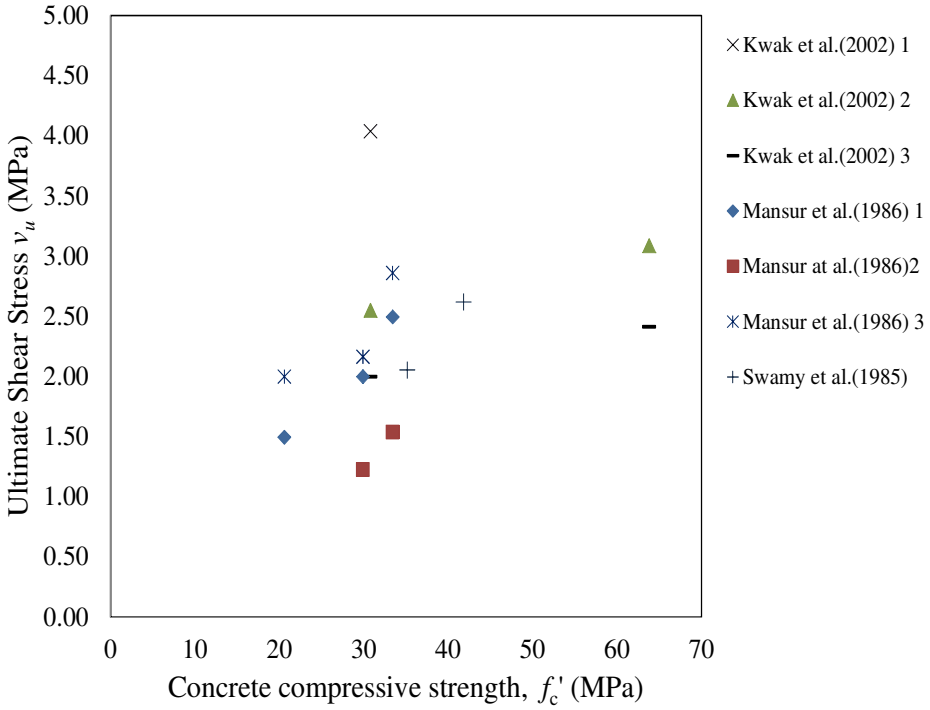

Figure 6.1: The effect of increasing the concrete compressive strength on the shear resistance for different fiber percentages

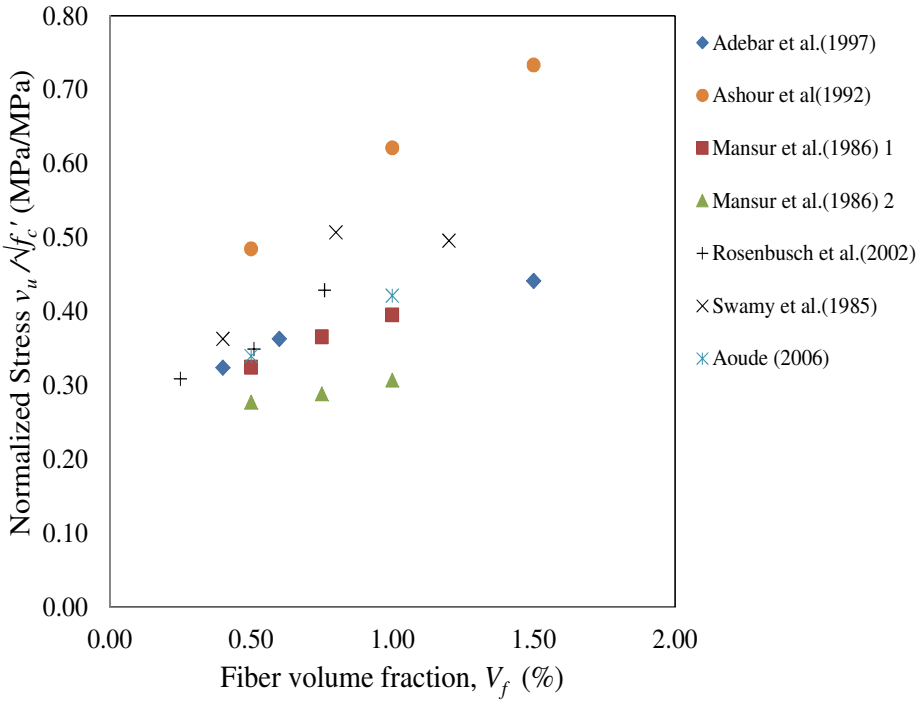

Figure 6.2: The effect of fiber volume fraction on the shear strength

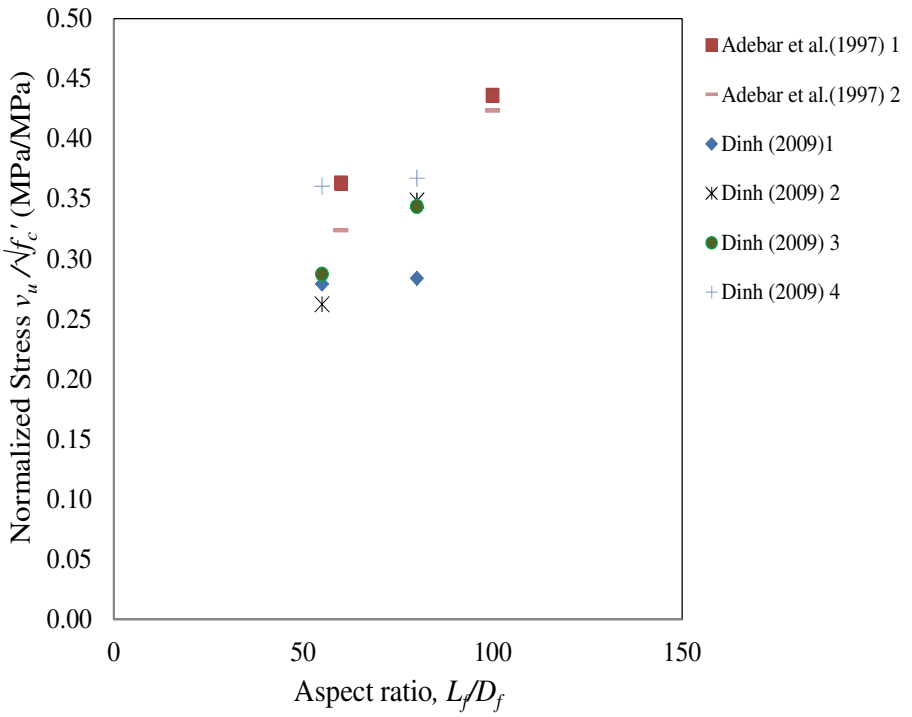

Figure 6.3: The effect of fiber aspect ratio on the normalized shear stress

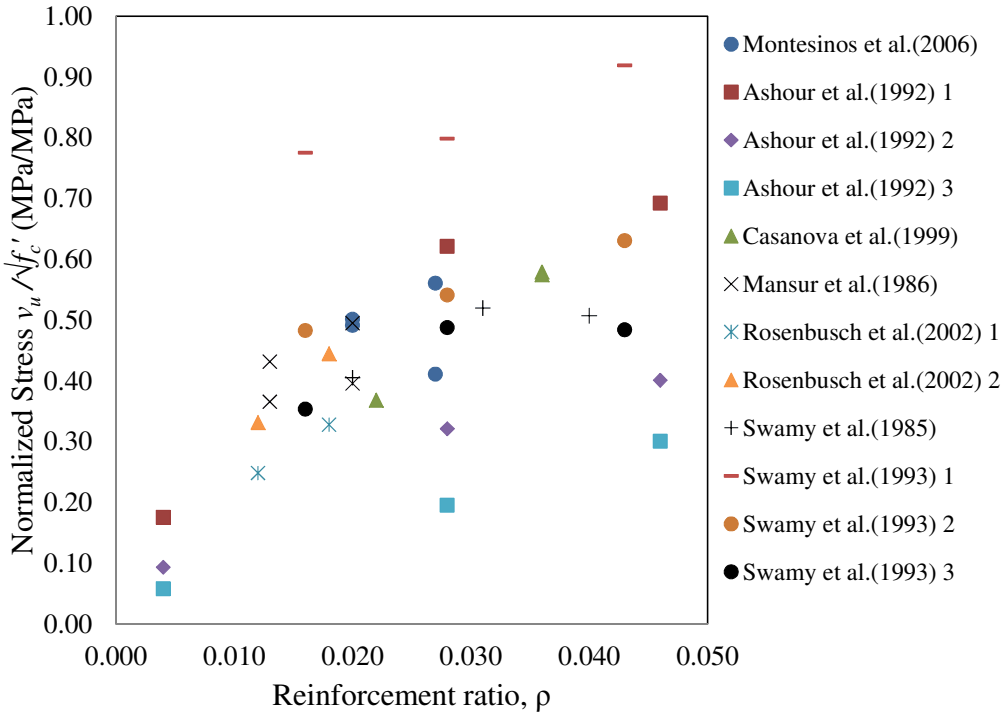

Figure 6.4: The effect of the longitudinal reinforcement ratio (ρ)

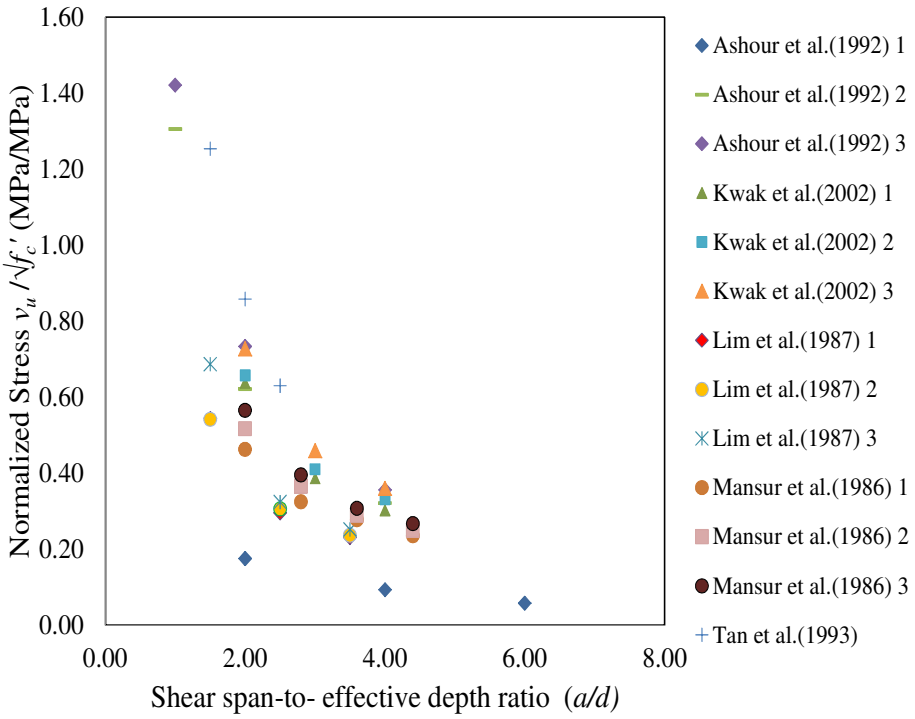

Figure 6.5: The effect of shear span-to-effective depth ratio on the shear strength

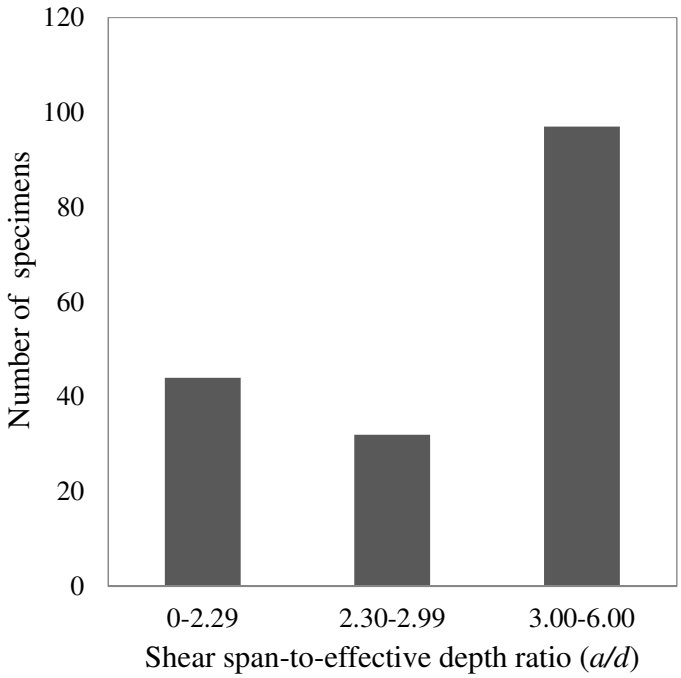

Figure 6.6: Number of studies on SFRC beams as a function of *a/d* ratio

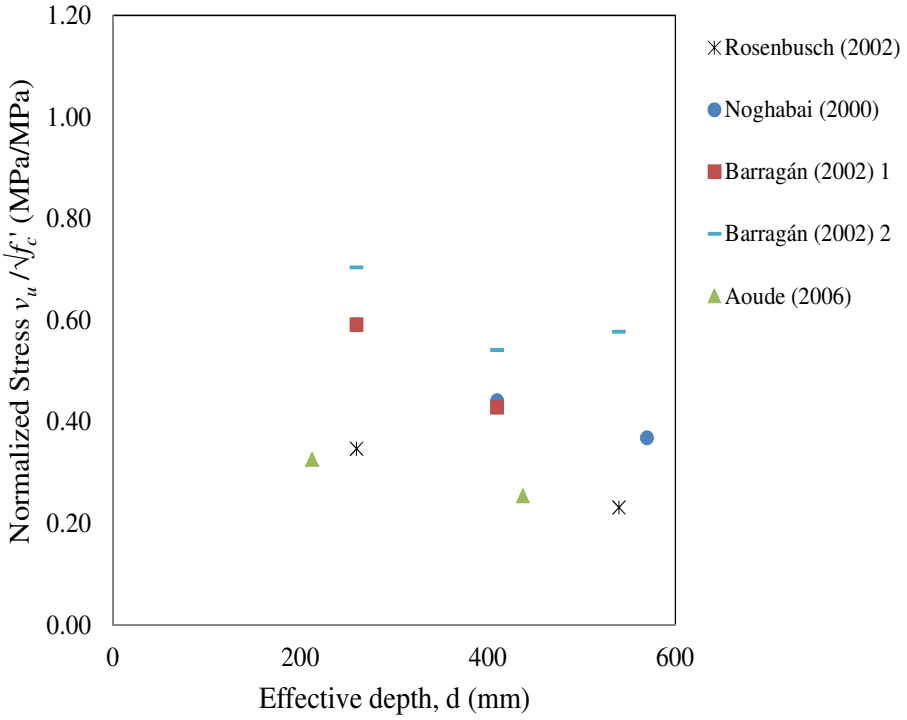

Figure 6.7: The effect of increasing the beam depth on the shear strength

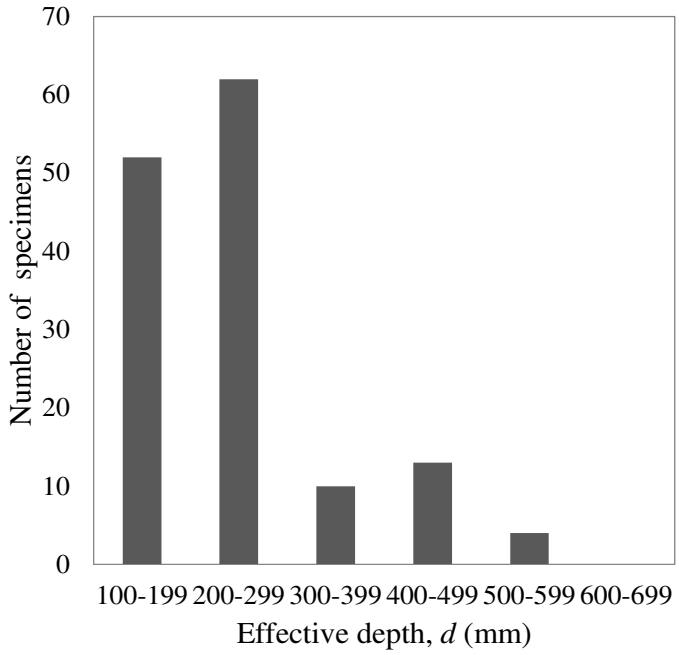

Figure 6.8: Number of studies on SFRC beams as a function of beam effective depth

6.3 Existing Models for Predicting the Shear Resistance of SFRC Beams

As discussed in the literature review, several researchers have proposed empirical equations for predicting the shear resistance of SFRC beams (refer to Chapter 2). As shown in **Table 6.2** most of these models can be broadly classified into two categories. The first category of models assumes that fibers improve the concrete shear resistance directly due to the improvement in tensile post-cracking resistance. These models use material tests to quantify the improvement in shear capacity. The second category considers that fibers provide a separate shear contribution that is additional to the concrete shear contribution. Many models in this category account for the fiber contribution empirically using a "fiber factor", F, which is a function of fiber volume ratio (V_f), diameter (D_f) and length (L_f) as shown in **Equation 6-1**. This equation is often scaled by an additional parameter to account for fiber typology. As discussed in the literature review and will be shown in section 6.5, due to the empirical nature of the expressions, the majority of these models do not produce accurate predictions for the resistance of SFRC beams.

$$F = V_f \frac{L_f}{D_f} \tag{6-1}$$

Table 6.2: Various models to predict shear resistance of SFRC beams (Category 1)

Category 1					
Model	**Fiber contribution is ...**		**Fiber effect accounted for using ...**		
	included in concrete contribution	separate term (additional to concrete contribution)	Split cylinder strength (or MOR)	Fracture mechanics /Bending test	Fiber factor
(Sharma, 1986) $\upsilon_u = kf_t \left(\frac{d}{a}\right)^{0.25}$	✓		✓		
(Li et al., 1992) $\upsilon_u = 1.25 + 4.7\left[\left(f_f f_{sp}\right)^{\frac{3}{4}}\left(\rho\frac{d}{a}\right)^{\frac{1}{3}} d^{-\frac{1}{3}}\right]$	✓		✓		
(Cassanova, 1996) $V = 0.9bd \cdot \overline{\sigma_p}(w) + V_s$	✓			✓	
(Minelli and Plizzari, 2006) $\upsilon_u = \left[\frac{0.18}{\gamma_c} k\left(100\rho_1\left(1+2.5\frac{f_{eq(0.6-3)}}{f_{ct}}\right)f_{ck}\right)^{1/3} + 0.15\sigma_{CP}\right]$	✓			✓	

Table 6.3: Various models to predict shear resistance of SFRC beams (Category 2)

Category 2					
Model	**Fiber contribution is ...**		**Fiber effect accounted for using ...**		
	included in concrete contribution	separate term (additional to concrete contribution)	Split cylinder strength (or MOR)	Fracture mechanics /Bending test	Fiber factor
(Imam et al., 1995) $v_u = 0.6\Psi\sqrt[3]{\omega}\left[\left(f_c\right)^{0.44} + 275\sqrt{\frac{\omega}{\left(a/d\right)^5}}\right]$		✓			✓
(Mansur et al., 1986) $v_u = \left(0.16\sqrt{f_c'} + 17.2\frac{\rho V d}{M}\right) + 0.41\left(\tau \cdot V_f \frac{L_f}{D_f}\right)$		✓			✓
(Narayanan and Darwish, 1987) $v_u = e\left(0.24 f_{spfc} + 80\rho\frac{d}{a}\right) + 0.41\left(\tau \cdot V_f \frac{L_f}{D_f} d_f\right)$		✓			✓
(Ashour et al., 1992) $v_u = \left(0.7\sqrt{f_c'} + 7 \cdot V_f \frac{L_f}{D_f} d_f\right)\frac{d}{a} + 17.2\rho\frac{d}{a}$		✓			✓
(Swamy et al., 1993) $v_u = v_c + 0.37\left(\tau \cdot V_f \frac{L_f}{D_f}\right)$		✓			✓
(Shin and Oh, 1994) $v_u = 0.19 f_{sp} + 93\left(\rho\frac{d}{a}\right) + 0.34\left(\tau \cdot V_f \frac{L_f}{D_f} d_f\right)$		✓			✓
(Khuntia et al., 1999) $v_u = \left(0.167\alpha + 0.25 \cdot V_f \frac{L_f}{D_f} d_f\right)\sqrt{f_c'}$		✓			✓
(Kwak et al., 2002) $v_u = 3.7 e f_{spfc}^{2/3}\left(\rho\frac{d}{a}\right)^{1/3} + 0.8\left(0.41\tau V_f \frac{L_f}{D_f} d_f\right)$		✓			✓

6.4 Proposed Model for Predicting the Shear Resistance of SFRC Beams

This section describes a procedure for predicting the shear resistance of SFRC beams without web reinforcement. As noted previously, several existing models and design guidelines consider the fiber contribution to shear capacity to be additional to the concrete contribution, much in the same way stirrups improve shear capacity. Other models propose that the fibers should modify the concrete contribution directly, In the present model, the former approach

is used and the shear resistance of an SFRC beam is assumed to be equivalent to the expected shear strength of a traditional reinforced concrete beam (V_{no}) plus the additional shear resistance provided by the fibers (V_{fib}) as shown in **Equation 6-2**:

$$V_{nf} = V_{no} + V_{fib} \tag{6-2}$$

6.4.1 RC contribution to shear resistance

In order to compute the RC contribution to shear resistance, V_{no}, the general shear design method of the 2004 CSA Standard can be used (see **Equation 6-3**). This method which is based on the Modified Compression Field Theory (MCFT) has been shown to provide accurate estimates of the shear resistance of traditional RC beams.

$$V_{no} = V_c + V_s \tag{6-3}$$

Where, V_c and V_s are the concrete and transverse steel contributions to shear resistance respectively. The concrete contribution, V_c, is computed using **Equation 6-4**:

$$V_c = \phi_c \beta \sqrt{f_c'} b_w d_v \tag{6-4}$$

and in case of using transverse steel reinforcement, its contribution, V_s, can be calculated using **Equation 6-5**

$$V_s = \frac{\phi_s A_V f_{yh} d_v \cot\theta}{s} \tag{6-5}$$

Where $b_w d_v$ is the effective shear area represented by the web width multiplied by the effective shear depth of the beam. The factor ϕ_c is a material reduction factor for concrete (can be taken as 1.0 for the purposes of analysis). The value β accounts for the ability of the concrete to transmit tensile stresses between the cracks. The angle θ is the angle of inclination of the diagonal compressive stresses to the longitudinal axis of the member. In the general design method both these parameters are a function of the longitudinal strain at mid-depth of the cross-section, ε_x, as shown in **Equation 6-6** and **Equation 6-7.** The effective crack spacing parameter, s_{ze}, is a function of the maximum aggregate size.

$$\beta = \frac{0.40}{1+1500\varepsilon_x} \times \frac{1300}{1000+s_{ze}} \tag{6-6}$$

$$\theta = 29° + 7000\varepsilon_x \tag{6-7}$$

The longitudinal strain at mid-depth of the cross section, ε_x, is computed using **Equation 6-8** for the case of moment and shear:

$$\varepsilon_x = \frac{\left(\frac{M}{d_v}\right)+V}{2\times E_s \times A_s} \tag{6-8}$$

To determine the shear strength, the shear, V, should correspond to the expected maximum shear resistance of the beam. The moment, M, represents the corresponding moment at the critical section in the beam (for the beams in this analysis the critical section is taken at a distance d_v from the loading point). A_s and E_s are the cross-sectional area and modulus of elasticity of the longitudinal tension reinforcement, respectively.

6.4.2 Pullout strength of hooked-end fibers

As mentioned in Chapter 2, studies have shown that anchorage properties play an important role in improving the pullout resistance of hooked-end steel fibers. Alwan et al. (1999) suggested that the mechanical contribution of the hook, $\Delta P'$, is a function of the cold work needed to straighten the fiber as it is being pulled out from the matrix. Using **Equation 2-2** (refer to Chapter 2), the simplified expression for $\Delta P'$ is shown in **Equation 6-9**:

$$\Delta P' = \frac{3.05}{\cos\left(45^o \times \pi/180^o\right)}\left(f_{fy} * \frac{\pi\left(D_f/2\right)^2}{6}\right) \tag{6-9}$$

The value f_{fy} is the fiber yield strength (in psi) and D_f is the fiber diameter (in inches). As an example for a typical Dramix ZP305 fiber, $\Delta P'$ is found to be 34 lbs (152 N).

Therefore, in the case of hooked-end fibers, taking into account the hook contribution, an estimate of the pullout strength, $F_{pullout}$, can be made using **Equation 6-10**, where the contribution of the hook ($\Delta P'$) is added to the load needed to cause debonding of the fiber:

$$F_{pullout} = \left(\tau_{bond} \times \pi \times D_f \times \frac{L_{f,straight}}{2} \right) + \Delta P' \quad (6\text{-}10)$$

The parameter $L_{f,straight}$ is the length of the straight portion of the fiber.

6.4.3 Pullout strength of crimped fibers

In order to take into account the enhancement in pullout strength provided by the deformed shape of a crimped fiber, the present model suggests using a "deformation contribution factor", α_m which scales the expected pullout strength of a straight smooth fiber as shown in **Equation 6-11**. As shown in **Table 6-4**, using data on the pullout strength of crimped fibers in the literature**,** α_m was taken as the average of the ratio of the bond strength of the deformed fiber (taken as measured pullout load divided by the surface area of the fiber) and the expected bond strength of a straight smooth fiber (see section 2.2.4.2). Based on this analysis, α_m was estimated to be 2.84 for the case of crimped fibers.

$$F_{pullout} = \tau_{bond} \times \pi \times d_f \times \frac{L_f}{2} \times \alpha_m \quad (6\text{-}11)$$

6.4.4 Alternate expression for the pullout strength of hooked-end fibers

In lieu of using **Equation 6-10**, the simplified approach used for crimped fibers can also be used to predict the pullout strength of hooked-end fibers by scaling the expected pullout strength of a straight smooth fiber to account for the contribution of the anchorage as shown in **Equation 6-11**. Using data on the pullout strength of hooked-end fibers in the literature, it was determined that α_m can be taken as 2.0.

Table 6.4: Several studies used to predict α_m for crimped fibers

Author	Pullout Load (N)	Fiber type	Aspect ratio (L_f/D_f)	f_c' (MPa)	Bond Strength $\tau_{straight}$ (MPa)	Bond Strength $\tau_{deformed}$ (MPa)	deformed fiber coefficient
Chanvillard & Aitcin (1996)	647	Crimped	50	29	2.42	8.23	3.41
Chanvillard & Aitcint (1996)	650	Crimped	50	49	3.45	8.27	2.4
Chanvillard & Aitcint (1996)	689	Crimped	50	78	4.72	8.77	1.86
Banthia & Trottier (1994)	675	Crimped	40	40	3.01	10.74	3.57
Banthia & Trottier (1994)	675	Crimped	40	52	3.59	10.74	2.99
						α_m **(Average)**	**2.84**

6.4.5 Bond-shear strength

The bond-shear strength, τ_{bond}, is a function of the concrete matrix strength, and it can be approximated using the values in **Table 2.1** (refer to Chapter 2). As discussed previously, the values listed in **Table 2.1** are based on a literature review performed by Kützing (2000) on the average bond shear strength from single fiber pull-out tests.

In the present work the simplified formula shown below was developed to estimate the bond-shear strength, τ_{bond}:

$$\tau_{bond} = 1.11 \times (f_{ct})^{1.354} \tag{6-12}$$

Where f_{ct} is the tensile strength of concrete and can be found using the following equation:

$$f_{ct} = 0.33\sqrt{f_c'} \text{ (MPa)} \tag{6-13}$$

Figure 6.9 shows that the proposed formula provides a good fit to the data in **Table 2.1**.

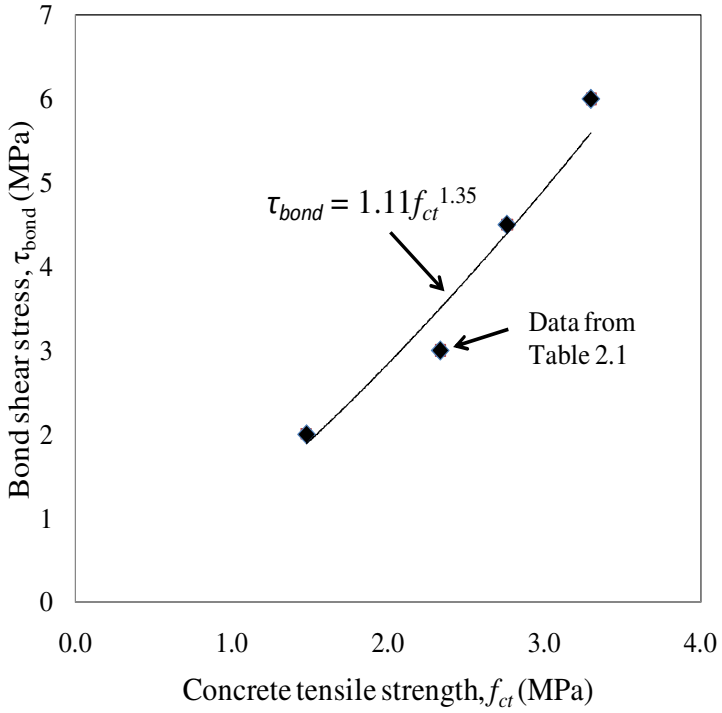

Figure 6.9: Bond strength equation

6.4.6 Fiber contribution to shear resistance

In order to account for the influence of the fibers on shear strength one can examine the free-body diagram of an SFRC beam with a crack inclination θ (see **Figure 6.10**). The fiber contribution to shear resistance, V_{fib}, can be related to the pullout strength of the fibers crossing this cracking plane as shown in **Equation 6-14**:

$$V_{fib} = \psi \times K \times \left(N_{fibres} \times \alpha_v F_{pullout}\right) \times b_w d_v \times \cot\theta \tag{6-14}$$

The above equation simplifies an iterative model previously proposed by Aoude (2008).

As mentioned in Chapter 2, the effective number of fibers per unit area, N_{fibers}, for fibers randomly oriented in three dimensions can be calculated using **Equation 6-15**:

$$N_{fibers} = \frac{V_f}{A_f} \times \alpha_\theta \times \eta_l \tag{6-15}$$

Where A_f is the cross-sectional area of the fiber, and where V_f is the volume fraction of fibers in the matrix. The orientation factor, α_θ, is used to account for the random orientation of the fibers crossing any arbitrary cracking plane and is taken as 3/8. The length factor η_l is used to account for the variability in the fiber embedment length across the cracking plane and is taken as 0.5.

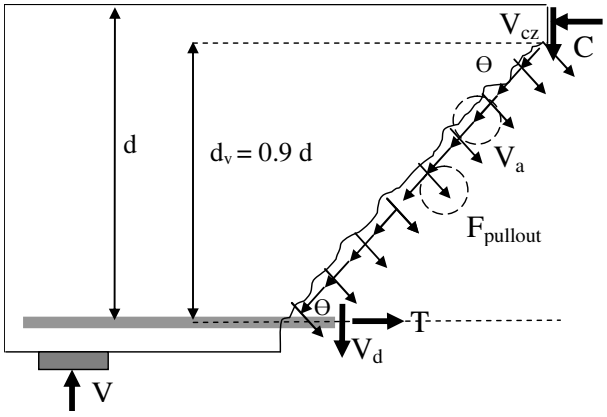

Figure 6.10: Fiber pullout resistance contributing to shear resistance

The pullout strength, $F_{pullout}$, is valid for the situation of pure tensile pullout. However in a beam, the fibers will resist tension along the diagonal cracks while undergoing a shear deformation (see **Figure 6.11**). Hence, in the proposed model it is assumed that the fibers will have reduced pullout efficiency in the situation of combined tension and shear. Using regression analysis, an empirically determined modification factor "Pullout Reduction Factor" of 0.8, α_v, was used to reduce the pullout resistance of the fibers (the pullout reduction factor was previously proposed in the model of Aoude (2008)).

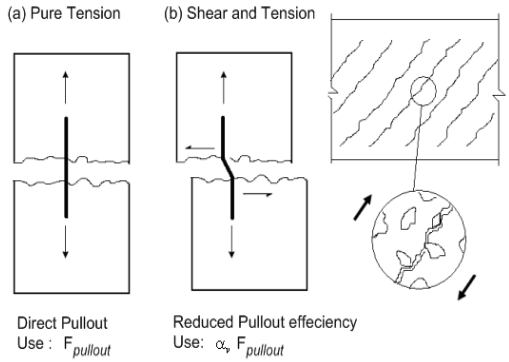

Figure 6.11: Reduced pullout resistance in the case of combined tension and shear [Adapted from Aoude (2008)]

As shown in **Figure 6.5**, the *a/d* ratio has a significant influence on the shear resistance of SFRC beams. In the proposed model a factor, K, is used to account for the effect of the *a/d* ratio as shown in **Equation 6-16**. This expression was determined based on regression analysis using a large database of experimental results from the literature.

$$K = 1.72 \times \frac{d}{a} \tag{6-16}$$

Figure 6.12 shows the relationship between normalized shear stress and *a/d* ratio from four different studies in the literature. It can be seen that as the *a/d* ratio increases, the normalized shear stress reduces. It can be seen that at an *a/d* ratio of 2.0, the normalized shear strength of the beams approaches a value of 0.75. Assuming that the fiber participation is full at an *a/d* ratio of 2.0 and reduces beyond the point, **Figure 6.13** plots the relationship of normalized shear strength divided by 0.75 as a function of *a/d* ratio. It can be seen that the empirically-derived expression for K gives a reasonably good correlation to the experimental data reported in the literature.

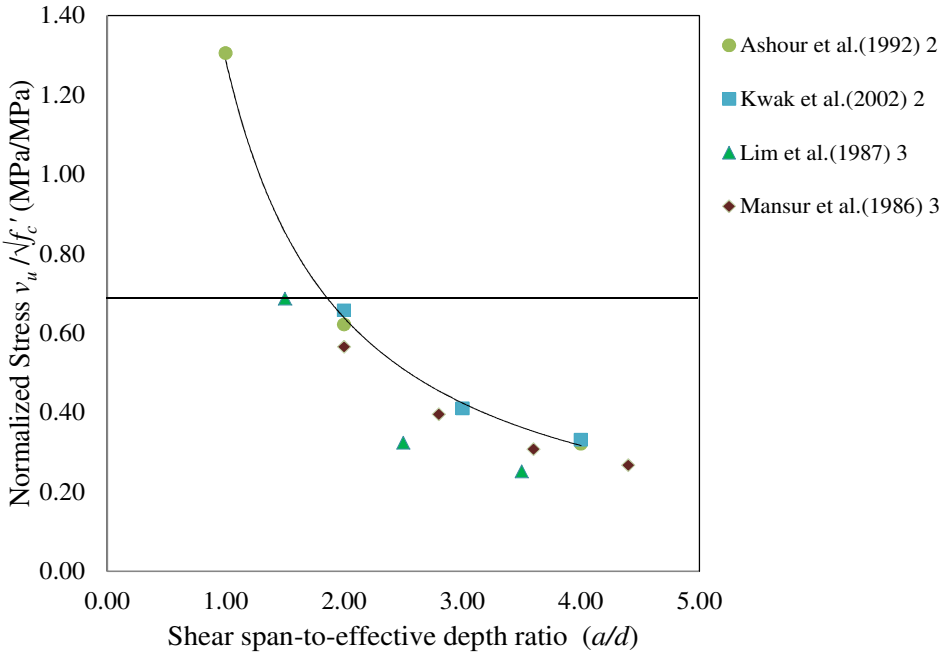

Figure 6.12: Normal shear stress as a function of *a/d* ratio

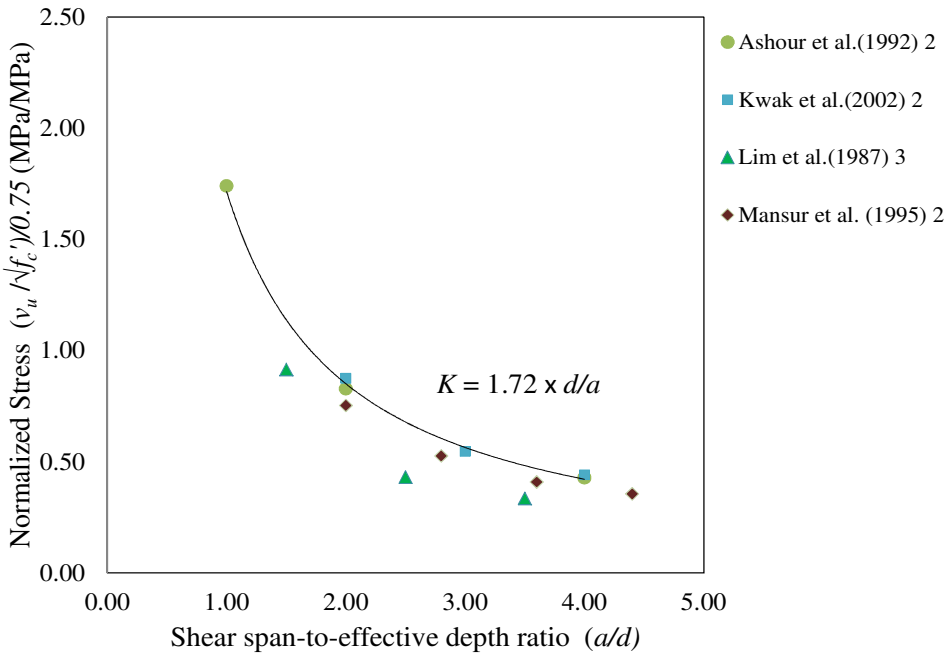

Figure 6.13: Correlation between normalized data and participation factor, K.

Research has shown that the shear stress at failure in RC beams without web reinforcement reduces as the size increase. Some researchers have postulated that this "size effect" is eliminated in SFRC beams. Although there is very limited data on the shear behaviour of larger SFRC beams, **Figure 6.7** indicates that there may be a size effect in larger SFRC beams. In the proposed model this size effect is taken into account using the size effect factor, ψ. The expression shown in **Equation 6-17** is the same expression suggested by Zararis and Papadakis (2001) for accounting for size effect in traditional RC beams:

$$\psi = \left(1.2 - 0.2\frac{a}{d}d\right) \tag{6-17}$$

The various steps needed to determine the shear resistance of SFRC beams (V_{nf}) as proposed in the present model are summarized in **Figure 6.14**.

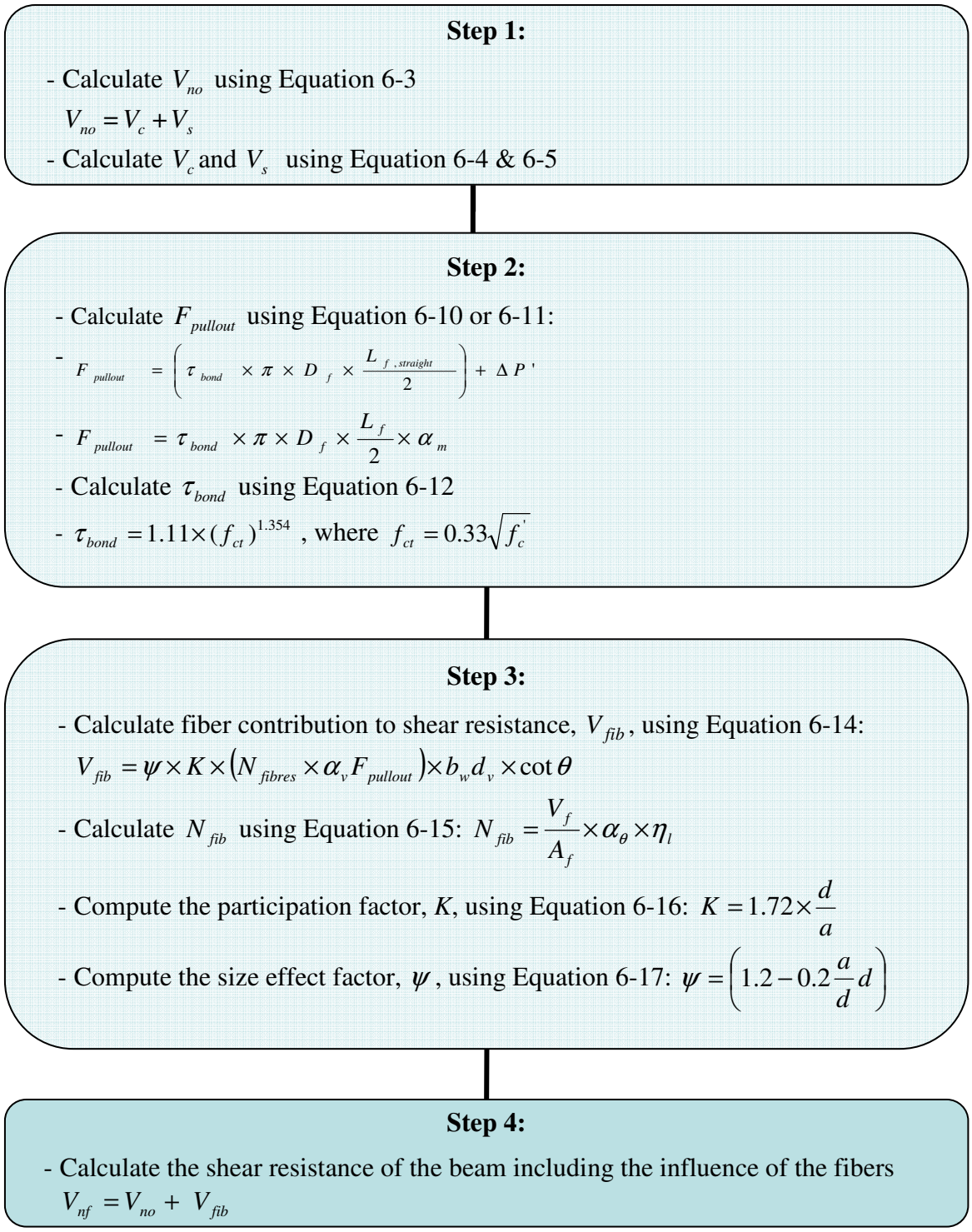

Figure 6.14: Proposed model procedure to calculate shear resistance of SFRC beams

6.5 Prediction of Shear Strength of SFRC beams

In this section, the models proposed by other researchers and the author are used to predict the shear capacities of a large database of SFRC beams from the literature (the beam properties are summarized in **Table A1**). The database includes the results from 173 SFRC beams (120 beams with hooked-end fibers and 53 with crimped fibers), including 137 beams that failed in shear.

It should be noted that many of the experimental tests available in the literature present the results of beams that have small *a/d* ratio. Such beams carry load by strut and tie action and in such cases the strength of the beams is strongly influenced by the details near the supports (Collins and Mitchell, 1997). From the database of 173 beam test results taken from the literature (see **Table A1**), 129 beams have *a/d* ratio greater than 2.3 (with 97 beams in this category failing in shear).

Figure 6.15 shows the predictions of the beams using six different models proposed in the literature and considering all 173 beams in the database. **Figure 6.16** includes only those beams having an *a/d* ratio greater than 2.3 (also shown in **Table A2** for hooked-end fibers and **Table A3** for crimped fibers). With the exception of the Narayanan & Darwish (1987) and the Ashour et al. (1992) models, one can note that the majority of the models proposed in the literature show high scatter.

Figures 6.17 (a), **6.18 (a)** and **6.19 (a)** compare the experimental shear capacities of all 173 beams in the database to those predicted using the analytical models for hooked-end and crimped fibers proposed in this thesis. **Figures 6.17 (b)**, **6.18 (b)** and **6.19 (b)** compares the experimental and predicted shear capacities of only those beams with *a/d* ratio greater than 2.3 (also shown in **Tables A2** and **A3**). One can see that the predictions using the models proposed in the present study agree reasonably well with the actual capacities for the majority of the beams for the case of slender beams (see mean and standard deviation values reported in **Tables A2** and **A3**).

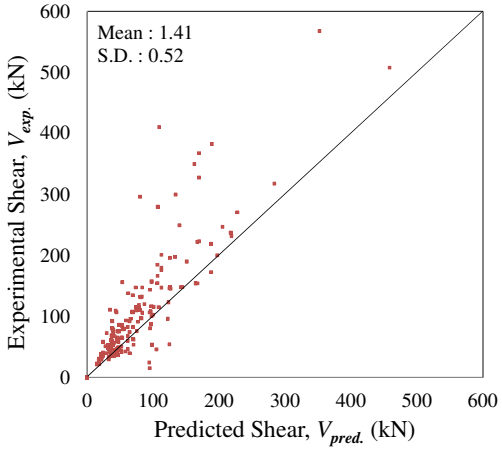

(a) Khuntia et al. (1999)

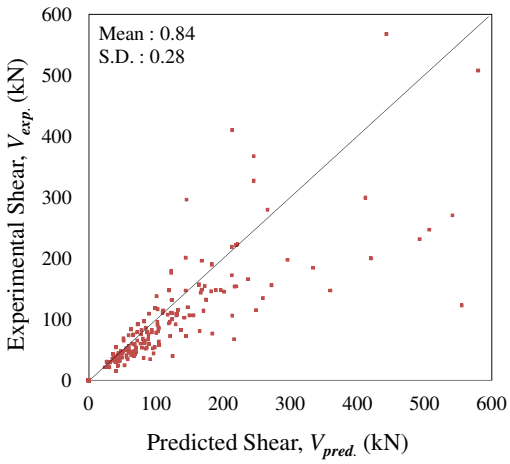

(b) Imam et al. (1995)

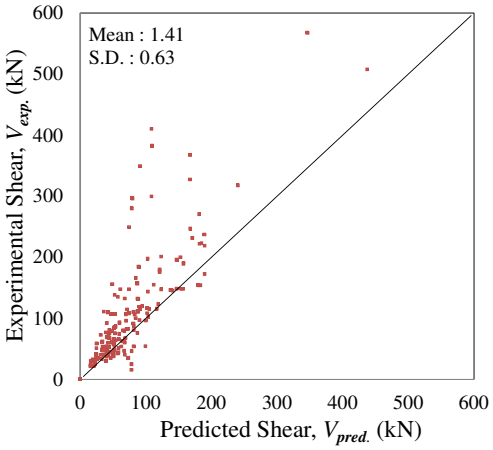

(c) Mansur et al. (1986)

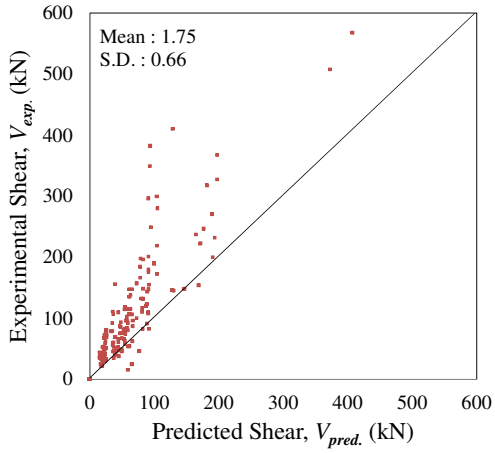

(d) Sharma et al. (1986)

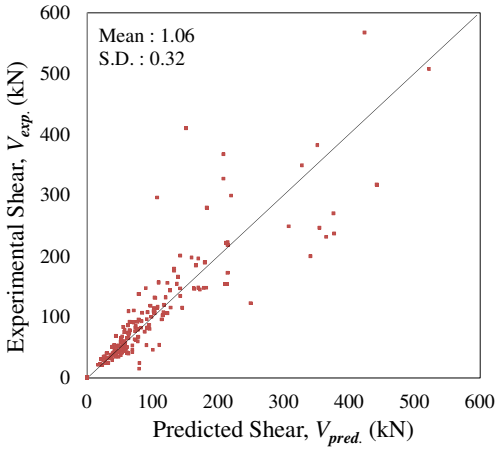

(e) Narayanan & Darwish (1987)

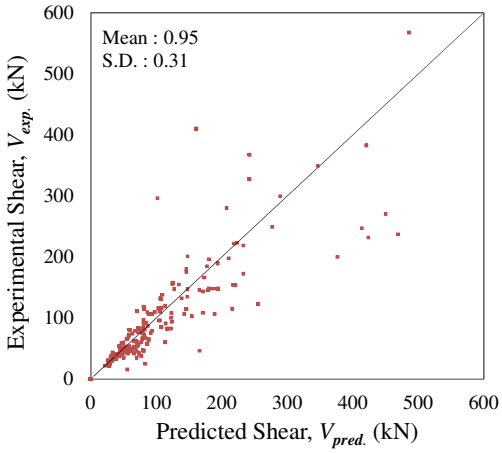

(f) Ashour et al. (1992)

Figure 6.15: Experimental vs. predicted shear capacities using equations suggested by other researchers and including all beams in the database.

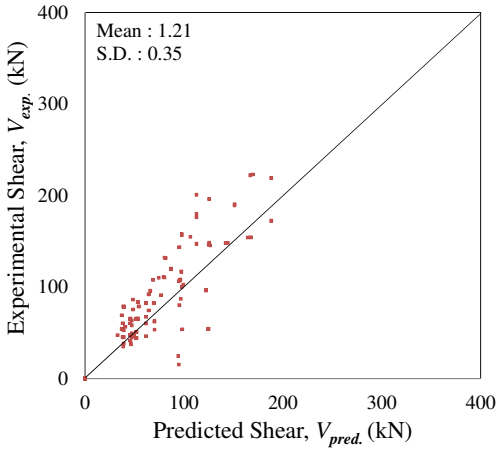

(a) Khuntia et al. (1999)

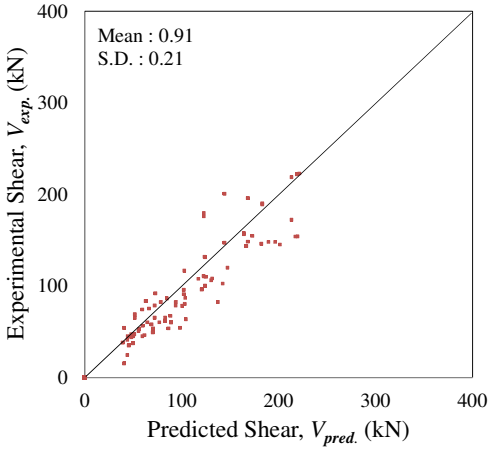

(b) Imam et al. (1995)

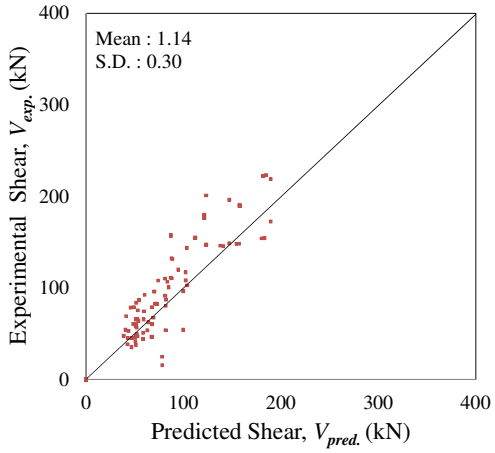

(c) Mansur et al. (1986)

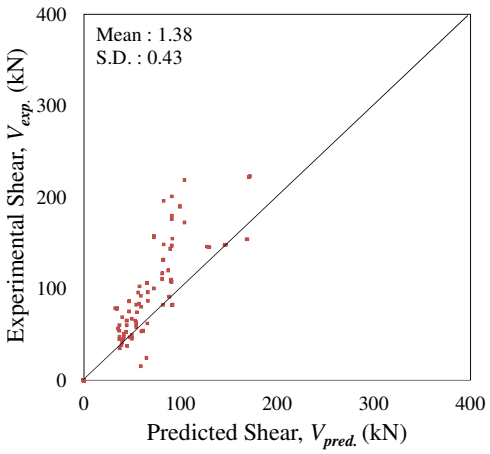

(d) Sharma et al. (1986)

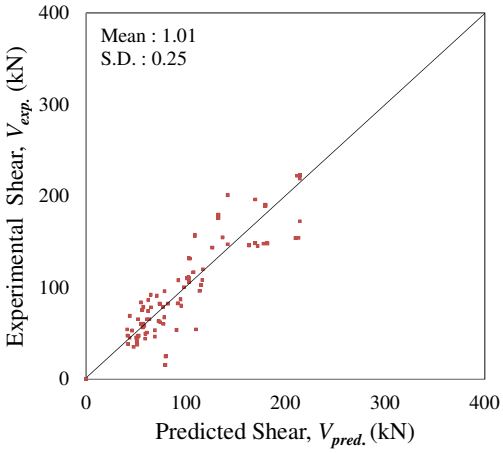

(e) Narayanan & Darwish (1987)

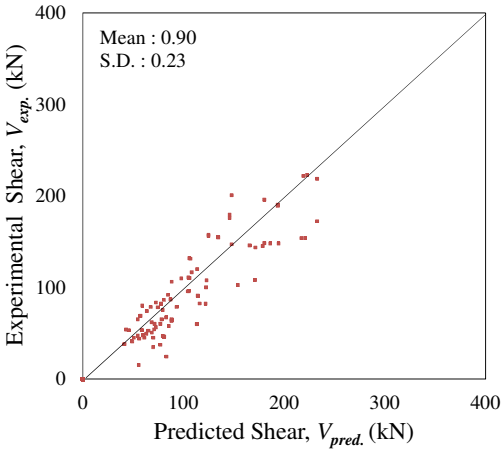

(f) Ashour et al. (1992)

Figure 6.16: Experimental vs. predicted shear capacities using equations suggested by other researchers and including only those beams with *a/d* ratio > 2.3.

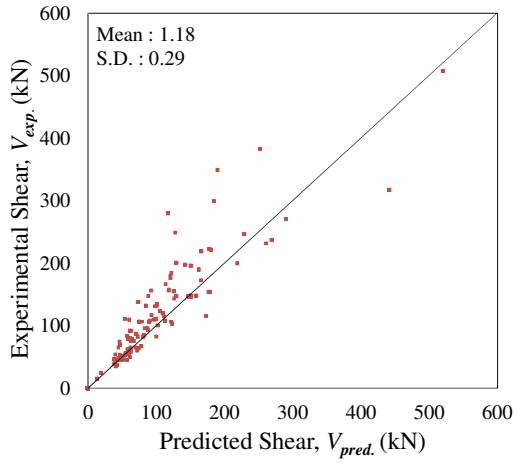

(a) Experimental vs. predicted shear capacities of all the beams

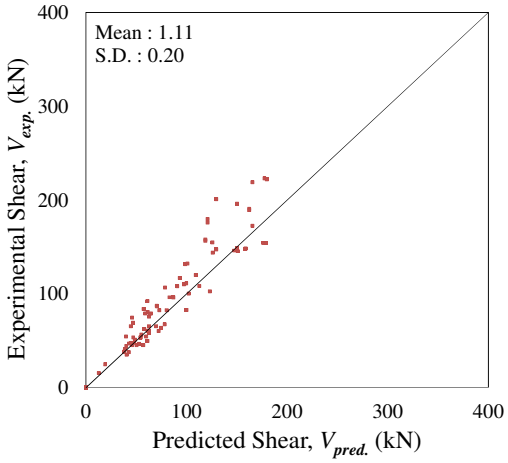

(b) Experimental vs. predicted shear capacities of beams with $a/d > 2.3$

Figure 6.17: Experimental vs. predicted shear capacities using the proposed model for hooked-end fiber with pullout predicted using Equation 6-10

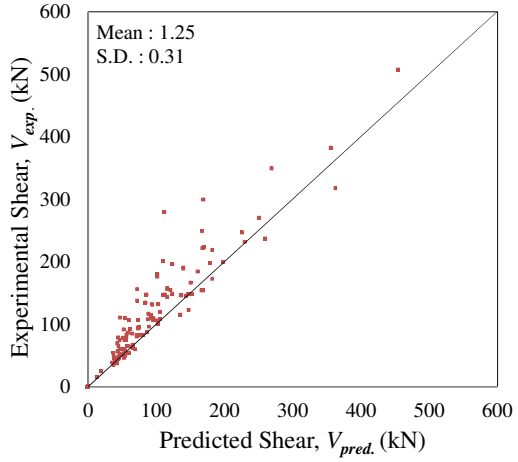

(a) Experimental vs. predicted shear capacities of all the beams

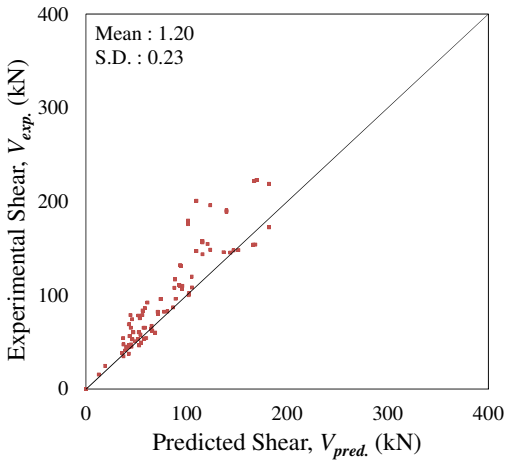

(b) Experimental vs. predicted shear capacities of beams with $a/d > 2.3$

Figure 6.18: Experimental vs. predicted shear capacities using other proposed model for hooked-end fiber with pullout predicted using Equation 6-11

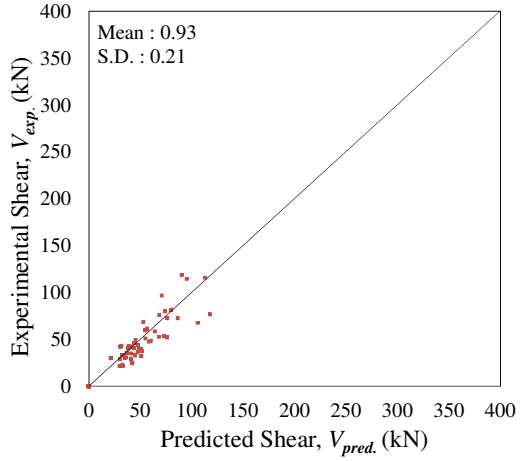

(a) Experimental vs. predicted shear capacities of all the beams

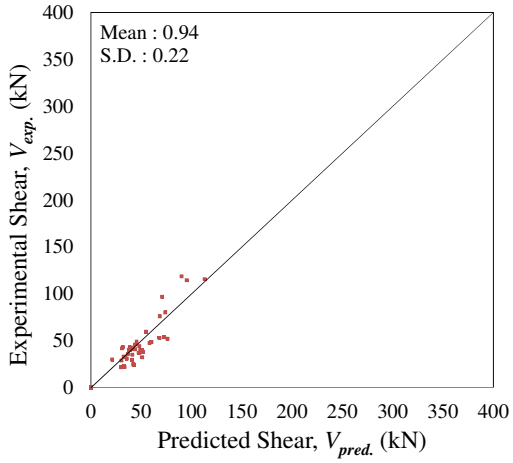

(b) Experimental vs. predicted shear capacities of beams with $a/d > 2.3$

Figure 6.19: Experimental vs. predicted shear capacities using the proposed model for crimped fiber with pullout predicted using Equation 6-11

6.6 Prediction of Shear Strength of SCFRC beams

In this section the shear resistance of the specimens in this experimental program that failed in shear (beams M15-0.5%, M15-0.5%H, M20-0.75%, M20-1.0%, M20-1.0%A, M20-1.0%B) and four other SCFRC beams tested in two other studies are predicted using various equations proposed in the literature, including **Equations 2-41** and **2-42** that were proposed in the study of Greenough and Nehdi (**Table 6.5** shows the properties of the beams). **Table 6.6** summarizes the results of the analysis. As can be clearly seen most of the SFRC models show wide scatter. For the expressions proposed by Greenough and Nehdi (2008), the first equation shows high scatter, while the second equation gives better results although it over-predicts the shear capacity of the beam tested in this study and under-predicts the capacity of the beam tested in the study of Zighuo et al. (2010).

The model proposed in this study was also used to predict the shear capacities of the SCFRC beams. The results show that the model gives reasonably accurate predictions when compared to the models proposed by other researchers. It is noted that for the majority of the

beams, including all the beams tested in this study, the model over-predicts the shear capacity of the SCFRC beams.

It should be noted that the shear capacity of the plain concrete as represented in the term V_{no} may be slightly over-predicted in the case of SCC beams. There is limited published data in the literature on the behaviour of plain SCC beams in shear, however as discussed in the literature review, Lachemi et al. (2004) tested a series of beams to examine the influence of SCC on shear behaviour. The authors of this study found that the SCC beams had reduced capacity when compared to the companion reinforced concrete beams. The authors also found that a decrease in aggregate size decreased ultimate shear capacity. Similarly the authors found that an SCC with the same aggregate size but having a reduced coarse aggregate content showed a reduction in ultimate shear resistance. The reduction in capacity was linked to the reduced contribution of aggregate interlock (and therefore lower post-cracking shear resistance) in beams having reduced aggregate size and aggregate content, which is typical in SCC (see **Figure 6.20** which shows a more smooth and straight shear path in the case of SCC having reduced aggregate size). It is noted that further research is required to study the effect of these two parameters on post-cracking shear transfer mechanisms in SCC and SCFRC beams.

Table 6.5: Parameters of SCFRC beams tested in this study and other researchers

Beam I.D.	b (mm)	d (mm)	ρ	a/d	f_c' (MPa)	D_f (mm)	L_f/D_f	V_f (%)	V_{exp} (kN)
M15-0.5% *	125	212	0.015	3.77	50	0.55	55	0.50	43.33
M15-0.5%H *	125	212	0.015	3.77	50	0.38	79	0.50	45.17
M20-0.75% *	125	212	0.023	3.77	50	0.55	55	0.75	44.03
M20-1.0% *	125	212	0.023	3.77	50	0.55	55	1.00	57.50
M20-1.0%A *	125	212	0.023	3.77	54.5	0.55	55	1.00	59.02
M20-1.0%B *	125	212	0.023	3.77	52.5	0.55	55	1.00	51.46
S-HE-50-0.5 **	200	265	0.017	3.02	40	1.00	50	0.50	90.80
S-HE-50-0.75 **	200	265	0.017	3.02	40	1.00	50	0.75	105.60
S-HE-50-1.0 **	200	265	0.017	3.02	40	1.00	50	1.00	148.90
SFSCCB50-∞ †	200	260	0.028	3.00	56	0.55	64	0.50	137.50

* Beams tested in this study

**Beams tested by Greenough and Nehdi (2008)

† Beams tested by Zighuo et al. (2010)

Table 6.6: Prediction of shear capacities using models proposed in this study and by other researchers

Beam I.D.	V_{exp} (kN)	Predictions (V_{exp} /V_{pred})							
		Khuntia et al. (1999)	Imam et al. (1995)	Mansur et al. (1986)	Sharma et al. (1986)	Ashour et al. (1992)	Greeenough & Nehdi		Proposed Model*
							Eq. 2-41	Eq. 2-42	
M15-0.5%	43.33	0.84	0.93	0.98	0.93	0.87	1.02	0.74	0.97
M15-0.5%H	45.17	0.79	0.88	0.91	0.97	0.81	0.95	0.71	0.97
M20-0.75%	44.03	0.72	0.71	0.87	0.95	0.78	0.92	0.68	0.79
M20-1.0%	57.50	0.86	0.84	1.01	1.24	0.91	1.07	0.81	0.93
M20-1.0%A	59.02	0.86	0.84	1.02	1.22	0.91	1.08	0.83	0.94
M20-1.0%B	51.46	0.76	0.74	0.89	1.09	0.80	0.95	0.72	0.83
S-HE-50-0.5	90.80	1.18	0.89	1.12	1.03	0.80	1.49	1.00	0.95
S-HE-50-0.75	105.60	1.21	0.92	1.14	1.19	0.82	1.53	1.07	0.96
S-HE-50-1.0	148.90	1.52	1.18	1.43	1.68	1.03	1.92	1.39	1.20
SFSCCB50-∞	137.50	1.43	0.89	1.39	1.34	1.00	1.86	1.36	1.13
Mean:		**1.02**	**0.88**	**1.08**	**1.16**	**0.87**	**1.28**	**0.93**	**0.96**
S.D.:		**0.29**	**0.13**	**0.20**	**0.23**	**0.09**	**0.39**	**0.27**	**0.12**

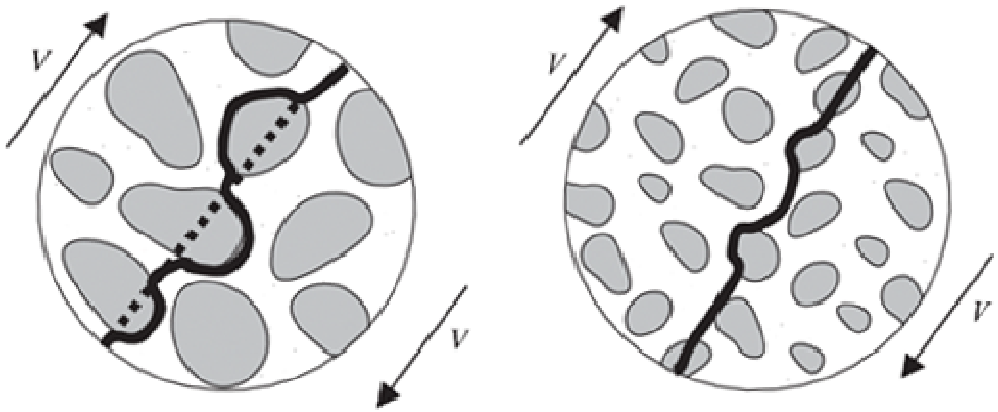

Figure 6.20: Influence of a reduction in coarse aggregate size on crack shear plane [Adapted from Lachemi et al. (2005)]

6.7 Proposed Code-Based Equations

6.7.1 Existing Design Guidelines Related to Use of SFRC in Beams

Design guidelines for the use of SFRC in beams have been proposed in several European and Nordic countries. As seen in **Table 6.7** and discussed in Chapter 2 it can be noted that the majority of the equations consider the fiber contribution to be separate from the concrete contribution, the exception being the equation proposed by the Italian Recommendation which modifies the concrete contribution directly. Similarly, in North America, the 2008 ACI-318 code includes provisions permitting the use of SFRC to replace minimum shear reinforcement in flexural members. In order to qualify as an alternative to traditional shear reinforcement, the SFRC must have a minimum fiber dosage of 60 kg/m^3 (0.75 % by volume) and meet the performance requirements defined in Chapter 5 of the ACI code.

Although the ACI provisions are a positive step in the recognition of SFRC as a structural material in North America, the provisions do not include a code-based design equation for computing the shear resistance of SFRC. It is noted that the CSA A23.3 standard does not contain any provisions related to the use of SFRC in beams.

Table 6.7: Design guidelines and equations for predicting shear resistance of SFRC beams

Design Guidelines	Design Equation
RILEM σ-ϵ method	$V_u = V_c + 0.7 k_f k_1 \tau_{fd} b_w d$ where $\tau_{fd} = 0.12 f_{Rk,4}$
German Guidelines	$V_u = V_c + 0.7 k_f k_1 \tau_{fd} b_w d$ where $\tau_{fd} = 0.37 f_{Rk}$
Norwegian Guidelines	$V_u = V_c + 0.8 f_{ftd,res} b_w d$
Italian Recommendation	$V_u = \left[\frac{0.18}{\gamma_c} k \left(100 \rho_1 \left(1 + 7.5 \frac{f_{Ftuk}}{f_{ctk}} \right) f_{ck} \right)^{1/3} + 0.15 \sigma_{CP} \right] b_w d$
ACI 318-08 CSA A23.3-04	No Design Equation

6.7.2 Proposed Design Equation

6.7.2.1 Design equation

This section proposes a design equation which can be used to predict the shear capacity of SFRC beams. The expression shown in **Equation 6-18** is based on the prediction model discussed in section 6.4 and is used to predict the shear resistance attributed to steel fiber reinforced concrete, $V_{c,fib}$.

$$V_{c,fib} = \phi_c \left[\left(\frac{230}{1000 + s_{ze}} \sqrt{f_c'} b_w d_v \right) + \left(1.72 \frac{d}{a} \times \left(0.6 \times N_{fibres} F_{pullout} \right) \times b_w d_v \times \cot\theta \right) \right] \qquad (6\text{-}18)$$

The first component in **Equation 6-18** is used to estimate the shear resistance provided by concrete and is the same expression used in the simplified method of the CSA A23.3 standard for sections containing no transverse reinforcement and can be used for all aggregate sizes. The term $\frac{230}{1000 + s_{ze}}$ is derived from the MCFT and general shear design method of the CSA A23.3 standard by assuming a value of 0.85 x 10^{-3} for the strain at mid-depth, ε_x (Bentz and Collins, 2005). The expression has been shown to account for the effect of beam size and aggregate size on shear resistance and is a simplified equation which is suitable for design (Lubell, 2006; Sherwood, 2008).

The second component in **Equation 6-18** is used to estimate the shear resistance provided by steel fibers and is the same expression used in the predictive model in section 6.4 with the exception being that the pullout reduction factor, α_v, is reduced from 0.8 to 0.6 to produce more conservative estimates of pullout strength for design.

Figure 6.21 compares the experimental to predicted shear capacities (V_{exp}/V_{pred}) using **Equation 6-18** and with ϕ_c taken as 1.0 for the database of SFRC beam test results in **Table 6.1** and including only the results from specimens that failed in shear. The results are plotted as a function of fiber content (V_f), shear span-to-depth ratio (a/d) and beam effective depth (d). **Figure 6.22** shows the predictions for the reduced set of beams having an a/d ratio greater than 2.3. It can be seen that the majority of the V_{exp}/V_{pred} ratios exceed 1.0 producing safe design with only 2.3% of the results having a V_{exp}/V_{pred} ratio < 1.0. When only slender beams are included the mean V_{exp}/V_{pred} is 1.43 with a standard deviation of 0.25.

Figure 6.23 compares the experimental to predicted shear capacities but with ϕ_c taken as 0.65 as specified in the CSA A23.3 standard. One can see that the proposed design equation produces safe predictions of SFRC shear resistance for a wide range of beam tests reported in the literature.

6.7.2.2 Need for reliability analysis

It is noted that the above was a first attempt at developing a shear design equation for SFRC beams. However, detailed reliability analysis needs to be conducted in order to measure the safety and reliability of the proposed equation. For example in the proposed equation a pullout reduction factor of 0.6 was suggested for design; the reliability associated with the choice of this factor needs to be verified. As a rough check, using the mean of 1.43 and the standard deviation of 0.25, the first percentile value is 1.43-2.33(0.25) = 0.85.

6.7.2.3 Additional recommendations

If **Equation 6-18** is to be used for design, the following additional requirements and limitations are recommended:

- It is proposed that a minimum fiber content of 0.75% be required when SFRC is used as a complement to the shear resistance provided by concrete.
- The maximum shear resistance computed using **Equation 6-18** should be limited to $0.3\phi_c\sqrt{f'_c}b_w d_v$ which corresponds to the conservative lower bound value reported by Parra-Montesinos (2006).
- It is proposed that SFRC be only permitted in members having d ≤ 570 mm due to the lack of experimental results on larger SFRC beams failing in shear.
- It is proposed that minimum performance requirements related to the toughness parameters obtained from the ASTM C1609 be required when SFRC is used to enhance the shear capacity of beams (e.g. requirements similar to those proposed in the current edition of the ACI-318 code).

It is noted that the above recommendations apply to regular SFRC; as discussed in the thesis more research is required for shear design of SCFRC beams.

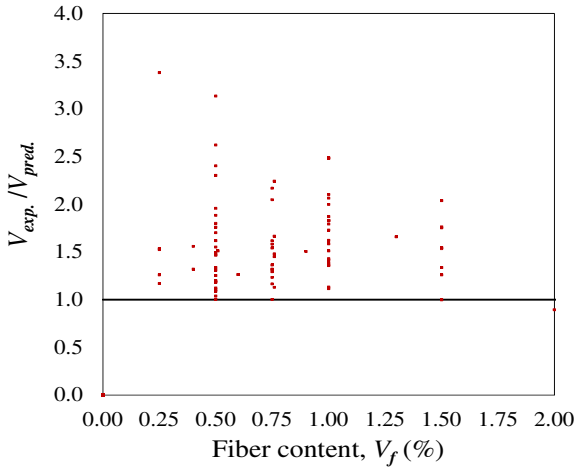

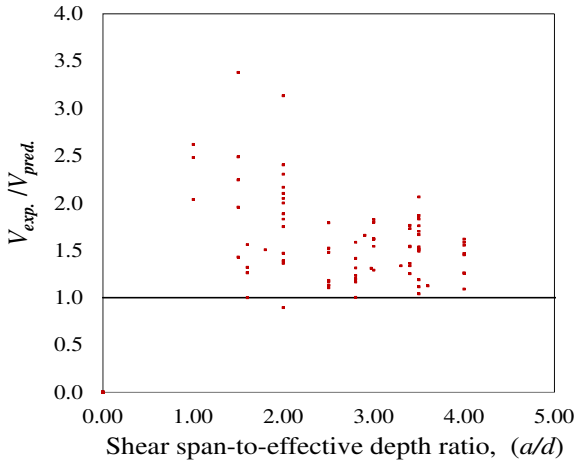

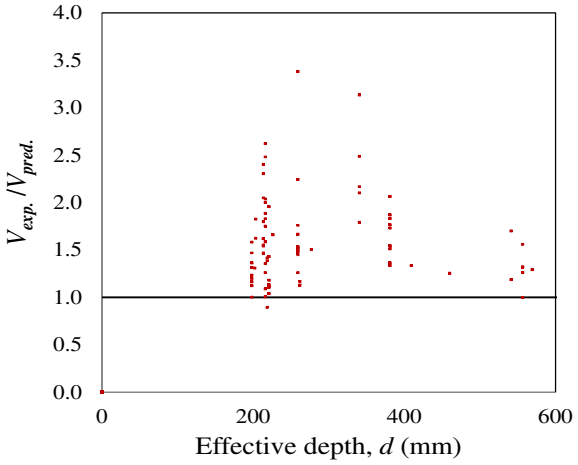

Figure 6.21: Validity of the design model using all beam results, and taking ϕ_c as 1.0

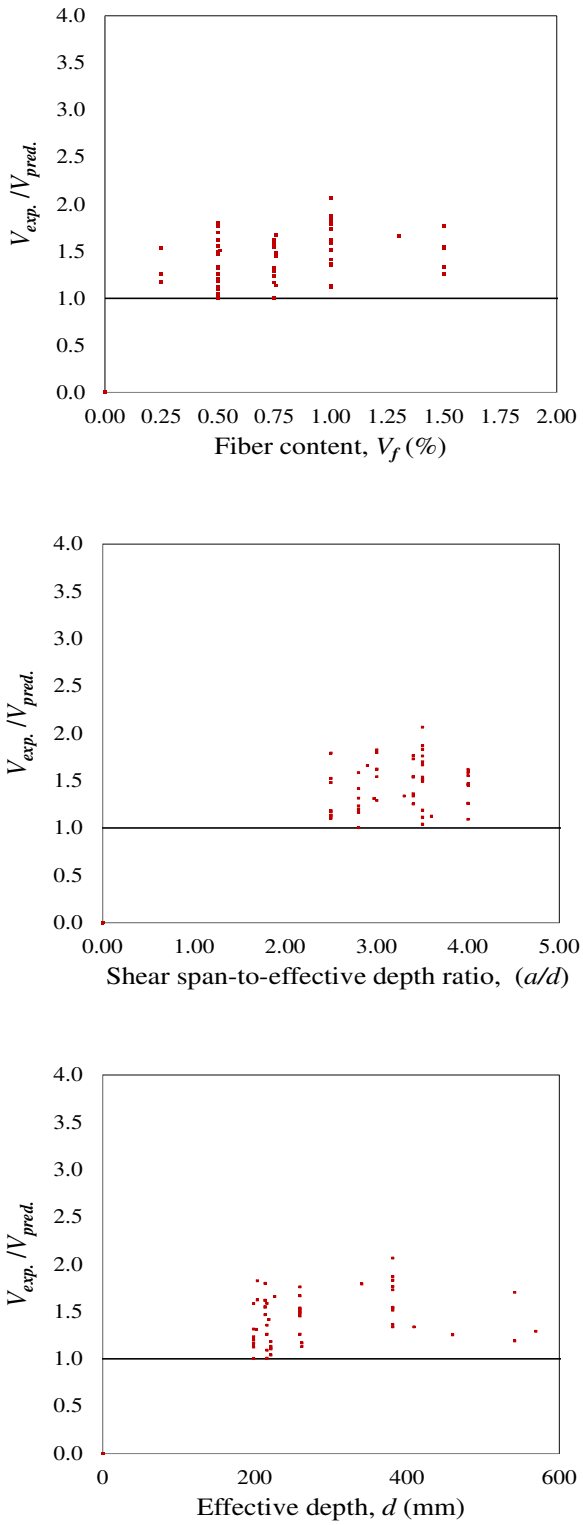

Figure 6.22: Validity of the design model using only beams with an $a/d > 2.3$, and taking ϕ_c as 1.0

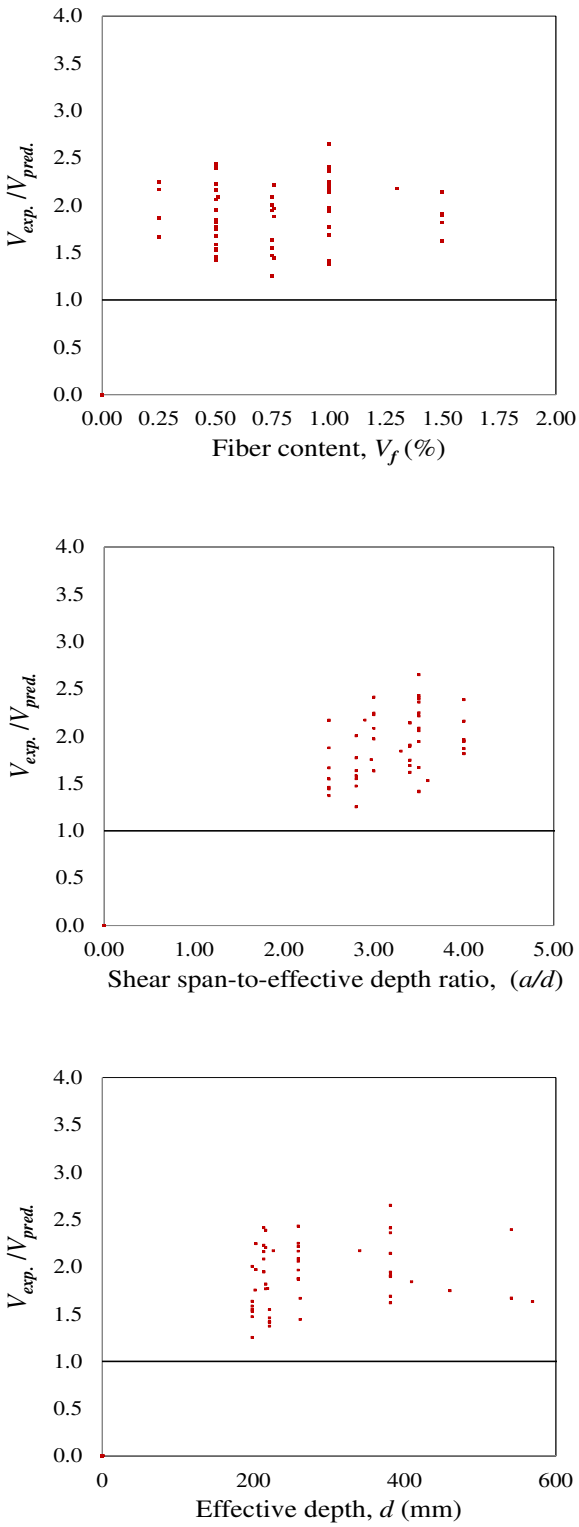

Figure 6.23: Validity of design model using only beams with an $a/d > 2.3$, and with $\phi_c = 0.65$

Chapter Seven: Conclusions

7.1 Overview

Steel Fiber Reinforced Concrete is a promising material which offers many advantages that can be adopted for structural applications. This thesis provided a comprehensive investigation into the potential of using steel fibers in combination with self-consolidating concrete in beams. Furthermore, the thesis proposed a method to predict the shear strength of SFRC beams. The concluding remarks concerning the experimental and the analytical program are summarized in the following sections.

7.1.1 Experimental program

Twelve beam specimens, having identical geometrical properties but constructed with different types of self-consolidating concrete and fiber types, were tested under four-point loading to evaluate the effect of steel fibers on the structural response of SCFRC beams. The results obtained from the experimental program lead to the following conclusions:

1. The addition of fibers reduces the workability of SCC, however adequately workable mixtures can be obtained with moderate fiber contents.
2. The addition of fibers to a SCC mix improves the shear capacity of reinforced concrete beams.
3. The addition of a sufficient amount of fibers could alter the brittle shear failure mode into a more ductile flexural response in shear-critical beams.
4. The addition of steel fibers leads to an improvement in cracking behaviour, which was evidenced by a better control of crack widths and reductions in crack spacings.

7.1.2 Analytical Program

The following conclusions can be drawn from the analytical phase of the research program:

1. Based on an evaluation of a large database of results, existing equations in the literature are empirical and many do not accurately predict the shear resistance of SFRC and SCFRC beams, there is thus a need to develop reliable and accurate prediction equations.
2. An analytical model which can predict the ultimate shear resistance of SFRC and SCFRC beams was proposed. The model accounts for:
   - The effect of fiber deformation on pullout strength (with equations developed for both hooked end and crimped steel fibers);
   - The influence of bond-shear strength on pullout strength (with an equation which computes bond strength based on matrix strength);
   - The influence of shear span-to-depth ratio (*a/d*) on the shear strength of SFRC beams (with a factor that accounts for *a/d* ratio);
   - The influence of beam size on the shear strength of SFRC beams (with a factor that accounts for the effect of increased beam size).
3. The results show that the analytical model provides accurate and reliable predictions for a large database of SFRC beam test results reported in the literature. The model also provides reasonable predictions for SCFRC beams.
4. An equation for estimating the shear design strength of SFRC beams was proposed. The design equation was shown to reliable results and a series of recommendations were proposed for design purposes.

7.2 Future Research

The following suggestions are proposed for future research:

1. Further experimental research and the development of an analytical model which more accurately accounts for the effect of reduced aggregate size and content in self-consolidating concrete (for beams with and without steel fibers).
2. Further research focusing on the shear behaviour of larger SFRC and SCFRC beams, to more clearly examine the effect of increased beam size on shear response.
3. The effectiveness of combining steel fibers with traditional transverse reinforcement and the effect of this approach on the shear response of SFRC and SCFRC beams.
4. The use of nonlinear Finite Element (FE) modeling to predict the complete shear deflection response of SFRC and SCFRC beams. Specialized computer-aided software such as VecTor2D can be utilized for this purpose.
5. An experimental program on SFRC and SCFRC beams subjected to cyclic and reversed cyclic loads, in order to evaluate the effect of steel fibers on the shear response and flexural ductility of beams subjected to load reversals.

References

ACI Committee 318 (1963) “Building Code Requirements for Reinforced Concrete (ACI 318-63).” *American Concrete Institute*, Farmington Hills, Michigan, USA, 144 pp.

ACI Committee 318, (2005) “Building Code Requirements for Structural Concrete (ACI 318-05) and Commentary (ACI 318-05).” *American Concrete Institute*, Farmington Hills, Michigan, USA, 430 pp.

ACI Committee 318, (2008) “Building Code Requirements for Structural Concrete (ACI 318-08) and Commentary.” *American Concrete Institute*, Farmington Hills, Michigan, USA, 473 pp.

ACI Committee 544, (1988). “Design Considerations for Steel Fiber Reinforced Concrete (ACI 544.4R-88).” *American Concrete Institute*, Farmington Hills, Michigan, USA, 18 pp.

ACI-ASCE Committee 326 (1962) “Shear and Diagonal Tension.” *Journal of the AmericanConcrete Institute, Proceedings*, 59(1, 2, 3) January pp. 1-30, February pp. 277-334, March pp. 352-396.

Adebar, P., Collins, M. P. (1996) “Shear Strength of Members Without Transverse Reinforcement.” *Canadian Journal in Civil Engineering*, 23 (1), pp. 30-41.

Adebar, P., Mindess, S., St.Pierre, D., & Olund, B. (1997) "Shear Tests of Fiber Concrete Beams without Stirrups." *ACI Structural Journal*, 94 (1), pp. 68-76.

Alwan, J. M., Namman, A. E. & HNSEN, W. (1991) “Pull-Out Work of Steel Fibers From Cementitious Composites: Analytical Investigation.” *Cement and Concrete Composites*, 13 (4), pp. 247-255.

Alwan, J. M., Naaman, A. E., & Guerrero, P. (1999) “Effect of Mechanical Clamping on the Pullout Response of Hooked Steel Fibers Embedded in Cementitious Matrices.” *Concrete Science and Engineering*, 1, pp. 15-25.

Ando, T. et al. (1990) “Fabrication and Properties for a New Carbon Fiber Reinforced Cement Products, Thin-Section FRC and Ferrocement.” *American Concrete Institute Special Publication, ACI SP*, (124) 3, pp. 39–60.

Aoude, H. (2008) “*Structural Behaviour of Steel Fiber Reinforced Concrete Members*.” PhD thesis, Department of Civil Engineering and Applied Mechanics, McGill University, Montreal, Canada.

Aoude, H., Mitchell, D., & D. Cook, W. D. (2008) “Tension Behaviour of Reinforced Concrete Specimens Constructed with Steel Fibers and SCC.” *Fiber Reinforced Concrete - Design and Applications*: Proceedings of the 7th RILEM International Symposium on Fiber Reinforced Concrete, BEFIB, Chennai, India, pp. 689-698.

Aoude, H., Mitchell, D. & Cook W.D. (2009) "Behaviour of Columns Constructed with Fibers and Self-Consolidating Concrete." *ACI Structural Journal*, (106) 1, pp. 349-357.

Ashour, S. A., Hasanain, G. S., & Wafa, F. F. (1992). "Shear Behaviour of High-Strength Fiber Reinforced Concrete Beams." *ACI Structural Journal*, 89(2), pp. 176-184.

ASTM C1018 (1998) "*Standard Test Method for Flexural Toughness and First Crack Strength of Fiber Reinforced Concrete*." Philadelphia, American Society of Testing and Materials.

ASTM C1399 (1998b) " *Test Method for Obtaining Average Residual-Strength of Fiber Reinforced Concrete*." Philadelphia, American Society of Testing and Materials.

ASTM C1550 (2010a) "Standard Test Method for Flexural Toughness of Fiber Reinforced Concrete (Using centrally loaded round panel).' Philadelphia, American Society of Testing and Materials.

ASTM C1609 (2010b) "*Standard Test Method for Flexural Performance of Fiber Reinforced Concrete (Using Beam with Third-Point Loading).*' Philadelphia, American Society of Testing and Materials.

Banthia N. & Sappakittipakorn M. (2007) "Toughness Enhancement in Steel Fiber Reinforced Concrete through Fiber Hybridization." *Cement and Concrete Research*, 37, pp. 1366-1372.

Banthia, N. & Mindess, S. (2004) "Toughness Characterization of Fiber-Reinforced Concrete: Which Standard to Use." *Journal of Testing and Evaluation*, 32 (2), pp. 138-42.

Banthia, N. & Trottier, J. F. (1995) "Test Methods for Flexural Toughness Characterization of Fiber Reinforced Concrete: Some Concerns and a Proposition." *ACI Materials Journal*, 92 (1), pp. 48-57.

Barragan, B. E. (2002) "*Failure and toughness of steel fiber reinforced concrete under tension and shear."* PhD Thesis, Universitat Politècnica de Catalunya, Barcelona, Spain..

BEKAERT (2007) Dramix steel fibers, http://www.bekaert.com/en.aspx, accessed October 15th, 2010.

Bentz, E. C. & Collins, M. P. (2005) "Development of the 2004 Canadian Standards Association (CSA) A23.3 Shear Provisions for Reinforced Concrete." *Canadian Journal of Civil Engineering*, 33 (5), pp. 521-534.

Bentz, E. C. (2000) "*Sectional Analysis of Reinforced Concrete Membrane*." PhD Thesis, University of Toronto, Toronto, Canada.

Bentz, E. C. (2000) "RESPONSE 2000: Reinforced Concrete Sectional Analysis Program." 1.05 ed. Toronto, Canada.

Bernard, S. (2003) "Release of New ASTM Round Panel Test." *Shotcrete Corner*, 5 (2), pp. 20-23.

Bui, V. K., Geiker, M. R., & Shah, S. P. (2003) "Rheology of Fiber-Reinforced Cementitious Materials." *RILEM PRO30 High Performance Fiber Reinforced Composites HPFRCC4*, pp. 221-232.

Bui, V. K. & Attiogbe, E. (2005) "*Degussa Admixtures Inc."* Seminar at University of Michigan, USA.

Cassanova, P. (1996) "Bétons renforcés de fibers métalliques: Du matériau à la structure." *Division Bétons et Ciments pour Ouvrages d'art* Paris, Ecole Nationale des Ponts et Chaussées, Paris, France.

Chanvillard, G. & Aiticin, P.C. (1996) "Pull-Out Behaviour of Corrugated Steel Fibers Qualitative and Statistical Analysis." *Advanced Cement Based Materials*, 4 (1), pp. 28-41.

Chen, L. (1995) "*Flexural Toughness of Fiber Reinforced Concrete*." PhD thesis, University of British Columbia, Vancouver, Canada, 42 pp.

Choi, K., Park, H., & Wight, J., (2007) "Shear Strength of Steel Fiber Reinforced Concrete Beams without Web Reinforcement." *ACI Structural Journal*, 104 (1), pp. 12-21.

CNR-DT 204 (2006) "Guide for the Design and Construction of Fiber-Reinforced Concrete Structures." *Consiglio Nazionale Delle Ricerche,* Rome, Italy, 60 pp.

Collins, M. P., Mitchell, D. (1997) "*Prestressed Concrete Structures*", Response Publication, Toronto and Montreal, Canada.

CSA (2004) "*CSA A23.3-04: Design of Concrete Structures*." Canadian Standards Association, Mississauga, Canada.

Cucchiara, C., La Mendola, L., & Papia, M. (2004) "Effectiveness of Stirrups and Steel Fibers as Shear Reinforcement." *Cement and Concrete Composites*, 26 (7), pp. 777-786.

DAfStb UA SFB N 0146 (2005) "*DAfStb-Richtlinie Stahlfaserbeton-Draft march*." (In German), 60 pp.

Dehn F. (2005) "Private communication with Naaman, A.E." Leipzig Germany.

Dinh, H. H. (2009) "*Shear Behaviour of Steel Fiber Reinforced Concrete Beams without Stirrups Reinforcement*." PhD Thesis, Department of Civil Engineering, University of Michigan, Michigan, USA.

Dupont, D. (2003) "*Modeling and Experimental Validation of the Constitutive Law and Cracking Behaviour of Steel Fiber Reinforced Concrete*." Department of Civil Engineering. Heverlee, Catholic University of Leuven, Belgium.

Fantilli, A. P. (2009) "Multiple Cracking and Strain Hardening in Uniaxial Tension." *Cement and Concrete Research*, 39, pp. 1217–1229.

FiberMesh (2010) Crimped Fibers, http://www.fibermesh.com, accessed on June 12th, 2012.

Foster, J. & VOO, J., (2003) "Variable Engagement Model for Fiber Reinforced Concrete in Tension." University of New South Wales, Sydney, Australia.

Foster, S. J. & Attard, M. M. (2001) "Strength and Ductility of Fiber-Reinforced High-Strength Concrete Columns." *Journal of Structural Engineering*, 127 (1), pp. 28-34.

Furlan Jr. S., & Hanai J. B. (1997) "Shear Behaviour of Fiber Reinforced Concrete Beams." *Journal of Cement and Concrete Composites*, 19, pp. 359-366.

Greenough, T & Nehdi, M. (2008) "Shear Behaviour of Fiber-Reinforced Self-Consolidating Concrete Slender Beams.". *ACI Structural Journal*, 105 (5), pp. 468-477.

Groth, P. (2000) "Steel Fiber Reinforced SCC, Final Report of Task 6." *LTU Journal*, Swedish Cement and Concrete Institute., RT6 (1).

Grunewal, S. & Walraven, J. (2001) "Parameter-Study on The Influence of Steel Fibers and Coarse Aggregate Content on the Fresh Properties of Self-Compacting Concrete." *Cement and Concrete Research*, 31 (12), pp. 1793-1798.

Grunewald, S. (2004) "*Performance-Based Design of Self-Compacting Fiber Reinforced Concrete*." Department of Structural and Building Engineering, Delft University of Technology, Delft, Germany, 20-24 pp.

Gurjar, A. (2004) "*Mix Design and Testing of Self-Consolidating Concrete Using Florida Materials*." Report No. BD 503, Daytona Beach, the Florida Department of Transportation.

Gustaffso J. & Noghabai K. (1999) "Steel Fibers as Shear Reinforcement in High Strength Concrete Beams." *International Journal of Nordic Concrete Research*, 22, 16 pp.

Hannant, D. J. (1978) "*Fiber Cements and Fiber Concretes*." John Wiley and Sons Ltd., New York, USA.

Hsu, L. S. & Hsu, C. T. T. (1994) "Stress-Strain Behaviour of Steel Fiber High-Strength Concrete Under Compression." *ACI Structural Journal* 91 (4)**,** pp. 448-457.

Imam, M., Vandewalle, L. & Mortelmans, F. (1995) "Shear-Moment Analysis of Reinforced High Strength Concrete Beams Containing Steel Fibers." *Canadian Journal of Civil Engineering,* 22 (3)**,** pp. 462-470.

Jansson, A. (2007) "*Analysis and Design Methods for Fiber Reinforced Concrete: A State-of-The-Art Report*." Department of Civil and Environmental Engineering, Division of Structural Engineering, Chalmers University of Technology, Göteborg, Sweden, 196 pp.

Johnston, C. D. (1996) "*Proportioning, Mixing and Replacement of Fiber-Reinforced Cement and Concrete*." Production Methods and Workability of Concrete, Edited by Bartos, Marrs and Cleland, E. and FN Spon, London, pp. 155-179.

JSCE (1984) "Standard SF-4: Method of Test for Flexural Toughness and First Crack Strength of Fiber Reinforced Concrete." *Japan Society of Civil Engineers*.

Khuntia, M., Stojadinovic, B. & Goel, S. C. (1999) "Shear Strength of Normal and High-Strength Fiber Reinforced Concrete Beams without Stirrups." *ACI Structural Journal,* 96 (2)**,** pp. 282-289.

Kosmatka, S. H., Kerkhoff, B., Panarese, W. C., Macleod, N. F., & McGrath, R. J. (2002) "*Design and Control of Concrete Mixtures*." Cement Association of Canada, 7th Canadian Edition, 356 pp.

Kützing, L. (2000) "*Trafahigkeitsermittlung stahlfaserverstarkter Betone*." (in German), PhD Thesis, University of Leipzig, Stuttgart, Germany.

Kwak, Y. K., Eberhard, M. O., Kim, W. S., & Kim, J. (2002) "Shear Strength of Steel Fiber-Reinforced Concrete Beams without Stirrups." *ACI Structural Journal*, 99 (4), pp. 530-538.

Lachemi, M., Hossain, K., & Lambros, V. (2005) "Shear Resistance of Self Consolidating Concrete Beams-Experimental Investigations." *Civil Engineering Journal,* NRC Canada, 32, pp. 1103-1113.

Lee, C. D. (1990) "*Constitutive Modeling and Flexural Analysis of Steel Fiber Reinforced Concrete for Structural Applications*." Department of Civil and Environmental Engineering. Ann Arbor, Michigan State University.

Li, V. C. (2000) "Large Volume, High Performance Application of Fibers in Civil Engineering." *Journal of Applied Polymer Science*, 83, 660-686

Li, V. C., Ward, R., & Hamza, A. M. (1992) "Steel and Synthetic Fibers as Shear Reinforcement." *ACI Materials Journal*, 89 (5), pp .499-508.

Liao W., Chao S., Park S., & Naaman A. (2006) "*Self-Consolidating High Performance Fiber Reinforced Concrete (SCHPFRC)-Preliminary Investigation*." Department of Civil and Environmental Engineering, University of Michigan, USA.

Lim, T. Y., Paramasivam, P., & Lee, S. L. (1987) "Shear and Moment Capacity of Reinforced Steel-Fiber-Concrete Beams." *Magazine of Concrete Research*, 39 (140), pp. 148-160.

Löfgren, I. (2005) "*Fiber-Reinforced Concrete for Industrial Construction: A Fracture Mechanics Approach to Material Testing and Structural Analysis*". PhD Thesis, Department of Civil and Environmental Engineering, Chalmers University of Technology, Göteborg, Sweden, 268 pp.

Lubell, A.S. (2006) "*Shear in Wide Reinforced Concrete Members*." PhD Thesis, Department of Civil Engineering, University of Toronto, Toronto, Canada, 267 pp.

Maage, M. (1977) "Interaction Between Steel Fibers and Cement Based Matrices." *Materials and Structures Journal*, 10 (59), pp. 297-301.

Mansur, M. A., Chin, M. S. & Wee, T. H. (1999) "Stress-Strain Relationship of High-Strength Fiber Concrete in Compression." *Journal of Materials in Civil Engineering,* 11 (1)**,** pp. 21-29.

Mansur, M. A., Ong, K. C. G., & ParamasivamA, P. (1986) "Shear Strength of Fibrous Concrete Beams without Stirrups", *ASCE Journal of Structural Engineering*, 112 (9), pp. 2066-2079.

Minelli, F. (2005) "*Plain and Fiber Reinforced Concrete Beams under Shear Loading*." PhD Thesis, Department of Civil Engineering, University of Brescia, Italy.

Minelli, F. and Plizzari, G.A. (2006) "Steel Fibers as Shear Reinforcement for Beams." *Proceedings of the Second International Fib Congress*, 12 pp.

Mitchell, D. & Collins, M. P. (1974) "Diagonal Compression Field Theory: A Rational Model for Structural Concrete in Pure Torsion." *Journal of the American Concrete Institute*, 71, pp. 396-408.

Molins et al. (2009) “Double Punch Test to Control the Energy Dissipation in Tension of FRC (Barcelona test).” *Materials and Structures*, 42 (4), pp. 415-425.

Mörsch, E. (1905) “*Concrete-Steel Construction (Der Eisenbetonbau).*” English translation of the 3rd German Edition, McGraw-Hill Book Company, New York, USA, 368 pp.

Naaman, A. E., and Reinhardt H. W. (2006) “High Performance Fiber Reinforced Cement Composites: Classification and Application.” *Proceedings of the Second International RILEM Workshop*, RILEM Publications, Cachan Cedex, France, pp. 1-24.

Naaman, A. E, Namur, G. G, Alwan, J. M., & Najim (1991) “High Strength Fiber Pullout and Bond Slip Relationship: Analytical Study.” *Journal in Structural Engineering*, 117 (9), pp. 2769-90.

Narayanan, R. & Darwish, I. Y. S. (1987) "Use of Steel Fibers as Shear Reinforcement." *ACI Structural Journal*, 84 (3), pp. 216-227.

Narayanan, R. & Darwish, I. Y. S. (1988) "Fiber Concrete Deep Beams in Shear." *ACI Structural Journal*, 85 (2), pp. 141-149.

Nataraja, M. C., Dhang, N. & Gupta, A. P. (1999) “Stress-Strain Curves for Steel-Fiber Reinforced Concrete Under Compression.” *Cement and Concrete Composites,* 21 (5)**,** pp. 383-390.

Noghabai, K. (2000). "Beams of Fibrous Concrete in Shear and Bending: Experiment and Model." *ASCE Journal of Structural Engineering*, 126(2), pp. 243-251.

Park, R., & Paulay, T. (1975) “*Reinforced Concrete Structure*” Willey-Interscience Publication, New York, USA.

Parra-Montesinos, G. J. (2006) “Shear Strength of Beams with Deformed Steel Fibers”, *Journal of American Concrete Institute*, 28 (11), pp. 57-66.

RILEM (2001) “RILEM TC 162-TDF: Test and Design Methods for Steel Fiber Reinforced Concrete - Bending Test.” *Materials and Structures Journal*, 35 (253), pp. 579-582.

RILEM (2003) “Rilem TC 162-TDF: Test and Design Methods for Steel Fiber Reinforced Concrete - $\sigma - \varepsilon$ Design Method.” *Materials and Structures*, 36, pp. 560-567.

Rosenbusch, J. & Teutsch, M. “*Trial Beams in Shear*.” Brite/Euram Project 97-4163, Final Report, Sub Task 4.2, Technical University of Braunschweig, Braunschweig, Germany.

Sahmaran, M., Yurtseven, Alperen, & Yaman, I. O. (2005) “Workability of Hybrid Fiber Reinforced Self-Compacting Concrete.” *Building and Environment* 40, pp. 1672-1677.

Sharma, A. K. (1986) “Shear Strength of Steel Fiber Reinforced Concrete Beams.” *Journal of the American Concrete Institute,* 83 (4), pp. 624-628.

Sherwood, E. G. (2008) “*One-Way Shear Behaviour of Large, Lightly Reinforced Concrete Beams and Slabs”* PhD Thesis, Department of Civil Engineering, University of Toronto, Toronto, Canada, 333 pp.

Shin, S. W., Oh, J. G., & Ghosh, S. K. (1994) "Shear Behaviour of Laboratory-Sized High-Strength Concrete Beams Reinforced with Bars and Steel Fibers." *ACI Special Publication*, 142, pp. 181-200.

Skazlic, M. & Bjecovic, D. (2009) “Toughness Testing of Ultra-High Performance Fiber Reinforced Concrete.” *Materials and Structures*, (42), pp. 1025-1038.

Swamy, R. N. & Bahia, H. M. (1985) “Effectiveness of Steel Fibers as Shear Reinforcement.” *Concrete International*, 7 (3), pp. 35-40.

Swamy, R. N., Jones, R., & Chiam, A. T. P. (1993) "Influence of Steel Fibers on The Shear Resistance of Lightweight Concrete I- Beams." *ACI Structural Journal*, 90 (1), pp. 103-114.

Swamy, R. N. and Mangat, P. S. (1974) “Influence of Fiber-Aggregate Interaction on Some Properties of Steel Fiber Reinforced Concrete.” *Materials and Structures Journal*, 7 (5), September 1974, pp. 307-314.

Swedish Concrete Society (1997) (Svenska Betongföreningen). *Steel Fiber Concrete Recommendations for Construction, Performance and Testing*.” Report no4 -2nd edition (In Swedish: Stålfiberbetong-rekommendationer för konstruktion, utförande och provning. Rapport nr 4 - utgåva 2), 2nd ed.

Tan, K. H., Murugappan, K., & Paramasivam, P. (1993) "Shear Behaviour of Steel Fiber Reinforced Concrete Beams." *ACI Structural Journal*, 90 (1), pp. 3-11.

Thorenfeldt, E., Sandaker, T., Bosnjak, D., Martinsen, T., Olsen, O., Maage, M., & Fjeld, S. (2006) "*Veiledning stålfiberarmert betong*." (in Norwegian), 42 pp.

Vecchio, F. J. & Collins, M. P. (1986) “Modified Compression Field Theory for Reinforced Concrete Elements Subjected to Shear.” *Journal of the American Concrete Institut*e, 83 (2), pp. 219-231.

Wight J. K. & MacGregor J. G. (2009) “Reinforced Concrete Mechanics and Design”, 5th Edition, USA, 1112 pp.

Zararis P. D. & Papaakis G. Ch. (2001) “Diagonal Shear Failure and Size Effect in RC Beams without Web Reinforcement.” *ASCE Journal of Structural Engineer*ing, 127 (7), pp. 733-742.

Zhiguo Y., Yining D., & Christoph N. (2010) “Replacing Stirrups of Self-Compacting Concrete Beams with Steel Fibers.” *Tianjin University and Springer-Verlag Berlin Heidelberg*, Berlin, Germany, 16, pp. 411-416.

Appendix A

Table A1: Database and properties of various SFRC beams tested by other researchers

Study	**Beam I.D.**	b_w (mm)	h (mm)	d (mm)	ρ	a/d	f_c' (MPa)	Fiber Type	L_f (mm)	D_f (mm)	L_f/D_f	V_f %	(Fiber Factor) F_p	$V_{exp.}$ (kN)
Parra-Montesinos et al. (2006)	1	152	457	381	0.020	3.50	38	H	30	0.51	60	1.00	0.59	176.03
	2	152	457	381	0.020	3.50	38	H	30	0.51	60	1.00	0.59	179.63
	3	152	457	381	0.027	3.50	38	H	30	0.51	60	1.00	0.59	200.83
	4	152	457	381	0.027	3.50	38	H	30	0.51	60	1.00	0.59	147.22
	7	152	457	381	0.027	3.40	31	H	30	0.51	60	1.50	0.89	148.42
	8	152	457	381	0.027	3.40	31	H	30	0.51	60	1.50	0.89	196.03
	9	152	457	381	0.027	3.40	45	H	30	0.51	60	1.50	0.89	190.43
	10	152	457	381	0.027	3.40	45	H	30	0.51	60	1.50	0.89	189.23
	11	152	457	381	0.027	3.40	49	H	60	0.51	80	1.00	1.18	172.43
	12	152	457	381	0.027	3.40	49	H	60	0.51	80	1.00	1.18	218.83
Adebar et al. (1997)	FC2	150	610	556	0.023	1.60	54	H	30	0.51	60	0.75	0.44	270.52
	FC3	150	610	556	0.023	1.60	50	H	30	0.51	60	1.50	0.89	317.62
	FC8	150	610	556	0.023	1.60	55	H	30	0.51	60	0.40	0.24	199.88
	FC9	150	610	556	0.023	1.60	56	H	30	0.51	60	0.60	0.35	231.74
	FC10	150	610	556	0.023	1.60	47	H	50	0.51	100	0.40	0.39	246.86
	FC11	150	610	556	0.023	1.60	41	H	50	0.51	100	0.60	0.59	237.08
Ashour et al. (1992)	B-2-1.0-L	127	254	216	0.004	2.00	92	H	60	0.79	75	1.00	0.76	46.10
	B-4-1.0-L	127	254	216	0.004	4.00	93	H	60	0.79	75	1.00	0.76	24.56

Study	**Beam I.D.**	b_w (mm)	h (mm)	d (mm)	ρ	a/d	f_c' (MPa)	Fiber Type	L_f (mm)	D_f (mm)	L_f/D_f	V_f %	(Fiber Factor) F_p	$V_{exp.}$ (kN)
	B-6-1.0-L	127	254	216	0.004	6.00	94	H	60	0.79	75	1.00	0.76	15.30
	B-1-0.5-A	127	254	216	0.028	1.00	99	H	60	0.79	75	0.50	0.38	249.18
	B-2-0.5-A	127	254	216	0.028	2.00	99	H	60	0.79	75	0.50	0.38	132.24
	B-4-0.5-A	127	254	216	0.028	4.00	95	H	60	0.79	75	0.50	0.38	62.15
	B-6-0.5-A	127	254	216	0.028	6.00	96	H	60	0.79	75	0.50	0.38	53.46
	B-1-1.0A	127	254	216	0.028	1.00	95	H	60	0.79	75	1.00	0.76	349.31
	B-2-1.0-A	127	254	216	0.028	2.00	95	H	60	0.79	75	1.00	0.76	166.25
	B-4-1.0-A	127	254	216	0.028	4.00	97	H	60	0.79	75	1.00	0.76	86.90
	B-6-1.0-A	127	254	216	0.028	6.00	101	H	60	0.79	75	1.00	0.76	53.65
	B-1-1.5-A	127	254	216	0.028	1.00	96	H	60	0.79	75	1.50	1.14	382.56
	B-2-1.5-A	127	254	216	0.028	2.00	97	H	60	0.79	75	1.50	1.14	197.61
	B-4-1.5-A	127	254	216	0.028	4.00	97	H	60	0.79	75	1.50	1.14	96.16
	B-6-1.5-A	127	254	216	0.028	6.00	101	H	60	0.79	75	1.50	1.14	54.22
	B-2-1.0-M	127	254	216	0.046	2.00	95	H	60	0.79	75	1.00	0.76	184.57
	B-4-1.0-M	127	254	216	0.046	4.00	94	H	60	0.79	75	1.00	0.76	106.36
	B-6-1.0-M	127	254	216	0.046	6.00	95	H	60	0.79	75	1.00	0.76	80.29
Casanova et al. (1999)	HSFRC1	127	254	226	0.036	2.90	90	H	30	0.51	60	1.30	0.77	157.65
	HSFRC2	127	254	226	0.036	2.90	90	H	30	0.51	60	1.30	0.77	156.47
	HSFRC3	127	254	226	0.022	2.90	90	H	30	0.51	60	1.30	0.77	100.29
Cucchiara et al. (2004)	A10	150	249	218	0.019	2.80	41	H	30	0.51	60	1.00	0.59	95.86

Study	**Beam I.D.**	b_w (mm)	h (mm)	d (mm)	ρ	a/d	f_c' (MPa)	Fiber Type	L_f (mm)	D_f (mm)	L_f/D_f	V_f %	(Fiber Factor) F_p	$V_{exp.}$ (kN)
	A20	150	249	218	0.019	2.80	43	H	30	0.51	60	2.00	1.18	102.62
	B10	150	249	218	0.019	2.00	41	H	30	0.51	60	1.00	0.59	114.58
	B20	150	249	218	0.019	2.00	43	H	30	0.51	60	2.00	1.18	115.25
Kwak et al. (2002)	FHB2-2	127	254	213	0.015	2.00	64	H	50	0.79	63	0.50	0.32	137.97
	FHB3-2	127	254	213	0.015	2.00	69	H	50	0.79	63	0.75	0.48	147.49
	FHB2-3	127	254	213	0.015	3.00	64	H	50	0.79	63	0.50	0.32	83.64
	FHB3-3	127	254	213	0.015	3.00	69	H	50	0.79	63	0.75	0.48	92.04
	FHB2-4	127	254	213	0.015	4.00	64	H	50	0.79	63	0.50	0.32	65.34
	FHB3-4	127	254	213	0.015	4.00	69	H	50	0.79	63	0.75	0.48	74.31
	FNB2-2	127	254	213	0.015	2.00	31	H	50	0.79	63	0.50	0.32	109.40
	FNB2-3	127	254	213	0.015	3.00	31	H	50	0.79	63	0.50	0.32	69.08
	FNB2-4	127	254	213	0.015	4.00	31	H	50	0.79	63	0.50	0.32	54.14
Li et al. (1992)	-	127	229	203	0.022	3.00	23	H	30	0.51	60	1.00	0.59	78.77
	-	127	229	203	0.022	3.00	26	H	50	0.51	100	1.00	0.99	78.77
Lim et al. (1987)	2/0.5/1.5	152	254	221	0.012	1.50	34	H	30	0.51	60	0.50	0.30	106.74
	2/0.5/2.5	152	254	221	0.012	2.50	34	H	30	0.51	60	0.50	0.30	58.01
	2/0.5/3.5	152	254	221	0.012	3.50	34	H	30	0.51	60	0.50	0.30	45.25
	2/1.0/1.5	152	254	221	0.012	1.50	34	H	30	0.51	60	1.00	0.59	106.27
	2/1.0/2.5	152	254	221	0.012	2.50	34	H	30	0.51	60	1.00	0.59	60.10
	2/1.0/3.5	152	254	221	0.012	3.50	34	H	30	0.51	60	1.00	0.59	46.41

Study	**Beam I.D.**	b_w (mm)	h (mm)	d (mm)	ρ	a/d	f_c' (MPa)	Fiber Type	L_f (mm)	D_f (mm)	L_f/D_f	V_f %	(Fiber Factor) F_p	$V_{exp.}$ (kN)
	4/0.5/1.5	152	254	221	0.024	1.50	34	H	30	0.51	60	0.50	0.30	134.81
	4/0.5/2.5	152	254	221	0.024	2.50	34	H	30	0.51	60	0.50	0.30	63.58
	4/0.5/3.5	152	254	221	0.024	3.50	34	H	30	0.51	60	0.50	0.30	49.42
	4/1.0/1.5	152	254	221	0.024	1.50	34	H	30	0.51	60	1.00	0.59	147.34
	4/1.0/2.5	152	254	221	0.024	2.50	34	H	30	0.51	60	1.00	0.59	82.61
	4/1.0/3.5	152	254	221	0.024	3.50	34	H	30	0.51	60	1.00	0.59	67.29
Mansur et al. (1986)	B1	152	229	198	0.013	2.00	29	H	30	0.51	60	0.50	0.30	75.31
	B2	152	229	198	0.013	2.80	29	H	30	0.51	60	0.50	0.30	52.84
	B3	152	229	198	0.013	3.60	29	H	30	0.51	60	0.50	0.30	45.14
	B4	152	229	198	0.013	4.40	29	H	30	0.51	60	0.50	0.30	38.28
	C1	152	229	198	0.013	2.00	30	H	30	0.51	60	0.75	0.44	85.29
	C2	152	229	198	0.013	2.80	30	H	30	0.51	60	0.75	0.44	60.33
	C3	152	229	198	0.013	3.60	30	H	30	0.51	60	0.75	0.44	47.64
	C4	152	229	198	0.013	4.40	30	H	30	0.51	60	0.75	0.44	41.19
	C5	152	229	201	0.008	2.80	30	H	30	0.51	60	0.75	0.44	37.50
	C6	152	229	198	0.020	2.80	30	H	30	0.51	60	0.75	0.44	65.32
	D1	152	229	198	0.013	2.00	30	H	30	0.51	60	1.00	0.59	93.41
	D2	152	229	198	0.013	2.80	30	H	30	0.51	60	1.00	0.59	65.32
	D3	152	229	198	0.013	3.60	30	H	30	0.51	60	1.00	0.59	50.76
	D4	152	229	198	0.013	4.40	30	H	30	0.51	60	1.00	0.59	44.10

Study	**Beam I.D.**	b_w (mm)	h (mm)	d (mm)	ρ	a/d	f_c' (MPa)	Fiber Type	L_f (mm)	D_f (mm)	L_f/D_f	V_f %	(Fiber Factor) F_p	$V_{exp.}$ (kN)
	E1	152	229	201	0.008	2.80	21	H	30	0.51	60	0.75	0.44	34.98
	E2	152	229	198	0.013	2.80	21	H	30	0.51	60	0.75	0.44	45.14
	E3	152	229	198	0.020	2.80	21	H	30	0.51	60	0.75	0.44	60.33
	F1	152	229	201	0.008	2.80	33	H	30	0.51	60	0.75	0.44	46.99
	F2	152	229	198	0.013	2.80	33	H	30	0.51	60	0.75	0.44	75.31
	F3	152	229	198	0.020	2.80	33	H	30	0.51	60	0.75	0.44	86.33
Noghabai (2000)	4 type A	201	249	180	0.045	3.30	95	S-H	30	0.61	50	0.50	0.25	296.20
	5 type B	201	300	236	0.043	2.80	102	S-H	30	0.61	50	0.50	0.25	410.19
	5 type C	201	500	409	0.030	2.90	82	S-H	30	0.61	50	0.50	0.25	367.50
	6 type C	201	500	409	0.030	2.90	82	S-H	30	0.61	50	0.50	0.25	327.35
	3 type D	300	701	569	0.029	3.00	82	S-H	30	0.61	50	0.50	0.25	567.50
	4 type D	300	701	569	0.029	3.00	68	H	60	0.71	86	0.75	0.63	507.58
Rosenbusch et al. (2002)	1.2/2	201	300	259	0.036	3.50	47	H	60	0.89	67	0.25	0.17	109.96
	1.2/3	201	300	259	0.036	3.50	44	H	60	0.89	67	0.51	0.34	119.99
	1.2/4	201	300	259	0.036	3.50	48	H	60	0.89	67	0.76	0.51	154.74
	2.2/2	201	300	259	0.018	1.50	41	H	60	0.89	67	0.25	0.17	279.75
	2.2/3	201	300	259	0.018	1.50	40	H	60	0.89	67	0.76	0.51	299.45
	2.3/2	201	300	262	0.012	2.50	40	H	60	0.89	67	0.25	0.17	82.47
	2.3/3	201	300	262	0.012	2.50	39	H	60	0.89	67	0.76	0.51	108.15

Study	**Beam I.D.**	b_w (mm)	h (mm)	d (mm)	ρ	a/d	f_c' (MPa)	Fiber Type	L_f (mm)	D_f (mm)	L_f/D_f	V_f %	(Fiber Factor) F_p	$V_{exp.}$ (kN)
	2.4/2	201	300	259	0.018	2.50	40	H	60	0.89	67	0.25	0.17	107.82
	2.4/3	201	300	259	0.018	2.50	39	H	60	0.89	67	0.76	0.51	143.63
	2.6/2	201	300	259	0.018	4.00	41	H	60	0.89	67	0.25	0.17	82.38
	2.6/3	201	300	259	0.018	4.00	40	H	60	0.89	67	0.76	0.51	116.77
	20x30-SFRC Series 1	201	300	259	0.028	3.50	38	H	60	0.89	67	0.50	0.34	110.32
	20x45-SFRC Series 1	201	450	409	0.031	3.30	38	H	60	0.89	67	0.50	0.34	145.30
	20x60-SFRC Series 1	201	599	541	0.027	3.50	38	H	60	0.89	67	0.50	0.34	154.09
	20x30-SFRC Series 2	201	300	259	0.028	3.50	39	H	60	0.89	67	0.50	0.34	131.46
	20x50-SFRC Series 2	201	500	460	0.026	3.40	39	H	60	0.89	67	0.50	0.34	148.10
	20x60-SFRC Series 2	201	599	541	0.027	3.50	39	H	60	0.89	67	0.50	0.34	222.90
Sharma (1986)	S3F	152	305	277	0.045	1.80	49	H	51	0.61	83	0.90	0.75	122.97
Swamy & Bahia. (1985)	B52	175	249	211	0.040	4.50	36	C	50	0.51	100	0.40	0.39	79.94
	B53	175	249	211	0.040	4.50	37	C	50	0.51	100	0.80	0.79	114.56
	B54	175	249	211	0.040	4.50	40	C	50	0.51	100	1.20	1.18	115.58
	B55	175	249	211	0.031	4.50	38	C	50	0.51	100	0.80	0.79	118.63
	B56	175	249	211	0.020	4.50	42	C	50	0.51	100	0.80	0.79	96.74
	B63R	175	249	211	0.020	4.50	35	C	50	0.51	100	0.80	0.79	75.86
Swamy et al. (1993)	1TLF-1	56	305	264	0.043	2.00	36	C	51	0.51	100	1.00	1.00	80.96
	1TLF-2	56	305	264	0.043	3.40	41	C	51	0.51	100	1.00	1.00	59.50

Study	**Beam I.D.**	b_w (mm)	h (mm)	d (mm)	ρ	a/d	f_c' (MPa)	Fiber Type	L_f (mm)	D_f (mm)	L_f/D_f	V_f %	(Fiber Factor) F_p	$V_{exp.}$ (kN)
	1TLF-3	56	305	264	0.043	4.90	36	C	51	0.51	100	1.00	1.00	42.82
	2TLF-1	56	305	264	0.028	2.00	38	C	51	0.51	100	1.00	1.00	72.41
	2TLF-2	56	305	264	0.028	3.40	33	C	51	0.51	100	1.00	1.00	45.97
	2TLF-3	56	305	264	0.028	4.90	36	C	51	0.51	100	1.00	1.00	43.12
	3TLF-1	56	305	264	0.016	2.00	36	C	51	0.51	100	1.00	1.00	68.35
	3TLF-2	56	305	264	0.016	3.40	34	C	51	0.51	100	1.00	1.00	41.80
	3TLF-3	56	305	264	0.016	4.90	32	C	51	0.51	100	1.00	1.00	29.70
Tan et al. (1993)	2	61	376	340	0.034	2.00	35	H	30	0.51	60	0.50	0.30	110.79
	3	61	376	340	0.034	2.00	33	H	30	0.51	60	0.75	0.45	91.92
	4	61	376	340	0.034	2.00	36	H	30	0.51	60	1.00	0.60	106.79
	5	61	376	340	0.034	2.50	36	H	30	0.51	60	1.00	0.60	78.34
	6	61	376	340	0.034	1.50	36	H	30	0.51	60	1.00	0.60	155.97
Barragan (2002)	R20X30 Series1	200	300	260	0.0283	3.50	38	H	60	0.92	65	0.50	0.33	111.00
	R20X30 Series2	200	300	260	0.0283	3.50	39	H	60	0.92	65	0.50	0.33	132.00
	R20X45 Series1	200	450	410	0.0294	3.50	38	H	60	0.92	65	0.50	0.33	146.00
	R20X50 Series2	200	500	460	0.0262	3.50	39	H	60	0.92	65	0.50	0.33	148.00
	R20x60 Series1	200	600	540	0.0273	3.50	38	H	60	0.92	65	0.50	0.33	154.00
	R20x60 Series2	200	600	540	0.0273	3.50	39	H	60	0.92	65	0.50	0.33	222.00
Aoude H. (2008)	B 0.5%	150	250	202	0.0133	2.97	21	H	30	0.55	55	0.50	0.27	47.50

Study	**Beam I.D.**	b_w (mm)	h (mm)	d (mm)	ρ	a/d	f_c' (MPa)	Fiber Type	L_f (mm)	D_f (mm)	L_f/D_f	V_f %	(Fiber Factor) F_p	$V_{exp.}$ (kN)
	B 1.0%	150	250	202	0.0133	2.97	20	H	30	0.55	55	1.00	0.55	56.50
Greenough & Nehdi (2008)	S-HE-50-0.5	200	300	265	0.017	3	40	H	50	1.00	50	0.50	0.25	91.16
	S-HE-50-0.75	200	300	265	0.017	3	40	H	50	1.00	50	0.75	0.38	105.47
	S-HE-50-1.0	200	300	265	0.017	3	40	H	50	1.00	50	1.00	0.50	148.93
	S-FE-50-0.5	200	300	265	0.017	3	40	S	50	1.00	50	0.50	0.25	115.54
	S-FE-50-0.75	200	300	265	0.017	3	40	S	50	1.00	50	0.75	0.38	144.16
	S-FE-50-1.0	200	300	265	0.017	3	40	S	50	1.00	50	1.00	0.50	146.81
	S-FE-30-0.5	200	300	265	0.017	3	40	S	30	0.70	43	0.50	0.21	106.53
	S-FE-30-0.75	200	300	265	0.017	3	40	S	30	0.70	43	0.75	0.32	122.96
	S-FE-30-1.0	200	300	265	0.017	3	40	S	30	0.70	43	1.00	0.43	151.58
Narayanan & Darwish (1987)	SF1	85	150	130	0.020	2.00	61	C	30	0.3	100	0.25	0.19	32.71
	SF2	85	150	130	0.020	2.50	61	C	30	0.3	100	0.25	0.19	29.50
	SF3	85	150	130	0.020	3.00	61	C	30	0.3	100	0.25	0.19	30.61
	SF4	85	150	130	0.020	2.00	39	C	30	0.3	100	0.25	0.19	29.95
	SF5	85	150	130	0.020	2.50	39	C	30	0.3	100	0.25	0.19	22.87
	SF6	85	150	130	0.020	3.00	39	C	30	0.3	100	0.25	0.19	21.44
	B1	85	150	130	0.020	3.00	61	C	40	0.3	133	0.50	0.50	35.69
	B2	85	150	130	0.020	3.00	66	C	40	0.3	133	1.00	1.00	40.44
	B3	85	150	130	0.020	3.00	59	C	30	0.3	100	1.50	1.12	40.22

Study	**Beam I.D.**	b_w (mm)	h (mm)	d (mm)	ρ	a/d	f_c' (MPa)	Fiber Type	L_f (mm)	D_f (mm)	L_f/D_f	V_f %	(Fiber Factor) F_p	$V_{exp.}$ (kN)
	B4	85	150	130	0.020	3.00	63	C	30	0.3	100	2.00	1.50	41.33
	B5	85	150	130	0.020	3.00	64	C	30	0.3	100	2.50	1.90	41.55
	B6	85	150	130	0.020	3.00	61	C	30	0.3	100	3.00	2.25	42.54
	B7	85	150	130	0.020	3.00	36	C	40	0.3	133	0.50	0.50	21.77
	B9	85	150	130	0.020	3.00	37	C	30	0.3	100	1.00	0.75	32.82
	B11	85	150	130	0.020	2.00	61	C	40	0.3	133	0.50	0.50	51.05
	B12	85	150	130	0.020	2.50	61	C	40	0.3	133	0.50	0.50	40.77
	B13	85	150	130	0.020	3.50	49	C	40	0.3	133	0.50	0.50	28.84
	B14	85	150	130	0.020	2.00	57	C	40	0.3	133	1.00	1.00	61.55
	B15	85	150	130	0.020	2.50	57	C	40	0.3	133	1.00	1.00	48.84
	B16	85	150	130	0.020	3.50	57	C	40	0.3	133	1.00	1.00	32.82
	B17	85	150	128	0.0369	3.00	49	C	40	0.3	133	0.50	0.50	32.20
	B18	85	150	126	0.0572	3.10	49	C	40	0.3	133	0.50	0.50	38.02
	B19	85	150	128	0.0369	3.00	36	C	40	0.3	133	0.50	0.50	24.37
	B20	85	150	126	0.0572	3.10	36	C	40	0.3	133	0.50	0.50	24.95
	B23	85	150	128	0.0369	3.00	57	C	40	0.3	133	1.00	1.00	47.55
	B24	85	150	126	0.0572	3.10	57	C	40	0.3	133	1.00	1.00	53.55
	B25	85	150	126	0.0572	3.10	63	C	30	0.3	100	1.50	1.12	51.94
	B26	85	150	126	0.0572	3.10	51	C	30	0.3	100	2.00	1.50	52.80
	B27	85	150	128	0.0369	3.00	63	C	30	0.3	100	1.50	1.12	48.52

Study	**Beam I.D.**	b_w (mm)	h (mm)	d (mm)	ρ	a/d	f_c' (MPa)	Fiber Type	L_f (mm)	D_f (mm)	L_f/D_f	V_f %	(Fiber Factor) F_p	$V_{exp.}$ (kN)
	B28	85	150	126	0.0572	2.00	59	C	30	0.3	100	0.50	0.37	58.48
	B29	85	150	126	0.0572	2.00	54	C	30	0.3	100	1.00	0.75	72.51
	B30	85	150	126	0.0572	2.00	63	C	30	0.3	100	1.50	1.12	76.58
	B31	85	150	126	0.0572	2.00	51	C	30	0.3	100	2.00	1.50	67.47
Furlan & Hanai (1997)	P3B	100	100	86	0.066	3.50	55	C	25	0.20	127	1.00	1.27	40.00
	P4B	100	100	86	0.066	3.50	50	C	25	0.20	127	2.00	2.54	44.00
	P5B	100	100	86	0.066	3.50	49	C	38	0.20	191	1.00	1.91	37.00
	P6B	100	100	86	0.066	3.50	54	C	38	0.20	191	2.00	3.81	40.00
	P7B	100	100	86	0.066	3.50	54	C	38	0.20	191	0.50	0.95	35.00

Table A2: Predictions of shear capacities of beams containing hooked-end fibers and having an *a/d* ratio greater than 2.3 using the model proposed in this thesis and models proposed by other researchers.

		Prediction models													
		Khuntia et al. (1999)		Imam et al. (1995)		Mansur et al. (1986)		Sharma et al. (1986)		Narayanan & Darwish (1987)		Ashour et al. (1992)		Proposed model	
Study	**Beam I.D.**	V_{pred} (kN)	$\frac{V_{exp}}{V_{pred}}$	V_{pred} (kN)	$\frac{V_{exp}}{V_{pred}}$	V_{pred} (kN)	$\frac{V_{exp}}{V_{pred}}$	V_{pred} (kN)	$\frac{V_{exp}}{V_{pred}}$	V_{pred} (kN)	$\frac{V_{exp}}{V_{pred}}$	V_{pred} (kN)	$\frac{V_{exp}}{V_{pred}}$	V_{pred} (kN)	$\frac{V_{exp}}{V_{pred}}$
Parra-Montesinos et al. (2006)	1	112.72	1.56	122.85	1.43	121.34	1.45	91.08	1.93	132.90	1.32	145.91	1.21	122.78	1.43
	2	112.72	1.59	122.85	1.46	121.34	1.48	91.08	1.97	132.90	1.35	145.91	1.23	122.78	1.46
	3	112.72	1.78	144.24	1.39	123.34	1.63	91.08	2.20	142.19	1.41	147.90	1.36	131.68	1.53
	4	112.72	1.31	144.24	1.02	123.34	1.19	91.08	1.62	142.19	1.04	147.90	1.00	131.68	1.12
	7	125.53	1.18	168.25	0.88	147.10	1.01	82.76	1.79	169.86	0.87	180.29	0.82	153.13	0.97
	8	125.53	1.56	168.25	1.17	147.10	1.33	82.76	2.37	169.86	1.15	180.29	1.09	153.13	1.28
	9	151.10	1.26	183.18	1.04	157.63	1.21	99.62	1.91	180.03	1.06	193.85	0.98	165.26	1.15
	10	151.10	1.25	183.18	1.03	157.63	1.20	99.62	1.90	180.03	1.05	193.85	0.98	165.26	1.15
	11	188.15	0.92	213.33	0.81	189.67	0.91	104.25	1.65	214.61	0.80	232.84	0.74	168.71	1.02
	12	188.15	1.16	213.33	1.03	189.67	1.15	104.25	2.10	214.61	1.02	232.84	0.94	168.71	1.30
Ashour et al. (1992)	B-4-1.0-L†	94.28	0.26	43.95	0.56	78.21	0.31	64.85	0.38	79.92	0.31	83.18	0.30	19.09	1.29
	B-6-1.0-L†	94.84	0.16	40.52	0.38	78.30	0.20	58.95	0.26	79.57	0.19	55.63	0.28	12.75	1.20
	B-4-0.5-A	70.22	0.89	82.82	0.75	63.92	0.97	65.83	0.94	74.18	0.84	68.44	0.91	58.38	1.06
	B-6-0.5-A	70.35	0.76	70.51	0.76	62.89	0.85	59.60	0.90	69.18	0.77	45.68	1.17	47.27	1.13
	B-4-1.0-A†	96.74	0.90	103.71	0.84	82.14	1.06	66.54	1.31	94.76	0.92	87.21	1.00	71.44	1.22

		Prediction models													
		Khuntia et al. (1999)		Imam et al. (1995)		Mansur et al. (1986)		Sharma et al. (1986)		Narayanan & Darwish (1987)		Ashour et al. (1992)		Proposed model	
Study	**Beam I.D.**	V_{pred} (kN)	$\frac{V_{exp}}{V_{pred}}$	V_{pred} (kN)	$\frac{V_{exp}}{V_{pred}}$	V_{pred} (kN)	$\frac{V_{exp}}{V_{pred}}$	V_{pred} (kN)	$\frac{V_{exp}}{V_{pred}}$	V_{pred} (kN)	$\frac{V_{exp}}{V_{pred}}$	V_{pred} (kN)	$\frac{V_{exp}}{V_{pred}}$	V_{pred} (kN)	$\frac{V_{exp}}{V_{pred}}$
	B-6-1.0-A†	98.23	0.55	86.34	0.62	81.70	0.66	61.06	0.88	90.69	0.59	58.63	0.92	54.89	0.98
	B-4-1.5-A	122.24	0.79	120.77	0.80	99.80	0.96	66.40	1.45	114.01	0.84	105.37	0.91	84.50	1.14
	B-6-1.5-A†	124.86	0.43	98.34	0.55	99.63	0.54	61.29	0.88	110.36	0.49	70.92	0.76	59.80	0.91
	B-4-1.0-M	94.88	1.12	130.47	0.82	83.42	1.27	65.26	1.63	103.35	1.03	88.42	1.20	79.61	1.34
	B-6-1.0-M	95.50	0.84	103.16	0.78	81.90	0.98	59.36	1.35	95.37	0.84	59.15	1.36	62.22	1.29
Casanova et al. (1999)	HSFRC1	97.70	1.61	164.24	0.96	87.17	1.81	72.54	2.17	109.26	1.44	125.02	1.26	120.97	1.30
	HSFRC2†	97.70	1.60	164.24	0.95	87.17	1.79	72.54	2.16	109.26	1.43	125.02	1.25	120.97	1.29
	HSFRC3†	97.70	1.03	124.05	0.81	84.79	1.18	72.54	1.38	98.17	1.02	122.64	0.82	102.15	0.98
Cucchiara et al. (2004)	A10	65.81	1.46	102.18	0.94	70.16	1.37	56.23	1.70	78.86	1.22	104.42	0.92	88.48	1.08
	A20†	99.40	1.03	142.41	0.72	103.97	0.99	57.82	1.77	115.47	0.89	154.18	0.67	123.19	0.83
Kwak et al. (2002)	FHB2-3	53.34	1.57	62.97	1.33	51.61	1.62	57.17	1.46	55.05	1.52	72.92	1.15	58.07	1.44
	FHB3-3	64.23	1.43	72.91	1.26	60.22	1.53	59.29	1.55	64.97	1.42	84.84	1.08	61.31	1.50
	FHB2-4	53.34	1.23	51.88	1.26	51.03	1.28	53.20	1.23	52.34	1.25	54.69	1.19	44.56	1.47
	FHB3-4	64.23	1.16	59.29	1.25	59.64	1.25	55.17	1.35	62.26	1.19	63.63	1.17	45.94	1.62
	FNB2-3	37.06	1.86	51.63	1.34	41.04	1.68	39.72	1.74	44.01	1.57	57.51	1.20	47.39	1.46
	FNB2-4	37.06	1.46	40.54	1.34	40.46	1.34	36.96	1.46	41.30	1.31	43.13	1.26	40.28	1.34
Li et al. (1992)	-	38.64	2.04	72.06	1.09	48.82	1.61	32.45	2.43	57.44	1.37	67.45	1.17	59.99	1.31
	-	54.35	1.45	93.78	0.84	67.55	1.17	34.74	2.27	77.34	1.02	93.26	0.84	64.62	1.22

		Prediction models													
		Khuntia et al. (1999)		Imam et al. (1995)		Mansur et al. (1986)		Sharma et al. (1986)		Narayanan & Darwish (1987)		Ashour et al. (1992)		Proposed model	
Study	**Beam I.D.**	V_{pred} (kN)	$\frac{V_{exp}}{V_{pred}}$	V_{pred} (kN)	$\frac{V_{exp}}{V_{pred}}$	V_{pred} (kN)	$\frac{V_{exp}}{V_{pred}}$	V_{pred} (kN)	$\frac{V_{exp}}{V_{pred}}$	V_{pred} (kN)	$\frac{V_{exp}}{V_{pred}}$	V_{pred} (kN)	$\frac{V_{exp}}{V_{pred}}$	V_{pred} (kN)	$\frac{V_{exp}}{V_{pred}}$
Lim et al. (1987)	2/0.5/2.5	47.25	1.23	68.93	0.84	51.09	1.14	54.26	1.07	58.45	0.99	85.56	0.68	63.73	0.91
	2/0.5/3.5†	47.25	0.96	49.79	0.91	50.29	0.90	49.88	0.91	50.30	0.90	61.11	0.74	50.42	0.90
	2/1.0/2.5†	61.73	0.97	89.01	0.68	67.99	0.88	54.26	1.11	77.57	0.77	113.37	0.53	72.17	0.83
	2/1.0/3.5†	61.73	0.75	61.56	0.75	67.20	0.69	49.88	0.93	69.19	0.67	80.98	0.57	52.93	0.88
	4/0.5/2.5	47.25	1.35	104.41	0.61	53.87	1.18	54.26	1.17	72.93	0.87	88.34	0.72	75.46	0.84
	4/0.5/3.5	47.25	1.05	70.30	0.70	52.28	0.95	49.88	0.99	59.54	0.83	63.10	0.78	61.75	0.80
	4/1.0/2.5	61.73	1.34	137.33	0.60	70.77	1.17	54.26	1.52	92.05	0.90	116.15	0.71	101.83	0.81
	4/1.0/3.5	61.73	1.09	88.42	0.76	69.18	0.97	49.88	1.35	78.42	0.86	82.97	0.81	79.45	0.85
Mansur et al. (1986)	B2	39.20	1.35	56.03	0.94	43.62	1.21	43.75	1.21	46.21	1.14	65.38	0.81	54.80	0.96
	B3	39.20	1.15	44.41	1.02	43.08	1.05	41.08	1.10	43.72	1.03	50.85	0.89	46.33	0.97
	B4†	39.20	0.98	39.16	0.98	42.74	0.90	39.07	0.98	42.13	0.91	41.61	0.92	38.26	1.00
	C2	45.84	1.32	64.54	0.93	51.56	1.17	44.37	1.36	55.05	1.10	77.09	0.78	61.62	0.98
	C3†	45.84	1.04	50.35	0.95	51.03	0.93	41.67	1.14	52.56	0.91	59.96	0.79	47.93	0.99
	C4†	45.84	0.90	43.94	0.94	50.68	0.81	39.63	1.04	50.97	0.81	49.06	0.84	39.21	1.05
	C5†	46.43	0.81	49.81	0.75	51.28	0.73	44.94	0.83	51.38	0.73	77.14	0.49	42.61	0.88
	C6	45.84	1.43	82.95	0.79	52.86	1.24	44.37	1.47	61.09	1.07	78.39	0.83	70.85	0.92
	D2†	51.99	1.26	72.16	0.91	59.17	1.10	44.42	1.47	63.46	1.03	88.27	0.74	62.85	1.04

		Prediction models													
		Khuntia et al. (1999)		Imam et al. (1995)		Mansur et al. (1986)		Sharma et al. (1986)		Narayanan & Darwish (1987)		Ashour et al. (1992)		Proposed model	
Study	**Beam I.D.**	V_{pred} (kN)	$\frac{V_{exp}}{V_{pred}}$	V_{pred} (kN)	$\frac{V_{exp}}{V_{pred}}$	V_{pred} (kN)	$\frac{V_{exp}}{V_{pred}}$	V_{pred} (kN)	$\frac{V_{exp}}{V_{pred}}$	V_{pred} (kN)	$\frac{V_{exp}}{V_{pred}}$	V_{pred} (kN)	$\frac{V_{exp}}{V_{pred}}$	V_{pred} (kN)	$\frac{V_{exp}}{V_{pred}}$
	D3†	51.99	0.98	55.49	0.91	58.63	0.87	41.71	1.22	60.97	0.83	68.66	0.74	48.89	1.04
	D4†	51.99	0.85	47.96	0.92	58.29	0.76	39.67	1.11	59.38	0.74	56.17	0.79	40.00	1.10
	E1†	38.53	0.91	45.38	0.77	46.74	0.75	37.30	0.94	47.85	0.73	70.03	0.50	40.54	0.86
	E2	38.05	1.19	59.38	0.76	47.07	0.96	36.83	1.23	51.56	0.88	70.07	0.64	57.09	0.79
	E3	38.05	1.59	77.00	0.78	48.37	1.25	36.83	1.64	57.60	1.05	71.37	0.85	63.79	0.95
	F1†	49.08	0.96	51.28	0.92	52.81	0.89	47.50	0.99	52.72	0.89	79.53	0.59	43.09	1.09
	F2†	48.46	1.55	66.25	1.14	53.07	1.42	46.90	1.61	56.36	1.34	79.45	0.95	62.69	1.20
	F3	48.46	1.78	84.92	1.02	54.37	1.59	46.90	1.84	62.40	1.38	80.75	1.07	72.02	1.20
Rosenbusch et al. (2002)	1.2/2	74.48	1.48	125.15	0.88	81.09	1.36	90.50	1.22	101.43	1.08	97.95	1.12	97.90	1.12
	1.2/3	86.99	1.38	147.31	0.81	94.63	1.27	87.39	1.37	117.37	1.02	113.73	1.06	110.34	1.09
	1.2/4	106.55	1.45	172.83	0.90	112.29	1.38	91.75	1.69	136.98	1.13	134.69	1.15	127.32	1.22
	2.3/2	69.47	1.19	94.07	0.88	72.53	1.14	91.82	0.90	82.14	1.00	122.11	0.68	80.99	1.02
	2.3/3	96.32	1.12	131.47	0.82	102.33	1.06	90.22	1.20	116.62	0.93	171.05	0.63	112.85	0.96
	2.4/2	68.79	1.57	117.32	0.92	73.98	1.46	90.93	1.19	92.52	1.17	123.07	0.88	91.55	1.18
	2.4/3	95.38	1.51	166.60	0.86	103.48	1.39	89.35	1.61	126.66	1.13	171.53	0.84	128.13	1.12
	2.6/2	69.79	1.18	78.52	1.05	72.33	1.14	82.02	1.00	73.73	1.12	77.76	1.06	73.39	1.12
	2.6/3	97.40	1.20	102.73	1.14	102.16	1.14	81.12	1.44	107.79	1.08	108.40	1.08	94.45	1.24

		Prediction models													
		Khuntia et al. (1999)		Imam et al. (1995)		Mansur et al. (1986)		Sharma et al. (1986)		Narayanan & Darwish (1987)		Ashour et al. (1992)		Proposed model	
Study	**Beam I.D.**	V_{pred} (kN)	$\frac{V_{exp}}{V_{pred}}$	V_{pred} (kN)	$\frac{V_{exp}}{V_{pred}}$	V_{pred} (kN)	$\frac{V_{exp}}{V_{pred}}$	V_{pred} (kN)	$\frac{V_{exp}}{V_{pred}}$	V_{pred} (kN)	$\frac{V_{exp}}{V_{pred}}$	V_{pred} (kN)	$\frac{V_{exp}}{V_{pred}}$	V_{pred} (kN)	$\frac{V_{exp}}{V_{pred}}$
Tan et al. (1993)	5	39.44	1.99	100.42	0.78	45.94	1.71	34.40	2.28	65.12	1.20	74.55	1.05	64.50	1.21
Barragan (2002)	R20X30 Series1†	79.26	1.40	122.48	0.91	87.08	1.27	81.14	1.37	102.49	1.08	104.90	1.06	100.91	1.10
	R20X30 Series2†	80.41	1.64	123.44	1.07	87.82	1.50	82.32	1.60	103.20	1.28	105.82	1.25	101.91	1.30
	R20X45 Series1†	124.99	1.17	182.22	0.80	137.76	1.06	127.95	1.14	163.70	0.89	165.86	0.88	148.83	0.98
	R20X50 Series2†	142.26	1.04	189.50	0.78	154.43	0.96	145.64	1.02	178.18	0.83	186.27	0.79	159.71	0.93
	R20x60 Series1†	164.62	0.94	217.37	0.71	180.30	0.85	168.52	0.91	210.28	0.73	217.30	0.71	180.59	0.85
	R20x60 Series2†	167.00	1.33	219.09	1.01	181.84	1.22	170.96	1.30	211.75	1.05	219.23	1.01	181.66	1.22
Aoude (2008)	B 0.5%	32.89	1.44	47.90	0.99	38.77	1.23	37.03	1.28	41.74	1.14	54.77	0.87	45.92	1.03
	B 1.0%	40.70	1.39	59.65	0.95	51.92	1.09	35.52	1.59	56.82	0.99	72.91	0.77	55.28	1.02
		mean:	1.22	**mean:**	0.92	**mean:**	1.14	**mean:**	1.38	**mean:**	1.02	**mean:**	0.90	**mean:**	1.10
		S.D.:	0.34	**S.D.:**	0.21	**S.D.:**	0.30	**S.D.:**	0.43	**S.D.:**	0.26	**S.D.:**	0.23	**S.D.:**	0.19

† Beams failed in flexural mode

Table A3: Predictions of shear capacities of beams containing crimped fibers and having an *a/d* ratio greater than 2.3 using the model proposed in this thesis and models proposed by other researchers.

		Prediction models													
		Khuntia et al. (1999)		Imam et al. (1995)		Mansur et al. (1986)		Sharma et al. (1986)		Narayanan & Darwish (1987)		Ashour et al. (1992)		Proposed model	
Study	**Beam I.D.**	V_{pred} (kN)	$\frac{V_{exp}}{V_{pred}}$	V_{pred} (kN)	$\frac{V_{exp}}{V_{pred}}$	V_{pred} (kN)	$\frac{V_{exp}}{V_{pred}}$	V_{pred} (kN)	$\frac{V_{exp}}{V_{pred}}$	V_{pred} (kN)	$\frac{V_{exp}}{V_{pred}}$	V_{pred} (kN)	$\frac{V_{exp}}{V_{pred}}$	V_{pred} (kN)	$\frac{V_{exp}}{V_{pred}}$
Swamy & Bahia (1985)	B52	56.32	1.42	87.28	0.92	65.67	1.22	52.58	1.52	76.61	1.04	60.30	1.33	74.84	1.07
	B53	77.81	1.47	111.16	1.03	91.35	1.25	53.94	2.12	102.30	1.12	81.57	1.40	96.68	1.18
	B54	100.95	1.14	132.83	0.87	117.27	0.99	55.65	2.08	127.67	0.91	103.06	1.12	113.00	1.02
	B55	78.60	1.51	98.58	1.20	90.44	1.31	54.48	2.18	96.74	1.23	80.65	1.47	91.74	1.29
	B56†	82.27	1.18	82.44	1.17	90.60	1.07	57.03	1.70	91.21	1.06	80.76	1.20	70.88	1.36
	B63R†	75.41	1.01	77.92	0.97	87.41	0.87	52.27	1.45	88.11	0.86	77.66	0.98	68.38	1.11
Swamy et al. (1993)	1TLF-2	36.99	1.61	67.75	0.88	43.42	1.37	24.15	2.46	51.18	1.16	49.99	1.19	55.97	1.06
	1TLF-3	34.70	1.23	44.56	0.96	41.51	1.03	20.68	2.07	45.70	0.94	33.85	1.26	39.44	1.09
	2TLF-2	33.31	1.38	50.29	0.91	40.80	1.13	21.75	2.11	44.53	1.03	46.94	0.98	44.27	1.04
	2TLF-3	34.67	1.24	36.19	1.19	40.72	1.06	20.66	2.09	42.07	1.03	33.06	1.30	31.81	1.36
	3TLF-2	33.96	1.23	37.02	1.13	40.17	1.04	22.18	1.88	40.61	1.03	46.38	0.90	30.77	1.36
	3TLF-3†	32.96	0.90	27.06	1.10	39.40	0.75	19.65	1.51	38.53	0.77	31.82	0.93	21.25	1.40
Narayanan & Darwish (1987)	SF2	18.10	1.63	32.16	0.92	18.90	1.56	23.86	1.24	24.71	1.19	30.98	0.95	41.33	0.71
	SF3	18.10	1.69	26.80	1.14	18.65	1.64	22.79	1.34	21.23	1.44	25.81	1.19	35.67	0.86

		Prediction models													
		Khuntia et al. (1999)		Imam et al. (1995)		Mansur et al. (1986)		Sharma et al. (1986)		Narayanan & Darwish (1987)		Ashour et al. (1992)		Proposed model	
Study	**Beam I.D.**	V_{pred} (kN)	$\frac{V_{exp}}{V_{pred}}$	V_{pred} (kN)	$\frac{V_{exp}}{V_{pred}}$	V_{pred} (kN)	$\frac{V_{exp}}{V_{pred}}$	V_{pred} (kN)	$\frac{V_{exp}}{V_{pred}}$	V_{pred} (kN)	$\frac{V_{exp}}{V_{pred}}$	V_{pred} (kN)	$\frac{V_{exp}}{V_{pred}}$	V_{pred} (kN)	$\frac{V_{exp}}{V_{pred}}$
	SF5	14.51	1.58	29.06	0.79	16.16	1.42	19.12	1.20	20.14	1.14	26.18	0.87	32.89	0.70
	SF6	14.51	1.48	23.70	0.90	15.91	1.35	18.27	1.17	17.14	1.25	21.82	0.98	30.27	0.71
	B1	24.08	1.48	34.90	1.02	24.45	1.46	22.76	1.57	27.06	1.32	32.97	1.08	36.65	0.97
	B2	35.14	1.15	46.76	0.86	34.41	1.18	23.67	1.71	38.75	1.04	45.39	0.89	38.62	1.05
	B3	35.41	1.14	47.88	0.84	35.85	1.12	22.32	1.80	43.99	0.91	46.98	0.86	38.32	1.05
	B4	44.35	0.93	56.03	0.74	43.54	0.95	23.22	1.78	52.76	0.78	56.59	0.73	39.92	1.04
	B5	52.47	0.79	63.28	0.66	51.11	0.81	23.31	1.78	61.12	0.68	65.95	0.63	41.14	1.01
	B6	58.20	0.73	68.66	0.62	57.40	0.74	22.83	1.86	69.19	0.61	73.65	0.58	41.82	1.02
	B7	18.53	1.17	30.63	0.71	21.28	1.02	17.51	1.24	23.03	0.95	28.34	0.77	33.38	0.65
	B9	22.41	1.46	36.06	0.91	26.05	1.26	17.63	1.86	28.48	1.15	34.25	0.96	34.01	0.96
	B12	24.08	1.69	43.09	0.95	24.71	1.65	23.82	1.71	30.61	1.33	39.57	1.03	43.98	0.93
	B13	21.62	1.33	28.49	1.01	22.86	1.26	19.66	1.47	25.34	1.14	26.50	1.09	30.43	0.95
	B15	32.79	1.49	57.66	0.85	33.71	1.45	23.12	2.11	43.35	1.13	52.79	0.93	45.41	1.08
	B16	32.82	1.00	38.42	0.85	33.28	0.99	21.28	1.54	37.96	0.86	37.72	0.87	32.45	1.01
	B17	21.29	1.51	46.09	0.70	23.74	1.36	20.12	1.60	30.68	1.05	31.50	1.02	52.04	0.62
	B18	20.95	1.81	56.51	0.67	24.51	1.55	19.64	1.94	35.47	1.07	31.21	1.22	52.26	0.73
	B19	18.25	1.34	43.20	0.56	22.00	1.11	17.24	1.41	27.58	0.88	28.96	0.84	43.11	0.57
	B20	17.96	1.39	53.21	0.47	22.79	1.09	16.83	1.48	32.41	0.77	28.79	0.87	42.97	0.58

		Prediction models													
		Khuntia et al. (1999)		Imam et al. (1995)		Mansur et al. (1986)		Sharma et al. (1986)		Narayanan & Darwish (1987)		Ashour et al. (1992)		Proposed model	
Study	**Beam I.D.**	V_{pred} (kN)	$\frac{V_{exp}}{V_{pred}}$	V_{pred} (kN)	$\frac{V_{exp}}{V_{pred}}$	V_{pred} (kN)	$\frac{V_{exp}}{V_{pred}}$	V_{pred} (kN)	$\frac{V_{exp}}{V_{pred}}$	V_{pred} (kN)	$\frac{V_{exp}}{V_{pred}}$	V_{pred} (kN)	$\frac{V_{exp}}{V_{pred}}$	V_{pred} (kN)	$\frac{V_{exp}}{V_{pred}}$
	B23	32.31	1.47	64.08	0.74	34.00	1.40	21.77	2.18	43.11	1.10	44.38	1.07	58.51	0.81
	B24	31.81	1.68	79.03	0.68	34.60	1.55	21.26	2.52	47.71	1.12	43.49	1.23	72.75	0.74
	B25	35.62	1.46	85.03	0.61	37.41	1.39	22.27	2.33	49.01	1.06	46.97	1.11	76.01	0.68
	B26	38.51	1.37	95.55	0.55	42.95	1.23	20.00	2.64	53.70	0.98	53.28	0.99	68.24	0.77
	B27	36.18	1.34	68.93	0.70	36.85	1.32	22.81	2.13	44.43	1.09	48.04	1.01	60.23	0.81
Furlan&Hanai (1997)	P3B	28.73	1.39	67.18	0.60	31.46	1.27	16.13	2.48	29.64	1.35	35.07	1.14	50.13	0.80
	P4B	44.76	0.98	96.52	0.46	49.53	0.89	15.40	2.86	46.31	0.95	54.10	0.81	48.05	0.92
	P5B	35.85	1.03	81.67	0.45	40.20	0.92	15.29	2.42	37.97	0.97	44.22	0.84	47.58	0.78
	P6B	64.33	0.62	124.76	0.32	68.40	0.58	15.96	2.51	62.98	0.64	74.13	0.54	50.47	0.79
	P7B	23.91	1.46	58.19	0.60	26.71	1.31	15.93	2.20	25.47	1.37	30.02	1.17	42.16	0.83
		Mean:	1.31	**Mean:**	0.81	**Mean:**	1.19	**Mean:**	1.89	**Mean:**	1.04	**Mean:**	1.01	**Mean:**	0.94
		S.D.:	0.28	**S.D.:**	0.22	**S.D.:**	0.26	**S.D.:**	0.43	**S.D.:**	0.19	**S.D.:**	0.21	**S.D.:**	0.22

† Beams failed in flexural mode